Characterisation of a novel interaction partner for Atg16L1 and its role in regulating autophagy

By Laura Catherine Vaux

3454223

Faculty of Medicine and Health Sciences

University of East Anglia

January 2015

Abstract

Macroautophagy (hereafter referred to as autophagy) is a highly conserved eukaryotic cellular response to starvation, resulting in the formation of double-membrane vesicles known as autophagosomes. These sequester cytoplasmic contents to the lysosome, where they are degraded to generate amino acids which can be used for protein synthesis during periods of nutrient deprivation. Membrane targeting of LC3, the major structural protein of the autophagosome, is essential for autophagy. LC3 is processed from its cytosolic form (LC3-I) to its lipidated form (LC3-II) in a series of ubiquitin-like conjugation events. Of particular importance is Atg16-like-1 (Atg16L1), which through its interactions with Atg5-Atg12, specifies the site of LC3 incorporation into the expanding autophagosomal membrane.

In this study tools have been generated for the study and characterisation of Atg16L1 domains in cell culture. Atg16L1 -/- MEFs have also been generated and used for reconstitution experiments, which confirm that the coiled-coil domain of Atg16L1 is sufficient to restore autophagy in response to starvation and to a surrogate pathogen.
A novel interaction between Atg16L1 and the serine/threonine kinase MEKK4 has been characterised in this study. Existing research has established an interaction between the pathogen recognition receptors NOD1/2 and Atg16L1. The NOD receptors are activated by bacterial peptidoglycan (PG), which has been shown to drive autophagy. Interestingly, MEKK4 inhibits NOD2 signalling by binding the downstream adaptor protein RIP2, leading to the hypothesis that MEKK4 may play a role in autophagy. The interaction was verified by co-immunoprecipitation, with domain analysis indicating that MEKK4 binds to the linker region of Atg16L1. The kinase activity of MEKK4 was also required for the interaction. The complex between Atg16L1 and MEKK4 persisted during starvation induced autophagy. Lipidation of LC3 in response to starvation required expression of MEKK4, with a redistribution of LC3 to large perinuclear aggregrates that co-localised with p62 and ubiquitin in siRNA silenced cells and CRISPR/Cas MEKK4 knockout cells. The aggregates were also able to recruit LC3 I, indicating a role of aggresome-like induced structures (ALIS).
This thesis documents an interaction between Atg16L1 and MEKK4 that is vital for LC3 processing. The potential role for MEKK4 in regulating autophagy through Atg16L1 is discussed and experiments proposed to further explore this interaction in the context of autophagy.

Contents

Abbreviations

ABM – Atg16L1 binding motif
AID – autoinhibitory domain
ALIS - aggresome-like induced structures
ATG - autophagy-related
ATP – adenosine triphosphate
BCA - bicinchoninic acid
CAS - CRISPR associated gene
CCD – coiled-coil domain
CD – Crohn's disease
CD4 – cluster of differentiation 4
CRISPR - clustered regularly interspaced short palindromic repeats
DAPI - 4',6-diamidino-2-phenylindole
DCFP1 - double FYVE-containing protein 1
DMEM Dulbecco's Modified Eagles Media
DNA – deoxyribonucleic acid
DSB – double stranded break
DSP - dithiobis(succinimidylpropionate)
ER – endoplasmic reticulum
FACS - Fluorescence-activated cell sorting
FCS – foetal calf serum
FIP200 – focal adhesion kinase family interacting protein of 200 kDa
GABARAP - GABA receptor-associated protein
GADD45 growth arrest and DNA damage inducible 45 genes
GFP – green fluorescent protein
GWAS – genome-wide association studies
HA - Human influenza hemagglutinin
HBSS - Hank's Balanced Salt Solution
HDAC6 - histone deacetylase 6
HEK293 cells - Human embryo kidney 293 cells
IB - immunoblot
IBD – inflammatory bowel disease
IgG - immunoglobulin G
IL – interleukin
INDEL – insertion/deletion mutation
IP - immunoprecipitation
KO - knock out
LRR - leucine rich repeats
MAPK - mitogen activated protein kinase
MAP3K4/MEKK4 - Mitogen-activated protein kinase kinase kinase 4
MDP - muramyl dipeptide
MEF cells – mouse embryonic fibroblast cells
MHC - major histocompatibility complex
mPER - mammalian protein extraction reagent
MTOC - microtubule organising centre
mTOR - mammalian target of rapamycin
MVB - multivesicular body
NDS - normal donkey serum
NEAA – non-essential amino acids
NF-κB - nuclear factor-kappa B
NHEJ – non-homologous end joining
NLR - NOD-like receptor
NOD - nucleotide-binding oligomerization domain receptor
PAM – protospacer adjacent motif
PAMPs - pathogen associated molecular patterns

PBS – phosphate buffered saline

PCR – polymerase chain reaction

PE - phosphatidylethanolamine

PI – phosphatidylinositol

PI3K – phosphatidylinositiol 3-kinase

PI3P - phosphatidylinositol 3-phosphate

PRR - pathogen recognition receptor

P/S – penicillin-streptomycin

RFP – red fluorescent protein

RIP2 - receptor-interacting serine/threonine-protein kinase 2

ROI – region of interest

SCR – scrambled

sgRNA – single guide ribonucleic acid

shRNA – short hairpin ribonucleic acid

siRNA – short interfering ribonucleic acid

SNP – single nucleotide polymorphism

TLR – toll-like receptor

TVA – tubulovesicular autophagosome

UC – Ulcerative colitis

Ub - ubiquitin

ULK - unc-51-like-kinase

WIPI - WD-repeat PI3P-effector protein

List of figures and tables

Acknowledgements

Firstly I would like to thank my supervisors, Tom Wileman and Ulrike Mayer for all the support and advice they have provided throughout the last four years. With their guidance and patience, they have allowed me to develop this thesis and work towards becoming an independent scientist. I have benefited so much from learning new skills and techniques and challenging myself with this PhD, and I will always be grateful that you let me find my own way. I'd especially like to thank Ernst Pöschl and Ulrike with whom I have had countless discussions in lab meetings, and the knowledge and encouragement they have imparted has been so very helpful. I'd also like to thank my mentor, Lindsay Hall who has provided all means of support over the last two years. I am sincerely grateful for all the advice shared over coffee and email, and she continues to be an inspiration to me.

I'd like to thank the past and present members of the Wileman and Mayer laboratories for their help, advice and scientific discussion over the years; Eleanor, Matt J, Zhou and Isabelle. I'd especially like to thank Devina and Louise, who have both been incredibly helpful scientifically and are wonderful people. It has been a pleasure knowing you. I am also indebted to everyone in the BMRC who has helped me during this PhD, especially Milka and Debbie for their advice with immunoprecipitations, Meghan M and Stuart for their expertise on siRNAs, and Darren for his help and astounding FACs knowledge. I'd also like to thank Matt Y for working opposite me and sharing my dark sense of humour. Thanks also to Jasmine W and Andy L who work so incredibly hard in the day to day running of the BMRC. I'd like to extend my thanks to the undergraduate students I have had the pleasure to teach, namely Jamie, Kieran and Rukky. The work you produced was invaluable in helping this thesis progress, and you helped me realise I actually knew something about science! I wish you all the best in your futures.

To two people who helped me realise that I was capable of doing a PhD in the first place and then helped me realise this ambition; Dr Kate Bowers and my father-in-law John Baker. I will never forget how you encouraged me all those years ago. Thank you so much.

I owe an enormous debt of gratitude to the orthopaedic department at the NNUH, the staff at the UEA Medical Centre and the amazing team of Physiotherapists (Chris, Michelle, Cathy and Carly), who have got me back on my feet again and allowed me to complete my PhD. This has meant the world to me and I cannot thank you all enough for the amazing job you do.

A huge thanks to my wonderful family for all their love and for listening. Especially my Mum, Sheila, who has been amazingly supportive of me. Lastly to my husband Andy. I dedicate this thesis to you. Thank you for absolutely everything, for all the support in the many forms you have given it and for always being able to make me laugh. The ninja experiment is now over.

Chapter 1

Introduction

1: Introduction

1.1 Overview of Autophagy

Autophagy was originally discovered more than forty years ago as a cellular response to starvation, where cells digest portions of the cytosol to generate amino acids. This catabolic process involves the trafficking of proteins and organelles to the lysosome for degradation, with subsequent amino acids recycled back to the cytosol. Autophagy is highly conserved from simple eukaryotes such as yeast to complex higher eukaryotes such as humans (Yang and Klionsky., 2009).

Three distinct forms of autophagy have been described in eukaryotic cells – macroautophagy, microautophagy and chaperone mediated autophagy. Microautophagy involves the direct engulfment of cytoplasm at the lysosome surface by invagination, protrusion and septation of the lysosomal membrane (Yang and Klionsky., 2009). In contrast, chaperone mediated autophagy does not involve this type of membrane rearrangement. Instead, chaperone proteins interact with targeting sequences on cargo proteins, resulting in translocation of unfolded, soluble proteins directly across the limiting membrane of the lysosome (Bandyopadhyay et al., 2008).

Macroautophagy, the subject of this report and herein referred to as autophagy, involves formation of new membranes that engulf and sequester cytoplasmic components into double membrane vesicles, known as autophagosomes. These fuse with lysosomes, forming autolysosomes, where the contents are degraded in the lumen by lysosomal enzymes, with the resulting amino acids recycled to the cytosol through membrane permeases (Figure 1.1). Autophagy occurs at basal levels within the majority of cells, performing 'housekeeping' functions including the turnover of proteins and organelles and as such, acts as a quality control system. However, it is dramatically upregulated during cellular stress e.g. nutrient starvation or growth factor withdrawal (Yang and Klionsky., 2009). Autophagy also provides a detoxification pathway that removes toxic cytosolic components, protein aggregates, damaged organelles and intracellular pathogens for degradation and recycling (Shintani and Klionsky., 2004). It can play a role during developmental processes, allowing cells to meet amino acid-poor growth conditions (Levine and Klionksy., 2004). Autophagy has an essential role in cell survival, development and homeostasis, and is implicated in the pathogenesis of human diseases, such as cancer, neurodegenerative disorders including Alzheimer's and Parkinson's disease, infection and inflammatory disorders (Huang and Klionksy., 2007; Mizushima et al., 2008; Levine and Kroemer., 2008). Importantly, autophagy is also an effector of innate and adaptive immunity providing a defence against intracellular pathogens, and influencing MHC II presentation of antigens (Paludan et al., 2005; English et al., 2009).

1.1.1 The core molecular machinery in mammalian autophagy

The molecular regulators of autophagy have been studied in detail, with many essential ATGs (autophagy-related genes) first identified in yeast and their orthologs found in other organisms; confirming the conservation of autophagic machinery across eukaryotes (Huang and Klionsky., 2007). To date more than 30 ATGs have been identified (Yang and Klionksy., 2009). Among these proteins, one subset is essential for autophagosome formation, and is referred to as the core molecular machinery; this drives the initiation, expansion and closure of the autophagosome (Xie and Klionksy., 2007; Mehrpour et al., 2010b). The core ATG proteins can be grouped into four subgroups; the ATG1/unc-51-like-kinase (ULK) complex; the class III phosphatidylinositol 3-kinase (PI3K)/Vps34 complex I; the transmembrane protein mATG9, and lastly the two ubiquitin-like protein (ATG12-ATG5:ATG16L and ATG8/LC3) conjugation systems. These core ATG proteins are recruited to the site of autophagosome formation; the phagophore assembly site (PAS) (Yang and Klionksy., 2010; Proikas-Cezanne et al., 2004).

This report focuses on mammalian autophagy, which differs in some part to the yeast autophagy pathway.

The mammalian target of rapamycin complex 1 (mTORC1) plays a key role in the control of autophagy. mTORC1 is a highly conserved serine/threonine protein kinase that acts as a central sensor of growth factors, nutrient signals and the energy status of the cell (Yang and Klionsky., 2010). When the cell has a ready supply of nutrients, mTORC1 inhibits the induction of autophagy. However during starvation or in the presence of the drug rapamycin, mTORC1 is inhibited and consequently autophagy is upregulated (Yang and Klionsky., 2009).

Under nutrient rich conditions, mTORC1 inhibits autophagy by binding the ULK complex, which contains ULK1/2, ATG13 and FIP200. mTOR inactivates ULK1/2 by phosphorylation (Chan et al., 2009; Ragusa et al., 2012; Mehrpour et al., 2010a).

Inactivation of mTORC1 by starvation or rapamycin leads to the dissociation of the ULK complex from mTORC1, and activation of ULK1/2 kinase activity, resulting in the phosphorylation of Atg13 and FIP200 (Chan et al., 2009; Ragusa et al., 2012; Mehrpour et al., 2010a).

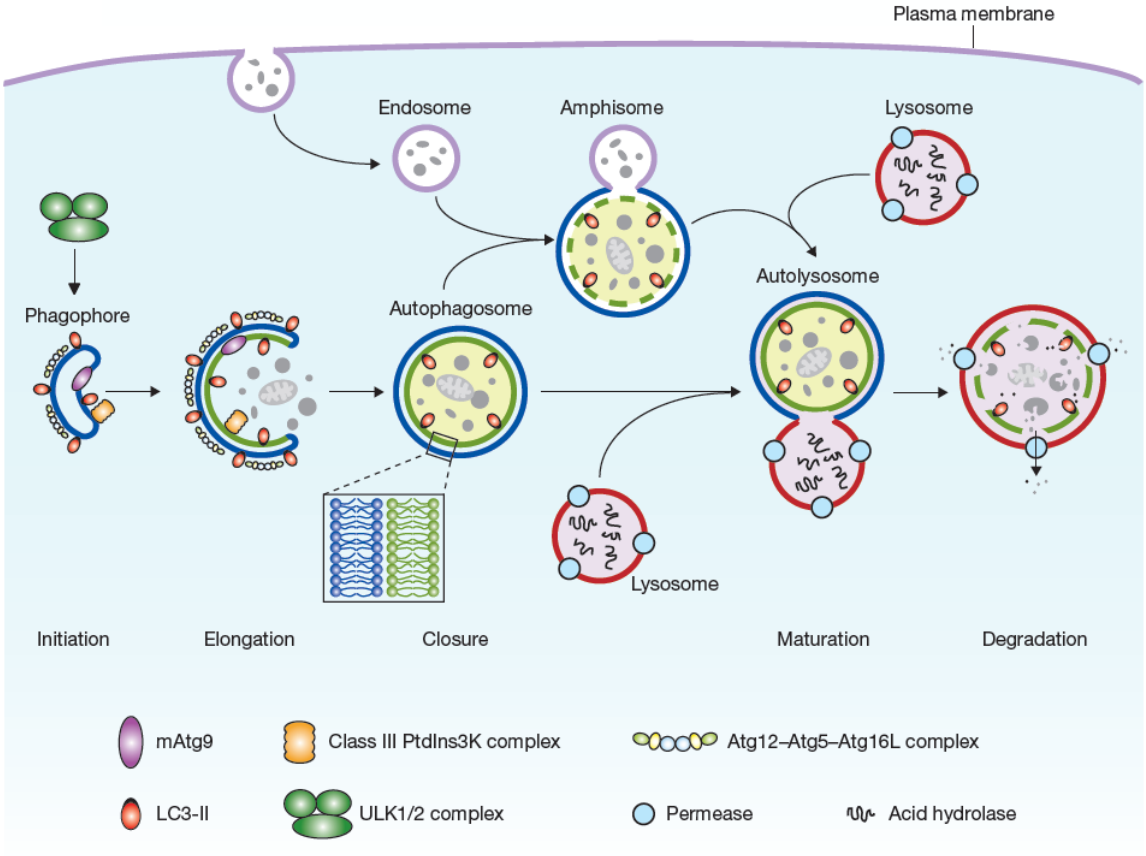

Figure 1.1: A schematic representation of the autophagy pathway

Autophagy involves the formation of double membrane vesicles known as autophagosomes, which sequester cytoplasmic components and protein aggregates. Their initiation, elongation and closure are regulated by the core machinery of the autophagy pathway. In yeast, following maturation, the autophagosome will fuse with a lysosome, generating an autolysosome; the contents of which are degraded and recycled back to the cytosol through membrane permeases. In mammalian autophagy, the autophagosome is thought to fuse with components of the endocytic pathway forming an amphisome, prior to lysosomal fusion.

Image from Yang and Klionsky, 2010

The endoplasmic reticulum (ER) is a well characterised site of autophagosome formation, with early autophagosomes (phagophores) arising from ER-derived omegasomes (Axe et al., 2008). Other subcellular compartments have also been shown to contribute to the membrane of the autophagosome e.g. plasma membrane and Golgi (Ravikumar et al., 2010; Ge et al., 2014). The nucleation and assembly of the early autophagosome depends upon the PI3K complex. This consists of hVps34, its regulatory protein kinase hVps15, Beclin1 and ATG14L/Barkor (Itakura et al., 2008; Sun et al., 2008). The class III Vps34 lipid kinase is activated (Wirth et al, 2013), translocates to the ER along with the ULK complex, and produces an autophagosome specific pool of phosphatidylinositol 3-phosphate (PtdIns(3)P or PI3P) (Russell et al., 2013). The activity of this complex is tightly regulated; positive regulators include vacuole membrane protein 1 (VMP1) and myeloid differentiation factor 88 (MyD88) (Cecconi and Levine., 2008; Mehrpour et al., 2010a).

During autophagosome formation, the increased levels of PI3P at the membrane of the elongating phagophore leads to the recruitment of autophagy specific PI3P effectors, such as DCFP1 (double FYVE-containing protein 1) and the WIPI (WD-repeat PI3P-effector protein) family of proteins (Karanasios et al., 2013; Koyama-Honda et al., 2013; Polson et al., 2010). The WIPI proteins are phospholipid-binding effectors, which can act as a PI3P scaffold in the early stages of autophagy (Proikas-Cexanne et al., 2004).

The only known transmembrane autophagy protein is mATG9 or ATG9L1. During nutrient rich conditions, mATG9 traffics between the *trans*-Golgi network and late endosomes (Young et al., 2006). In response to autophagy activation, mATG9 translocates to a peripheral pool where it co-localises with the autophagosome markers LC3 and Rab7. The trafficking of mAtg9 is dependent upon the p38α mitogen-activated protein kinase and its binding protein p38IP (Webber and Tooze., 2010). The putative role(s) of mAtg9 in autophagy is to serve as a platform for recruiting effectors to the developing autophagosome and/or act as a lipid carrier (Longatti and Tooze., 2009).
To enable expansion of the forming autophagosome, two vital protein complexes are required; the multimeric ATG12–ATG5-ATG16L complex and the lipidated form of LC3 and its family members GATE16 and GABARAP (GABA receptor-associated protein)

(Kabeya et al., 2000; Mizushima et al., 2003). Both utilise evolutionarily conserved ubiquitin-like conjugation systems which allow association with the autophagosome and eventual incorporation of LC3 into the membrane. ATG12 is activated by ATG7 in a process homologous to the E1 ubiquitin-activating enzyme. The activated ATG12 is then conjugated to ATG5 via an internal lysine residue by ATG10 in a reaction similar to the E2 ubiquitin-conjugating enzyme (Figure 1.2). The ATG12–ATG5 conjugate is then able to interact with ATG16L in a non-covalent manner, which subsequently oligomerises to form a large multimeric complex referred to as the ATG16L complex (Mizushima et al., 2003; Mehrpour et al., 2010b). This complex is thought to generate curvature in the autophagosome membrane. The interaction between ATG16L1 and WIPI2 drives recruitment of the ATG16L1 complex to the membrane of the developing autophagosome, which is dependent on PI3P formation (Figure 1.2) (Dooley et al., 2014; Itakura and Mizushima et al., 2010). Interactions between ATG16L1, FIP200 and ubiquitin have also been shown to play a role in the recruitment of ATG16L1 to the autophagosome membrane (Gammoh et al., 2013; Nishimura et al., 2013; Fujita et al., 2013). In a separate reaction ATG8/LC3 is cleaved by ATG4 at its C-terminus, exposing a glycine residue. At this point LC3 is referred to as LC3 I. In the absence of autophagy this form of LC3 remains cytosolic and diffuse. During autophagy the E1-like activating enzyme ATG7 activates LC3, and ATG3 binds to and is activated by ATG12, allowing ATG3 (E2-like) to transfer PE (phosphatidylethanolamine) to the C-terminus of ATG8/LC3 (Ichimura et al., 2000; Sakoh-Nakatogawa et al., 2013). This generates LC3 II, its lipidated form. The ATG16L complex actively recruits LC3 I to the expanding phagophore membrane, defining the site where it is conjugated to PE (Saitoh et al., 2008). The lipidated form of LC3 associates with both the inner and outer membranes of the developing phagophore/autophagosome. Membrane expansion leads to the sequestration of cytosol and closure of the autophagosomal membrane. When the autophagosome is fully formed, the ATG16L complex and other Atg associated proteins dissociate from the membrane, with LC3 remaining attached (Mizushima et al, 2003; Mizushima et al, 2001). LC3 present on the outer/cytosolic membrane is cleaved from the PE by the protease ATG4, and recycled back to the cytosol (Mehrpour et al., 2010b). At this point only LC3 remains associated with the inner autophagosomal membrane. The LC3 family members assist the expansion and closure of the autophagosome (Fujita and Hayashi-Nishino et al., 2008; Weidberg et al.,2011), and as such are a useful marker for the identification of autophagosomes. The next stage of the autophagy pathway involves the maturation of the autophagosome. This consists of the docking and fusion of the autophagosome with lysosomal compartments, which then becomes the autolysosome. The autolysosome is a functional degradative compartment, acquiring lipases and proteases

from the lysosome (Simonsen and Tooze., 2009). Though there is plenty of data to support this model in yeast, there is a lack of evidence in mammalian cells. It has been suggested that the autophagosome matures following input from the endocytic pathway, prior to fusion with the lysosome. The autophagosome can merge with endocytic compartments, such as the early and late endosomes, and MVBs (multivesicular bodies) (Liou et al., 2997; Razi et al., 2009), resulting in the formation of amphisomes. The lumen of the amphisome is more acidic than that of the autophagosome, gaining hydrolytic enzymes from the endocytic vesicle. This stage of autophagy depends on the acidification of autophagic compartments, and the proteins that regulate the fusion of autophagosomes with components of the endocytic pathway (Mehrpour et al., 2010b). The final stage of the pathway is vesicular breakdown and degradation of the lumenal contents of the autophagosome/amphisome, carried out by lysosomal cathepsins, among other enzymes. The inner membrane of the autophagosome is also degraded along with associated LC3 II, which is released into the lumen of the autolysosome. The digested lipids and amino acids are subsequently exported back into the cytoplasm to be recycled (Xie and Klionsky., 2007; Yang and Klionsky., 2009).

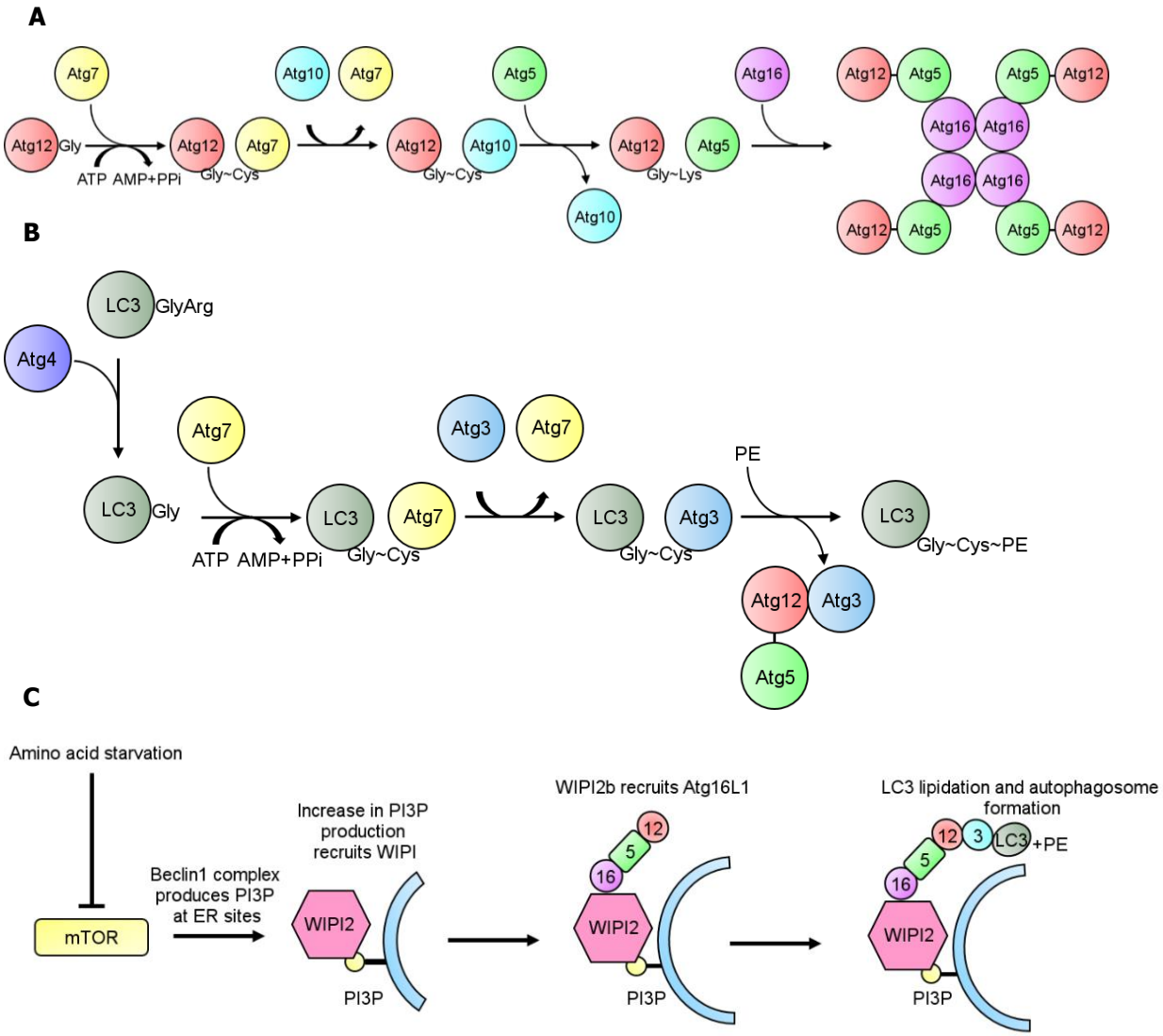

Figure 1.2: Two ubiquitin like systems involved in autophagosome formation

The two ubiquitin-like conjugation systems are utilised during autophagosome formation. (A) Atg12 is activated in an E1-like manner by Atg7. Atg12 can then be conjugated to Atg5 through an E2-like reaction with Atg7. This complex can then associate with Atg16L, which can actively recruit LC3 to the developing autophagosome.

(B) Atg8/LC3 is processed using another ubiquitin-like conjugation system utilising Atg7 (E1-like), Atg3 (E2-like) and the ATG16L complex (E3-like) (Geng and Klionsky., 2008).

(C) The Atg16L1-complex is recruited to the phagophore in early autophagy by WIPI2. The Atg16L complex specifies the site of LC3 lipidation and incorporation of LC3 into the autophagosomal membrane. For the sake of simplicity, "Atg" has been omitted from this section of the diagram.

Images modified from Geng and Klionsky, 2008; Dooley et al., 2014.

1.1.2 Autophagy in health and disease

In recent years, it has become clear that autophagy has a role to play in various aspects of human health. Autophagy promotes health by performing 'housekeeping' functions in the cells, eliminating defective or long-lived proteins and organelles, preventing abnormal protein aggregate accumulation and removing intracellular pathogens (Figure 1.3). This enables autophagy mediated protection against ageing, neurodegenerative diseases and pathogen infection (Levine and Kroemer., 2008). Conversely, defective or dysregulated autophagy has also been linked with the pathogenesis of disease, including neurodegeneration, cancer and inflammatory disease.

The role of autophagy in immunity and inflammation has become a great area of interest. The innate and adaptive immune response in mammals aims to provide defence mechanisms against invading pathogens which threaten the host, including bacteria, fungi and viruses (Medzhitov., 2007). Autophagy has been implicated in the homeostasis of T and B cells, the positive and negative selection of CD4 T cells, thymic selection enabling the regulation of self-tolerance and the delivery of antigenic peptides to MCH II processing compartments (Mehrpour et al., 2010a; Deretic and Levine., 2009; Schmid et al., 2007).

As part of the innate immune response, autophagy aids the targeted removal of microorganisms that invade the cell; this is termed xenophagy (Figure 1.3). Many medically important microorganisms are eliminated from the cell by this process including the bacteria *Staphylococcus aureus* and *Mycobacterium tuberculosis*, and the parasite *Toxoplasma gondii* (Deretic and Levine., 2009). During xenophagy invading microbes and their intermediates are captured and delivered to various cellular compartments, where they subsequently activate pathogen recognition receptors (PRRs), resulting in proinflammatory signalling. Interestingly, autophagy can also downregulate the proinflammatory response, including interleukin (IL) -1β, IL-18 and type I interferon production (Deretic and Levine., 2009). It appears that the immune system and autophagy are intricately linked, supporting its importance in health and disease.

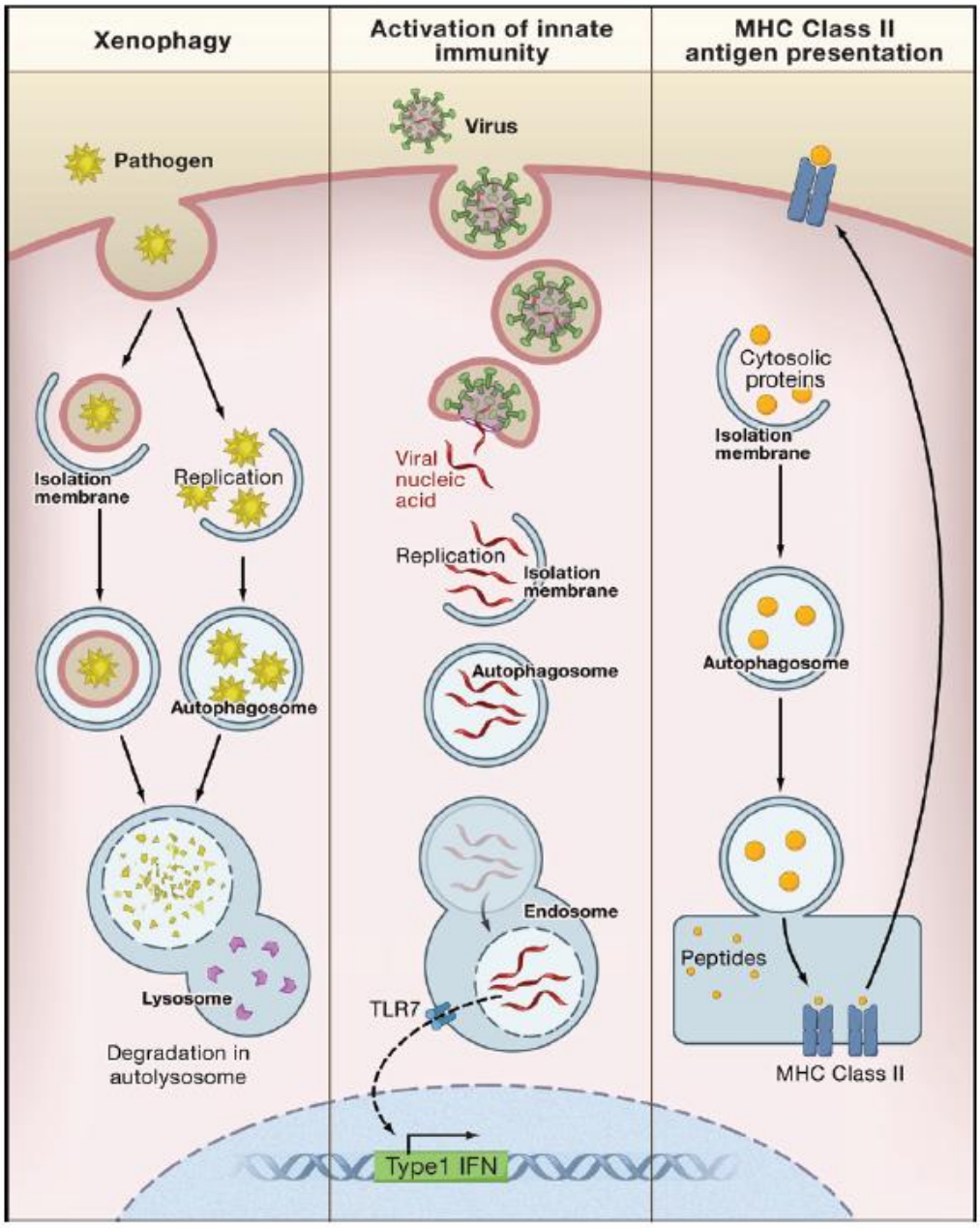

Figure 1.3: Autophagy in innate and adaptive immunity

In xenophagy, invading pathogens are engulfed by autophagosomes and degraded in the autolysosome. Autophagy can also activate innate immunity by delivering viral nucleic acids to compartments contain the PRR Toll-like receptor 7. When activated, this receptor can signal the induction of a type 1 interferon response. Autophagy is also involved in the delivery of antigenic pathogens to MHC-II processing compartments. Antigenic peptides can then be presented on the surface of APCs, where they are recognised by CD4+ T cells, which activates the adaptive immune response

Image from Levine and Kroemer (2008).

1.2 A mutation in the autophagy gene ATG16L1 is associated with Crohn's disease

Increasing evidence suggests a strong link between mutations in autophagy and autophagy-related genes and inflammatory bowel disease (IBD); two main subsets of which are ulcerative colitis (UC) and Crohn's disease (CD). Epidemiological data strongly supports a genetic contribution in the pathogenesis of Crohn's disease. Fifteen percent of patients with CD have a family member affected by IBD; the relative risk to siblings is approximately 17x population risk with around 50% concordance in identical twins, compared to less than 10% in non-identical twins (Stappenbeck et al., 2011; Breslin et al., 1997).

Genome-wide association studies (GWAS) have found that a point mutation in the autophagy gene *ATG16L1* is implicated in CD (Barrett et al., 2008; Hampe et al., 2007; Rioux et al., 2007; Consortium., 2007; Cheng et al., 2010). The mutation in question encodes a base pair substitution from an adenine to a guanine, which results in a single amino acid exchange from a polar threonine to a non-polar alanine at position 300 amino acid of ATG16L1 (T300A). This single nucleotide polymorphism (SNP) appears to carry nearly all the disease risk exerted by ATG16L1 (Hampe et al., 2007). Studies have shown that the ATG16L1 protein is expressed in the colon, small intestine, intestinal epithelial cells, leukocytes and spleen (Fujita et al, 2008). Additionally, the T300A mutation has been associated with the onset of a specific subtype of CD; ileal CD (Sventoraityte et al., 2010).

Crohn's disease and ulcerative colitis are both chronic and debilitating inflammatory disorders affecting the gastrointestinal tract. CD differs from ulcerative colitis in that CD inflammation mostly involves the ileum and colon, though it can affect any region of the gut. The inflammation associated with the disease is transmural, typically discontinuous and associated with granulomas. Ulcerative colitis, on the other hand, is usually limited to the colon and rectum, with continuous inflammation that is confined to the superficial mucosal and submucosal layers of the intestinal wall (Cho, 2008, Stappenbeck et al., 2011). It is apparent that the barrier function of the gut epithelium, commensal bacteria and appropriate intestinal immune response are important to the maintenance of a healthy gut. In CD, these factors no longer appear to function correctly, leading to prolonged activation of the immune response and chronic inflammation. Impaired immune defence mechanisms against bacteria may be due to genetic susceptibility; this link is apparent in GWA studies. Research is beginning to point towards how the T300A polymorphism contributes towards the pathogenesis of CD, but to greater understand the significance of this mutation, the structure of ATG16L1 and its known functions will be outlined below.

Table 1.1. A comparison between mouse and human Atg16L1 on the genetic and protein level

Gene	Organism	Accession no.	cDNA length (bp)	Nucleotide homology	Number of residues (aa)	Protein homology
ATG16L1 γ	*Homo sapiens*	NM_030803.6	1875	89 %	624	94%
Atg16L1 γ	*Mus musculus*	NT_078297.6	1872		623	

1.2.1 Structure and function of ATG16L1

The ubiquitin-like conjugation systems, utilising the ATG8 system and the ATG16L1 complex, are evolutionarily conserved across eukaryotes. The protein ATG16L1 shares many similarities with its yeast counterpart ATG16. Both comprise of an N-terminal ATG5-binding domain, followed by a coiled-coil domain (CCD). In higher complex eukaryotes there is an additional linker region and a WD40 repeat domain at the C-terminus (Figure 1.4 a). The T300A polymorphism falls towards the end of this linker region, before the start of the WD40 repeat. Alignment of the amino acid sequence from *Saccharomyces cerevisiae* (yeast) and from *Mus musculus* (mouse) shows homology in the CCD. The homology, though weak, is significant and lies between amino acids 28-145 with around 22% identity and 43% similarity (Mizushima et al., 2003) . *Mus musculus* and *Homo sapiens* (human) *ATG16L1* share high nucleic acid identity (89%) and amino acid similarity (94%) (Table 1.1). Both contain a linker region and seven WD40 repeats at the C-terminal end, something which yeast ATG16 completely lacks (Mizushima et al., 2003). The WD40 motif was originally identified in the β subunits of G proteins, and forms blades which can assemble into a β-propeller structure. This symmetrical structure acts as a stable platform, allowing interactions with various proteins (Smith et al., 1999). The WD repeat itself is a 40-60 amino acid sequence that typically contains a GH dipeptide 11-24 residues from its N-terminus and the WD dipeptide at its C-terminus. The WD40 repeat domain in ATG16L1 is not required for autophagy, but is conserved across higher eukaryotes.

The crystal structure of yeast ATG16 has shown it forms a parallel coiled-coil dimer, in solution. Sequence alignment of ATG16 homologues suggests that this model is a conserved feature (Fujioka et al., 2010). However, more structural analysis is needed to confirm

whether the structure of ATG16L1 conforms to this model. Residues 22-46 of yeast ATG16 form an alpha helix that binds ATG5. Both the ATG5 binding region and the CCD are widely conserved. A model of the yeast ATG12–ATG5-ATG16 complex has been proposed (Figure 1.4 b), though it has yet to be experimentally determined. As the crystal structure of the full length mammalian ATG16L1 has not been determined, it is not clear whether the WD40 domain assembles into 7 or 8 blades. The number of predicted WD40 repeats has been disputed (Mizushima et al., 2003; Hampe et al., 2008), with the potential eighth WD40 repeat containing the T300A polymorphism. Until this structure is crystallised, the position of the T300A mutation will remain unknown.

A homologue of Atg16L1 was identified which is not required for autophagy; Atg16L2 (Ishibashi et al., 2011). Whilst the N-terminus (including the majority of the CCD) and the C-terminal WD40 domains are conserved (32.1% and 43% amino acid identity, respectively), the end of the CCD and linker region are relatively poorly conserved (20.7% amino acid identity). Characterisation of Atg16L2 determined that it was unable to localise to the autophagosome, and that this was likely due to the poor conservation in this region (Ishibashi et al., 2011).

To greater understand the role of ATG16L1 and the function of the T300A mutation in CD, various mouse models have been developed, which are discussed below.

1.2.2 Development of Atg16L1 mouse models

To further understand the role of Atg16L1 in autophagy and the significance of the T300A mutation, a number of mouse models have been generated. Attempts to create a complete knockout mouse of Atg16L1 have resulted in a post-natal phenotype, with mice dying within 1 day of delivery (Saitoh et al., 2008). This phenotype has occurred previously in Atg5- and Atg7- knockout mice, demonstrating the requirement of these autophagy proteins during the neonatal starvation period (Kuma et al., 2004; Komatsu et al., 2005).

The first Atg16L1 deficient mouse model was generated by deletion of the coiled-coil domain of Atg16L1, with the resulting mice expressing a truncated Atg16L1 protein (ΔCCD) (Saitoh et al., 2008). However, this was not a knockout of Atg16L1. As the linker and WD40 domains remain, this mouse model can be considered a functional knockout. Nonetheless, this mutation led to post-natal mortality, indicating how vital Atg16L1 is for survival. Mouse-embryonic fibroblasts (MEFs) harvested from these mice were deficient in autophagy following starvation. Additionally, Atg16L1 was required for conjugation of LC3 to PE, with an overall decrease in the bulk degradation of long lived proteins (Saitoh et al., 2008). Studies arising from the creation of these mice confirmed the vital importance of the CCD domain in the function of autophagy. Whilst this study highlights the importance of the CCD

in autophagy, it does not address the consequences of the T300A mutation, or the function of the WD40 repeat domain.

The issue of lethality in Atg16L1 functional knockout mice has been overcome in part by the development of a mouse hypomorphic for Atg16L1 protein expression by Cadwell et al 2008. The levels of Atg16L1 expression were confirmed to be 23-37% of expected levels. Whilst not a true knockout (recruitment of LC3 to the autophagosome was not completely ablated), this mouse can give an indication of the impact low levels of functional Atg16L1 may have on autophagy and the gut. Markers of autophagy were altered in Atg16L1^{HM} ileal lysates in a similar fashion to mice with diminished Atg5 expression demonstrating a consistent role for Atg16L1 and Atg5 in ileal autophagy (Cadwell et al., 2008). Infection of these mice with the bacteria *Listeria monocytogenes* found no increase in susceptibility to systemic infection when compared to controls, indicating that in this mouse model, Atg16L1 is not important for microbial processing. What was most striking however, was the Paneth cell abnormalities seen in Atg16L1^{HM} mice. Paneth cells are part of the intestinal epithelium and are located at the base of the intestinal crypt. They play an essential role in the control of intestinal microbiota by secretion of antimicrobial peptides and lysozyme packaged within granules (Porter et al., 2002). The Paneth cell abnormalities seen in the Atg16L1^{HM} mice affected the packaging of the lysozyme, granule number and organisation, which phenocopied abnormalities seen in CD patients carrying the *ATG16L1* risk allele (Cadwell et al., 2008).

The abnormalities seen in ATG16L1^{HM} mice were later found to be dependent upon persistent infection with murine norovirus (MNV) (Cadwell et al., 2010). ATG16L1^{HM} mice were rederived by embryo-transfer into an enhanced barrier facility, where more steps are taken to lower the risk of infection e.g. all cages, bedding and chow are autoclaved prior to use and sentinel mice are used and routinely screened for common mouse pathogens. When raised in the enhanced barrier facility the ATG16L1^{HM} mice gut morphology was comparable to wild type mice. The Paneth cell abnormalities could be reconstituted following infection with MNV (Cadwell et al., 2010; Simmons., 2010).

Tissue specific knockouts of Atg16L1 have been generated by Conway et al., 2013, who have studied the effects of Atg16L1 deficiency in the intestinal epithelium (IEC) and dendritic cells. The expression of Atg16L1 was conditionally knocked out using either the Villin-cre promoter for intestinal epithelial cre expression, or the CD11c-Cre promoter for dendritic mononuclear cell cre expression. Knockout of Atg16L1 was confirmed by Western blotting, with impaired LC3 conversion and accumulation of p62 (Conway et al., 2013). These mice were then infected with *Salmonella typhimurium* SL1344, a strain able to traverse the epithelium and disseminate systemically. These studies found an intestinal

specific requirement for autophagy in the clearance of bacteria and prevention of systemic infection, however this was not the case for the dendritic cells. Atg16L1 expression was essential for co-localisation of *S.typhi* with LC3, and furthermore, the Paneth cells in IEC specific Atg16L1 knockouts displayed abnormalities in lysosome granules, antimicrobial peptide expression, and a decrease in the overall number of Paneth cells per crypt compared to a control mouse. Whilst the Paneth cell abnormalities are similar between the IEC specific knockout and the $Atg16L1^{HM}$ mouse model, there is a difference in requirement of Atg16L1 in the prevention of systemic infection. The residual expression of Atg16L1 in the hypomorph may account for the lack of significant results in infection studies. Alternatively, the use of different types of bacteria (*Salmonella* and *Listeria*) could also have affected the outcomes of the studies, as the manner in which these bacteria interact with the host cell and autophagy machinery may not be comparable.

These mouse models show how genetic susceptibility, virus infection, injury to the gut mucosa, commensal and pathogenic bacteria all interact to initiate an inflammatory response, similar to that seen in CD in humans. CD pathogenesis is a very complex process, it is still unclear precisely what causes the disease, and as yet there is no known cure. Reproducing some, but not all, pathologies seen in CD patients raises the possibility that virus infection can interact with gene susceptibility to trigger chronic inflammation.

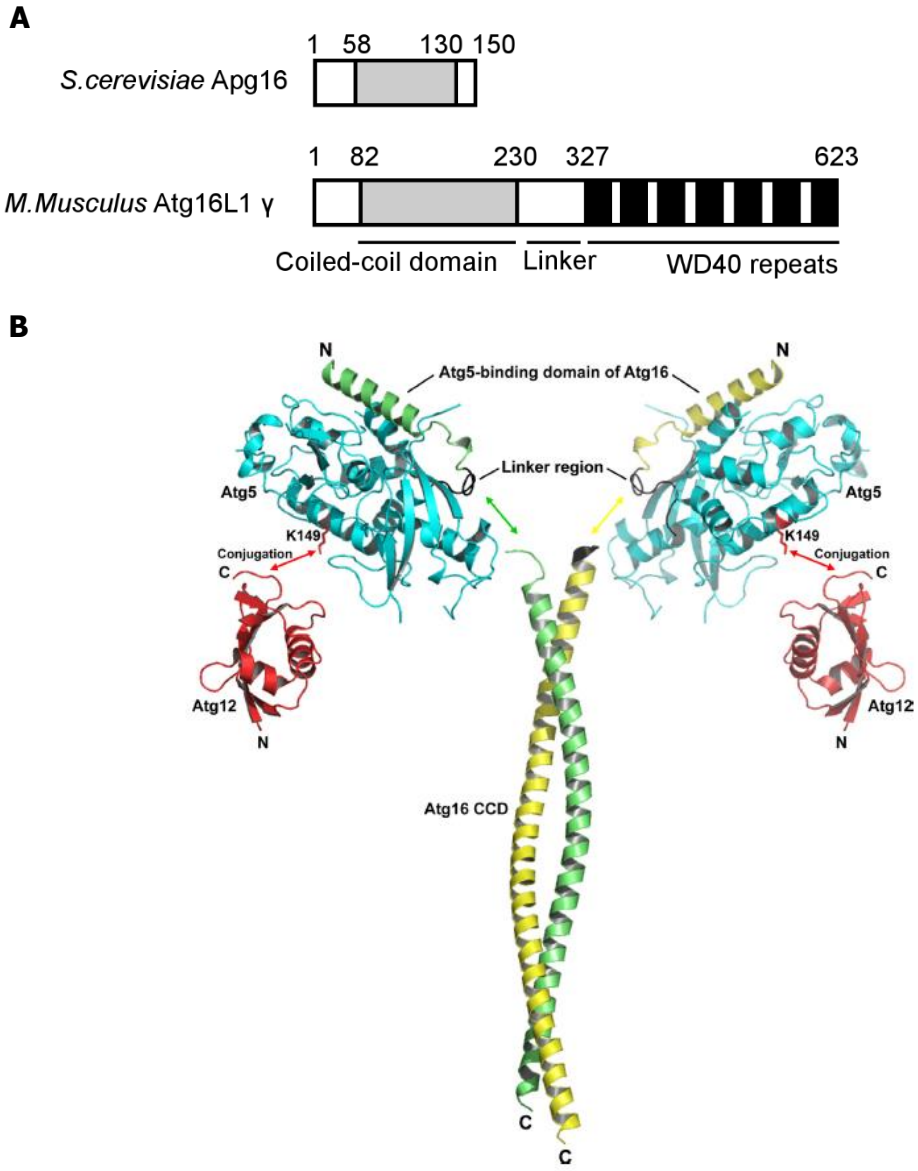

Figure 1.4: Conservation of Atg16L1 domains and proposed model of the yeast ATG12–ATG5-ATG16 complex

(A) Schematic representation of yeast Apg16 and murine Atg16L1 γ. The coiled-coil domain in yeast Apg16 is conserved in mouse Atg16L1, with the addition of a linker and WD40 repeat domain. Modified from Mizushima et al., 2003.

(B) Two ATG16 molecules are able to form a parallel coiled-coil dimer (shown in green and yellow), though more structural analysis is required to confirm whether this structure applies to ATG16L1. However, sequence alignment of ATG16 homologues suggests that this model is a conserved feature, and would explain how ATG16 oligomerises to form the tetrameric ATG12–ATG5-ATG16 complex. ATG5 and ATG12 are coloured cyan and red, respectively.

Image from Fujioka et al (2010).

1.2.3 Cell culture and mouse models of the CD associated mutation in Atg16L1

The consequences of the ATG16L1 T300A mutation are slowly being unravelled, aided early on by the development of the first Atg16L1 mouse models. A study by Fujita et al 2009, utilised MEFs from the Atg16L1 functional knockout mouse model developed by Saitoh et al, 2008. By expressing constructs containing the CCD of ATG16L1, or full length ATG16L1 T300A polymorphism they were able to reconstitute starvation induced autophagy (Fujita et al., 2009). This indicates that the T300A mutation and WD40 repeat domain are not required for starvation induced autophagy (Fujita et al., 2009). MEFs reconstituted with the CCD construct and the full length T300A construct were infected with *Salmonella typhimurium*. This resulted in no apparent difference in autophagosome formation around *S.typhimurium* which would suggest that the WD40 repeat domain and T300A mutation have no influence over xenophagy. However, an important point to note is that MEFs do not represent the highly specialised cells in the gut epithelium and mucosal immune system, as they lack important pathogen recognition receptors (PRRs) such as NOD2.

The findings of the Fujita et al, 2009 study conflicts with findings in cell culture studies. To elucidate the role of the ATG16L1 T300A polymorphism in CD, a study was carried out by Kuballa et al, 2008, using HeLa, Human embryo kidney 293 (HEK293) and the colonic Caco2 cell lines. Expression of the T300A polymorphism in ATG16L1 silenced cells did not affect basal autophagy, nor did it affect the ability of ATG16L1 to bind ATG5 (Kuballa et al., 2008). However, expression of the T300A variant diminished the cell's ability to handle intracellular pathogens when infected with *Salmonella typhimurium*. This decrease in the efficiency of xenophagy could have consequences for the gut mucosal immune system, as cells may not respond appropriately to pathogen invasion. This study suggests that the effect of the T300A mutation may be confined to a selective form of autophagy.

These previous papers utilise an overexpression method to study the Atg16L1 T300A variant. A cell culture based knock-in model was developed by Messer et al., 2013 using the colorectal cell line HCT116. Cells that expressed the CD associated T300A variant were protected against invasion by *Salmonella*, however those T300A expressing cells that were invaded by the bacteria showed an increase in intracellular bacterial growth due to reduced clearance of microbes by autophagy. The conflicting results in these cell culture based studies highlight the importance of cell type when monitoring xenophagy. Whilst all these studies have used the same bacteria (*Salmonella*), the cell lines have been the variable. It has also been shown that Salmonella invasion of fibroblasts occurs though distinct mechanisms compared to epithelial cells (Aistui et al., 2010), so the manner in which bacteria invade different cell types could impact the requirements for autophagy.

Additionally, genotyping of gastrointestinal cell lines has identified that the Caco2 cell line carried SNPs associated with IBD for ATG16L1 and NOD2 (Huebner et al., 2010). Therefore, results of studies using this particular cell line should be treated with caution, as it is difficult to decouple the results from the expression of the SNP. The study of the T300A mutation *in vivo* offers the best opportunity to resolve the effects of the ATG16L1 T300A mutation on autophagy and xenophagy.

Two independent groups developed a T300A knock-in mouse model in 2014, with both discovering and characterising a putative caspase cleavage motif that lies adjacent to the T300 residue (Murthy et al., 2014; Lassen et al., 2014). The cleavage of this motif is mediated by caspase 3 (Murthy et al., 2014) and possibly by caspase 7 (Lassen et al., 2014). Importantly, a functional consequence of the T300A mutation was identified using a combination of cells derived from the knock-in mouse model and human cells donated from carriers of the T300A mutation. The caspase mediated cleavage of Atg16L1 is enhanced in the T300A variant, which was shown to have a subsequent effect on autophagy (Murthy et al., 2014). Defects in Paneth cells were also observed, similar to those seen in the $Atg16L1^{HM}$, IEC specific knockout mouse models and CD patients. Infection of MEFs isolated from the T300A knock-in mice with *Shigella* confirmed a reduction in xenophagy (Lassen et al., 2014). Precisely how the caspase cleavage mechanism contributes to CD is unclear, though it paves the way for further studies focusing on activation and regulation of caspase pathways in the context of microbial infection, with the knock-in mice a valuable tool in achieving this.

1.2.4 Crohn's disease susceptibility gene interactions – NOD2 and ATG16L1

A vital arm of the innate immune system are the PRRs, which sense conserved pathogen associated molecular patterns (PAMPs); this includes viruses and their nucleic acid. PRR signalling is thought to affect autophagy, cytokine secretion and antigen presentation to effector immune cells (Simmons., 2010).

Polymorphisms in NOD2 were one of the first susceptibility risk factors identified in Crohn's disease (Cho., 2008). Two studies by Cooney et al, 2010 and Travassos et al, 2010 have demonstrated cross-talk between the NOD and autophagy pathways and a direct interaction between ATG16L1 and NOD2.

NOD2 belongs to the NOD-like receptor (NLR) family of PRRs, which play a key role in defence against pathogens and inflammation. NOD2 consists of two N-terminal CARD domains, a centrally located nucleotide-binding and oligomerisation domain and C-terminal leucine rich repeats (Figure 1.5) (Billmann-Born et al., 2011; Kumar et al., 2009). NOD2 receptors are specifically activated by a peptidoglycan-derived motif muramyl dipeptide (MDP), which is a component of Gram positive bacteria (Shaw et al., 2008). Following MDP recognition by the LRRs of NOD2, the receptor undergoes a conformational change and self oligomerisation via the NOD domain. Subsequently, they recruit a cytosolic serine/threonine kinase known as RIP2 through homotypic CARD/CARD interactions (Ogura et al., 2001). RIP2 then autophosphorylates on Y474, which is required for optimal NF-κB activation (Tigno-Aranjuez et al., 2010). RIP2 is also modified with K63-linked polyubiquitin, which is thought to be mediated by a number of E3 ubiquitin ligases including ITCH and IAP proteins (Figure 1.6) (Tao et al., 2009; Bertrand et al., 2009; Krieg et al., 2009). Following this polyubiquitination of RIP2, the IKK scaffolding protein IKKγ (NEMO) becomes poly-ubiquitinated via Lys^{63} linkages on Lys^{285} of NEMO. These ubiquitin chains are thought to provide a scaffold for the recruitment of TAK1 (TNF receptor-associated kinase 1), through its ubiquitin binding partners TAB2 and TAB3 (Figure 1.6) (Abbott et al., 2004; Abbott et al., 2007; Kanayama et al., 2004) enabling it to phosphorylate the activation loop of IKKβ (Figure 1.6). This eventually leads to the activation of nuclear factor-kappa B (NF-κB) transcription factors, the production of pro-inflammatory cytokines such as IL-1β, activation of mitogen activated protein kinases (MAPKs) ERK1/2, Jun-N-terminal kinase and p38.

The NOD2 receptor is constitutively expressed in immune cells such as monocytes, macrophages and dendritic cells. In relation to the gut, intestinal epithelial cells constitutively express NOD1, a member of the NLR family (Hisamatsu et al., 2003), with Paneth cells and intestinal stem cells expressing NOD2 (Ogura et al., 2003; Nigro et al., 2014), however the expression of NOD2 by intestinal epithelial cells is disputed (Billman-

Born et al., 2011; Hisamatsu et al., 2003). NOD2 induced signalling is involved in both systemic inflammatory responses and mediation of antimicrobial defence mechanisms through the secretion of α- and β-defensins along with other bactericidal proteins (Ogura et al., 2001). Therefore, it makes sense that mutations in NOD2 would lead to defective inflammation and defence against pathogenic bacteria. Three polymorphisms have been discovered in the NOD2 gene which contribute towards the development of CD. All three occur within the LRR region and result in a loss of function; L1007fsinsC is a one-base insertion, causing a frameshift mutation that results in a truncated LRR, whilst R702W and G908R are SNPs that result in single amino acid substitutions. (Figure 1.5) (Billmann-Born et al., 2011). It has been suggested this may cause epithelial barrier dysfunction due to facilitated bacterial entry into the base of the crypt-villus, as there is a failure to regulate the expression and secretion of defensins. Overall this would amount to a defective gut immune response to invasive pathogens.

The link between autophagy and NOD2 signalling was first demonstrated by Cooney et al. 2010. Initially they found that the NOD2 ligand, MDP, was able to induce autophagosome formation. This was dependent on NOD2 and required input from ATG5, ATG12, ATG16L1 and PI3K; all essential components of the core autophagy machinery (Cooney et al., 2010). Furthermore, MHC-II trafficking and antigen presentation in DCs was found to be influenced by NOD2 induced autophagy. Dendritic cells from CD patients carrying NOD2 or ATG16L1 polymorphisms were defective in MDP induced autophagy, were defective in MHC-II processing and failed to generate antigenic responses (Cooney et al., 2010). This may well lead to dysfunctional immune responses, resulting in the chronic tissue inflammation seen in CD.

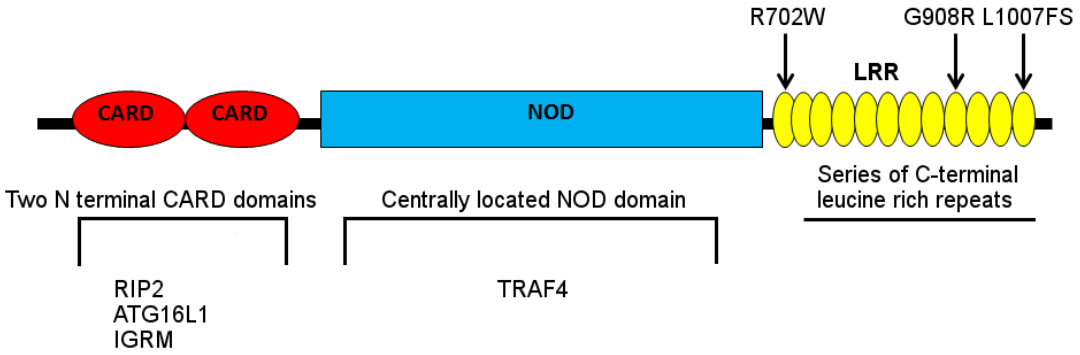

Figure 1.5: The domain structure of NOD2 and location of the CD associated polymorphisms

The NOD2 receptor consists of a trimodular structure, with two N-terminal CARD domains (red), a centrally located NOD domain (blue) and a series of C-terminal leucine rich repeats (yellow). The 3 CD associated polymorphisms in NOD2 occur in the leucine rich repeat region. In brackets are binding partners for the various domains. The interaction of NOD2 with RIP2 has been described by Tao et al., 2009, the interaction with ATG16L1 by Travassos et al., 2010 and Boada-Romero et al., 2013., the interaction with IGRM by Chauhan et al., 2015, and the interaction with TRAF4 by Marinis et al. 2011.

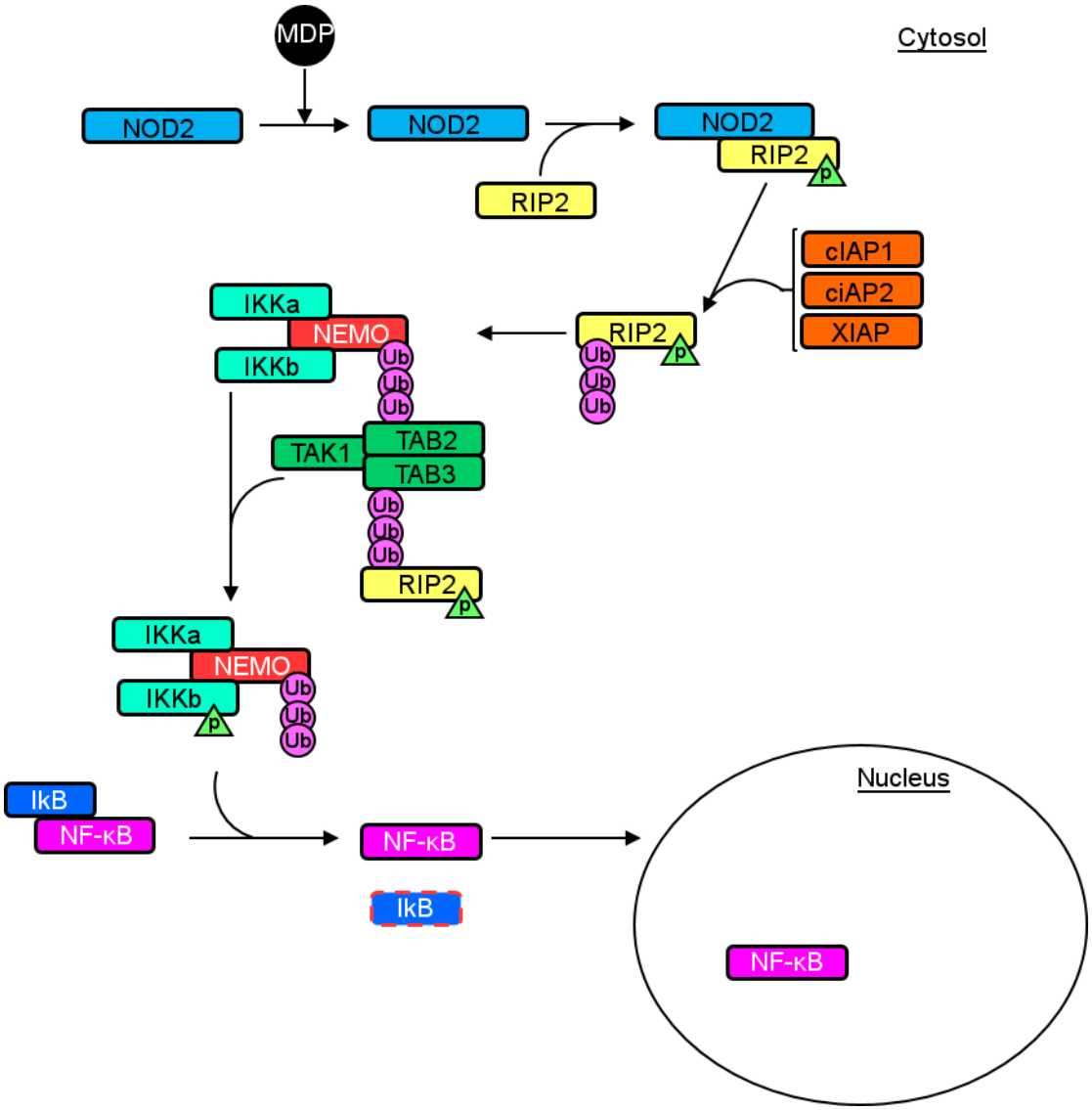

Figure 1.6 Activation of NOD2 signalling

Following MDP recognition by NOD2, the receptor undergoes a conformational change and can self oligomerise via its NOD domain. RIP2/RICK, a serine/threonine kinase is recruited to NOD2 via homotypic CARD/CARD interactions. This leads to the activation of the IκB-kinase/ NF-κB pathway and subsequent production of pro-inflammatory cytokines.

Assembled using data from Tigno-Aranjuez et al., 2010, Tao et al., 2009; Bertrand et al., 2009; Krieg et al., 2009, Abbott et al., 2004; Abbott et al., 2007; Kanayama et al., 2004.

A study published simultaneously by Travassos et al, 2010 confirmed a direct interaction between NOD2 and ATG16L1 (Figure 1.7). A series of *in vitro* and *in vivo* experiments confirmed that agonists of NOD1 and NOD2 receptors e.g. MDP, lead to the induction of autophagy. ATG16L1 was found to co-localise at the plasma membrane with NOD2, and when both constructs were co-expressed an ATG16L1-NOD2 complex could be precipitated, confirming that these two proteins can interact with each other. Furthermore, when cells were infected with the bacterium *Shigella flexneri*, NOD2 and ATG16L1 translocated to the site bacterial entry, forming LC3 positive autophagosomes around invading bacteria (Travassos et al., 2010). This mechanistic link between NOD2 and ATG16L1 provides great scope for research into a potential pathway involving these two CD risk alleles. The biological consequences of this pathway, and from mutations within it, would shed light on the development of CD, and may even provide future therapeutic targets.

This signalling axis has been explored in vivo with the use of the Atg16L1^{HM} and Nod2 -/- mouse models. The bacterial pathogen *Citrobacter rodentium*, which models infective colitis (Bhinder et al., 2013), was used to infect both these mouse stains, and revealed that the Atg16L1^{HM}conferred protection to infection whereas the Nod2 -/- mice displayed poor survival rates. This resistance in the Atg16L1^{HM} mice was due to a hyperimmune transcriptional response which was present before infection (Marchiando et al., 2013). This protective effect was lost when the Atg16L1^{HM} mice were crossed with Nod2 -/- mice, demonstrating that this effect is dependent on the expression of this PRR, and may be related to this important signalling axis.

The link between the two pathways was further investigated at the molecular level in cell cultures studies by Sorbara et al. 2013. Using Atg16L1 deficient MEFs that lack the CCD, they specifically show that Atg16L1 is able to regulate Nod driven cytokine production in response to infection. The mechanism behind this was Atg16L1 dependent interference with two important molecular events in Nod2 signalling; poly-ubiquitination of Rip2 and recruitment of Rip2 into large signalling complexes (Sorbara et al., 2013) (Figure 1.7). Interestingly the T300A variant of Atg16L1 had less of an effect on Rip2/Nod2. This study further illustrates the importance of the Nod2:Atg16L1 interaction in a physiologically relevant context.

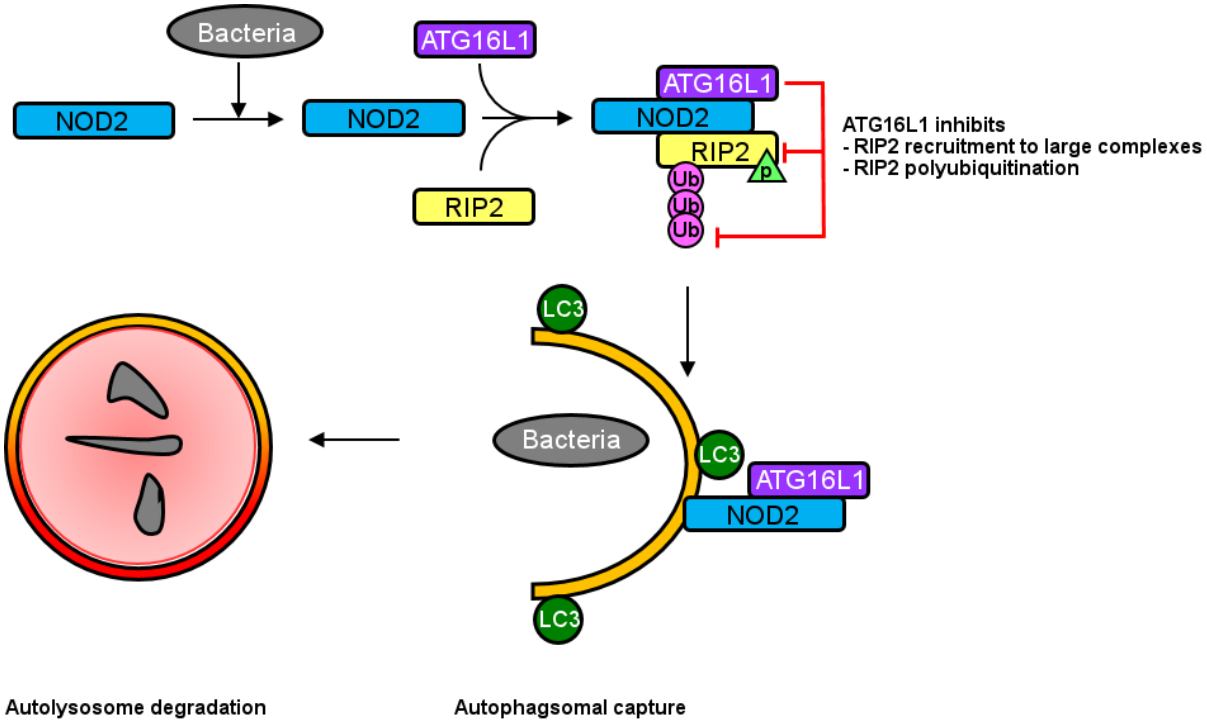

Figure 1.7 Crosstalk between the NOD2 and autophagy pathways

NOD2-activated autophagy involves a direct interaction between NOD2 and ATG16L1, and leads to the targeting of autophagosomes to intracellular bacteria. ATG16L1 negatively regulates NOD2 signalling by inhibiting the recruitment of RIP2 into large signalling complexes and preventing the polyubiquitination of RIP2.

Figure assembled using data from Travassos et al., 2010; Sorbara et al., 2013.

1.3. The aims and objective of the thesis

GWAS have identified mutations in ATG16L1 and NOD2 that are strongly associated with CD (Barrett et al., 2008; Hampe et al., 2007; Rioux et al., 2007; Consortium., 2007; Cheng et al., 2010). The main objective of this project was to gain further insight into the role of ATG16L1 by studying novel protein interactions which may impact on the NOD2:ATG16L1 signalling axis.

Aim 1. To determine the role played by different domains of ATG16L1 during autophagy and see if these roles are affected by the T300A mutation.

While the function of the coiled-coil domain of ATG16L1 is known, the role of the linker and WD40 repeat domain remains unclear. Deletion constructs of ATG16L1 were generated and tagged with eGFP at the C-terminus, to allow the study of the role of the individual domains of ATG16L1. Site directed mutagenesis was used to generate the CD associated T300A mutation and remove a putative phosphorylation site to study the contribution of these residues to autophagy. This work was carried out in the first results chapter, and generated vital tools for studies carried out in the second results chapter.

Aim 2. To validate a role for MEKK4 as a novel ATG16L1 interaction partner that may modulate NOD2 signalling. A yeast-two-hybrid screen had been carried out on behalf of the lab by Hybrigenics Global PBS®, using *Mus musculus* Atg16l1 as bait against a human colon cDNA library. The human colon cDNA library was chosen so as to identify interactions with proteins that are likely expressed in the gut. One of the interactions identified by this screen was the kinase MEKK4 (also referred to as MAP3K4 and MTK1). In order to validate this interaction, immunoprecipitation assays were carried out using the GFP-tagged Atg16L1 constructs (generated in the first results chapter) and an HA-tagged MEKK4 construct, obtained. Literature searches of MEKK4 found that the protein plays a key role in the regulation of NOD2 signalling (Clark et al., 2008). Previous studies have identified that stimulation of NOD2 signalling results in the activation of autophagy, and that NOD2 binds ATG16L1 following stimulation of NOD2 signalling with MDP (Cooney et al., 2010; Travassos et al., 2010) though the mechanisms by which stimulation of NOD2 leads to the activation of autophagy are unknown. It was therefore hypothesised that MEKK4 may interact with ATG16L1 to modulate NOD2 activated autophagy. To confirm whether the ATG16L1:MEKK4 interaction is involved in NOD activated autophagy, HA-tagged NOD2 constructs were used in complex immunoprecipitation assay.

Aim 3. To determine if interaction between ATG16L1 and MEKK4 controls autophagy. MEKK4 has been linked to the regulation of autophagy through p38 MAPK (Keil et al., 2012), and is required for NOD2 directed autophagy against intracellular bacteria (Homer et al., 2012). To study the role of MEKK4 in autophagy, siRNAs were used to silence MEKK4 and the effect on autophagy monitored by the formation of autophagosomes and the conversion of LC3. Furthermore, the effects of MEKK4 silencing were replicated using a genome editing technique to generate MEKK4 knockout cell lines, for future studies. This work is described in the third and final results chapter.

Overall, the findings of this thesis will contribute to a greater understanding of the ATG16L1:NOD2 axis through the characterisation and dissection of a novel interaction between ATG16L1 and MEKK4, a protein that also regulates NOD2 signalling.

Chapter 2:

Materials and Methods

2. Materials and Methods

2.1 Materials

2.1.1 Chemicals, reagents and materials

Chemicals were obtained from the companies Sigma-Aldrich (UK), Roche (UK) and Melford (UK). Restriction enzymes were from Roche (Germany). All media solutions and reagents were purchased from Invitrogen (Paisley, UK), and all chemical compounds purchased from Sigma (Dorset, UK), unless otherwise stated.

2.1.2 Kits used for molecular biology

Kits used in molecular cloning are detailed in table 2.1

Table 2.1 Kits used for molecular cloning

Kit	Company
Expand High Fidelity PCR system	Roche
VELOCITY DNA Polymerase	BIOLINE
Geneclean II DNA purification kit	MP Biomedicals
Ready-To-Go T4 DNA ligase	Amersham/GE Lifesciences
Fast DNA End repair kit	Thermo Scientific
GeneJET PCR Purification Kit	Thermo Scientific
QIAGEN Mini and MIDI plasmid prep kits	QIAGEN
Macherey-Nagel Nucleospin and Nucleobond plasmid prep kits	Macherey-Nagel
QuikChange Lightning Site-Directed Mutagenesis Kit	Agilent Technologies

2.1.3 Frequently used buffers and solutions

Buffers were prepared with ultrapure dH_2O unless otherwise stated. The full list of buffers and solutions is detailed in table 2.2

Table 2.2 List of buffers and solutions

Buffer	Formula	Buffer	Formula
50X TAE buffer	40 mM Tris acetate, 2 mM EDTA (pH 8.5)	PBS (10x)	80g NaCl, 2g KCl, 26.8g Na2HPO4 and 2.4g KH2PO4, up to 1 litre H_2O, pH 7.4
TE buffer	10 mM Tris/HCl (pH 8.5), 1 mM EDTA (pH 8.0)	TBS (10x)	500 mM Tris/HCl (pH 7.4) and 1.5 M NaCl
TFB I buffer	30 mM K acetate, 50 mM Mn2Cl, 100 mM RbCl, 10 mM CaCl2, 15 % (v/v) Glycerine (pH 5.8), filter sterile	DNA loading buffer (5x)	50% (v/v) Glycerol, 1X TAE, 0.5 % (w/v) Orange G
TFB II buffer	10 mM MOPS/NaOH (pH 7.0), 75 mM CaCl2, 10 mM RbCl, 15 % (v/v) Glycerine, filter sterile	TENS buffer	50 mM Tris/HCl (pH 8.0), 20 mM EDTA (pH 8.0), 100 mM NaCl, 1.0 % (w/v) SDS
SDS-PAGE Sample Buffer (5x)	2.5ml Glycerin (25%), 0.2423g Tris (200mM), 0.5g SDS (5%), 5mg bromophenol blue, pH 6.8	Ponceau-S	0.2% in 5% TCA
SDS-PAGE Running Buffer (10x)	25mM Tris base, 190 mM glycine, 0.1 % SDS, pH 8.3	Transfer Buffer (10x)	390 mM Glycine, 480 mM Tris, 0.3% SDS, pH 9.2

2.1.4 Tissue Culture media

All media solutions for tissue culture were made as follows:

- Dulbecco's Modified Eagles Media (DMEM) with 1g/L GlutaMAX (Invitrogen) was supplemented with 10% (v/v) foetal calf serum (FCS) and 1% (100 units/µl) penicillin-streptomycin (P/S) for culture of HeLa, the immortalised MEF cell lines MEF, Atg5 -/-, p62 -/- and African green monkey epithelial cells or Vero cell lines.

- DMEM with 1g/L GlutaMAX was supplemented with 10% FCS, 1% P/S, 1% (100 units/µl) of Non-essential amino acids (NEAA) and 1% (100 units/µl) of sodium pyruvate (Sigma) for culture of Human embryo kidney 293 (HEK293) cell lines.

- DMEM with 4g/L GlutaMAX was supplemented with 10% FCS and 1% P/S for culture of the primary MEF cell lines and Raw 264.7 cells.

- DMEM with 1g/L GlutaMAX was supplemented with 10% FCS, 1% P/S, 1% NEAA, 1% sodium pyruvate and 10 µg/ml of puromycin for the culture of HEK293 episomal cells containing the pCEP-Pu vector.

- DMEM with 1g/L GlutaMAX was supplemented with 10% FCS, 1% P/S, 1% NEAA, 1% sodium pyruvate and 200 µg/ml of hygromycin for the culture of HEK293 episomal cells containing the pCEP4 vector.

- Where both episomal vectors were maintained, both selective antibiotics were added to the media.

- DMEM with 1g/L GlutaMAX was supplemented with 10% FCS, 1% P/S 1 µg/ml puromycin and 10 µg/ml blasticidin for the culture of Platinum-E cells.

- DMEM with 4g/L GlutaMAX was supplemented with 10% FCS, 1% P/S and 2 µg/ml of puromycin for the culture of Raw 264.7 cells containing shRNA lentiviral vectors.

FCS was purchased from Biosera (Sussex, UK). PBS for use in tissue culture was purchased from Invitrogen. Trypsin 0.05% EDTA (Invitrogen) was used for passaging of HeLa, Vero, Platinum-E, MEF and HEK293 cell lines. Cell scraping was used to passage Raw 264.7 cell lines. Hank's Balance Salt Solution (HBSS) media with magnesium and calcium (Invitrogen) was used as a starvation media.

2.1.5 Additives and Transfection reagents

Torin1, an ATP-competitive inhibitor that suppresses both mTORC1 and mTORC2, was provided by Drs. Gray and Sabatini (Harvard Medical School, Boston) as a 1mM solution in DMSO. To prepare for use in tissue culture, Torin1 was diluted 1:4 in DMSO then 1:1000 in cell culture media. The final concentration of Torin1 applied to cell culture was 250 nM.
Muramyl dipeptide (MDP), a NOD2 agonist was obtained from Source Bioscience Life Sciences, (UK). Stock solutions were prepared in endotoxin free water to a concentration of 10mg/ml. To prepare for use in tissue culture, MDP was diluted 1:1000 in cell culture media to a final concentration of 10 µg/ml or 1:500 for a concentration of 20 µg/ml.

Puromycin, hygromycin B and blasticidin were purchased from Invitrogen. Puromycin and blasticidin were provided at stock concentrations of 10 mg/ml. Hygromycin B was provided at a concentration of 50 mg/ml and diluted to a stock concentration of 10 mg/ml in sterile PBS. The antibiotics were diluted and added to media as required.

Transfast (E2431) from Promega (UK), a cationic lipoplex carrier, was used as a surrogate pathogen associated molecular pattern, and prepared according to manufacturer's instructions.

Transfection of HeLa, HEK293 and Vero cells was carried out using the jetPRIME^{TM} DNA and siRNA transfection reagent (Polyplus transfection, UK), according to the manufacturers protocol. The transfection protocol was optimised for HeLa and HEK293 cells as shown in table 2.3. The 1:2 ratio of DNA to jetPRIME is maintained whilst reducing the DNA and jetPRIME content to 0.5X of the original.

Table 2.3 Optimisation of jetPRIME transfection protocol for HEK293 and HeLa cells

Transfection protocol for 24 well	Volume of jetPRIME buffer	Amount of DNA	Volume of jetPRIME reagent
Original	50 ul	0.5 µg	0.1 µl
HeLa/HEK293	50 ul	0.25 µg	0.5 µl

For dual transfections, the jetPRIME protocol was optimised as shown in table 2.4. Both transfection mixes are prepared separately, incubated for 10 min according to manufacturer's instructions, and then combined and the dual transfection mix added to cells

Table 2.4 Optimisation of jetPRIME transfection protocol for dual transfection

Transfection protocol for 100mm dish	**Volume of jetPRIME buffer (x 2)**	**Amount of DNA (x 2)**	**Volume of jetPRIME added (x 2)**	**Total combined transfection mix added to cells**
HEK293/HeLa cells	250 µl	3.75 µg	7.5 µl	500 µl
Other cell lines	375 µl	7.5 µg	15 µl	750 µl

siRNA transfections were carried out according to manufacturer's protocol at a concentration of 50nM per siRNA.

2.1.6 Fixation solutions

All coverslips were fixed with 100% ice cold methanol for 5 min (unless otherwise stated). For cells immunostained with mouse anti-HA, coverslips were fixed with 100% ice cold methanol for 10 min, followed by a 1' incubation with ice cold acetone for 1 min.

2.1.7 Cell lines

The HeLa (human cervix eptheloid carcinoma) cells (ECACC 93021013), HEK-293 (ECACC 85120602), Raw 264.7 (ECACC 91062702), Vero (ECACC 84113001) cell lines were obtained from the European Collection of Cell cultures (ECACC) (Porton Down, UK). The Platinum-E cell line for retroviral packaging was purchased from Cell Biolabs Inc. The MEF wild-type and MEF Atg5 -/- cell lines were a kind gift from Professor Noboru Mizushima of Tokyo Medical and Dental University (Mizushima et al., 2001). The p62 -/- cell line and wild type counterpart were a kind gift from Professor Terje Johansen of The Department of Medical Biology, University of Norway (Komatsu et al., 2007; Kirkin et al., 2009). The HEK293 cell line stably expressing eGFP-LC3 was a kind gift from Dr Sharon Tooze of Cancer Research UK, London Research Institute (Köchl et al., 2006). Atg16L1 KO MEFs were generated as part of the work in this thesis and are described later in the methods section, all cells were grown in the stated media at 37^{o}C and 5% CO_2.

2.1.8 DNA plasmids

The cDNA for mouse ATG16L1 γ isoform (Accession no NT_078297.6) was obtained from Geneservice (Source BioScience Life Sciences). Generation of the C-terminal tagged ATG16L1 and deletion constructs are outlined in the results section. The plasmid pEGFP-N1 was obtained from Clontech (GenBank Accession #U55762).

The MEKK4-HA plasmid was a kind gift from Dr Derek Abbott (Case Western Reserve University, Cleveland (Clark et al. 2008). The kinase dead MEKK4-HA plasmid was acquired from Addgene (plasmid 12188), deposited by Dr Gary L Johnson (University of Colorado Medical School) (Gerwins et al, 1997). The NOD1-HA and NOD2-HA plasmids were a kind gift from Professor Dana Philpott (University of Toronto, Canada) (Linderson et al., 2005). The pCEP4 plasmid was obtained from Invitrogen (Cat no. V044-50). The pCEP-Pu plasmid was a kind gift from Dr Eddie Kohfeldt (Max-Planck Institute of Biochemistry, Germany) (Kohfeldt et al., 1997). The pSpCas9-2A-GFP plasmid was acquired from Addgene (plasmid 48138), deposited by Dr Feng Zhang (MIT), (Ran et al., 2013). The GFP-LC3-G120A plasmid was a kind gift from Professor Zvulun Elazar of the Weizmann Institute of Science, Israel (Fass et al., 2006).

The RFP-Ub and GFP-Ub plasmids were obtained from Addgene (plasmid 11935 and 11928 respectively), were deposited by Professor Nico Dantuma (Bergink et al., 2006; Dantuma et al., 2006). The mCherry-LC3 plasmid was obtained from Addgene (plasmid 40827), deposited by Professor David Rubinsztein (Jahreiss et al., 2008). The Mekk4 shRNA lentiviral vector (Cat no: RMM3981-9592704, Oligo ID: TRCN0000025296) was purchased from Open Biosystems (GE Dharmacon).

2.1.9 siRNA probes

Predesigned siRNA probes were purchased from Ambion and are detailed in table 2.5

Table 2.5 List of siRNA probes

Catalogue number	Sequence target
4392420	Human MAP3K4 Silencer® Select siRNA 8673 Exon 3: nt 929
4392421	Human MAP3K4 Silencer® Select siRNA 8675 Exon 2: nt 415
AM4611	Silencer® Negative Control No. 1 siRNA Validated for human, mouse and rat cells.

2.1.10 Primary and secondary antibodies

Primary antibodies used for immunofluoresence, Western blotting and immunoprecipitation are detailed in table 2.6. Alexa Fluor® secondary antibodies for immunofluorescence were donkey anti-rabbit 488, donkey anti-mouse 488, donkey anti-mouse 568, donkey anti-rabbit 594, donkey anti-mouse 594, donkey anti-rabbit 647 and donkey anti-mouse 647 (Invitrogen). All were used at 1:500 dilution. Cell nuclei were stained with 4',6-diamidino-2-phenylindole (DAPI). All coverslips were mounted onto slides using with Gelvatol fluorescence mounting medium (made in house, described previously by Harlow et al., 2006).

IRDye® secondary antibodies for Western blotting were purchased from Li-Cor Biosciences. Donkey anti-mouse 680LT, donkey anti-rabbit 680LT, donkey anti-mouse 800CW and donkey anti-rabbit 800CW were all used at 1:10 000 dilution.

Table 2.6 Summary of antibodies used in immunofluorescence, immunoprecipitation and Western blotting

Application	Antibody name	Clone	Dilution	Source	Catalogue no.
Immunofluorescence	Rabbit anti-Atg16L	-	1:300	MBL	PM040
	Rabbit anti-LC3	-	1:1000	Sigma	L7543
	Mouse anti-LC3	166AT1234	1:200	Abgent	AM1800
	Mouse anti-WIPI2	2A2	1:1000	abcam	ab101985
	Rabbit anti p62	-	1:1500	Sigma	P0067
	Mouse anti-HA	HA-7	1:1000	Sigma	H9658
Western blotting	Mouse anti-Atg16L	1F12	1:1000	MBL	M150-3
	Rabbit anti-Atg16L	-	1:1000	MBL	PM040
	Rabbit anti-p62	-	1:1000	abcam	ab91526
	Rabbit anti-LC3	-	1:1000	Sigma	L7543
	Mouse anti-β actin	ACTN05 (C4)	1:10 000	abcam	ab3280
	Mouse anti-HA	HA-7	1:2500	Sigma	H9658
	Rabbit anti-GFP	-	1:1000	abcam	ab290
	Mouse anti-MEKK4	MEKK4-338	1:1000	Sigma	M7194
	Mouse anti-γ tubulin	GTU-88	1:10 000	Sigma	T6557
Immunoprecipitation	Mouse-anti-GFP	GFP-20	-	Sigma	G6539
	Mouse anti-HA	16B12	-	Biolegend (Covance)	MMS-101P
	Rabbit anti-Atg16L	-	-	MBL	PM040
	Mouse anti-MEKK4	MEKK4-338	-	Sigma	M7194
	Normal mouse IgG	-	-	Santa Cruz Biotechnology	Sc-2025

2.1.11 Immunofluoresence Microscopy

Fluorescence was visualised using a widefield fluorescence microscope (ApoTome Axio Imager M2, Carl Zeiss) using a Plan-APOCHROMAT 63x/1.4 Oil (Carl Zeiss) objective lens attached to a high definition camera (AxioCam HRm, Carl Zeiss). Filter sets are detailed in table 2.7

Table 2.7 Excitation and emission wavelength ranges of filter sets

Filter set (Zeiss)	Excitation (nm)	Emission (nm)
DAPI 49	365	445/50
GFP 38	470/40	525/50
DS RED 43	545/25	605/70
CY5 50	640/30	690/50

Image processing was carried out using Axiovision Software v.4.7.1 (Carl Zeiss), with deconvolution applied to Z-stack images. Images were analysed using Imaris software v.7.6.3 (Bitplane).

2.1.12 Reagents for Co-immunoprecipitation and Western Blotting

Lysis buffer for all experiments was the mammalian protein extraction reagent (mPER) lysis buffer (Pierce, UK), with added protease inhibitors (cOmplete mini EDTA-Free) and phosphatase inhibitors (PhosSTOP), both from Roche. Immunoprecipitation assays were carried out using Dynabeads® protein G (Invitrogen), according to manufacturer's protocol with the following amendments. The incubation for immunoprecipitating the target antigen was carried out overnight at 4°C. The dynabead-Ab-Ag complex was washed 5 times with wash buffer prior to elution. Elution was carried out using an in-house reducing sample buffer at 95°C for 10 min.
Where stated, crosslinking was carried out using Dithiobis[succinimidyl propionate] (DSP) (Pierce, UK).

SDS-PAGE gels were prepared following recipes specified by Roche Lab FAQs (2011). Both 30% acryl-bisacrylamide and TEMED was purchased from BioRad (Hemel Hemptead, UK). Gels were prepared at 6% or 8% to resolve immunoprecipitation experiments, unless stated otherwise, and 15% gels were prepared to resolve LC3 proteins. Precision Plus Protein™ All blue standards molecular weight ladder was purchased from BioRad. Pierce Protein Free T20 (TBS) (Thermo scientific) was used as a blocking buffer.

2.2 Methods

2.2.2 Molecular cloning

2.2.2.1 Preparation of competent cells

For preparation of competent cells DH5α were plated on antibiotic free LB-agar plates and grown at 37°C overnight for selection of single colonies. A single colony was picked with a sterile plastic tip and transferred to 2 ml LB media in 15 ml Polystyrene round bottom test tube and incubated in a shaker (200rpm) at 37°C overnight. The overnight culture was used to inoculate 100 ml of LB media (1:100 dilution) in a 1000ml beaker and left shaking at 37°C till at a wavelength of 600 nm an O.D. of approximately 0.3-0.55 was reached. The beaker was left on ice with gentle shaking from time to time to prevent precipitation of the bacteria. The cells were then transferred to pre-cooled centrifugation flasks and were centrifuged at 6000 rpm for 10 min at 4°C in a pre-cooled centrifuge. The pellet was then re-suspended carefully in 50 ml of TFB-I buffer taking care not to produce any air bubbles and was then centrifuged again same as above. The cells were then re-suspended again this time in 4 ml TFB-II buffer and 100 µl aliquots were made using the fume cupboard in 1.5 ml Eppendorf tubes which were pre-cooled on a mixture of dry ice and acetone. The cells were then stored at -80°C and checked for competency at a later date.

2.2.2.2 Molecular cloning and plasmid construction of GFP tagged domains of Atg16L1

The primers designed for all five constructs are detailed in table 2.8. All primers, unless otherwise stated, were from Invitrogen (Paisley, UK). Primers for PCR reactions were diluted to a 10pmol concentration, and the PCR performed using the Expand High Fidelity PCR system (Roche).

Sequences for Atg16L1 γ were obtained from Ensembl geneservice (www.ensembl.org), and the domains determined using online software available from www.expasy.org and data from ensemble SMART and ProSite profiles.

All PCR samples were resolved by electrophoresis in 0.6% agarose gels. Gels were prepared using a 1 x TAE buffer from the 50 x stock solution, with agarose powder. Appropriate volumes of DNA loading buffer was added to samples. A 1 kb + ladder was used for comparison (Invitrogen). Gel extraction was performed using GeneClean DNA II purification kit (Anachem).

A Klenow reaction was carried out on the extracted PCR products using a DNA polymerase Klenow fragment (Amersham Pharmacia Biotech) according to manufacturer's instructions. This was incubated at 37°C for 30 min, followed by a phenol-chloroform extraction extract the DNA.

DNA was isolated by sequential extractions by adding an equal volume of phenol-chloroform and then chloroform. The aqueous phase was separated by centrifugation and precipitated by adding 1/10th volume of NaAc 3M [pH 5.6] and 2.5 volumes of EtOH. This was incubated at – 20°C for 2 hrs to precipitate the DNA which was recovered by centrifugation (13k rpm, 30 min, 4°C). The pellet was washed three times with 70% EtOH, repelleted and dissolved in ddH_2O.

Ligations were carried out using a Ready to Go T4 DNA ligase kit (Amersham). The volumes of insert and vector were calculated to a 1:1 ratio. Where stated, a phosphatase alkaline reaction was performed on target vector DNA to remove the 5' phosphoryl termini, prevent self-ligation and decrease vector background. DNA fragments requiring sequence verification were ligated into the sequencing vector pUC18/19.

Ligation reactions were transformed into Subcloning Efficiency™ DH5α™ Chemically Competent *E.coli* cells using a 1:50 or a 1:20 ratio of DNA to cells, and plated on to LB + selective antibiotic agar plates. Successfully transformed colonies were selected for on the basis of antibiotic resistance, and grown in 2 ml of LB + selective antibiotic suspension. Plasmid DNA was extracted from the bacteria using a Mini-lyse DNA preparation protocol involving alkaline lysis and SDS extraction with TENS buffer. The plasmid DNA was then precipitated by adjusting the supernatant to 70% EtOH and cooling to – 20°C, washed once in 70% ethanol and dissolved in TE-RNAse (99:1 ratio).
Test restriction digests were performed on extracted plasmid DNA to verify the insert was of the expected size. Plasmid DNA for sequencing was extracted from 20ml of bacterial LB suspension using a QIAGEN® Plasmid Mini kit (QIAgen) with the following alterations; in wash step 10 the QIAGEN-tip 20 was washed with 4 x 2ml Buffer QC; in step 14 the DNA pellet was redissolved in 50 µl of TE buffer. Plasmid DNA was sequenced by The Genome Analysis Centre (TGAC) at the John Innes Centre, using a 3730XL sequencer (Life Technologies). Sequences were verified and aligned using the online tool MultAlin (Corpet et al., 1988).

Once verified, DNA for transfection was generated using a QIAGEN® Plasmid MIDI kit (QIAgen) with the following modifications; the volume of LB+antibiotic suspension was increased to 50 ml. After step 7 the supernatant was filtered through a damp tissue to

remove any suspended material. For step 11 the QIAGEN tip was washed with 4 x 10 ml Buffer QC. After addition of isopropanol in step 13 the mixture was incubated for 2 hr at 4°C.

For the generation of the Atg16L1 point mutants, the QuikChange Lightning Site-Directed Mutagenesis Kit was used, and manufacturer's instructions followed. The mutagenic primers were designed using the web-based QuikChange Primer Design Program www.agilent.com/genomics/qcpd and are detailed in table 2.8. Sequencing primers are shown in table 2.9.

Table 2.8. List of primers used in the generation of ATG16L1 domain plasmids

Primer Name	Primer Sequence 5′ → 3′	File no
3′ ATG16L1 For	TGTTTGCAGGATCCAGCTGC	171
3′ ATG16L1 Rev	GATCGGATCCAAGCTTACTAGTGTAGGCTGTGCCCACAGCAC	172
CCD For	GATCGTCGACATGTCGTCGGGCCTGCGC	173
CCD Rev	GATCGGATCCAAGCTTACTAGTGTTTCCTTTGCTGCTTCTGCAA	174
CCD+Linker Rev	GATCGGATCCAAGCTTACTAGTGTGACTCTCACATCTTTACCAG	175
Linker+WD40 For	GATCGTCGACACCATGCCTCTACCTGTTGAACAG	176
WD40 Rev	GCAGCTGGATCCTGCAAACA	177
WD40 For	GATCGTCGACACCATGCCAACTACTGCCTCGTAT	178
For_ATG16L1-S305A	GGAGACGCTCTGTCGCTTCCATCCCAGTC	294
Rev_ATG16L1-S305A	GACTGGGATGGAAGCGACAGAGCGTCTCC	295
For_ATG16L1-T300A	CCAGGATATCATGGACGCTCATCCTGCTTCTGG	296
Rev_ATG16L1-T300A	CCAGAAGCAGGATGAGCGTCCATGATATCCTGG	297

Table 2.9 List of in-house sequencing primers

Primer name	Primer sequence 5′-3′	File No.
pmCherryN1_438_Forseq	CCATTGACGTCAATGGGAG	280
pEGFPN1_807_Revseq	GGTGCAGATGAACTTCAGGGTC	284
WD40 Rev	GCAGCTGGATCCTGCAAACA	177
U6-Fwd	GAGGGCCTATTTCCCATGATTCC	348
Atg16L1 int.seq	CTGAACAGTTAAGTTCCTAG	223
Atg16L1 Kpn.int1.rev	CCAAGAGACACTGACATAGG	226

2.2.2.3 Molecular cloning kits for episomal plasmid cloning

Further molecular cloning was carried out to generate the episomal constructs used in this thesis. The following modifications were made to the cloning protocols:
Any PCR reactions were carried out using the Velocity DNA polymerase system (Bioline). The Klenow reaction was carried out using the Fast DNA End Repair Kit (Thermo Scientific). The phenol/chloroform reaction was replaced with the GeneJET purification Kit (Thermo Scientific). Both kits were used according to manufacturer's instructions. DNA for sequencing and transfection was generated by Macherey-Nagel Nucleospin and NucleoBond kits, respectively, and were used according to manufacturer's protocol. Plasmid DNA was sequenced using the Source BioScience Sanger Sequencing Overnight service, using a 3730XL DNA Analyser (Applied Biosystems).

2.2.2.4. CRISPR/Cas9 Cloning

The CRISPR Cas9 cloning was carried out according to the protocol specified by Ran et al., 2013. The sgRNA template was designed using online tools from www.e-crisp.org and later verified by the online software available at (http://tools.genome-engineering.org). sgRNA oligos were purchased from Invitrogen, and are detailed in table 2.10. The FastDigest BbsI restriction enzyme was purchased from Thermo Scientific. The T7 ligase was purchased from NewEngland Biolabs. Sequencing was carried out using the U6-Fwd primer detailed in table 2.9.

Table 2.10 sgRNA template oligos used to construct MEKK4 targeted CRISPR/Cas9 vectors

sgRNA ID	Sequence 5' – 3'
Hm MEKK4 gRNA FOR	CACCGAGAGAAGCCGCTGCCGCGC
Hm MEKK4 gRNA REV	AAACGCGCGGCAGCGGCTTCTCTC
Ms MEKK4 gRNA FOR	CACCGTGTCGGCGAGGGCAGGAGG
Ms MEKK4 gRNA REV	AAACCCTCCTGCCCTCGCCGACAC

2.2.2.5 Mapping Atg16L1 binding motifs

Atg16L1 binding motifs were mapped using the ProSite algorithm, available at the ScanProsite website (http://prosite.expasy.org/scanprosite/). (DeCastro et al., 2006)

2.2.3 Cell culture, Immunoprecipitation and Western blotting

2.2.3.1 Transfection and cell culture

For immunofluoresence studies cells were cultured on 13mm coverslips in 24 well plates. The coverslips were coated with 20 µg/ml collagen I prior to the seeding of cells. Cells were grown at 37°C 5% CO_2. Cells were seeded at 1.5 x 10^4 per well in 500 µl supplemented media and allowed to grow for 24 hr prior to transfection. Cells were washed once in PBS and mixed with DNA transfection mix was used as shown in tables 2.3 and 2.4. After the transfection mix had incubated for 10 minutes at room temperature, 50 µl was added to media and then incubated with cells for 4 hrs. The media was then replaced with fresh pre-warmed supplemented media, and the cells cultured for 48 hrs post plasmid transfection and 36 hrs post siRNA transfection prior to treatment and fixation.

For western blotting cells were cultured in a 6 well plates, and for immunoprecipitation assays cells were cultured in a 10 cm plate (NUNC), pre-treated for tissue culture use. For immunoprecipitation assays 2-3 dishes per condition were used. The cells were grown at 37°C, 5% CO_2 in DMEM supplemented media 24 hours prior to transfection (48 hours for episomal cells). For 6 well plates, cells were seeded at 1-2 x 10^5 in 3 ml of media. Cells were seeded at 0.75-1.25 x 10^6 per dish in 10 ml of media (dependent on cell type) for immunoprecipitation assays. The transfection was performed as previously stated (tables 2.3 and 2.4), and the cells cultures for 48 hours prior to treatment and/or lysis.

2.2.3.2 siRNA depletion

For siRNA depletion studies, cells were cultured on 13mm coverslips in 24 well plates for immunofluorescence studies, and in 6 well plates for Western blot assays. Cells were seeded at 1 x 10^4 per well and allowed to grow 24h prior to the first round of siRNA depletion. Cells were transfected with a combination of 50nM siRNA from both probes (transfection mix shown in table 2.11). The transfection mixes were combined and added to each well as described in table 2.11, then incubated for 4 hours. The cells were allowed 24 hours recovery then the siRNA transfection repeated. After another 24 hours recovery, the assays were carried out.

Table 2.11 Transfection mix for siRNA depletion

	Volume per 24 well 50nM	Volume per 6 well 50nM
jetPRIME buffer	50 µl	200 µl
siRNA (50 µM stock)	0.55 µl	2.2 µl
jetPRIME reagent	2 µl	4 µl
Total volume added for dual siRNA	75 µl	300 µl

2.2.3.3 Induction of Autophagy

To induce autophagy, cells were incubated with HBSS for 2-4 hrs or with 250nM Torin1 in supplemented media for 2 hrs. To induce NOD2 directed autophagy, cells were incubated with 10-20 µg MDP for 4-8 hrs as stated.

2.2.3.4 Immunofluoresence

Cells were washed with 1 x PBS and fixed with 100% ice cold methanol for 5 min unless otherwise stated. 1 x PBS was prepared from a 10 x stock solution, diluted with ultrapure H_2O and autoclaved. Cells were subsequently washed three times with 1 x PBS before blocking for 20 min in 5% Normal Donkey Serum (NDS) in 1 x PBS, unless otherwise stated. Primary and secondary antibodies were diluted in 2 % NDS and incubated with cells for 1hr. Primary antibody was removed by three washes with PBS + 0.1% Tween 20 (Sigma). After addition of secondary antibody coverslips were incubated for 40 min, then washed three times with 1 x PBST and stained with DAPI for 10 min. After a final wash with PBS, the coverslips were mounted onto glass slides using Gelvatol and left in the dark to dry. Immunofluorescence was visualised using a widefield fluorescence microscope (ApoTome Axio Imager M2, Carl Zeiss) using a Plan-APOCHROMAT 63x/1.4 Oil (Carl Zeiss) objective lens attached to a high definition camera (AxioCam HRm, Carl Zeiss).

2.2.3.5 Imaris Analysis and Statistical Analysis

Images were analysed using Imaris software v.7.6.3 (Bitplane) to count puncta formation and colocalisation by user-defined spot definition parameters. Statistical analysis was performed using an unpaired two-tailed Student's T-test assuming unequal variance, using GraphPad Prism 6 software (GraphPad), where stated. A diameter of 0.75 µm was assumed as the standard for autophagosome size (Mizushima., 2004), was used for analytical purposes. A diameter of 1.5 µm and above was assumed as an aggregate (Wileman., 2007).

All graphs were generated using GraphPad Prism 6. All statistical analysis was carried out within this programme. A Levene's test was used to measure if the variance between the Atg16L1 domain puncta was equal. If a significant p value was returned, then there was a difference in the variances of the population.

2.2.3.6 Cell Lysis and Protein concentration quantification

For immunoprecipitation assays cells were washed with ice cold PBS 3 times, then lysed with 500 µl of supplemented MPER lysis buffer (Fisher) on ice. The lysis was done sequentially, so 2-3 dishes were combined with one lysate. The cells were scraped and transferred to a 1.5 ml Eppendorf then incubated on ice for 30 min with regular pipetting. For cells in 6 well plates, lysis was carried out with 30-80 µl of lysis buffer, depending on the confluency of cells. The lysate was clarified by centrifugation at 14 000 rpm at 4^{o}C for 10 min. The supernatant was either used fresh or kept at -20^{o}C before use in immunoprecipitation or Western blotting.

Protein concentrations were quantified by bicinchoninic acid (BCA) assay, which was purchased from Thermo Scientific and used according to manufacturer's instructions. Samples were read on a colorimetric plate reader (Wallac Envision, Perkin Elmer) at 560nm.

2.2.3.7 Co-immunoprecipitation assay

Co-immunoprecipitations were carried out using Dynabeads® protein G (Invitrogen). In some experiments, protein interactions had been stabilised with a DSP crosslinker prior to cell lysis. The DSP crosslinking (where stated) was carried out according to manufacturer's instructions with the following alterations. The crosslinker solution was used at a concentration of 1 mM and the reaction mixture was incubated at room temperature for 1 hour. Equal concentrations of lysate were made up to 1ml with MPER in a 1.5 ml Eppendorf. 25 µl of dynabeads were prepared with 3 µg of normal mouse IgG in 200 µl of PBST (0.02% Tween 20), according to manufacturers protocol. The lysate was precleared at room temperature for 10 min with rotation. To separate the lysate from the antibody-bead complex, the tube was placed on a magnet and the supernatant aspirated and reserved for the next step. The precipitating antibody was prepared as follows. 6-10 µg of precipitating antibody (dependent on binding affinity) was added to 200 µl of PBST. This was added to 50 µl of Dynabeads and incubated at room temperature for 10 – 30 min with rotation. The supernatant was removed using the magnet to separate the beads, and the pre-cleared lysate added directly to the bead-precipitating antibody complex. This was incubated at 4^{o}C, overnight with rotation. Beads were washed 5 times in PBS with added protease and phosphatase inhibitors, and proteins eluted in sample buffer. A reducing agent, β-

mercaptoethanol (β-ME) was added to samples to break down di-sulphide bonds in the precipitating antibody. Whole cell lysates and non-bound fractions were prepared for SDS-PAGE by adding 2% of original immunoprecipitation lysate volume to sample buffer, β-ME and made up to 15 µl with ddH_2O. Samples for use in SDS-PAGE were denatured by incubation at 95°C for 10 min. Eluted proteins from beads were removed by placing tubes on a magnet and aspirating the eluate into a fresh Eppendorf.

2.2.3.8 SDS-PAGE and Western Blotting

After quantification, equal concentrations of protein (20-40 µg) were prepared with sample buffer, β-ME and made up to 15 µl with ddH_2O. The contents were mixed and denatured by incubation at 95°C for 10 min. Samples were run on SDS-PAGE gels at 150V for 60-90 in dependent on the gel percentage. The protein was transferred by semi-dry transfer to PVDF membrane (Immobilon®-FL, Millipore Limited). Protein transfer was confirmed using Ponceau-S staining. All incubation steps are carried out with rocking. The membrane was blocked for 1 hour at room temperature using the Pierce protein free blocking buffer (Thermo Scientific). Primary and secondary antibodies were diluted in a 1:1 ratio of blocking buffer and TBST (0.1% Tween 20), with indicated dilutions of antibody. Primary antibodies were incubated overnight at 4°C then washed three times with TBST. Secondary antibodies were incubated at room temperature for 1 hour, then washed three times with TBST and once with TBS. Proteins detected by the labelled secondary antibodies were visualised using the Odyssey Infrared Imaging System, (LI-COR Biosciences)

2.2.3.9 Generation of MEFs from embryos.

The timed matings to obtain the embryos were set up by Devina Devikar and Ulrike Mayer. The uterus of 13.5 post-coitum females was removed, washed with 70% ethanol and transferred to a tissue culture fume hood. The embryos were removed and placed in PBS. The head and internal organs were removed, and the carcass placed into 1-2ml of trypsin/EDTA.

The carcass was macerated using a sterile pair of dissection scissors, and incubated for 10 min at 37°C. The tissue was broken down manually by pipetting with a 10 ml pipette, and the embryo was incubated for a further 10 min at 37°C. After neutralising the trypsin/EDTA with the addition of high glucose supplemented media, the tissue mass was broken up by pipetting with a 5ml pipette. This was allowed to settle for 1 min, and the cells plated at the equivalent density of 2 embryos/10cm dish.

2.2.3.10 FACS sorting

A BD FACS Aria II (Becton Dickinson) flow cytometer was used to perform single-cell sorting following the manufacturer's aseptic sort protocol. FDG staining was carried out using a FluoReporter lacZ Flow Cytometry kit (Molecular Probes, Invitrogen), according to manufacturers protocol. Briefly, cells were trypsinised, the trypsin inactivated with FACS buffer (5% FCS in PBS) and pelleted at 1000 rpm for 5 min. The pellet was washed again with FACS buffer, repelleted and resuspended in 20 µl PBS and place on ice. A 2 mM working solution of FDG was prepared using ultrapure autoclaved H_2O for tissue culture use. 20 µl of the working FDG solution was added to the resuspended cells and incubated for 45 sec at 37^{o}C, then 500 µl of ice cold FACS buffer was added and the reaction incubated on ice for up to an hour. The cells were pelleted and washed as previously, then resuspended in an appropriate volume of FACS buffer prior to sorting. FDG staining and eGFP was detected using 488 nm laser excitation and 530/30 band pass-filter detection. Individual cells were sorted using the following gating criteria: debris discrimination using forward and orthogonal 488 nm laser scatter (cells selected), doublet discrimination using orthogonal pulse height and width (individual cells selected), and the above listed marker.

2.2.3.11 Generation of lentiviral particles from Plat-E cell line

The Plat-E cell line has been described previously (Morita et al., 2000). Cells were seeded in a T75 tissue culture flask at a density of 5-7 x 10^5 without selective antibiotics. After 24 hours, the lentiviral plasmid was transfected into the cells following the jetPRIME protocol. Retroviral supernatant was harvested 48 hrs and 96 hrs post transfection. The viral particles were concentrated by centrifugation at 8000 rpm overnight at 4^{o}C. The pellet was resuspended in Opti-MEM (Invitrogen) at 37^{o}C for 15 min, then centrifuged at 1000 rpm for 5 min to pellet cell debris. The supernatant containing the concentrated viral particles was aliquoted into 50 µl cryotubes, and stored at -80^{o}C.

2.2.3.12 Yeast two hybrid screen

The yeast two hybrid screen was carried out by Hybrigenics Global PBS®. The bait protein, Mus musculus ATG16L1γ was screened against a human colon cDNA library, to identify interactions likely to occur in the gut. The gamma isoform was chosen as it was the longest of the mouse Atg16L1 isoforms. The interactions were analysed by Hybrigenics Global, with each interaction assigned a ranking, representing confidence in the interaction. This ranking is based on Hybrigenics Global algorithms, which take into account the likelihood of the interaction being a false positive, proven experimental artefact, or a prey protein

likely to missfold. Upon receiving the results, a literature search was performed to ascertain how the high confidence hits may relate to autophagy. As well as MEKK4, one hit returned by the yeast two hybrid screen was FIP200, an interaction which has been described (Gammoh et al., 2013).

Chapter 3:

Characterisation of the Atg16L1 domains

Chapter 3: The characterisation of the domains of Atg16L1

3.1 Chapter Aims

The aims of this chapter were to characterise the function of the domains of Atg16L1 in autophagy, by use of GFP-tagged deletion constructs. The cellular distribution, ability to form autophagosomes and localise with autophagic markers are characterised, so that these constructs can be used in future experiments. Atg16L1 KO MEFs are generated for use in reconstitution experiments. This allows the characterisation of the Atg16L1 deletion constructs on a WT and null Atg16L1 background.

3.2 Introduction

In mammalian autophagy, the ubiquitin-like conjugation systems that utilize LC3/Atg8 and the ATG16L1 complex, are evolutionarily conserved across eukaryotes. The mammalian Atg16L1 was originally identified in *Mus musculus* (mouse) in 2003 by Mizushima et al, based on its weak but significant homology to *Saccharomyces cerevisiae* (yeast) Apg16 (Fig. 3.1). Three isoforms have been reported and experimentally verified; Atg16L1α, Atg16L1β and Atg16L1γ. Two further isoforms have been proposed, however experimental evidence to support a functional role in autophagy is lacking.

The protein ATG16L1 shares many similarities with its yeast counterpart Apg16. Both comprise of an N-terminal ATG5-binding domain, followed by a coiled-coil domain (CCD). In higher complex eukaryotes there is an additional linker region and a WD40 repeat domain at the C-terminus. The Crohn's disease associated T300A polymorphism falls towards the end of this linker region, before the start of the WD40 repeat (Figure 3.1). Alignment of the amino acid sequence from Saccharomyces cerevisiae (yeast) and from Mus musculus (mouse) shows homology in the CCD. The function of the linker and WD40 repeat domain in autophagy is poorly characterised. Whilst the yeast Apg16 lacks these domains, emerging research suggests that the linker and WD40 repeat domain govern interactions that are involved in selective forms of autophagy and the regulation of the innate immune response (Boada-Romero et al., 2013; Fujita et al., 2013). Additionally, phosphorylation sites have been identified within the linker region of Atg16L1, though their purpose has yet to be elucidated (Villén et al., 2007; Olsen et al., 2010).

Therefore, the domains of Atg16L1 require further characterisation in the context of canonical and selective autophagy. This will be explored in the following chapter.

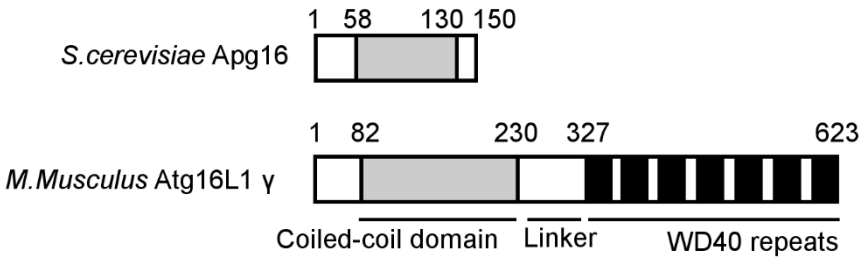

Figure 3.1 Schematic representation of the yeast Apg16 and Atg16L1 γ proteins. The coiled-coil domain in yeast Apg16 is conserved in mouse Atg16L1, with the addition of a linker and WD40 repeat domain. The CD associated mutation T300A, which has been mapped to the T316 residue in mouse Atg16L1 lies within the linker region. Modified from Mizushima et al., 2003.

.

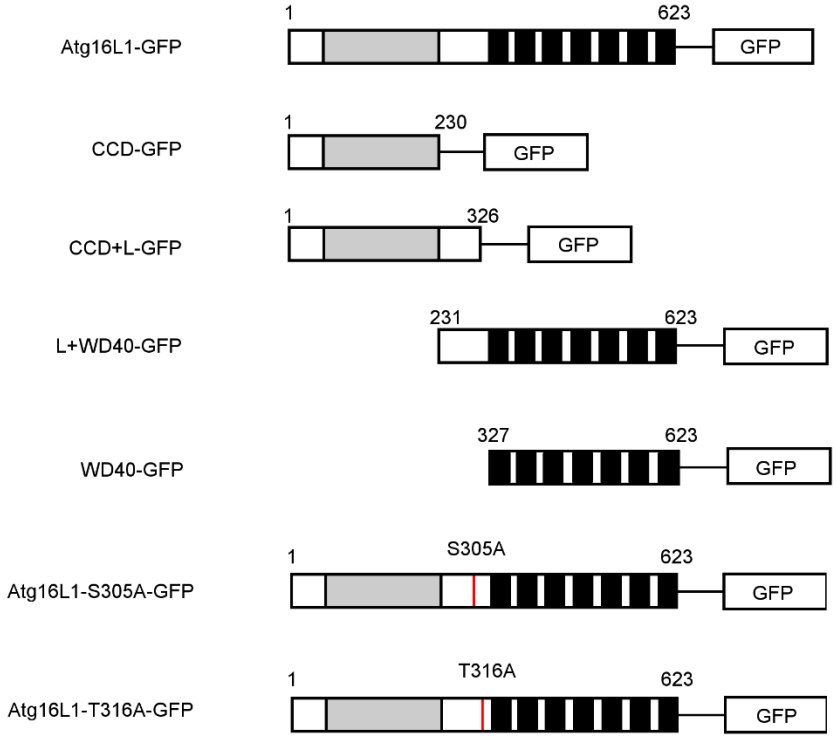

Figure 3.2 Summary of GFP-tagged Atg16L1 constructs

This diagram summarises the regions of Atg16L1 γ that were tagged with eGFP in the generation of the deletion constructs. The coiled-coil domain is depicted in grey and the WD40 repeat domain represented by repeated black boxes. The numbering refers to the amino acid sequence in murine Atg16L1 γ. The point mutations are indicated with a red line. The spacer region between the C-terminus of the Atg16L1 constructs and the N-terminus of eGFP is represented by a black line.

3.3 Results

3.3.1 Generation of GFP tagged Atg16L1 constructs

The Atg16L1 protein remains poorly characterised. To gain insight into the function of the domains of Atg16L1, deletion constructs of Atg16L1 were generated that are tagged at the C-terminus with eGFP. Three isoforms of Atg16L1 have been described, which arise from variation in exon splicing, and are referred to as Atg16L1 α, Atg16L1 β and Atg16L1 γ (Mizushima et al., 2003). The gamma isoform contains exons 1-19, the beta isoform does not contain exon 9, and the alpha isoform lacks exons 8 and 9 (Appendix 1).
The CD associated mutation lies within exon 10. The Atg16L1 γ isoform was chosen as a template for the generation of the deletion constructs, as this is the longest isoform, containing 623 amino acids.

The domains and features of Atg16L1 γ were mapped using SMART site profiling and data from Ensembl genome browser (table 3.1) to determine the regions that contain the coiled-coil domain, the linker region and the WD40 repeats.

Seven different constructs were generated using mouse Atg16L1 γ as a template. These are summarised in Figure 3.2 and are outlined below. The numbering of nucleotides/amino acids refers to the Atg16L1 γ isoform.

Table 3.1. The domains and features of mouse Atg16L1 γ determined from Ensembl data

Domain/Features	Amino acid residues	Nucleotides in cDNA	Spans exons
Coiled-coil region 1	82-102	244-306	3
Coiled-coil region 2	110-193	327-579	4 and 5
Coiled-coil region 3	195-230	587-690	5 and 6
Linker region	231-326	691-978	6, 7, 8, 9 and 10
WD40 repeat 1	327-366	978-1098	10 and 11
WD40 repeat 2	371-410	1111-1230	12 and 13
WD40 repeat 3	413-452	1237-1356	13 and 14
WD40 repeat 4	455-491	1363-1473	14 and 15
WD40 repeat 5	494-532	1480-1596	16
WD40 repeat 6	535-578	1603-1734	16, 17 and 18
WD40 repeat 7	581-621	1741-1863	18 and 19

3.3.1.1 Generation of Atg16L1-GFP

The 5'-end of Atg16L1 was generated from pYX-Asc-Atg16L1 by restriction digestion with SalI and BamHI. This fragment was ligated into the multiple cloning site (MCS) of the mammalian expression vector pEGFP-N1, which was digested with SalI and BamHI to create compatible ends. Primers were designed to amplify the 3'-end of Atg16L1, using pYX-Asc as a template (primers 171 and 172, see table 2.8 for primer details). The 3'-Atg16L1 forward primer simply targeted a region of Atg16L1 that contains a BamHI site in its nucleotide sequence. As the GFP tag is at the C-terminus, the stop codon of Atg16L1 had to be removed, and the reading frame with GFP maintained. To achieve this, the 3' Atg16L1 reverse primer was designed to remove the stop codon and insert two bases to maintain the reading frame. Three restriction sites, BamHI, HindIII and SpeI were also introduced by this primer.

The resulting PCR fragment was verified by sequencing, digested with BamHI and ligated into the 5'Atg16L1-pEGFPN1 plasmid to obtain the full length C-terminal tagged fusion protein; Atg16L1-GFP.

3.3.1.2 Generation of the Coiled-coil domain and Coiled-coil domain & Linker GFP constructs

Based on the SMART domain analysis, it was decided that the coiled-coil domain consisted of amino acids 1-230 of Atg16L1 γ, and that the coiled-coil domain and linker region consisted of amino acids 1-326 of Atg16L1 γ (Fig. 3.2 and table 3.1).

Primers 173 and 174 (table 2.8) were designed to amplify the coiled-coil domain, primers 173 and 175 (table 2.8) were designed to amplify the coiled-coil domain and linker region, both using pYX-Asc-Atg16L1 as a template. The CCD forward primer introduced a SalI site at the 5' end of Atg16L1. To maintain the reading frame with GFP, the reverse primers introduced two additional bases. As with the generation of Atg16L1-GFP, the reverse primers also introduced three restriction sites; BamHI, HindIII and SpeI. The resulting PCR products were verified by sequencing, digested with SalI and BamHI and ligated into the pEGFP-N1 plasmid to obtain the coiled-coil domain and coiled-coil domain and linker regions of Atg16L1 tagged at the C-terminus with GFP; CCD-GFP and CCD+Linker-GFP.

3.3.1.3 Linker and WD40 repeat domain and WD40 repeat domain

Based on the SMART domain analysis, the linker-WD40 domain of Atg16L1 γ was determined to consist of amino acids 326-623, and the WD40 domain consisting of amino acids 327-623 (Fig. 3.2 and table 3.1).

The 5'-region of the linker-WD40-GFP and WD40-GFP constructs was generated from pYX-Asc Atg16L1 using primers 176 and 177, and 177 and 178, respectively (table 2.8). The forward primer introduced a Kozak ATG site to enable initiation of transcription. The PCR products were verified by sequencing and ligated into pEGFP-N1 using SalI and BamHI sites. The remaining 3'-fragment was digested with BamHI and ligated into the 5'-linker-WD40-pEGFP-N1 and 5'-WD40-pEGFP-N1 plasmid to obtain the linker and WD40 repeat domain and WD40 repeat domain of Atg16L1 tagged at the C-terminus with eGFP; L+WD40-GFP and WD40-GFP.

3.3.1.4 Site directed mutagenesis: Atg16L1 point mutants – T316A and S305A

The CD associated T300A mutation was mapped to residue T316 of Atg16L1 γ. A serine phosphorylation site of unknown function was mapped to residue S305 of Atg16L1 γ. Using the completed Atg16L1-GFP construct as a template, primers were designed to introduce point mutations. For T316A primer pair 296 and 297 were used, for S305A primer pair 294 and 295 were used (table 2.8). Site directed mutagenesis was carried out using the QuikChange Lightning SDM kit (Agilent), and the mutations verified by sequencing. This resulted in the generation of the point mutants Atg16L1-T316A-GFP and Atg16L1-S305A-GFP.

All cloning strategies ensured an identical sequence between the 3' end of Atg16L1 and the 5' of eGFP (Thr-Leu-Val-Ser-Leu-Asp-Pro-Pro-Val-Ala-Thr). This should allow a degree of flexibility and space in-between the fusion protein, as the coiled-coil and WD40 β-propeller structures could prevent correct protein folding.

3.3.2 Characterising endogenous expression of ATG16L1 and Atg16L1-GFP

Before the full length and deletion constructs of Atg16L1 could be used, their stability, expression and ability to form autophagosomes had to be determined and compared to the function of endogenous Atg16L1. Therefore HeLa cells were cultured in supplemented media or media containing the mTOR inhibitor Torin1 to induce autophagy (Thoreen et al., 2009). Torin1 was used as a specific inducer of autophagy, to allow for fine control over early autophagosome formation and therefore puncta incorporating Atg16L1. The cells were fixed, stained for ATG16L1 and for the autophagosome markers LC3 and WIPI and visualised using widefield fluorescence microscopy. It should be noted that the antibody used to stain endogenous ATG16L1 was raised in rabbit, so LC3 was counterstained with an antibody raised in mouse. LC3 is a key marker of autophagosomes and is widely used to monitor autophagy (Klionsky et al., 2012; Mizushima, 2007). WIPI is recruited to the early autophagosome, and recruits Atg16L1 to the autophagosomal membrane, so will likely mark autophagosomes positive for Atg16L1 (Polson et al., 2010; Dooley et al., 2014).

To compare with endogenous ATG16L1, the full length Atg16L1-GFP was transiently transfected in HeLa cells. With respect to the experiments performed in this chapter, all transfections are transient. The cells were treated as above, with the following exception. LC3 was immunostained with an antibody raised in rabbit.

When there was a ready supply of nutrients both endogenous ATG16L1 and Atg16L1-GFP were evenly distributed in the cytoplasm, and not present in the nucleus (Fig. 3.3). When autophagy was induced with Torin1, the ATG16L1 and Atg16L1-GFP signals redistributed to punctate structures with LC3 and WIPI, indicating the formation of autophagosomes (Fig. 3.4 and 3.5). This indicates that Atg16L1-GFP is able to form autophagosomes, and that this function has not been compromised by the addition of GFP at its C-terminal end.

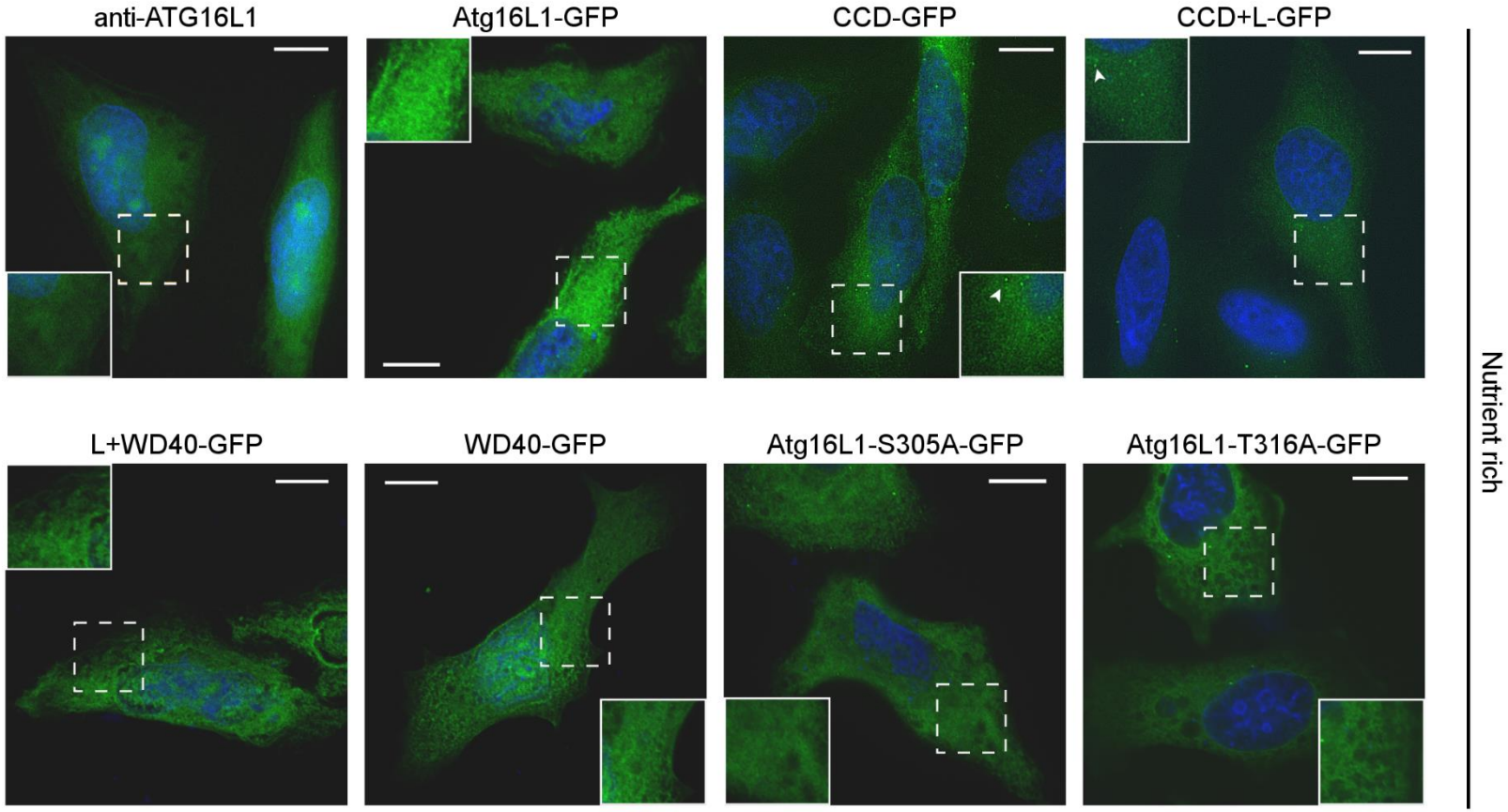

Figure 3.3 Characterisation of ATG16L1 and the GFP tagged constructs in the absence of autophagy activation

GFP-tagged Atg16L1 constructs were expressed in HeLa cells and compared to un-transfected cells. Atg16 was either visualised by anti-Atg16L immunostaining or GFP-tagged Atg16L1 construct expression. The nuclei were stained with DAPI. Regions of interest which show GFP positive puncta or filamentous structures are highlighted with dashed boxes and GFP puncta with indicated arrowheads.

Scale bars are 10 μm.

3.3.3 Characterisation of the deletion constructs of Atg16L1

The CCD of Atg16L1 is required for autophagy (Saitoh et al, 2008), however the function of the linker and WD40 repeat domain remains less characterised. To test and characterise the deletion constructs of Atg16L1, HeLa cells were transfected with CCD-GFP, CCD+L-GFP, L+WD40-GFP or WD40-GFP and counterstained for autophagy markers.

In the absence of autophagy, CCD-GFP and CCD+L-GFP were expressed diffusedly in cytosol and were absent from the nucleus, similar to endogenous ATG16L1. However in some cells, both constructs were able to form a few GFP positive puncta indicating early autophagosomes (Fig. 3.3). Following autophagy induction by Torin1, CCD-GFP and CCD+L-GFP formed punctate structures which partially co-localised with LC3 and WIPI (Fig. 3.4 and 3.5). These results indicate that CCD-GFP and CCD+L-GFP are capable of interacting with these autophagy proteins and have the ability to drive the formation of autophagosomes.

In the absence of autophagy and following induction through Torin1, both L+WD40-GFP and WD40-GFP differ from the full length and other deletion constructs. These constructs localise evenly throughout the cytoplasm and nucleus (Fig. 3.4, 3.5 and 3.6). Furthermore, they fail to form puncta in response to the activation of autophagy and do not localise with autophagosomes, indicated by the lack of co-localisation with LC3 and WIPI. In some cells, L+WD40-GFP and WD40-GFP had a filamentous distribution, with a fraction localising to the plasma membrane (Fig. 3.3 and 3.5). These results show that the L+WD40 domains of Atg16L1 are not incorporated into puncta and therefore do not play a role in canonical autophagy. In later experiments these constructs are used as a control for their inability to form puncta.

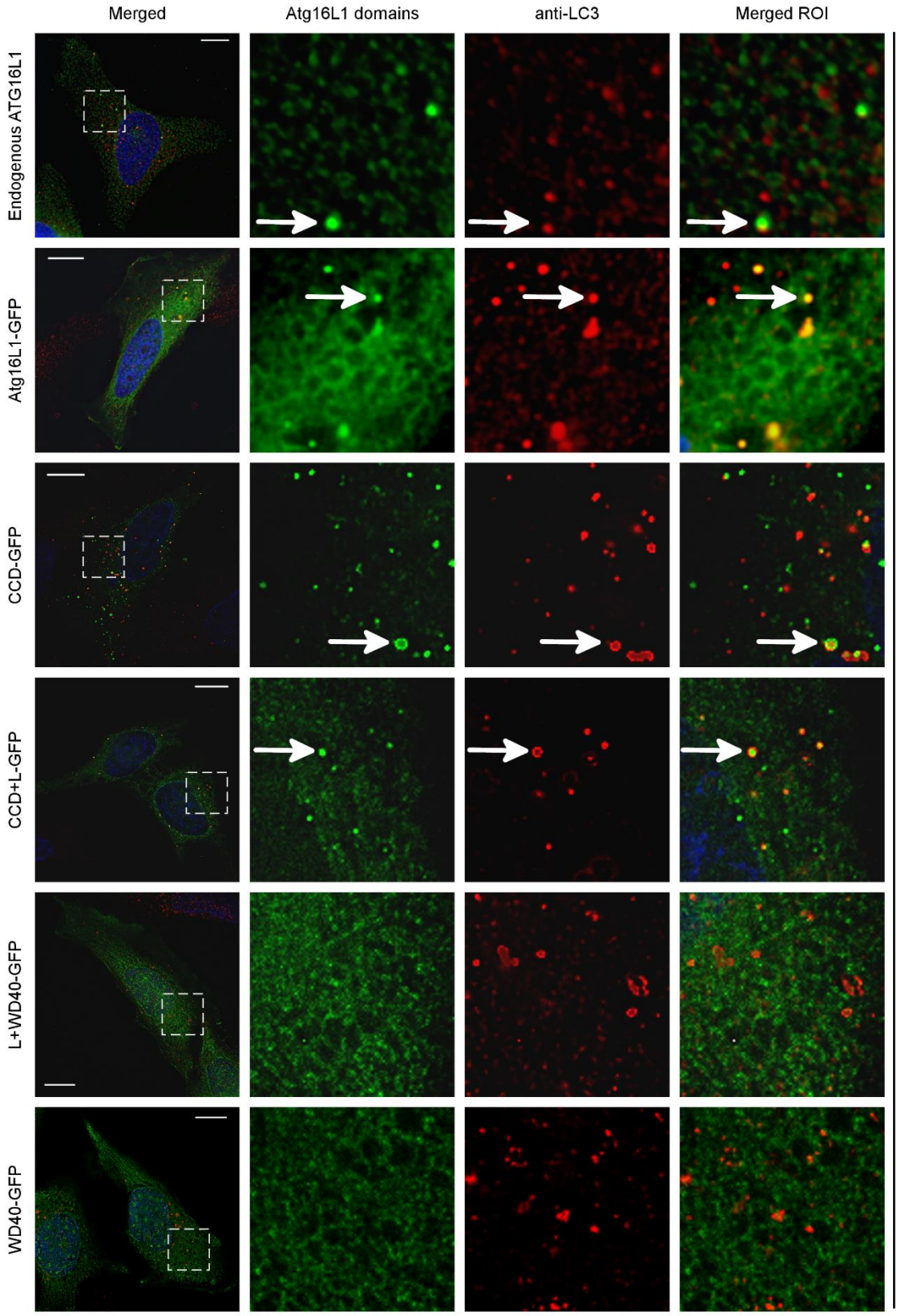

Figure 3.4 The endogenous ATG16L1, Atg16L1-GFP, CCD-GFP and CCD+L-GFP form puncta that partially colocalise with LC3 after Torin1 treatment

GFP-tagged Atg16L1 constructs were expressed in HeLa cells, and compared to endogenous Atg16 and LC3 distribution. After autophagy induction by Torin1 ATG16L1 was either visualised by immunostaining or GFP expression immunostained for ATG16L1. LC3 was immunostained and nuclei were stained with DAPI. Regions of interest are highlighted in boxes and colocalised puncta with arrows. Scale bars,10 μm.

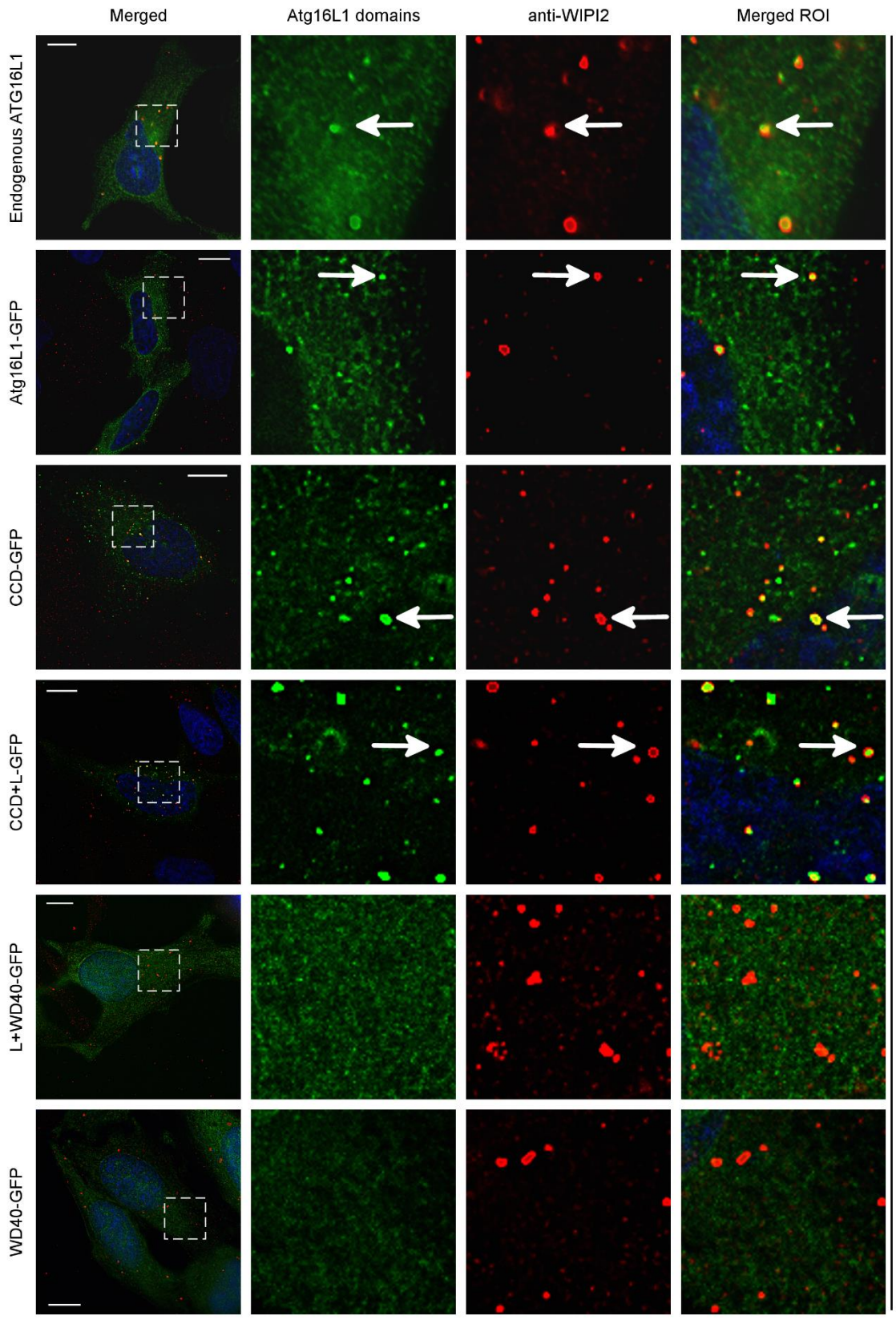

Figure 3.5 The endogenous ATG16L1, Atg16L1-GFP, CCD-GFP and CCD+L-GFP form puncta that partially colocalise with WIPI after Torin1 treatment

GFP-tagged Atg16L1 constructs were expressed in HeLa cells, and compared to endogenous Atg16 and LC3 distribution. After autophagy induction by Torin1 ATG16L1 was either visualised by immunostaining or GFP expression immunostained for ATG16L1. WIPI was immunostained and nuclei were stained with DAPI. Regions of interest are highlighted in boxes and colocalised puncta with arrows. Scale bars,10 μm.

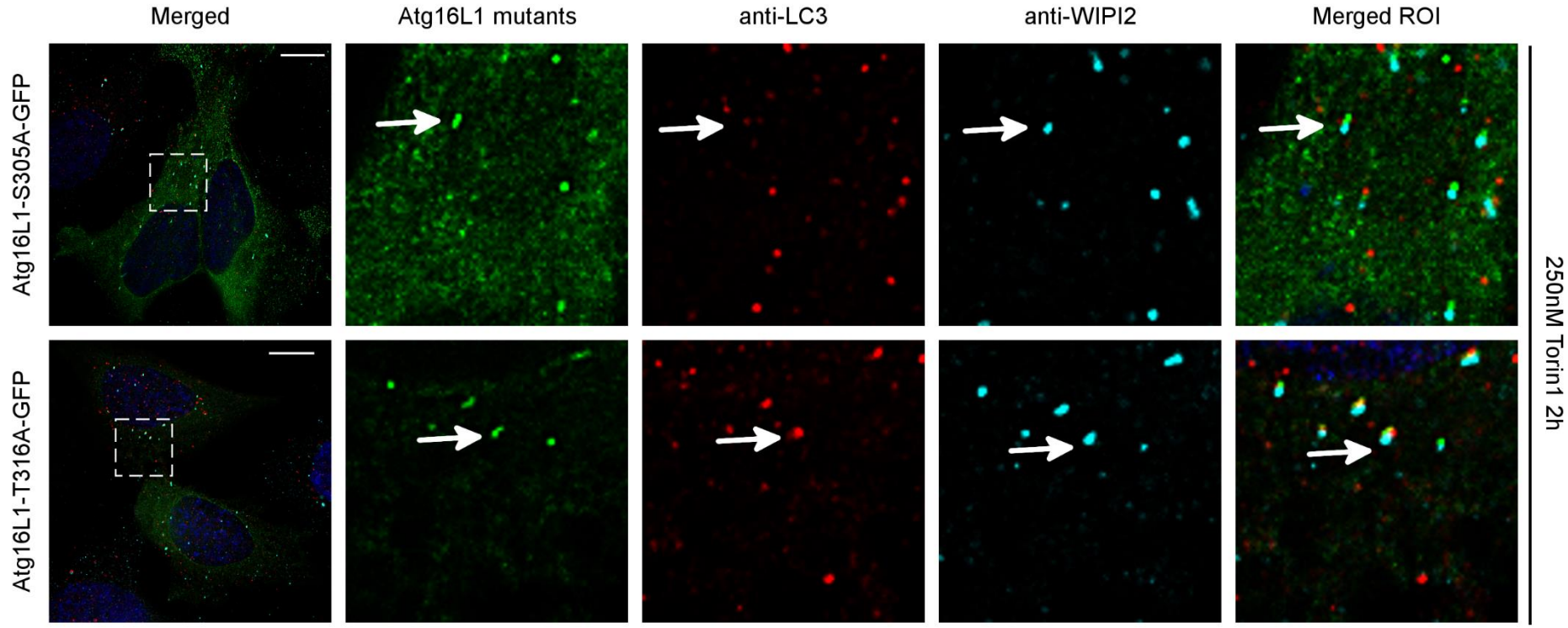

Figure 3.6 Autophagosome formation is not impaired by S305A and T316A mutations

Atg16L1-S305A-GFP or Atg16L1-T316A-GFP constructs were expressed in HeLa cells and compared to LC3 and WIPI distribution after the induction of autophagy by Torin1. LC3 (red) and WIPI (cyan) were immunostained and the nuclei stained with DAPI. Regions of interest are highlighted in boxes and colocalised puncta with arrows. Scale bars, 10 μm.

3.3.4 Characterisation of the point mutants of Atg16L1

Previous research has implicated the CD associated T316A variant of Atg16L1 with defective autophagy against invasive pathogens (Kuballa et al., 2008; Travassos et al., 2010). However, the role of this mutation during metabolic stress during canonical autophagy has been poorly explored. Furthermore, the linker region of Atg16L1 contains a serine phosphorylation site, the function of which is unknown (Villén et al., 2007). This serine, which has been mapped to position 305 of mouse Atg16L1 γ was mutated to alanine, to generate a putative phosphorylation defective mutant. Both point mutants were expressed in HeLa cells, to ascertain what role they play in autophagy.

In the absence of autophagy, both mutants were diffuse in the cytosol, and formed a small number of puncta. When autophagy was induced by Torin1, the point mutants formed puncta which co-localise with WIPI and LC3 (Fig. 3.7), indicating that these mutants were able to drive the formation of autophagosomes and interact with these autophagosome markers.

3.3.5 Quantification of Atg16L1 puncta

The ability of the GFP tagged constructs to form puncta can be further quantified to further assess their ability to function during the activation of autophagy. This would enable subtle changes between the deletion constructs to be detected. The Atg16L1 puncta were quantified using Imaris software (Bitplane), to convert pixels to digital data sets to accurately measure the number of GFP puncta, their diameter and the degree of co-localisation with the autophagosome markers WIPI and LC3. These parameters were normalised on a per cell basis (Klionsky et al., 2012). Highly overexpressing cells were excluded from the analysis, as they are likely undergoing ER stress and do not represent the physiological norm.

In response to the induction of autophagy, the numbers of puncta containing endogenous Atg16L1 (8) were approximately half those seen following expression of Atg16L1 constructs fused to GFP (13-25) (Fig 3.7a). This increase in Atg16L1-GFP puncta when compared to endogenous Atg16L1 puncta is significant. However, the CCD-GFP and CCD+L deletion constructs and the T316A and S305A mutants did not significantly differ from Atg16L1-GFP in the number of puncta per cell induced by autophagy (Fig 3.7a).

When the range of puncta/cell was plotted to ascertain the variable activity of each domain, the results indicated that endogenous Atg16L1, Atg16L1-GFP, S305A and T316A mutants were able to generate a consistent number of Atg16L1 containing puncta in response to

autophagy. The range of puncta/cell plotted for the CCD-GFP and CCD+L-GFP constructs were wider than endogenous ATG16L1, though the range was slightly smaller for the CCD+L-GFP compared to the CCD-GFP (Fig. 3.7b). A Levene's test was applied to the data which showed that the variance for the CCD-GFP construct was close to statistical significance, with a p-value of 0.0821, when compared to the Atg16L1-GFP construct. The other constructs were not deemed statistically significant. Whilst the mean puncta/cell generated by the CCD domain are not significantly different from Atg16L1-GFP, it's highly variable ability to form CCD containing puncta (as indicated by the Levene's statistic) indicates an altered ability to induce and maintain autophagosomes.

Next, the diameter of Atg16L1 puncta were measured to indicate the size of the developing autophagosome, to see whether the domains could efficiently generate autophagosomes above or below 0.75 μm diameter. This parameter was selected as autophagosomes are generally classified as 1 μm and above, though this varies by cell type (Mizushima, 2004). By focussing on Atg16L1 puncta above and below 0.75 μm diameter, it was intended to distinguish between early phagophore formation and the later stages of elongation and autophagosome formation, prior to the dissociation of Atg16L1. The number of puncta/cell below 0.75 μm containing endogenous Atg16L1 (7) were approximately half to a third of those seen following expression of the GFP tagged Atg16L1 constructs (12-27). This could correlate with an overall increase in the number of puncta in the cells expressing the Atg16L1-GFP constructs (Fig. 3.7a). The other constructs did not have a significantly different number of puncta below 0.75 μm when compared to Atg16L1-GFP. When the number of Atg16L1 puncta/cell above 0.75 μm was measured, the endogenous protein, Atg16L1-GFP, CCD-GFP, CCD+L-GFP and Atg16L1-S305A-GFP were shown to generate puncta above this threshold. However, the Atg16L1-T316A-GFP mutant was unable to form any puncta above 0.75 μm diameter (Fig 3.7d). This indicates that either the autophagosomes generated are of a smaller diameter, or that the mutant is out-recruited by endogenous Atg16L1 during the later stages autophagosome formation.

Next the colocalisation between Atg16L1 puncta and WIPI was quantified. WIPI recruits Atg16L1 to the site of the autophagosomal membrane (Dooley et al., 2014), so the degree of co-localisation between Atg16L1 and WIPI is an indicator of whether this interaction has been altered by the addition of GFP to the C-terminus of the deletion constructs. Endogenous Atg16L1 and Atg16L1-GFP co-localised with WIPI to a similar degree at 88.5% and 81.8%, respectively. There was a decrease in the co-localisation of CCD-GFP with WIPI compared to endogenous protein and the GFP-tagged Atg16L1 and CCD+L constructs (Fig

3.8a). The point mutations (T316A and S305A) did not affect co-localisation with WIPI (Fig 3.8a).

Next colocalisation between Atg16L1 and LC3 was determined. The Atg16L1 complex is vital for LC3 incorporation into the developing autophagosomal membrane, and dissociates from the mature autophagosome, leaving LC3 associated with the membrane. Therefore, not all LC3 puncta will be Atg16L1 positive, as some represent mature autophagosomes. The endogenous Atg16L1 and Atg16L1-GFP puncta co-localised with LC3 to a similar extent (56% and 51%, respectively) (Fig 3.8b). The same was true for the deletion constructs (excluding the L+WD40 and WD40) and the point mutants.

These results demonstrated that the full length GFP tagged Atg16L1 behaves in a similar manner to endogenous Atg16L1. Additionally, these results demonstrated that the CCD domain of Atg16L1 is less able to co-localise with WIPI than the full length Atg16L1 protein.

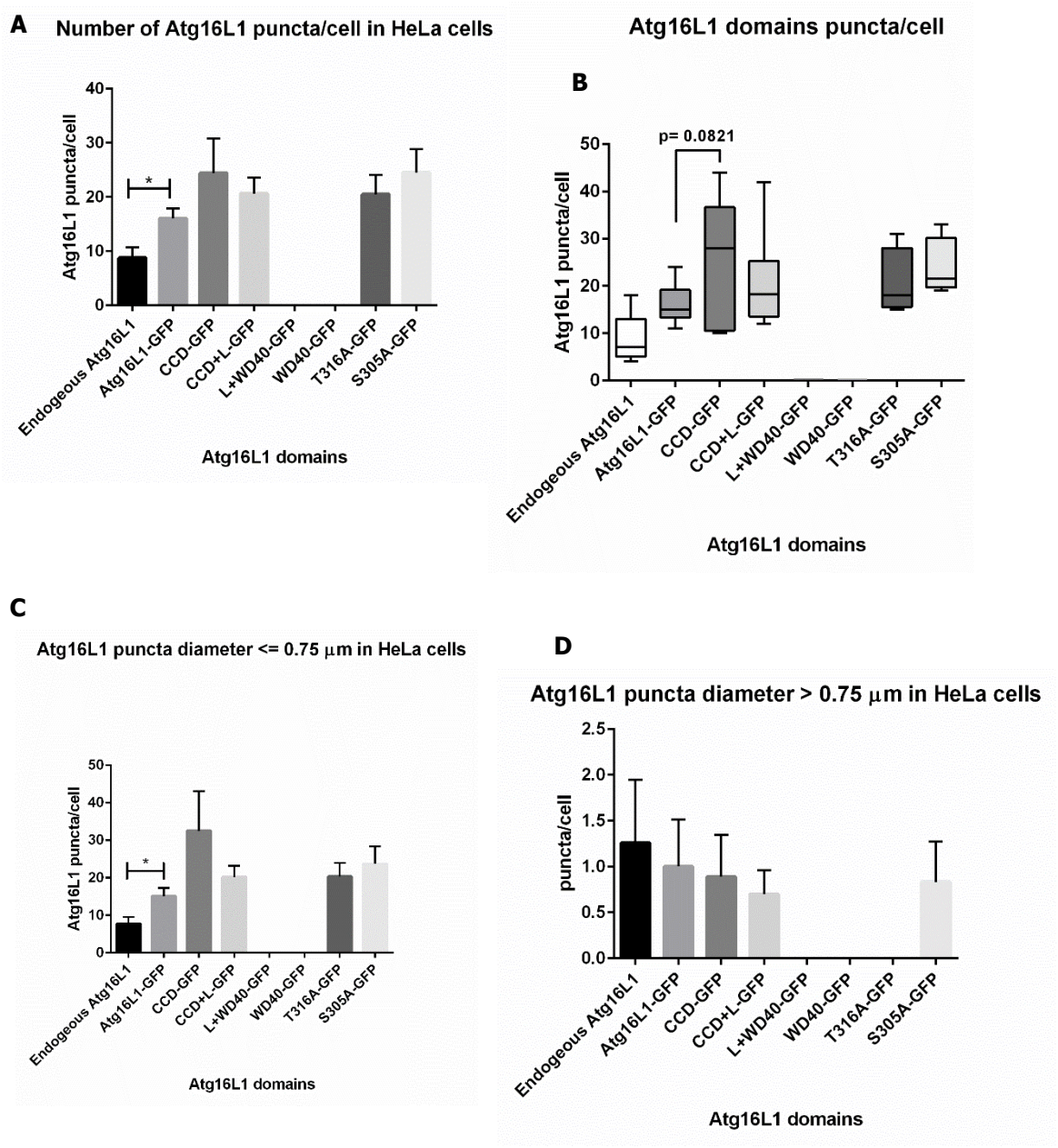

Figure 3.7 Quantification of Atg16L1 puncta/cell

(A) Quantification of Atg16L1 puncta/cell showing mean and SEM. 10 cells analysed per condition. * p = 0.0185

(B) Box plot of Atg16L1 puncta/cell, using data from (A). Levene's test calculated with an alpha value of 0.05

(C) Analysis of the data in (A) to show Atg16L1 puncta/cell less than or equal to 0.75 μm. * p = 0.0279

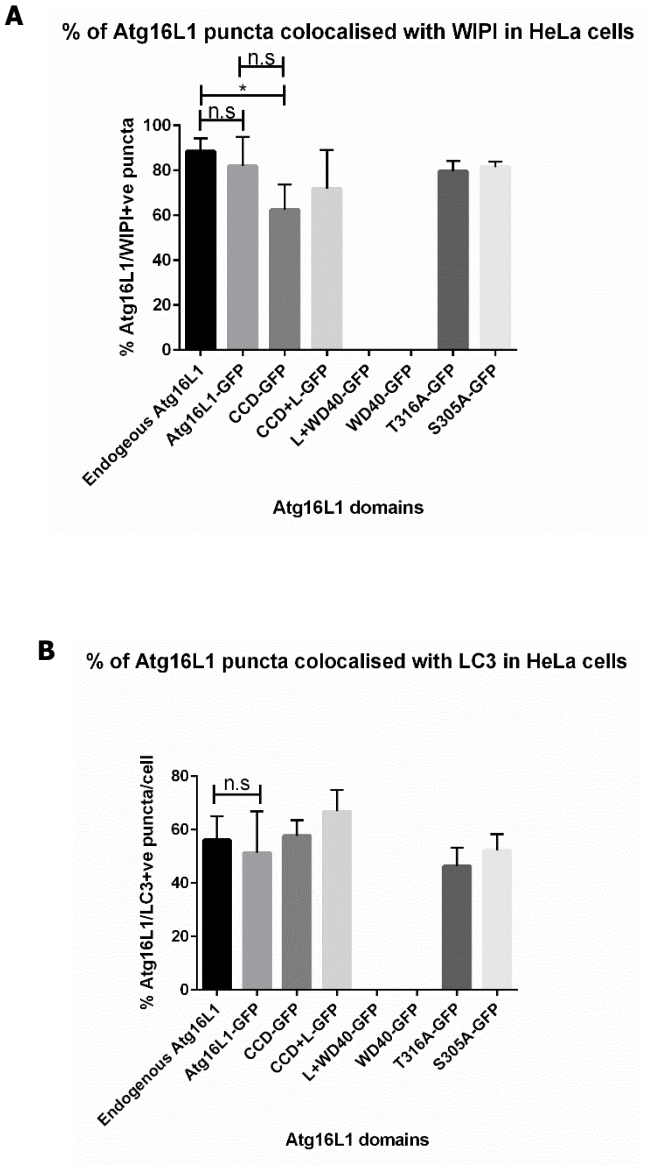

Figure 3.8 Quantification of colocalisation between Atg16L1 constructs and autophagosome markers WIPI2 and LC3

(A) Analysis of experiments in figures 3.5 and 3.6. Atg16L1 puncta that were positive for WIPI were converted to a percentage of the total number of Atg16L1 puncta/cell. Bars show mean and SEM. p * = 0.0396

(B) Analysis of experiments in figures 3.4 and 3.6. Atg16L1 puncta that were positive for LC3 were converted to a percentage of the total number of Atg16L1 puncta/cell. Bars show mean and SEM

3.3.6 Establishment of an Atg16L1 knockout MEF cell line

3.3.6.1 Breeding scheme to obtain Atg16L1 fl/fl Rosa LacZ embryos

To further characterise the role of the Atg16L1 domains and their ability to power autophagy, an Atg16L1 negative background was required. Therefore, a strategy to generate Atg16L1 KO MEFs using a conditional Atg16L1 knockout mouse model was utilised. The Atg16L1 flox/flox (fl/fl) mice were generated by Maryam Arasteh, and have been outlined in her thesis work. Briefly, exon 2 has been flanked by loxP sites, followed by a neomycin resistance cassette, flanked by Frt sites. The neomycin cassette has been removed by crossing heterozygous Atg16L1Fl/+ mice with mice carrying FlpO-recombinase, and is therefore not present in the mice used for the generation of the MEFs (Fig 3.9). The Atg16L1fl/fl mice were crossed with Rosa LacZ/LacZ mice (Fig 3.10) to obtain Atg16L1Fl/+//Rosa26LacZ/+ mice, which were then intercrossed to obtain Atg16L1fl/fl//Rosa26LacZ/+. E13.5 Atg16L1fl/fl // LacZ/+ embryos were obtained by time mating Atg16L1fl/fl with Atg16L1fl/fl //Rosa26LacZ/LacZ mice. This timed mating was set up by Devina Divekar and Ulrike Mayer. Since the disruption of Atg16L1fl/fl and the expression of the Rosa26-LacZ transgene are both controlled by the same Cre recombinase, LacZ expression/activity can serve as a useful marker of the cells with targeted gene disruption (Fig 3.10).

3.3.6.2 Extraction, immortalisation and clonal selection of MEFs from embryos

At E13 the pregnant mouse was humanely killed by a schedule 1 method. As the genotype of each embryo was identical, embryos were processed together. Immortalisation of MEFs can be achieved using serial passaging. In this method, immortalisation requires a stochastic genetic event, likely loss of p53 or less frequently loss of $p19^{ARF}$ (Kamijo et al., 1997; Sharpless., 2006/Cellis). MEFs were split twice a week during the rapid growth phase of the culture, which was between the first 1-6 passages. As the cells entered senescence, the cells were split 1:2 or just replated, to maintain cells at near 100% confluency since seeding cells too sparsely at this stage decreases the immortalisation frequency (Sharpless., 2005). Immortalised cells began to overgrow the cultures between passages 15-20, and were subsequently pooled for clonal selection to generate a homogenic population. Whilst the genotype of the immortalised MEFs were identical, other genetic variation between the pooled MEFs could not be accounted for e.g. immortalisation events and genetic variation between individual embryos.

Clones identified by clonal selection were expanded until enough cells were available for the adenoviral cre-recombinase expression, to knockout Atg16L1 expression.

3.3.6.3 Generation and verification of Adeno-Cre specific Atg16L1 knockout MEFs

The isolation of individual clones of immortalised Atg16L1 fl/fl LacZ +/- MEFs allowed for the generation of knockout Atg16L1 cells with Cre recombinase, while having a parental control genetically and morphologically identical to the Atg16L1-deficient cells. MEF Atg16L1 fl/fl cells were incubated with the AdenoCre virus (AdCre) to express cre-recombinase in induced cells. The cells were then analysed by FACS. LacZ expression and therefore Atg16L1 gene disruption can be determined using the fluorogenic β-galactosidase substrate fluorescein di β-D-galactopyranoside (FDG). The non-fluorescent FDG is sequentially hydrolysed by β-galactosidase, first to fluorescein monogalactoside (FMG) and then to highly fluorescent fluorescein (Guo and Wu., 2008). Parental fl/fl and AdCre treated cells were subjected to FDG stain, or left untreated as a control. The cells were then analysed and sorted by FACS. The parental fl/fl untreated, FDG treated and AdCre non FDG treated MEFs were negative for LacZ activity as determined by FACS (Fig 3.11). The AdCre FDG treated MEFs were positive for LacZ activity, and the population was sorted and collected for further analysis.

To determine if the AdCre treatment and FDG LacZ sorting of cells had been successful in knocking out Atg16L1 expression, PCR was used to analyse genomic DNA from cell lysates with the forward primer targets Atg16L1 intron 1 (primer 223) and the reverse primer targets Atg16L1 intron 2 (primer 226, Table 2.9). PCR genotyping was carried out on two populations of clonal cells, before and after AdCre treatment and FACs sorting. Both populations of parental Atg16L1 fl/fl cells were homozygous for the Atg16L1 fl/fl allele, generating a band of 801 bp (Figs 3.19, 3.12). PCR genotyping of the AdCre treated clones confirmed excision of exon 2 and generation of a homozygous Atg16L1 KO cell, with a single band of 253 bp (Fig.3.12). A weak band for Atg16L1 fl/fl was seen in clone 2, and further analysis lead to this clone being discarded.

Previous research has shown that Atg16L1 deficient MEFs are deficient in LC3 processing and accumulate long-lived proteins, such as p62 (Saitoh et al., 2008). To confirm that the MEFs were no longer expressing Atg16L1 at the protein level and were autophagy deficient, parental Atg16L1 fl/fl and AdCre FACS sorted Atg16L1 KO MEFs were subjected to an HBSS starvation time course, the protein lysates collected and analysed by Western blotting. HBSS

starvation was used as it is a standardised protocol for inducing autophagy, and can be used for starving the cells over a longer timecourse than Torin1, without potential pharmacological side effects. The Atg16L1 fl/fl MEFs expressed the α and β isoforms of the protein, whereas there was no Atg16L1 protein present in Atg16L1 KO MEFs (Fig. 3.13a). Following the induction of autophagy by HBSS starvation, Atg16L1 fl/fl MEFs were able to process LC3-I to LC3-II, and degrade p62, while in Atg16L1 KO MEFs, LC3-I was not processed, and p62 accumulated throughout the starvation time course (Fig. 3.13a-b). Indeed, prior to the induction of autophagy, there was a three-fold increase in the level of p62 compared to Atg16L1 fl/fl cells (Fig. 3.13b), indicating that the Atg16L1 KO MEFs are autophagy defective.

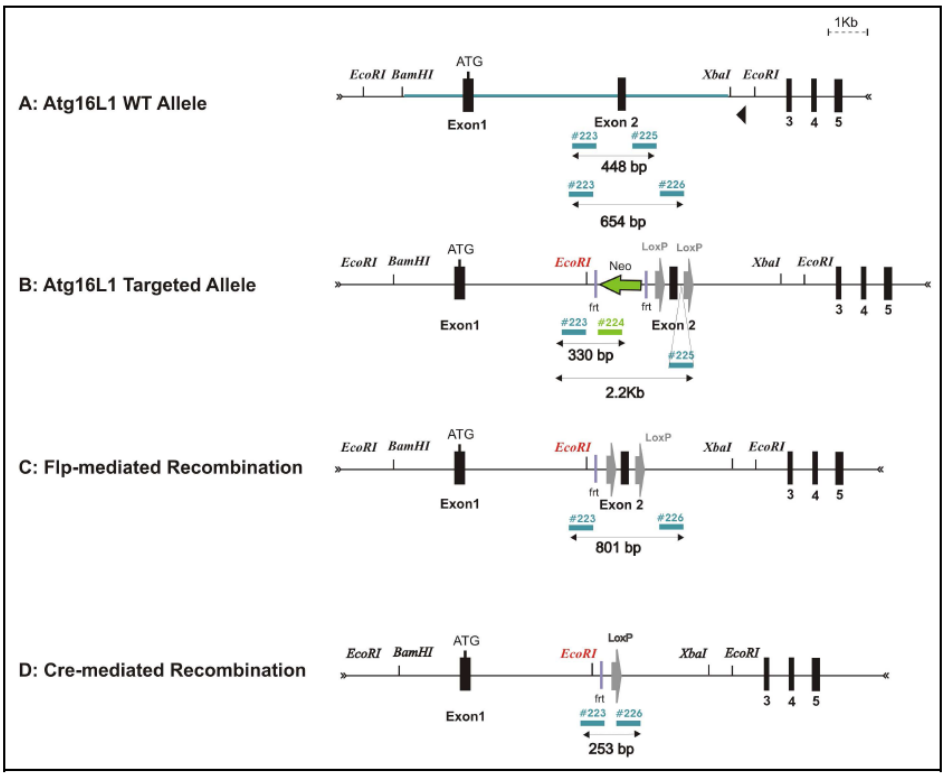

Figure 3.9 PCR strategy for genotyping Atg16L1 transgenic mice. Primers used to determine WT, Atg16l1 floxed, removal of the neomycin cassette after Flp-mediated recombination and removal of exon 2 after Cre mediated recombination in mice. Courtesy of Maryam Arasteh

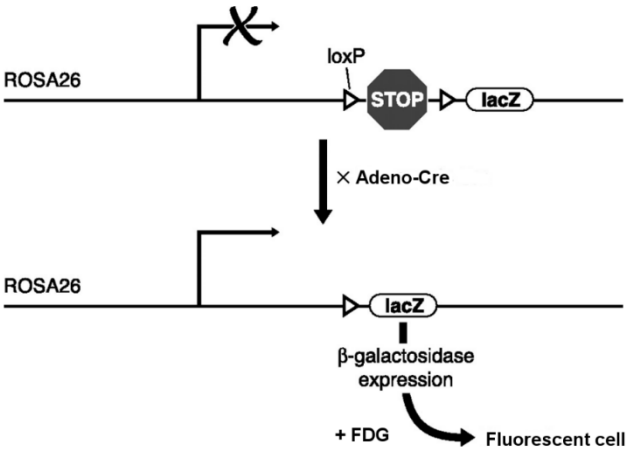

Figure 3.10 Diagrammatic representation of the Rosa26 LacZ locus. A stop codon is flanked by two loxP sites, preventing transcription of the LacZ gene. Following cre-mediated recombination, the stop codon is removed, and the lacZ gene can be transcribed and translated. Modified from Le Lay and Kaestner., 2010.

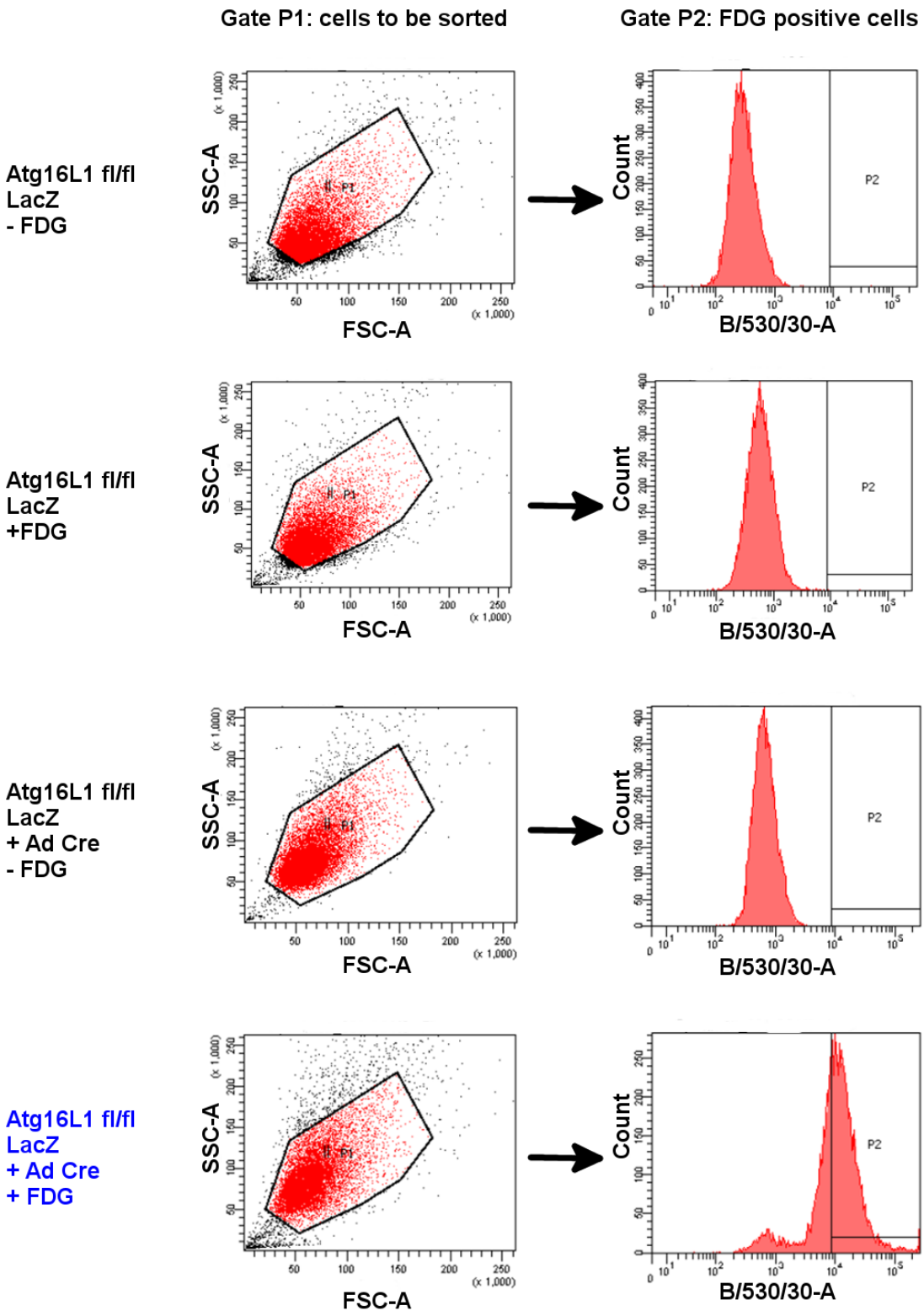

Figure 3.11 Atg16L1 fl/fl RosaLacZ AdCre induced MEFs are positive for LacZ activity determined by FDG staining and FACS sorting. Cells were treated with FDG to determine LacZ activity. Untreated and parental cells served as a control. Cells were gated using forward and sideward scatter (P1). Fluorescence was detected using the 530/30 filter, with fluorescent cells gated as P2. In blue typeface are MEFs induced with AdenoCre which are positive for LacZ activity.

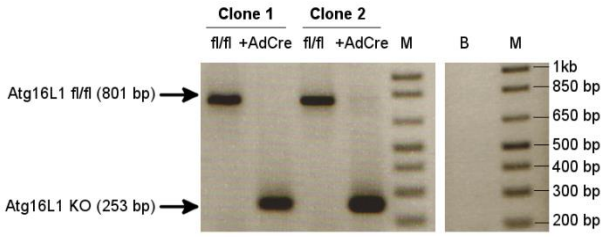

Figure 3.12 Adeno-cre specific knockout of Atg16L1 expression in FACS sorted MEFs as determined by PCR genotyping

PCR Genotyping of Atg16L1 fl/fl and Atg16L1 AdCre treated MEFs post FACS sorting. Genomic DNA was extracted from clonal cells that had been sorted for LacZ activity by FDG staining to confirm excision of exon2 of Atg16L1 by the presence of a 253 bp band. M = marker, B = blank.

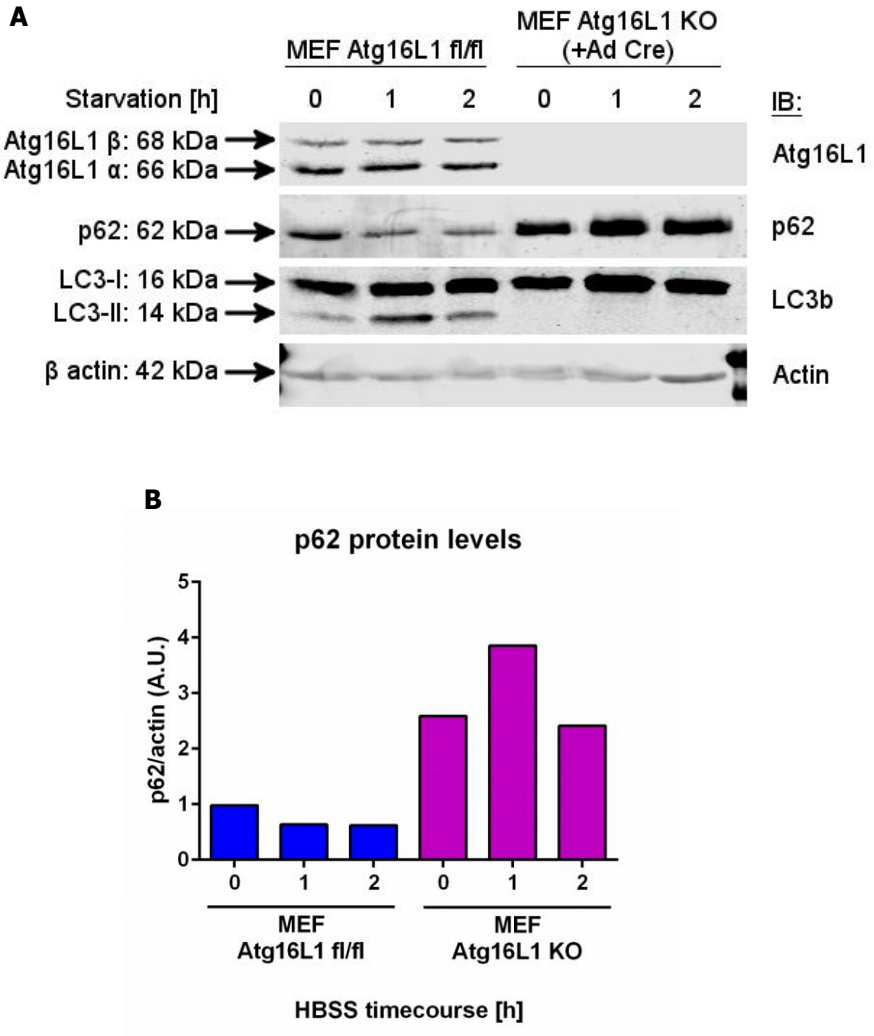

Figure 3.13 Atg16L1 KO MEFS are autophagy deficient

Autophagy deficiency in Atg16 KO MEFs. (A) Clonal Atg16L1 fl/fl or sorted Atg16L1 KO cells were cultured in nutrient rich medium or HBSS and lysates collected. The protein lysates were collected for analysis by Western blotting. (B) Quantification of the levels of p62 protein in (A) by densitometry.

Next, we tested whether Atg16L1 KO MEFs lacked the ability to form autophagosomes. Atg16L1 fl/fl and Atg16L1 KO MEFs were starved with HBSS for 2 h, fixed and immunostained for autophagosome markers. Atg16L1 fl/fl MEFs were able to form LC3 puncta which co-localised with WIPI2 (Fig. 3.14). Formation of autophagosomes was not observed in Atg16L1 KO MEFs (Fig. 3.14). These results confirm the generation of an Atg16L1 KO MEF cell line that is autophagy deficient, resulting in accumulation of long lived proteins, such as p62.

3.3.7 Reconstitution and quantification of Atg16L1 domains in Atg16L1 KO MEFs

Earlier in this chapter, the properties of the individual domains of Atg16L1 in autophagy had been characterised. To explore the role of these domains without endogenous Atg16L1 expression, full length, CCD, L+WD40 and CD associated Atg16L1-T316A mutant constructs were transfected in Atg16L1 KO MEFs, subjected to HBSS starvation to induce autophagy, and counterstained for the autophagosome marker LC3. In untransfected Atg16L1 KO MEFs, the distribution of LC3 remained diffuse during the activation of autophagy, with the exception of a few LC3 positive puncta (Fig. 3.15). In cells that were reconstituted with the full length Atg16L1-GFP, CCD-GFP and Atg16L1-T316A-GFP autophagosome formation was restored as indicated by the presence of GFP-positive puncta that co-localised with LC3 puncta (Fig. 3.15). As expected, in cells that were reconstituted with the L+WD40 domain of Atg16L1 no GFP- or LC3-positive puncta were apparent (Fig. 3.15).

Images from the reconstitution experiments were analysed to further quantify each domain's ability to form puncta and restore autophagy. The number of Atg16L1-GFP and Atg16L1-T316A-GFP puncta per cell were comparable, while the number of puncta were highly variable when the CCD-GFP domain was expressed, which is in line with the earlier results in this chapter (3.3.3, 3.3.5, Fig. 3.16a,b). A Levene's test showed that there was no significant difference in the variance between the CCD-GFP, T316A-GFP and the Atg16L1-GFP constructs, however the Levene's statistic for the CCD-GFP was nearing the threshold for significance indicating a trend towards difference in variance. Quantification of LC3 puncta confirmed that the full-length Atg161L1-GFP had restored autophagy (Fig. 3.16c). There was a small, non-significant decrease in cells expressing the CCD-GFP construct, highlighting the variability of this domain to effectively carry out autophagy. Interestingly, cells that expressed the Atg16L1-T316A-GFP construct showed a significant increase in the number of LC3 puncta generated (Fig. 3.16c).

The degree of co-localisation between Atg16L1 domains and LC3 was also analysed to determine how efficiently the domains could recruit LC3 to the site of the autophagosome. Atg16L1 puncta were classified as either LC3 positive or LC3 negative, with a larger proportion of Atg16L1/LC3 positive puncta indicating normal autophagosome maturation. Both the Atg16L1-GFP and Atg16L1-T316A-GFP constructs generated puncta that were predominantly LC3 positive during HBSS starvation (Fig. 3.16d). However, the CCD-GFP puncta were less likely to be associated with LC3, with fewer GFP/LC3 puncta compared to the other domains (Fig. 3.16d). Overall, this demonstrates that the CCD domain of Atg16L1 is sufficient to drive autophagic activity of Atg16L1.

3.3.8. The requirement of Atg16L1 domains in the formation of tubulovesicular autophagosomes

So far in this chapter, the role of the Atg16L1 domains during starvation induced autophagy has been explored. To determine the involvement of Atg16L1 in the selective recognition and degradation of pathogens via autophagy, lipoplex transfection reagents were chosen, as they act like pathogen associated molecular patterns (PAMPs) to activate selective autophagy (Roberts et al., 2013; Fujita et al., 2013). Lipoplex transfection reagents (e.g. *Transfast*) can induce the formation of tubulovesicular autophagosome (TVAs) in a wide variety of cell types (Roberts et al., 2013). Furthermore, it has been shown that beads coated with transfection reagents are selectively targeted by LC3-positive autophagosomes (Fujita et al., 2013). To simulate pathogen invasion and induce TVA formation, Atg16L1 KO MEFs expressing the Atg16L1-GFP, CCD-GFP, L+WD40 or Atg16L1-T316A-GFP constructs were cultured in nutrient rich media, with the addition of lipoplex reagent. The Atg16L1-GFP construct was able to restore the formation of large LC3 positive structures, which were clustered close to the nucleus. There was a degree of co-localisation between LC3 and Atg16L1-GFP, with the LC3 signal confined to a complex of vesicles and tubules (Fig. 3.18). Cells expressing CCD-GFP were also able to form TVAs. However, there were more CCD-GFP puncta observed which were LC3 negative (Fig. 3.18). The Atg16L1-T316A-GFP mutant was able to drive the formation of TVAs, which were both GFP and LC3 positive. Interestingly, there appeared to be an increase in the number of tubules and vesicles, though the tubules were shortened in length (Fig. 3.18). These results demonstrate that the CCD domain is sufficient to drive the autophagic response to surrogate PAMPS.

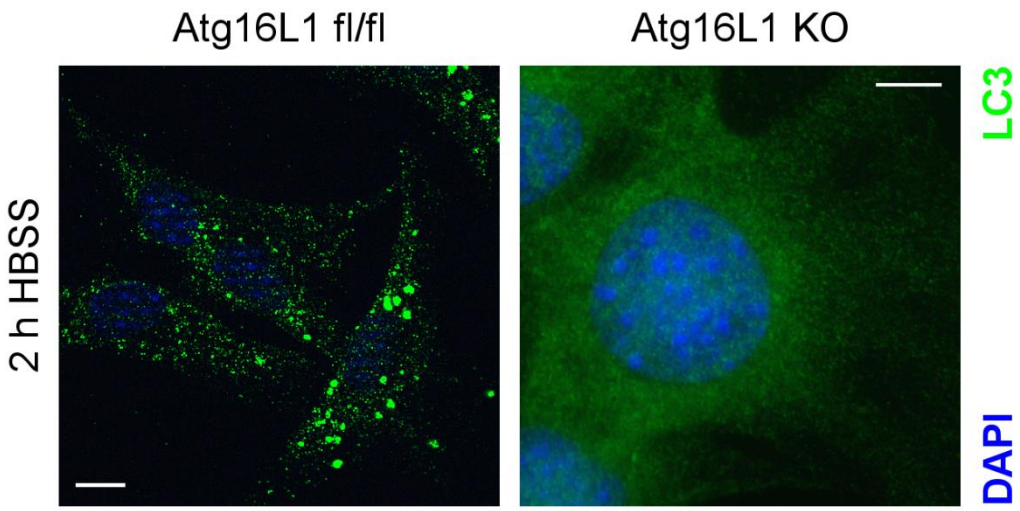

Figure 3.14 Atg16L1 KO MEFs do not form LC3 puncta

Distribution of autophagosome markers in Atg16L1 fl/fl and Atg16L1 KO MEFs.

Cells were incubated in HBSS for 2 h to induce autophagy. Cells were immunostained with LC3 and the nuclei were stained with DAPI. Scale bars, 10 μm.

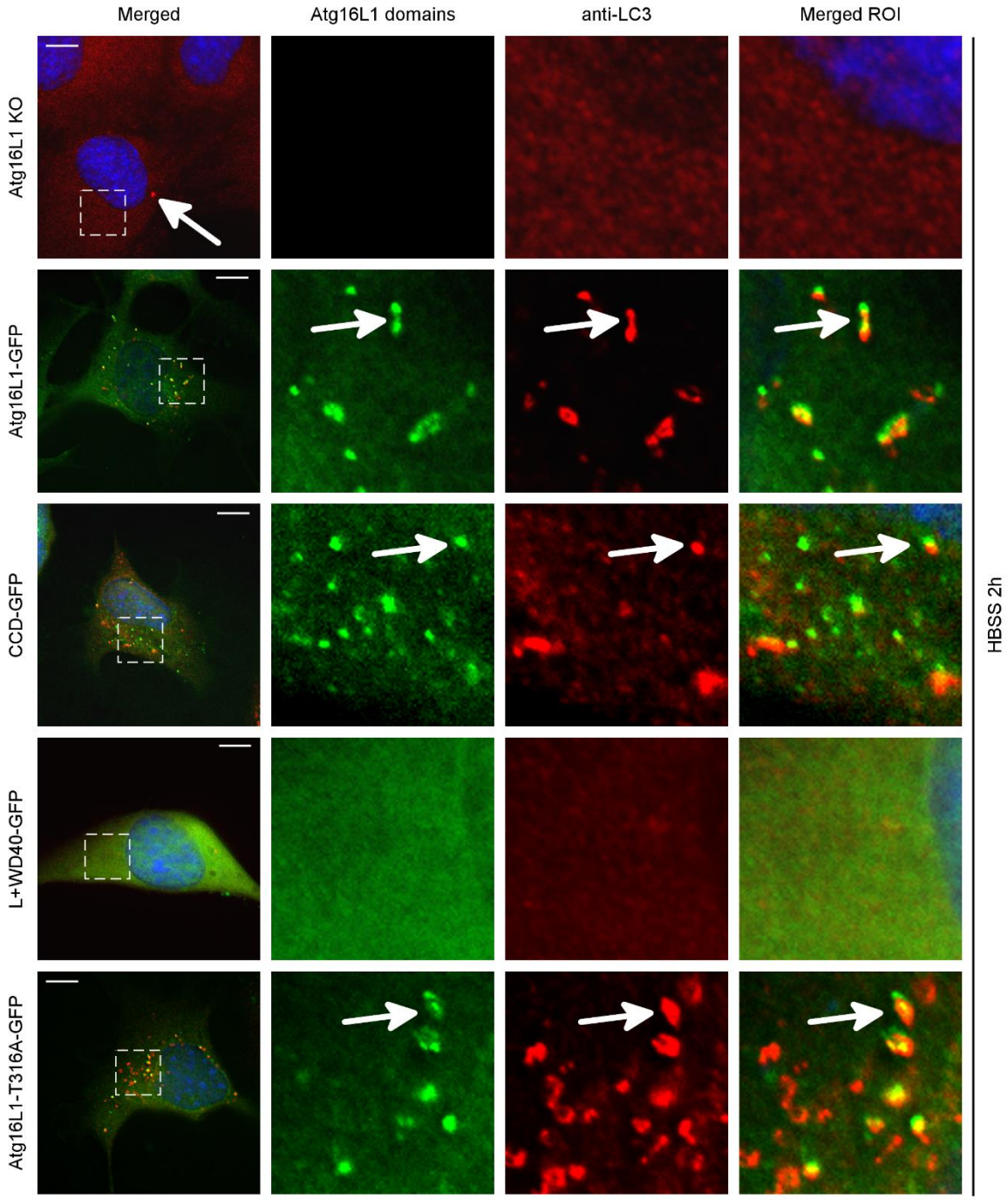

Figure 3.15 Reconstitution of Atg16L1 KO MEFs with GFP-tagged Atg16L1 constructs demonstrates that the CCD restores autophagy.

GFP-tagged Atg16L1 constructs were transfected in Atg16L1 KO MEFs and treated with HBSS for 2 h to induced autophagy. Autophagosomes were immunostained with LC3. The nuclei were stained with DAPI. Regions of interest are highlighted in boxes and puncta of interest with arrows. Scale bars, 10 μm

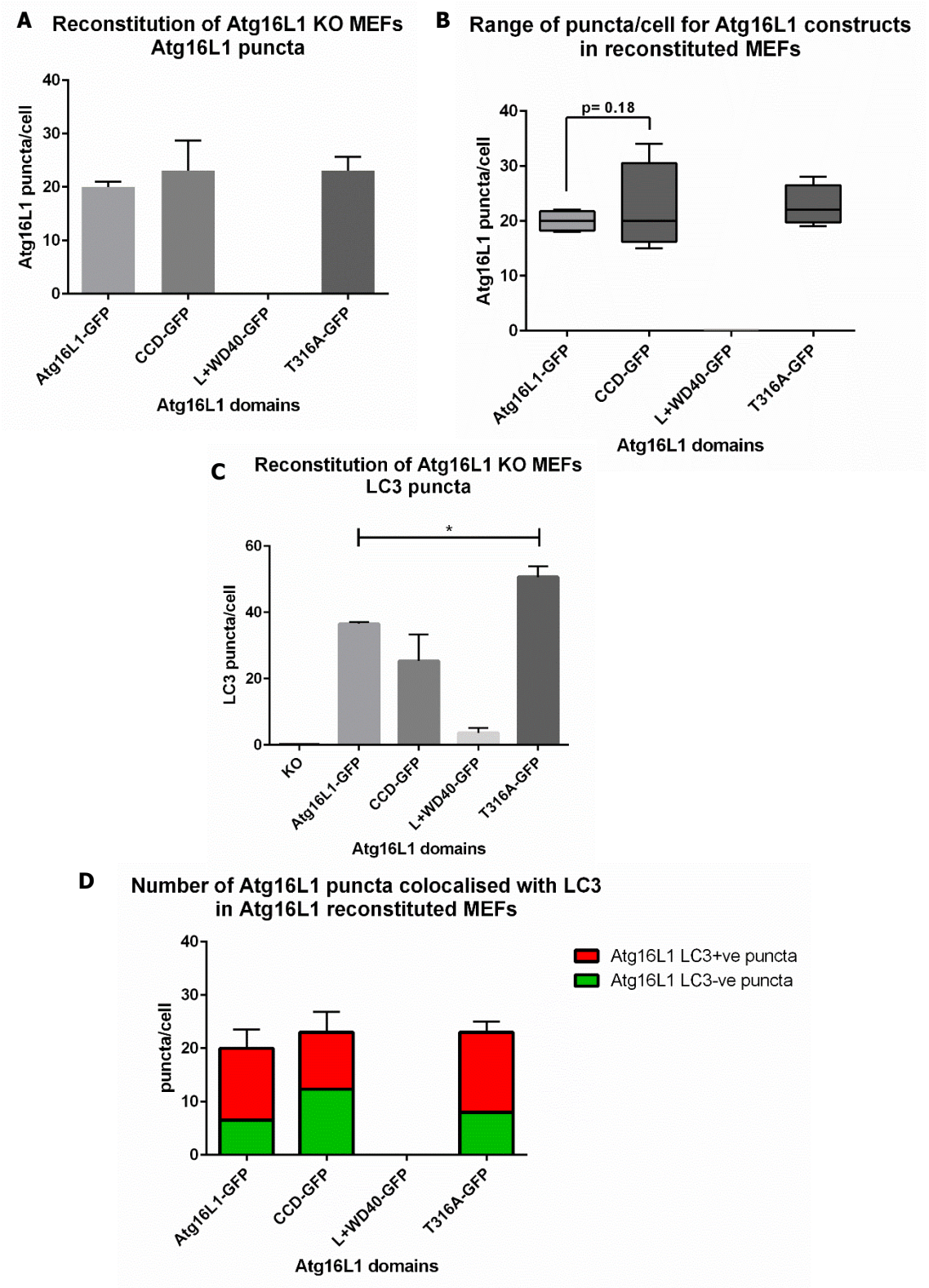

Figure 3.16 Quantification of Atg16L1 and LC3 puncta in reconstitution experiments

(A) Quantification of Atg16L1 puncta/cell from experiments in Figure 3.15.

(B) Box plot of Atg16L1/puncta/cell using data from (A). Levene's test calculated with an alpha value of 0.05

(C) Analysis of LC3 puncta/cell from experiments in Figure 3.15. * p = 0.0413

D) Analysis of Atg16L1 domain localisation with LC3 puncta from experiments in Figure 3.15.

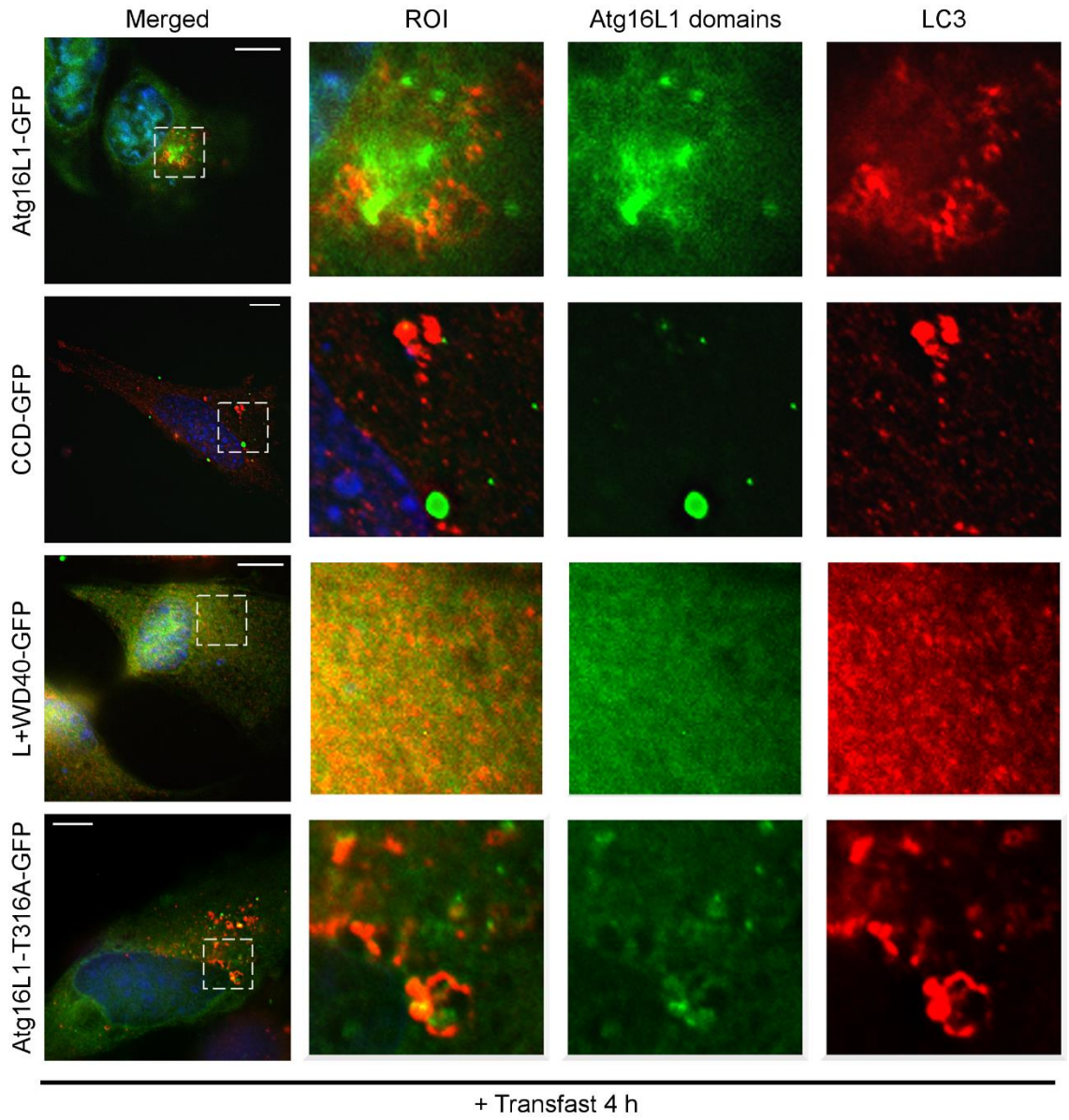

Figure 3.17 The CCD and the CD associated T316A mutant restore the autophagy response to surrogate pathogen in Atg16L1 KO MEFs

Atg16L1 KO MEFs were reconstituted with GFP-tagged Atg16L1 domains. Cells were incubated with lipoplex transfection reagent for 4 h to induce TVAs. LC3 was immunostained and the nuclei stained with DAPI (blue) Regions of interest are highlighted in boxes. Scale bars, 10 µm

3.4 Chapter Discussion

The main aims of this chapter were to determine the function of the Atg16L1 domains in autophagy. To study the function of the domains of Atg16L1, C-terminal GFP-tagged Atg16L1 constructs were generated. To ensure these constructs were stable when expressed, and to assess their contribution to autophagy, their localisation with autophagy markers was observed and quantified in cells with a background of ATG16L1 expression, and cells where Atg16L1 expression had been knocked out.

The full length Atg16L1-GFP behaves as endogenous ATG16L1 and can still form autophagosomes, confirmed by the localisation with the autophagosome markers LC3 and WIPI. The ability of Atg16L1-GFP to associate with these autophagosome markers in response to autophagy induction indicates that the autophagic function of Atg16L1 has not been disrupted by the addition of a C-terminal GFP tag, confirming that Atg16L1-GFP is able to function in canonical autophagy. The deletion constructs CCD-GFP and CCD+L-GFP were capable of localising to the autophagosome with WIPI and LC3. When expressed in Atg16L1 KO MEFs, the CCD-GFP construct was sufficient to restore LC3 puncta. However, a broad range of CCD-GFP puncta were detected (Fig. 3.18). This could indicate a potential loss of regulation or stability in the CCD, following deletion of the linker and WD40 domain. On the other hand, this could be caused by transfection efficiency varying between cells. The L+WD40-GFP and WD40-GFP deletion constructs did not form puncta and did not localise with LC3 and WIPI, and therefore do not play a role in driving the formation of autophagosomes.

If the varied range of puncta number generated by CCD-GFP is caused by the loss of the linker and WD40 domain, this could allude to important interactions or posttranslational modifications within these domains. These interactions and modifications could therefore play a key role in regulating canonical autophagy. The coiled-coil domain of Atg16 is conserved from yeast to higher eukaryotes, and whilst sufficient to reconstitute autophagy in this and other studies (Fujita et al., 2009), it is possible that mechanisms may have evolved in higher eukaryotes to fine tune the autophagy pathway which involve the linker and WD40 domain, though this is highly speculative. Another explanation for the results is that the addition of eGFP to the C-terminus of the CCD may have altered the important interaction between Atg16L1 and WIPI2. This interaction is crucial for the recruitment of the Atg5-12-Atg16L1 complex to the early autophagosome and is dependent on two residues in Atg16L1 which lie at the end of the coiled-coil domain; E226 and E230 (Dooley et al., 2014). It is possible that the presence of an eGFP tag so close to these residues

results in steric hindrance of WIPI2, which would also explain why there is a slight trend for reduced colocalisation between CCD-GFP and WIPI2, when compared to full length Atg16L1-GFP.

The putative phosphorylation mutant Atg16L1-S305A and the CD-associated mutant Atg16L1-T316A were also studied, to further understand the importance and function of these residues in autophagy. The S305A mutant was comparable to full length Atg16L1-GFP construct, and was able to function in autophagy. If this serine phosphorylation of Atg16L1 plays a role in autophagy, it may be a subtle regulatory mechanism, and could be associated with autophagic flux. Similar mechanisms have been demonstrated in the autophagy proteins, such as the threonine phosphorylation of Atg5 by p38 (Keil et al., 2013). The T316A mutant was able to incorporate into autophagosomes and was able to restore canonical autophagy, however, this construct was unable to form puncta above 0.75 µm in diameter. This was unusual, as all other autophagy competent constructs tested were able to generate some puncta above this threshold, which represents a near-mature autophagosome. However, the number of large autophagosomes containing the GFP tagged Atg16L1 constructs typically did not exceed 2 per cell. The biological relevance of this is as yet unclear. This inability of the T316A mutant to generate large puncta, comparable to the full length wild type Atg16L1 could lead to the formation of smaller autophagosomes (Fig 3.18), due to the vital role Atg16L1 plays in the incorporation of LC3 into the autophagosome, as less Atg16L1 is recruited to the phagophore (Fujita et al., 2008). Indeed, this hypothesis was confirmed by Murthy et al., 2014, who demonstrated that the T316A mutant generated smaller autophagosomes in response to starvation. Previously, the CD-associated mutation had been linked to defective autophagy in response to pathogen invasion, resulting in a failure to capture pathogens within the autophagosome (Kuballa et al., 2008; Travassos et al., 2010). Therefore, the T316A mutation also has an impact on canonical autophagy.

It has been established that the addition of transfection reagents such as lipoplex and polyplex can lead to the formation of tubulovesicular autophagosomes (TVAs) (Roberts et al., 2013). Previous studies have also shown that when latex beads coated with these transfection reagents are phagocytosed by cells, the autophagy machinery is activated and recruited to the bead in a response comparable to an invading microorganism (Fujita et al., 2013). In this chapter, the CCD of Atg16L1 was able to contribute to the formation of TVAs in response to lipoplex reagents, whereas the L+WD40 was unable to. This is likely linked to the interaction between Atg16L1 and WIPI2, which directs Atg16L1 to the site of early autophagosome formation (Dooley et al., 2014).

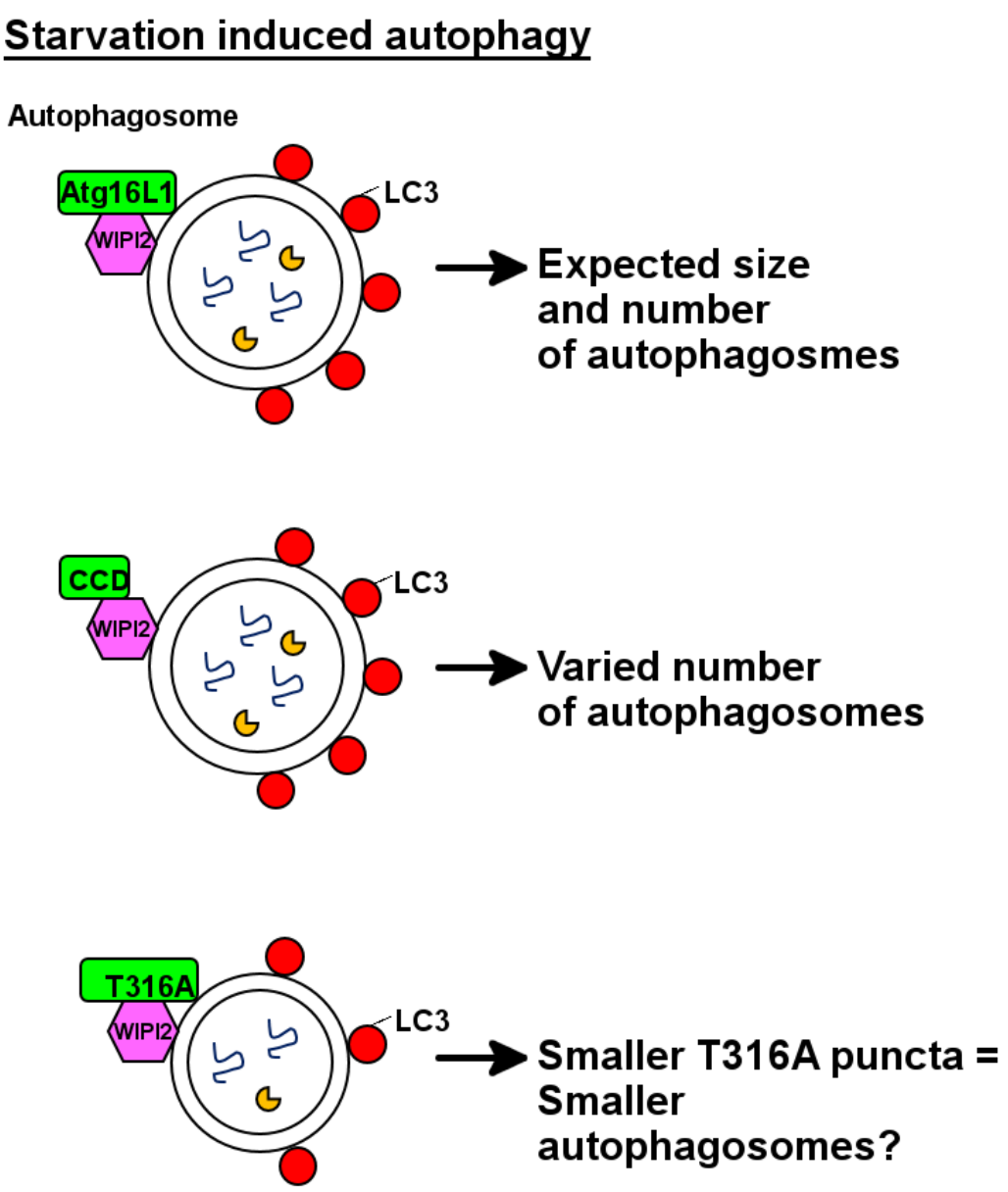

Figure 3.18 Schematic representation of autophagosome formation by domains and mutants of Atg16L1. In response to nutrient deprivation, CCD of Atg16L1 is able to drive the formation of autophagosomes, though the number of autophagosomes is varied The CD associated T316A mutant of Atg16L1 is able to power autophagosome formation, however the T316A mutant is unable to incorporate into large puncta, which could lead to the formation of smaller autophagosomes compared to those generated by wild type Atg16L1.

This interaction also plays a vital role in the clearance of pathogens, so it was not surprising that the CCD, which contains the residues responsible for the interaction with WIPI2, would be able to contribute to TVA formation. The CCD is also sufficient for the clearance of *Toxoplasma gondii* in macrophages (Choi et al., 2014). However, the efficiency of TVA formation by the CCD was not investigated, so the comparison to the full length Atg16L1 cannot be made. As the early results in this chapter have demonstrated, the loss of the L+WD40 domains affect the ability of the CCD to efficiently perform autophagy, and the same may be true of TVA formation. Whilst the CCD may be sufficient to recruit Atg16L1 to the autophagosome in response to infection, other mechanisms within Atg16L1 have been characterised (Fig 3.19). The WD40 domain of Atg16L1 has also been shown to bind ubiquitin, which decorates ruptured endosomal membranes containing *Salmonella* or transfection coated beads. Deletion of the WD domain and further mutation of Atg16L1 in the FIP200 binding region and within the CCD domain reduces the formation of LC3 and Atg16L1 positive vesicles around *Salmonella*, demonstrating that FIP200 and an additional unknown protein interaction also contribute to Atg16L1 recruitment. The interactions between Atg16L1 and the pathogen recognition receptors (PRR) NOD1/2 and TLR2 are also thought to enable recruitment to the invading microorganism via the PRR (Travassos et al., 2010; Boada-Romero et al., 2013). These separate regions and residues all appear to contribute towards different mechanisms in Atg16L1 recruitment in selective autophagy, indicating there are multiple ways in which Atg16L1 is recruited to the early autophagosome in response to many autophagic stimuli.

A clearer picture is emerging of the function of the domains of Atg16L1 in canonical and selective forms of autophagy. Whilst the CCD is recruited to the site of the early autophagosome and is responsible for the autophagic activity of Atg16L1, there are additional functions of the linker and WD40 repeat domain, as indicated by the alteration in autophagosome behaviour in the deletion constructs and the CD-associated T316A mutant. As more interactions with Atg16L1 are characterised and published, the role of the linker and WD40 domain in canonical and selective autophagy will become more apparent.

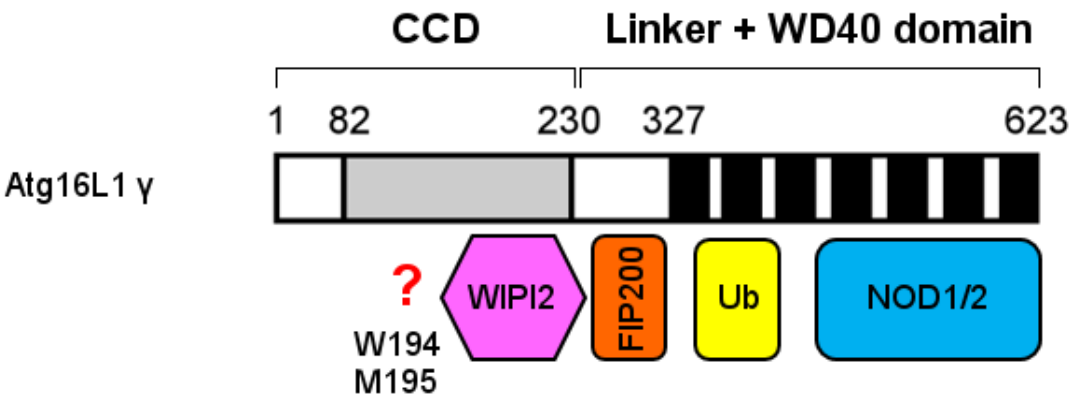

Figure 3.19 Schematic outline of proteins able to recruit Atg16L1 to autophagosomal/endosomal membranes. An unknown mechanism has been shown to affect the recruitment of Atg16L1 to the autophagosome in canonical and selective autophagy (Fujita et al., 2013).

Chapter 4:

Verification of a novel interaction between Atg16L1 and MEKK4

Chapter 4: Verification of a novel interaction between Atg16L1 and MEKK4

4.1 Chapter Aims

The aims of this chapter were to verify and characterise the novel interaction between Atg16L1 and the serine/threonine kinase MEKK4, an interaction that was intitially identified in a yeast two hybrid screen. Cell lines that stably express epitope tagged Atg16L1 and NOD2 for use in interaction studies are described. The interactions were investigated by immunoprecipitation and the cellular distribution observed by immunofluorescence microscopy. The proteins of interest were Atg16L1, Mekk4 and Nod2.

4.2 Introduction

To date, a number of proteins have been identified that interact with Atg16L1 (table 4.1). Those interactions that have been mapped to the N-terminus and the coiled-coil domain of Atg16L1 tend to be associated with canonical autophagy e.g. Atg5 and WIPI2 (Mizushima et al., 2003; Dooley et al., 2014). Interestingly, proteins which bind to the WD40 domain of Atg16L1 via the Atg16L1 interacting motif, identified by Boada-Romero et al in 2013 are involved in selective autophagy against intracellular pathogens e.g. Nod1/2 and TLR2.

As discussed in the previous chapter, there are a number of proteins that are capable of recruiting Atg16L1 to the autophagosome or endosomal membrane, however no molecular switch for autophagic activity of Atg16L1 has been identified. Interestingly, several serine phosphorylation sites within the linker region of Atg16L1 have been discovered, though their function is not known (Villén et al., 2007; Olsen et al., 2010).

Other components of the autophagy pathway have been shown to be tightly regulated by post-translational modifications. Under nutrient rich conditions, mTOR inhibits autophagy by phosphorylating the ULK complex, which contains ULK1/2, Atg13 and FIP200. (Hosokawa et al., 2009). Acetylation of Atg5, Atg7, Atg8 and Atg12 inhibits starvation induced autophagy (Lee and Finkel, 2009). Activity of Atg5 has been shown to be regulated by phosphorylation of a conserved threonine residue by p38 (Keil et al., 2012). Therefore, there is a possibility that Atg16L1 could be regulated by similar mechanisms during autophagy.

Table 4.1 A list of Atg16L1 interacting proteins determined from published data as of August 2014

Interacting protein	Region of Atg16L1 that binds to interacting protein	Species of Atg16L1 used in study	Function in Autophagy	Reference
Atg16L1	1-276	(*M.musculus)*	Atg16L1 homoligomerises via its coiled-coil domain (by similarity in yeast Apg16). Forms 800kDa complex with Atg5-12 conjugate.	Mizushima et al., 2003
Atg5	1-79 (N-term)	(*M.musculus)*	Atg5 is required for membrane targeting of Atg16L1	Mizushima et al., 2003
Rab33b	1-79 (N-term)	*M.musculus*	May be involved in modulation of autophagosome formation, though not during starvation induced autophagy.	Itoh et al., 2008.
NOD1	WD40 domain*	*H.sapiens*	Binds to Atg16L1 interacting motif (AIM). Is directed to site of bacterial entry by NOD1 and drives anti-bacterial autophagy to engulf pathogen.	Travassos et al., 2010. *Refined by Boada-Romero et al., 2013
NOD2	WD40 domain	*H.sapiens*	Binds to Atg16L1 interacting motif (AIM). Is directed to site of bacterial entry by NOD2 and drives anti-bacterial autophagy to engulf pathogen.	Travassos et al., 2010. *Refined by Boada-Romero et al., 2013
LC3B/GABARAP	Whole protein	*H.sapiens*	Interacts independently of LIR-LDS interface of LC3 (LC3-interaction region docking site). Atg16L1 known to specify site of LC3 lipidation and incorporation into autophagosome membrane.	Behrends et al., 2010.
Clathrin	2-77 (N-term)	*H.sapiens*	Atg16L1 interacts with clathrin heavy chain, and is involved in formation of early autophagosomes from plasma membrane precursors.	Ravikumar et al., 2010.
SNX18	Whole protein	Not cited	Recruits Atg16L1 to perinuclear recycling endosomes. Positive regulator of autophagy.	Knævelsrud et al., 2013.

Table 4.1 Continued

Interacting protein	Region of Atg16L1 that binds to interacting protein	Species of Atg16L1 used in study	Function in Autophagy	Reference
Human transmembrane protein 59 TMEM59	WD40 domain	*H.sapiens*	Identified Atg16L1 interacting motif (AIM). Promotes LC3 labelling of endocytic compartments and mediates autophagy in response to *Staphylococcus aureus* infection.	Boada-Romero et al., 2013.
Toll-like receptor 2 TLR2	WD40 domain	*H.sapiens*	Interacts via AIM. Is known to promote labelling of endocytic/phagocytic compartments with LC3	Boada-Romero et al., 2013.
FIP200	E235 D237 D238 D239 E241	*M.musculus*	Charge mutations from acidic residues to arginine weakened FIP200 binding. Was thought to regulate targeting of Atg16L1 to membrane, but this has been attributed to an interaction with WIPI2. However, other research has shown a role for FIP200 in targeting Atg16L1 to ubiquitinated endosomal membranes	Gammoh et al., 2013 Nishimura et al., 2013 Fujita et al., 2013 Dooley et al, 2014^ ^most recent and accurate data
Ubiquitin	WD40 domain	*H.sapiens*	Targets Atg16L1 to ubiquitin decorated endosomes containing pathogens/phagocytosed beads coated with transfection reagents.	Fujita et al., 2013.
WIPI2	E226 E230	*M.musculus*	Recruits Atg16L1 to site of early autophagosome formation. Required for both starvation induced autophagy and clearance of *Salmonella Typhimurium*.	Dooley et al., 2014
BTD **AVIL** **GARS** **CALU** **NOC1**	Whole protein	*H.sapiens*	Identified in a quantitative proteomics screen. siRNA depletion shows reduced LC3–Salmonella colocalization and intracellular bacterial replication assays, suggesting roles for these genes in antibacterial autophagy. Other proteins have been identified in this screen but not included in this table as they were not analysed.	Lassen et al., 2014

To identify novel protein interactions with Atg16L1 which may be responsible for the regulation of Atg16L1 activity, a yeast-two-hybrid screen was carried out using mouse Atg16L1 γ as bait against a human colon cDNA library. An interaction with a good confidence level was found for the protein MEKK4. MEKK4 belongs to the sterile (Ste) serine/threonine protein kinase family and is a member of the MAPK kinase kinase subfamily.

MEKK4 is a mitogen activated protein kinase kinase kinase (MAP3K), and is also referred to as MAP3K4, and MTK1. MEKK4 is involved in stress activated mitogen protein kinase pathways (SAPK), which enables cells to respond to life death decisions in the face of extra-cellular stress, e.g. physical stress such as UV radiation or biological stress such as DNA damage or cytokines (Miyake et al., 2007, Bettinger and Amberg., 2007). It consists of an N terminal autoinhibitory domain and C-terminal kinase domain (Takekawa et al., 1997; Gerwins et al., 1997). The MAP3Ks facilitate downstream signalling by activating an intermediate MAP kinase kinase (MAP2K) by phosphorylation, which subsequently phosphorylate and activate their target MAP kinase (Fig. 4.1). Similar to other MAP3Ks, MEKK4 activation is regulated by the release of autoinhibition, allowing MEKK4 to go from a closed to an open conformation (Miyake et al., 2007). One of the most characterised activators of MEKK4 is the GADD45 (growth arrest and DNA damage inducible) family of proteins, which bind to the N-terminus of MEKK4 and trigger the release of autoinhibition. Full activation is achieved when MEKK4 homodimerises and transautophosphorylates, allowing it to phosphorylate downstream targets. MEKK4 has been shown to phosphorylate various MAP2Ks, including MKK4 and MKK6, which function in both the p38 and JNK pathways (Gerwins et al., 1997, Takekawa et al., 1997). Recently, MEKK4 has been linked to autophagy regulation. The GADD45β-MEKK4-p38 pathway was shown to direct phosphorylated p38 to autophagosomes, where a subsequent interaction between p38 and Atg5 lead to inhibition of autophagy (Keil et al., 2012). However a specific role for MEKK4 in the regulation of autophagy has not been described.

MEKK4 has also been shown to play a key role in the NOD2 pathway, by binding the effector kinase RIP2 and preventing NOD2 signalling (Clark et al., 2008; Fig. 4.2a-b). The interaction between ATG16L1 and NOD2 has been investigated in the context of selective autophagy and the CD associated mutations in these two genes (Travassos et al., 2010; Sorbara et al., 2013). Activation of NOD receptors by bacterial cell wall peptidoglycan results in the activation of autophagy (Travassos et al., 2010, Cooney et al., 2010; Homer et al, 2010). ATG16L1 can specifically regulate NOD-driven cytokine responses, with knockdown of ATG16L1 but not ATG5 leading to up regulation of cytokine production (Sorbara et al.,

2013). Furthermore, ATG16L1 can inhibit polyubiquitination of RIP2, the mechanism by which activation of RIP2 is controlled. As yet, the precise molecular mechanism that governs the activation of NOD2 directed autophagy is unclear. The CD associated ATG16L1 mutant has been reported as defective in selective autophagy against intracellular pathogens (Kuballa et al., 2008; Travassos et al., 2010), though retains the ability to bind NOD2. Therefore a proximity model of activation cannot be solely responsible for ATG16L11 activation following NOD2 stimulation. Further post-translational modification of ATG16L1 might be required, with MEKK4 a likely candidate for crosstalk between the autophagy and NOD signalling pathways.

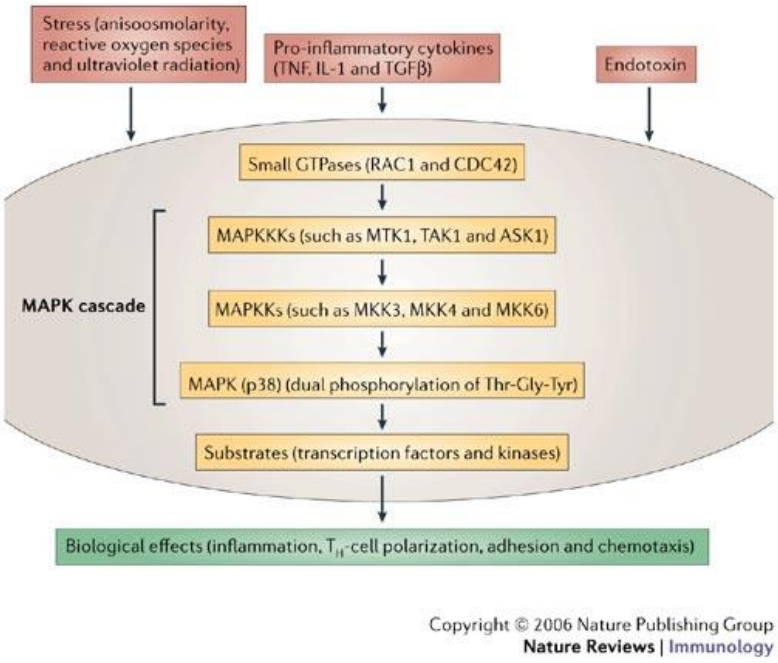

Figure 4.1 The MAPK signalling cascade. Activation of MAP3Ks by small GTPases in response to a variety of extracellular stresses. MAP3Ks phosphorylate and activate MAP2Ks that subsequently phosphorylate and activate MAPKs (only p38 shown). Modified from Ashwell (2006).

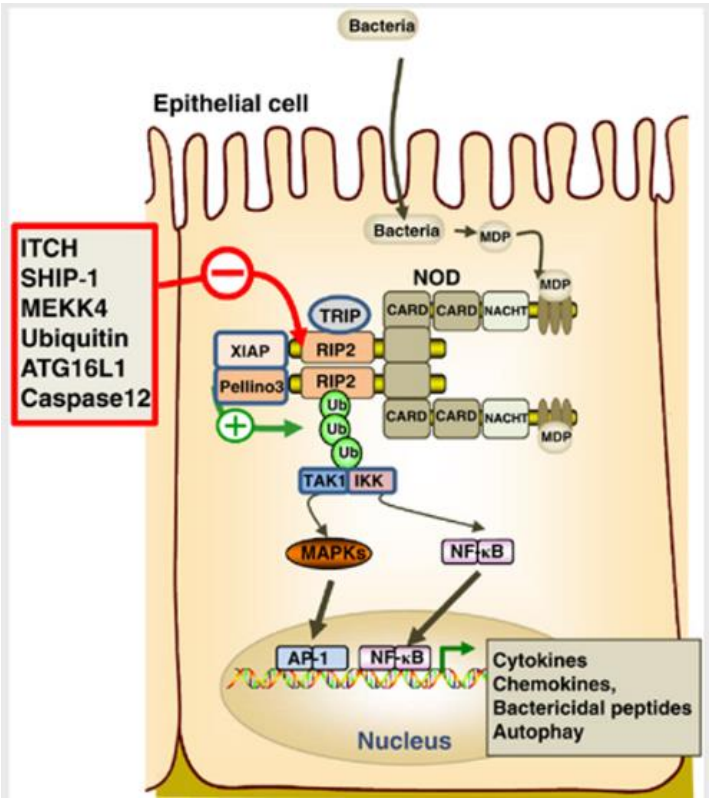

A

Figure 4.2 Diagrammatic representation of the interactions and regulators of Nod2 signalling

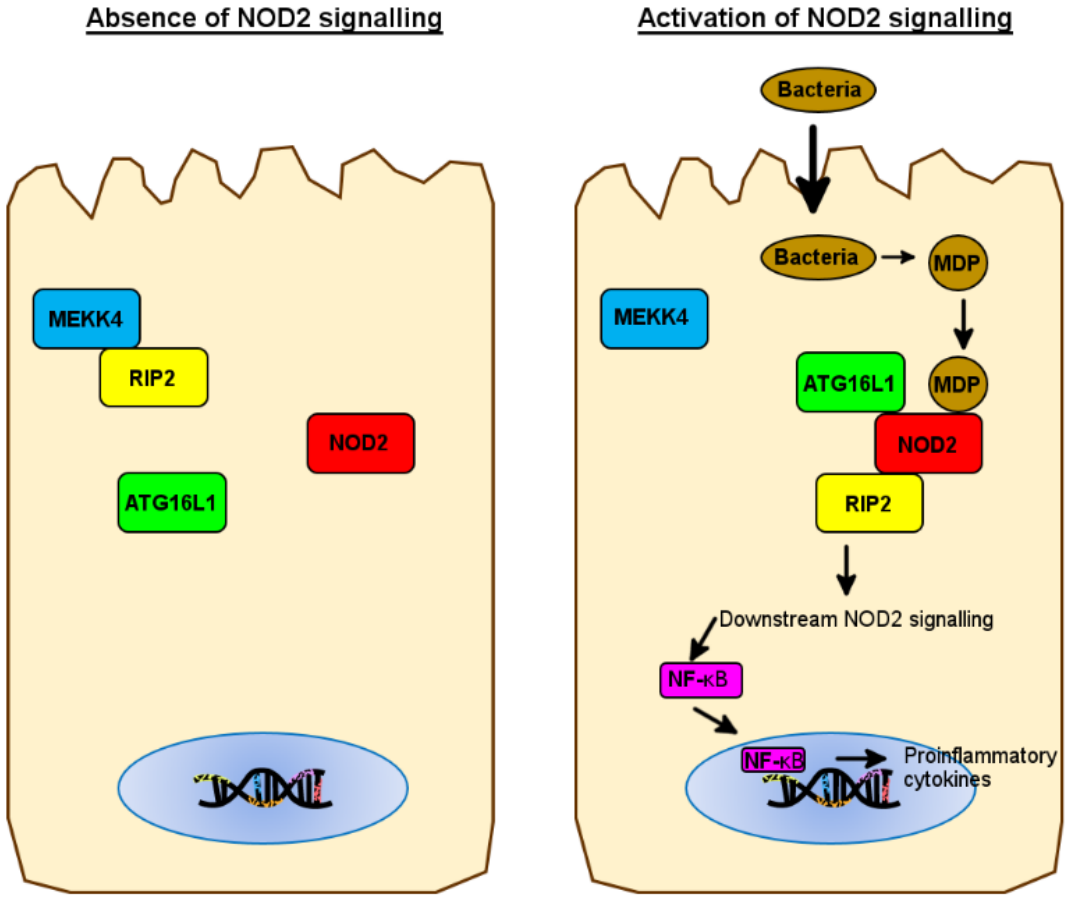

Figure 4.2 Continued

(A) Bacterial invasion of epithelial cells results in the stimulation of NOD2 proteins by peptidoglycan-derived peptides such as MDP. Once activated, NOD2 undergoes homoligomerisation via the NACHT/NOD domain. RIP2 is recruited via homotypic CARD:CARD interactions, followed by binding of TRIP protein to RIP2 and XIAP and Pellino3-mediated polyubiquitination of RIP2. The results in recruitment of TAK1 and IKK complexes and downstream activation of NF-κB, MAPKs and AP-1, driving the expression of proinflammatory responses. ATG16L1 negatively regulates NOD2 signalling by interfering with the polyubiquitination of RIP2 and the recruitment of RIP2 into NOD-signalling complexes. MEKK4 also negatively regulates NOD2 signalling by sequestering RIP2 and preventing the formation of the NOD2:RIP2 complex

(B) Established interactions between MEKK4, NOD2, ATG16L1 and RIP2 in the context of bacterial invasion. In the absence of NOD2 activation, MEKK4 is bound to RIP2 and NOD2 is inactive. When NOD2 is active, it undergoes a conformational change allowing it to outcompete MEKK4 for RIP2 binding (Clark et al., 2008). ATG16L1 is also bound to NOD2 and is recruited to the site of bacterial entry (Travassos et al., 2010). Modified from Humphries et al. (2014).

4.3 Results

4.3.1 Yeast two hybrid screen identifies MEKK4 as a novel binding partner of Atg16L1

To identify novel protein interactions with ATG16L1, a yeast-two-hybrid screen was carried out with the aid of Hybrigenics Global PBS®. The bait protein, Mus musculus ATG16L1γ was screened against a human colon cDNA library, to identify interactions likely to occur in the gut epithelium. Positive interactions were identified, analysed and assigned a grade to indicate confidence in the interaction. An interaction with a good confidence level was found for the protein MEKK4. To verify MEKK4 as a binding partner of Atg16L1, cell lines that constitutively express Atg16L1 and or NOD2 had to be generated for use in immunoprecipitation experiments.

4.3.2 Generation of Atg16L1-GFP and NOD2-HA episomal vector constructs

The conditions under which MEKK4 binds Atg16L1 are unknown. Transient transfection is known to activate autophagy (Roberts et al., 2013), with transfection of NOD known to activate downstream NOD signalling (Inohara et al., 2000). To overcome these issues, and to ensure even expression of two plasmids in the same cells, an episomal expression system was utilised.

The two episomal vectors used in this project were pCEP-Pu, which contains a puromycin resistance gene, and pCEP4 (Invitrogen) which contains a hygromycin resistance gene. The episomal expression vectors utilise the Epstein-Barr virus replication origin (oriP) and nuclear antigen (EBNA-1) to maintain extrachromasomal replication of the plasmid within cells (Craenenbroeck et al., 2000). This system allows a high transfection efficiency, with stable protein expression maintained by selective antibiotics, without chromosomal integration into the host cell genome (Belt et al., 1991; Craenenbroeck et al., 2000).

The Atg16L1-GFP sequence was cloned into the pCEP-Pu vector as follows. The 3'-end of Atg16L1-GFP was digested with NotI, then blunted with a Klenow reaction. The 5'-end of Atg16L1-GFP was digested with NheI in a separate reaction, to generate the Atg16L1-GFP insert. To prepare the pCEP-Pu vector, the MCS was digested with XhoI, then blunted with a Klenow reaction. A second digest with NheI was carried out on pCEP-Pu, and the Atg16L1-GFP fragment ligated into the plasmid. This resulted in the generation of full length Atg16L1-GFP in the episomal vector pCEP-Pu.

The NOD2-HA plasmid was a kind gift from Prof. Dana Philpott (UT, Canada). The NOD2-HA sequence was cloned into the pCEP4 vector as follows. The NOD2-HA fragment was generated by restriction digestion with NheI and XhoI. This was ligated into the MCS of pCEP4, which was digested with NheI and XhoI to create compatible ends. This resulted in the generation of NOD2-HA in the episomal vector pCEP4.

4.3.3 Generation of stable HEK293 episomal cell lines

To generate stable episomal cell lines, the pCEP-Pu-Atg16L1-GFP or pCEP4-NOD2-HA vectors were transfected into HEK293 cells. Two days post transfection, media containing a pre-determined concentration of antibiotics (10 µg/ml puromycin or 200 µg/ml hygromycin) was added to the cells and changed every 3-4 days until antibiotic resistant colonies were identified. These colonies were picked and expanded until enough cells were available for analysis. This process of transfection and selection was repeated with cells that were positive for pCEP4-NOD2-HA, to transfect and select for pCEP-Pu-Atg16L1-GFP. This resulted in the generation of the following cell lines; HEK293 Atg16L1-GFP, HEK293 NOD2-HA and HEK293 Atg16L1-GFP & NOD2-HA.

4.3.4 Confirmation of Atg16L1-GFP and NOD2-HA expression in episomal cell lines by immunofluorescence

The subcellular localisation of the proteins encoded in the episomal vectors and their ability to respond to key signalling pathways are indicators of how well they are expressed by the episomal vector. The episomal cell line HEK293 Atg16L1-GFP was cultured in nutrient rich medium or media with Torin1 to induce autophagy, and stained for the autophagosome markers WIPI2 and LC3. The HEK293 NOD2-HA cells were cultured in supplemented medium alone, or media with 10 µg/ml muramyl di-peptide (MDP), a NOD2 agonist, to induce NOD2-directed autophagy. The cells were stained for HA and the autophagosome marker LC3. The HEK293 Atg16L1-GFP cell line was able to respond to the induction of autophagy with the formation of GFP positive puncta which co-localised with WIPI2 and LC3 (Fig 4.3). The HEK293 NOD2-HA cells were able to respond to the presence of MDP with an increase in the number of LC3 puncta (Fig 4.4). The subcellular distribution of NOD2 is consistent with that reported in the literature, which is mainly cytosolic, with a fraction located at the plasma membrane (Barnich et al., 2005).

The ability of the HEK293 Atg16L1-GFP & NOD2-HA cell line to respond to both starvation induced autophagy and NOD2-directed autophagy was tested and quantified by Imaris, to determine how suitable these cells were for analysis during autophagy. Both 10 µg/ml and 20 µg/ml MDP were used, based on earlier papers (Clarke et al., 2008; Travassos et al., 2010; Homer et al., 2010). The formation of autophagosomes was followed over 6 hours at the indicated time points, and the autophagosomes stained with LC3. The HEK293 Atg16L1-GFP & NOD2-HA cell line was able to respond to starvation induced autophagy and NOD2 activation by generating Atg16L1 puncta and LC3 puncta (Fig 4.5). The LC3 puncta were quantified by Imaris, which showed that for starvation induced autophagy, LC3 puncta after 60 min starvation increased over 4 h, but then reduced slightly after 6 h (Fig 4.6). For treatment with 10 µg/ml MDP, an increase in LC3 puncta was seen after 30 min, and a small increase was only seen after 4 hrs (Fig 4.6). When cells were treated with 20 µg/ml MDP, a higher number of LC3 puncta were observed after 30 min compared to the 10 µg/ml MDP treatment. However, this level decreased and never reached the level obtained with treatment of cells with 10 µg/ml MDP for the rest of the time course, with the exception of the 90 min time point (Fig 4.6). Based on these results, the 10 µg/ml concentration was chosen for future experiments focussing on NOD2 activation in the context of autophagy, and the time points of 2h and 4h for both starvation induced and NOD2-directed autophagy were chosen as points of interest for future experiments.

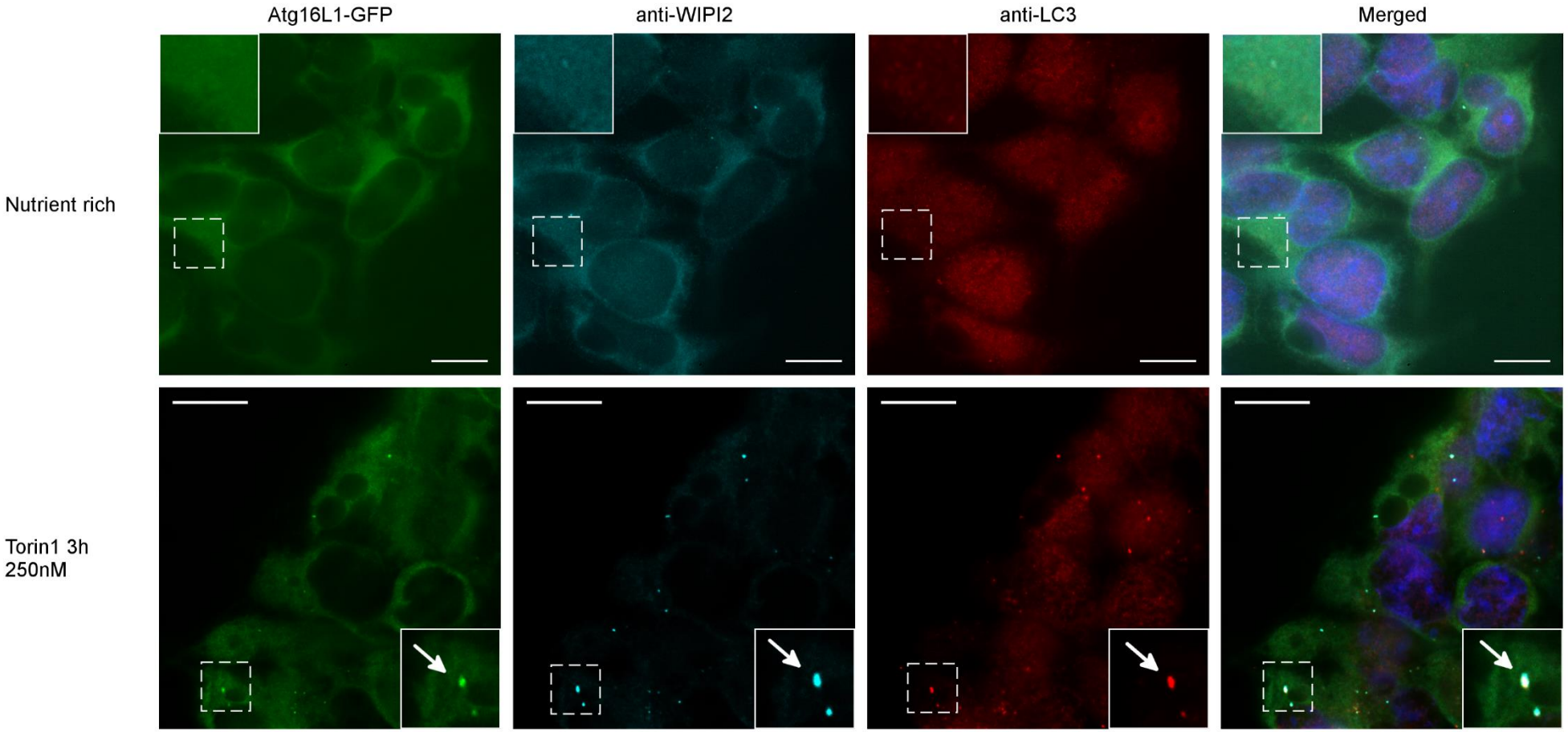

Figure 4.3 The HEK293 Atg16L1-GFP episomal cell line is able to respond to autophagy induced by Torin1. The episomal cells were stained for WIPI2 (false colour cyan, Alexa 647) and LC3 (red Alexa 594) to mark autophagosomes. The nuclei were stained with DAPI. Cells were fixed with methanol and viewed by widefield fluorescence microscopy.Regions of interest highlighted with dashed boxes, co-localised autophagosomes indicated with arrows. Scale bars, 10 μm.

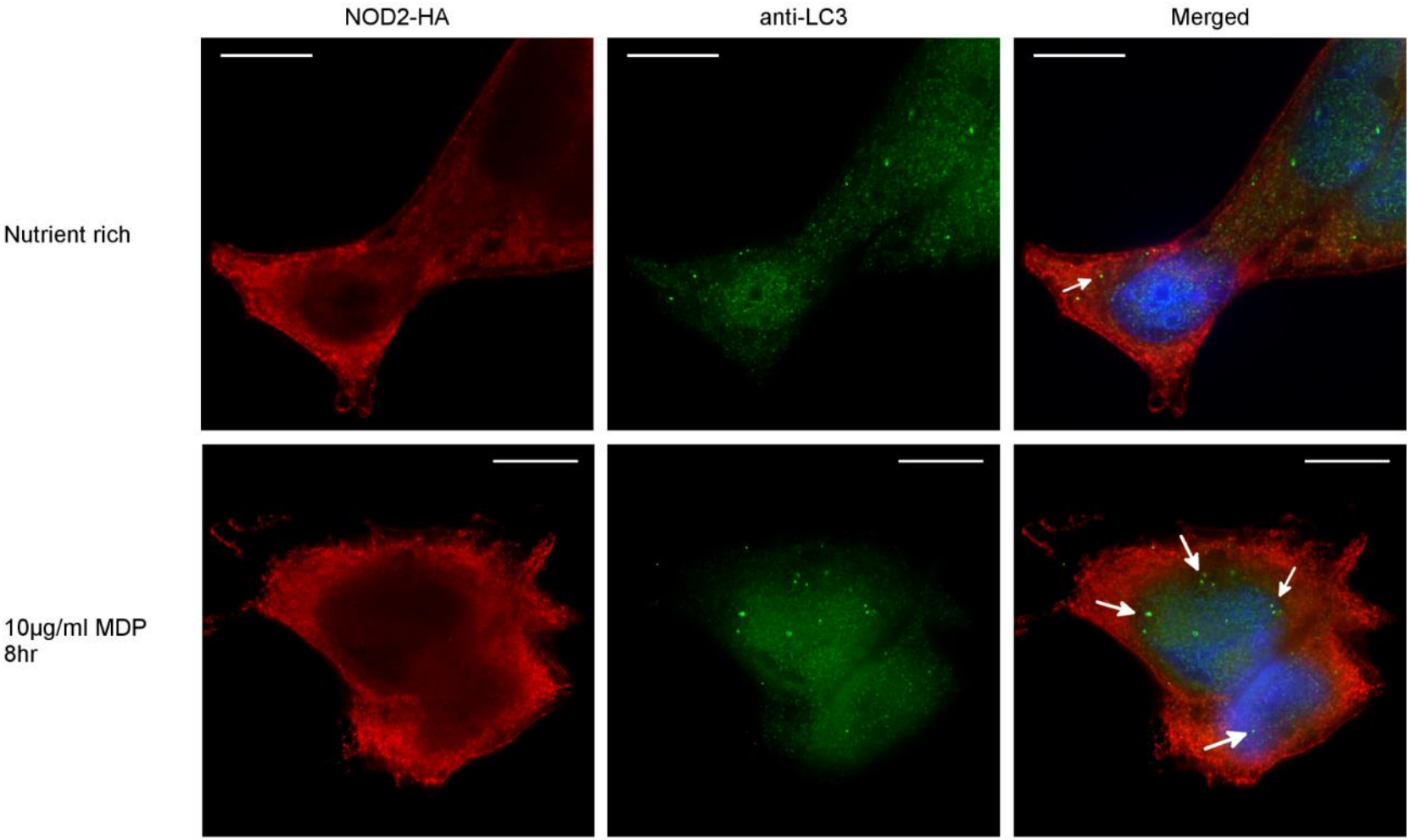

Figure 4.4 The HEK293 NOD2-HA episomal cell line is able to respond to MDP stimulation and activate autophagy. NOD2-HA was visualised by staining with HA (red Alexa 594) and autophagosomes by LC3 (green Alexa 488). Cells were fixed with methanol and viewed by widefield fluorescence microscopy. Scale bars, 10 µm.

4.3.5 Expression and retention of Atg16L1-GFP and NOD2-HA in episomal cell lines by Western blotting

Antibiotic selection is the primary method used to maintain the expression of proteins encoded in the Atg16L1-GFP and NOD2-HA episomal vectors. However, removal of the selective antibiotic is required when transfecting other plasmids e.g. Mekk4-HA.

To show that the episomal cells could retain the plasmids in the absence of the antibiotic (which has been reported by Sclimenti et al., 1998 and Yates et al., 1985), the selective antibiotic media was replaced with supplemented media for 1 or 3 days. This was the maximum length of time prior to cell lysis and subsequent immunoprecipitation experiment, hence why this time point was chosen. Lysates were collected and analysed by Western blotting. After three days without antibiotic selection Atg16L1-GFP could be detected in both episomal cell lines, and NOD2-HA could be detected in HEK293 Atg16L1-GFP NOD2-HA cells (Fig 4.7). This confirms that the episomal vectors are retained and expressed following the removal of selective antibiotics.

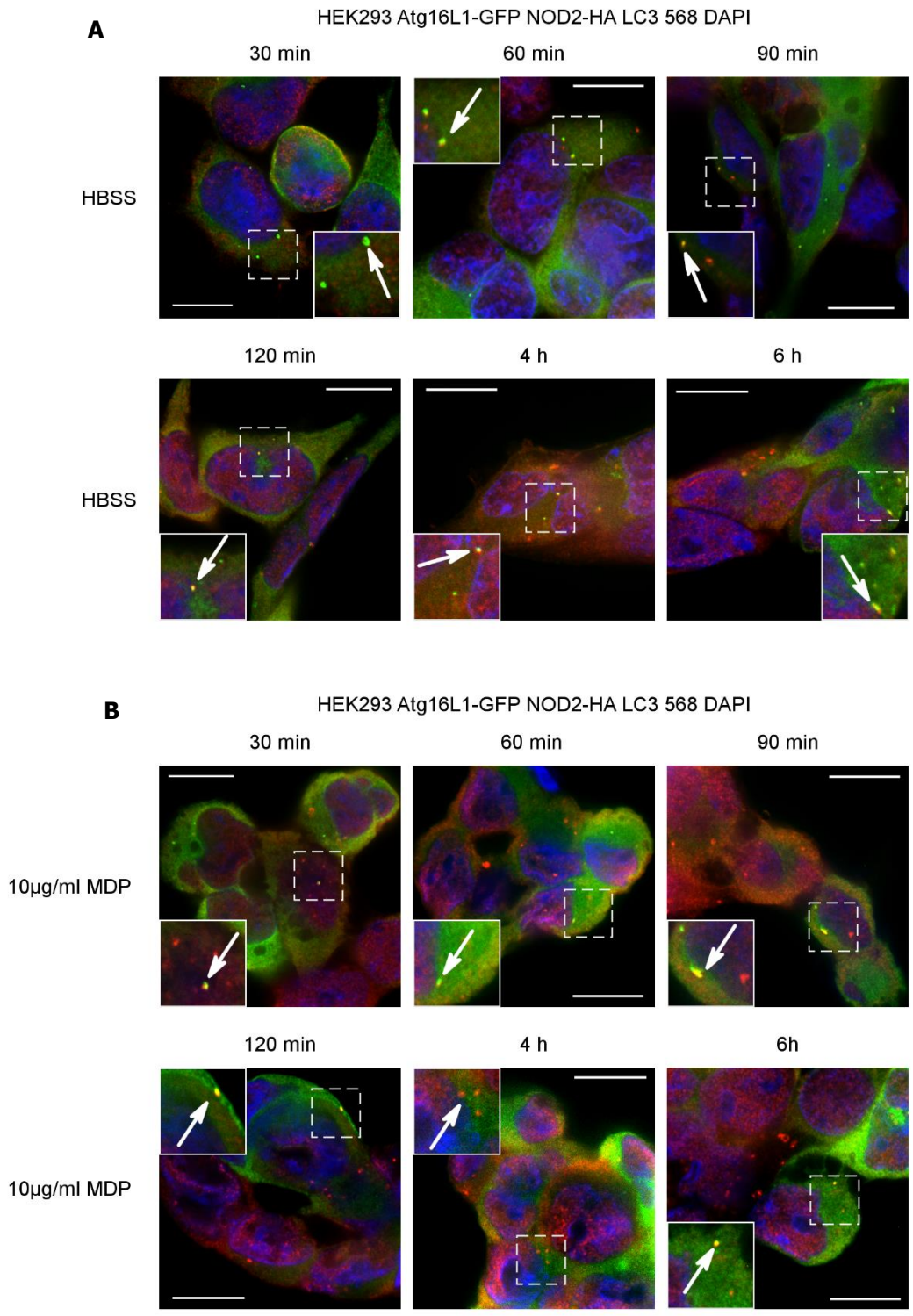

Figure 4.5 HEK293 Atg16L1-GFP & NOD2-HA cells are able to form autophagosomes in response to autophagy induction. Cells were cultured in HBSS (a) or supplemented media with MDP (b) and (c) at the specified concentration. Cells were fixed at the specified time point and stained for NOD2-HA (not shown) and LC3 (red Alexa 568). Atg16L1-GFP is in green, and the nuclei were stained with DAPI (blue). Regions of interest are highlighted with boxes, and arrows indicate Atg16L1 puncta that colocalise with LC3. Part (c) is continued on the next page. Scale bars, 10 µm.

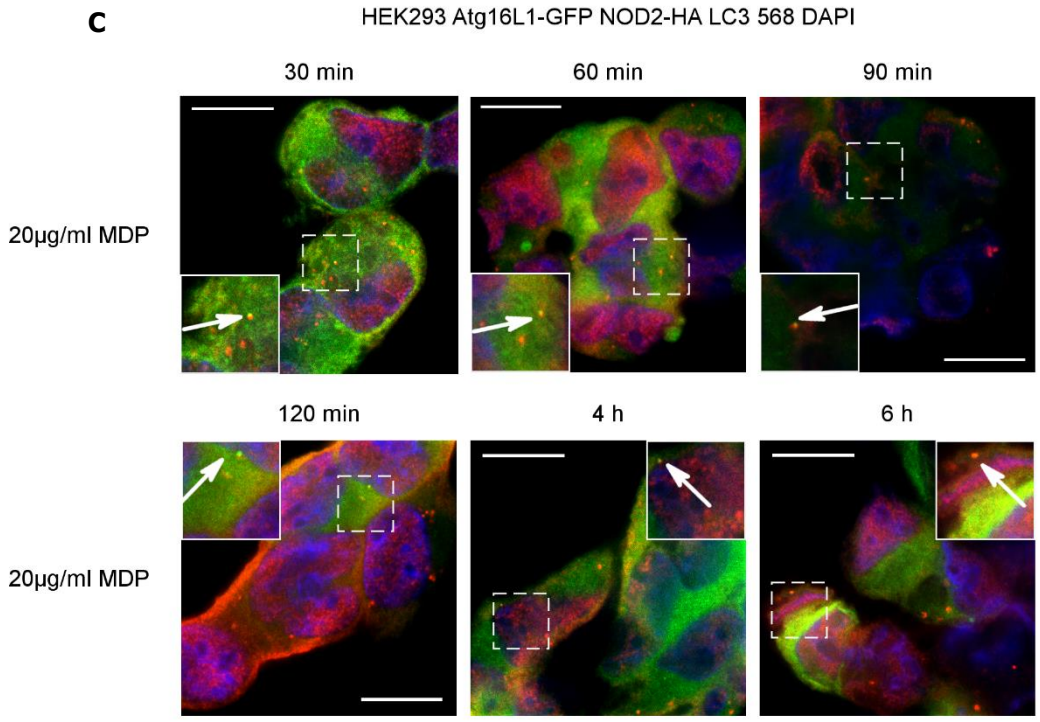

Figure 4.5 (c) HEK293 Atg16L1-GFP & NOD2-HA cells are able to form autophagosomes in response to autophagy induction. Cells were cultured in supplemented media with MDP (c) at the specified concentration. Cells were fixed at the specified time point and stained for NOD2-HA (not shown) and LC3 (red Alexa 568). Atg16L1-GFP is in green, and the nuclei were stained with DAPI (blue). Regions of interest are highlighted with boxes, and arrows indicate Atg16L1 puncta that colocalise with LC3. Scale bars, 10 µm.

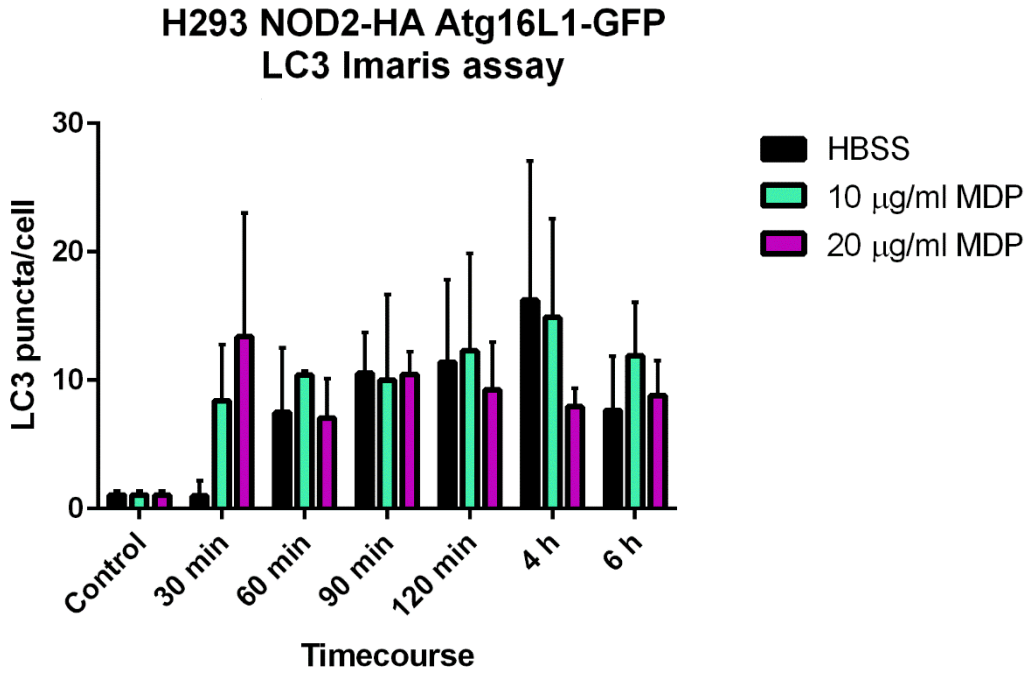

Figure 4.6 Analysis of the HEK293 Atg16L1-GFP & NOD2-HA episomal cell time course. The images from the experiments in figure 4.5 were analysed by Imaris to determine the number of LC3 puncta per cell.

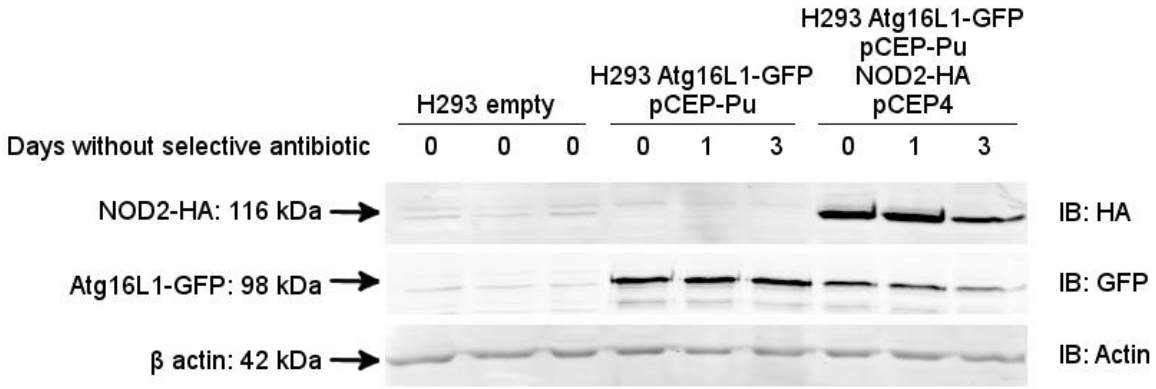

Figure 4.7 Atg16L1-GFP and NOD2-HA are retained in HEK293 episomal cells after removal of selective antibiotics.

Lysates from HEK293 Atg16L1-GFP and HEK293 Atg16L1-GFP & NOD2-HA episomal cells were analysed by SDS-PAGE and immunoblotting after being cultured without selective antibiotic for 0, 1 or 3 days.

4.3.6 Verification of interaction between Atg16L1-GFP and Mekk4-HA

To confirm the results of the yeast-two-hybrid screen, a co-immunoprecipitation was carried out. For this the HEK293 Atg16L1-GFP episomal cell line was transfected with HA-tagged Mekk4 from *Mus musculus*. Atg16L1-GFP was immunoprecipitated from cell lysates with antibodies against GFP. Western blotting with antibodies specific for HA then confirmed the findings of the yeast-two-hybrid screen that Mekk4-HA was bound to Atg16L1-GFP (Fig. 4.8).

4.3.7 Atg16L1 binds Mekk4 during starvation induced autophagy, but does not localise to the autophagosome

To further determine the functional role of this interaction, the effect of autophagy activation on the interaction between Mekk4 and Atg16L1 was investigated. Mekk4-HA was transfected into HEK293 Atg16L1-GFP episomal cells, which were cultured in nutrient rich conditions, or deprived of amino acids to induce autophagy, and a co-immunoprecipitation was carried out. As before, in the absence of autophagy, Mekk4 was bound to Atg16L1. When autophagy was induced through amino acid starvation in HBSS, Mekk4 remained bound to Atg16L1 (Fig. 4.9). Next, the cellular localisation of Mekk4 and Atg16L1 was observed, to determine whether Mekk4 translocates to the early autophagosome with Atg16L1. To study autophagy activation following starvation or NOD2 activation, Vero cells were used as they are able to form LC3 puncta in response to MDP. Vero cells were cotransfected with Mekk4-HA and Atg16L1-GFP, and autophagy induced by amino acid starvation or 10 µg/ml MDP. When cultured in nutrient rich conditions, both Atg16L1 and Mekk4 appeared diffuse in the cytoplasm and showed some co-localisation (Figure 4.10), indicating they are either bound, or that they may localise to the same subcellular structure within the cytosol, which could be the endoplasmic reticulum or cytoskeleton. When autophagy was induced by amino acid starvation or NOD2 activation through MDP, Atg16L1-GFP formed puncta, which were negative for Mekk4-HA. Some of the Atg16L1 puncta did co-localise with LC3, confirming the presence of autophagosomes. However, there was still co-localisation between Mekk4-HA and Atg16L1-GFP in the cytoplasm during autophagy (Fig. 4.10). This suggests that the Atg16L1:Mekk4 complex does not localise to autophagosomes and may not directly contribute towards the autophagosome development, though Mekk4 may bind the cytosolic fraction of Atg16L1 that does not take part in autophagy.

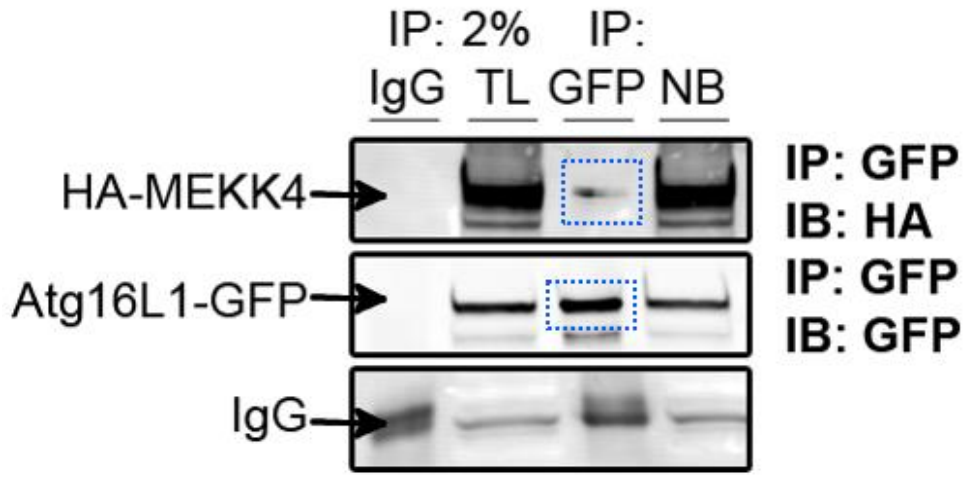

Figure 4.8 Atg16L1-GFP binds Mekk4-HA in HEK293 cells

Mekk4-HA was transiently expressed in HEK293 Atg16L1-GFP episomal cells, the lysate collected and the complex immunoprecipitated with anti GFP antibody. The proteins were separated by SDS-PAGE. Mekk4-HA binding was analysed by immunoblotting with antibodies against GFP and HA. Mekk4-HA was shown to bind Atg16L1-GFP (highlighted with blue boxes).

IP = immunoprecipitation. TL = total lysate. NB = non bound protein. IB = immunoblot.

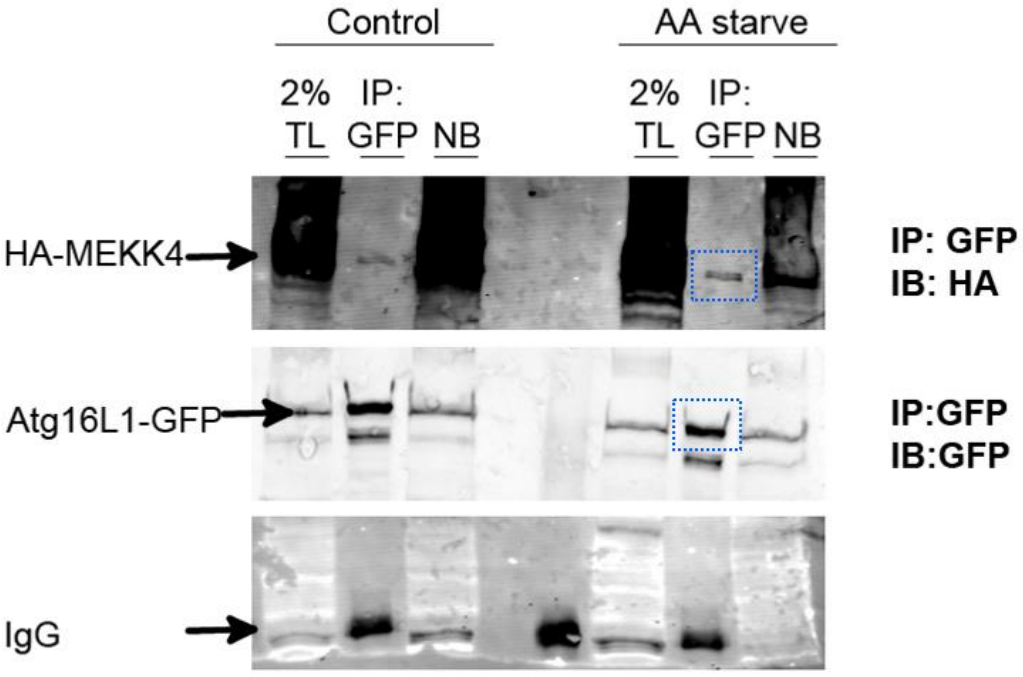

Figure 4.9 Atg16L1-GFP binds Mekk4-HA during starvation induced autophagy in HEK293 cells

Mekk4-HA was transiently expressed in HEK293 Atg16L1-GFP episomal cells, which were cultured in nutrient rich media or HBSS for 2h to induce autophagy. The lysate was collected and the complex immunoprecipitated with anti GFP antibody. The proteins were separated by SDS-PAGE. Mekk4-HA binding was analysed by immunoblotting with antibodies against GFP and HA. Mekk4-HA was shown to bind Atg16L1-GFP after activation of autophagy by starvation (highlighted with blue boxes).

IP = immunoprecipitation. TL = total lysate. NB = non bound protein. IB = immunoblot.

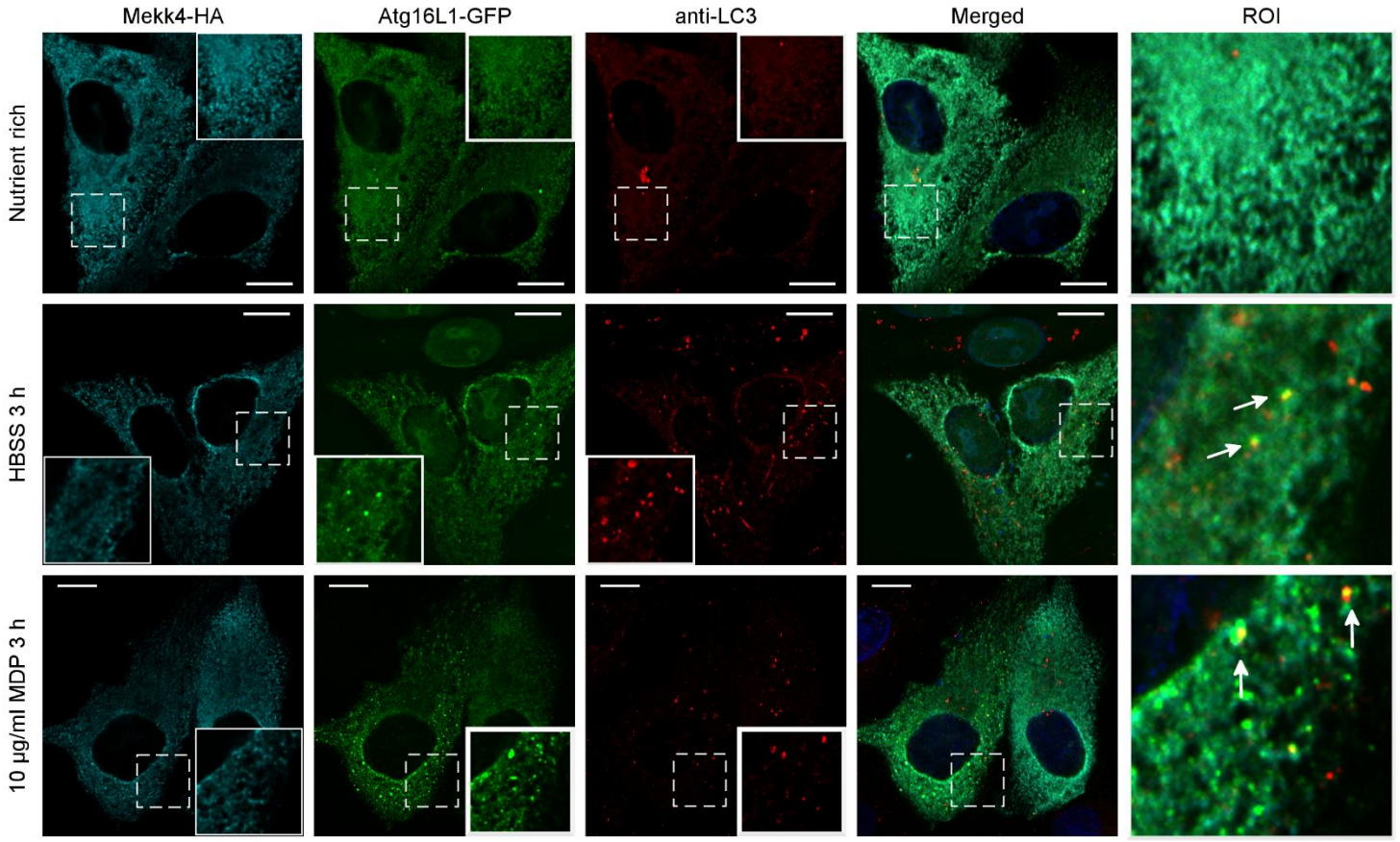

Figure 4.10 Subcellular distribution of Atg16L1-GFP and HA-MEKK4 in Vero cells
Atg16L1-GFP and Mekk4-HA (far red Alexa 647, false coloured cyan) were co-expressed in HeLa cells to observe their subcellular localisation. Both Atg16L1 and MEKK4 show an even cytosolic distribution and are absent from the nucleus. In nutrient rich conditions, there is colocalisation between Atg16L1-GFP and Mekk4-HA in the cytosol. Activation of autophagy by HBSS or MDP results in Atg16L1-GFP and LC3 positive puncta (red Alexa 594) which are negative for Mekk4-HA. Scale bars 10 µm

4.3.8 Mekk4 binds the linker region of Atg16L1

The results of the yeast-two-hybrid screen do not detail where Mekk4 binds to Atg16L1. Understanding the regions of Atg16L1 required for Mekk4 binding could help elucidate the function of the Atg16L1-Mekk4 interaction. To investigate this, the Atg16L1 deletion mutants CCD-GFP, CCD+L-GFP, L+WD40-GFP or WD40-GFP (chapter 3; figure 3.2 and 3.4 for details) were co-transfected with Mekk4-HA in HEK293 cells. Reciprocal immunoprecipitations were carried out with either Mekk4-HA or GFP tagged Atg16L1 deletion constructs precipitated from the lysates, and binding assayed by Western blotting. The CCD+L-GFP but not the CCD-GFP domain was able to bind to Mekk4-HA (Fig. 4.11 and 4.12). Similarly, the WD40-GFP alone was unable to bind Mekk4-HA, but addition of the linker region to the WD40 domain enabled L+WD40-GFP to bind Mekk4-HA (Fig. 4.11 and 4.12). Though the interactions were weak, as suggested by the intensity of the bands in Fig 4.11 and 4.12, they were consistent. This suggests that the linker region of Atg16L1 is responsible for the binding of Atg16L1 to Mekk4. To see whether the Atg16L1 binding motif identified by Boada-Romero et al (2013) was present in Mekk4, the motif ([YW]-X($_{2,6}$)-[ED]-X($_{2,6}$)-[YWF]-X$_2$-L) was run against multiple Mekk4 sequences across different species using the Prosite algorithm. The results of this search confirmed the presence of the motif in the N-terminus of Mekk4, and the conservation of this motif among higher eukaryotes (Fig 4.13).

4.3.9 The Atg16L1 mutants T316A and S305A are able to bind Mekk4

The CD risk associated mutation T316A and the putative phosphorylation defective S305A mutations lie within the linker region of Atg16L1. To determine whether these mutations affected the interaction between Atg16L1 and Mekk4, Atg16L1-GFP, Atg16L1-T316A-GFP or Atg16L1-S305A-GFP (chapter 3; figure 3.2 and 3.6 for details) were co-expressed with Mekk4-HA in HEK293 cells. Mekk4-HA was immunoprecipitated from the lysate and binding of Atg16L1 mutants assayed by Western blotting. Both the CD associated T316A mutant and the S305A mutant retained the ability to bind Mekk4-HA (Fig. 4.14), indicating that these residues are not essential for the interaction between Atg16L1 and Mekk4. However, further reciprocal immunoprecipitations are required to confirm that these residues are not required for the interaction with Mekk4, as the quality of the interaction in Fig 4.14 was not to a high standard.

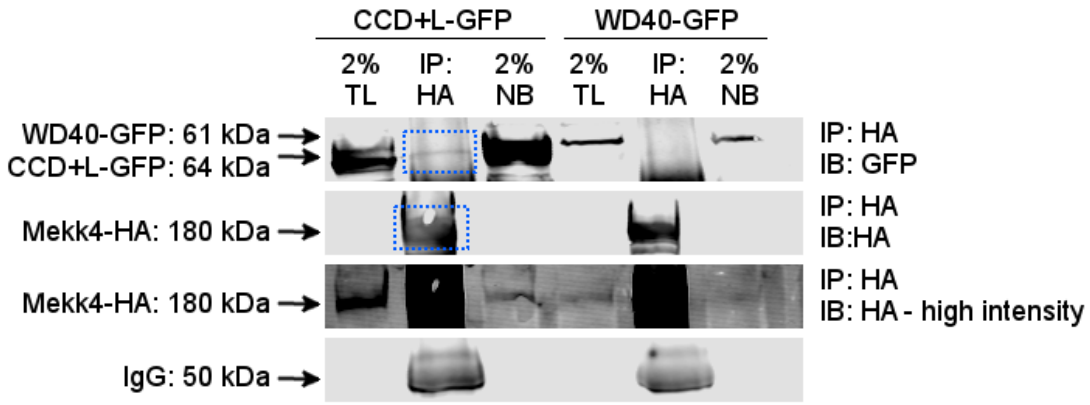

Figure 4.11 The CCD+L of Atg16L1 binds Mekk4

The CCD+L-GFP or WD40-GFP domains of Atg16L1 were transiently co-expressed with Mekk4-HA in HEK293 cells. The lysate was collected and the complex immunoprecipitated with anti HA antibody. The proteins were separated by SDS-PAGE. Domain binding was analysed by immunoblotting with antibodies against GFP and HA. The CCD+L was shown to bind Mekk4-HA (highlighted with blue boxes), and the WD40 domain was unable to bind Mekk4.

IP = immunoprecipitation. TL = total lysate. NB = non bound protein. IB = immunoblot.

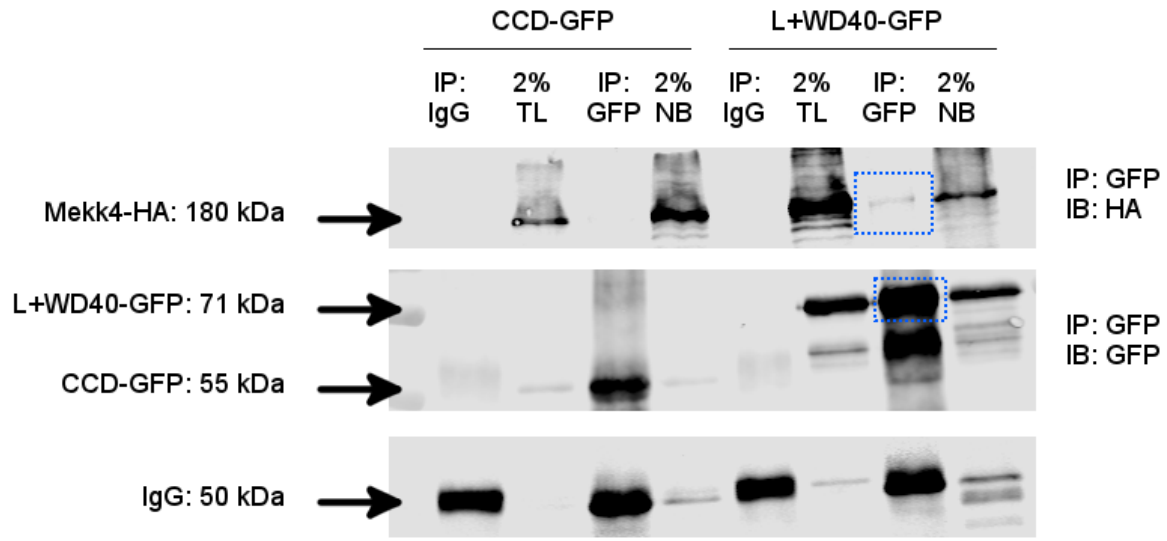

Figure 4.12 The L+WD40 of Atg16L1 binds Mekk4

The CCD-GFP or L+WD40-GFP domains of Atg16L1 were transiently co-expressed with Mekk4-HA in HEK293 cells. The lysate was collected and the complex immunoprecipitated with anti GFP antibody. The proteins were separated by SDS-PAGE. Domain binding was analysed by immunoblotting with antibodies against GFP and HA. The L+WD40 was shown to bind Mekk4-HA (highlighted with blue boxes), and the CCD domain was unable to bind Mekk4. A crosslinker was used to stabilise this interaction.

IP = immunoprecipitation. TL = total lysate. NB = non bound protein. IB = immunoblot.

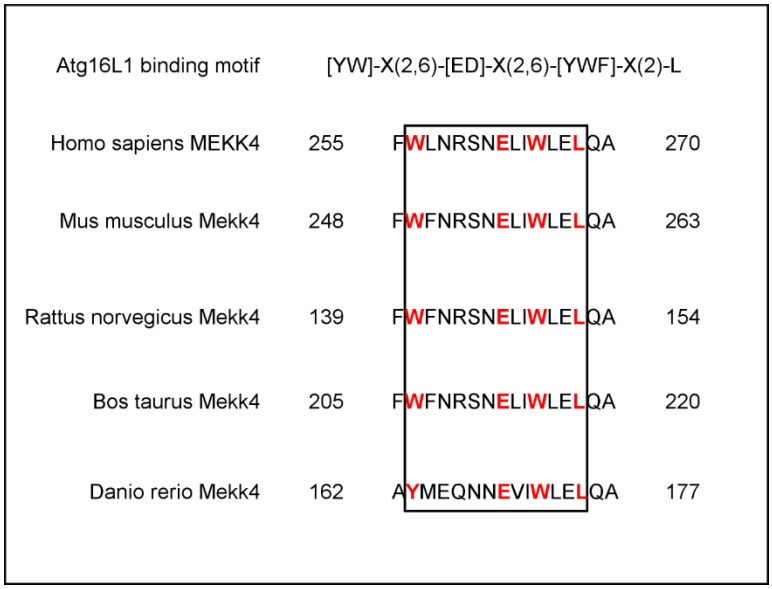

Figure 4.13 Conservation of the Atg16L1 binding motif in Mekk4

The amino acid sequences of Mekk4 from various higher eukaryotes were analysed using the Prosite Scan algorithm, to identify Atg16L1 binding motifs. In bold and red typeface are the residues consistent with the Atg16L1 binding motif published by Boada-Romero et al (2013). This shows evolutionary conservation of the Atg16L1 binding motif in this region of Mekk4.

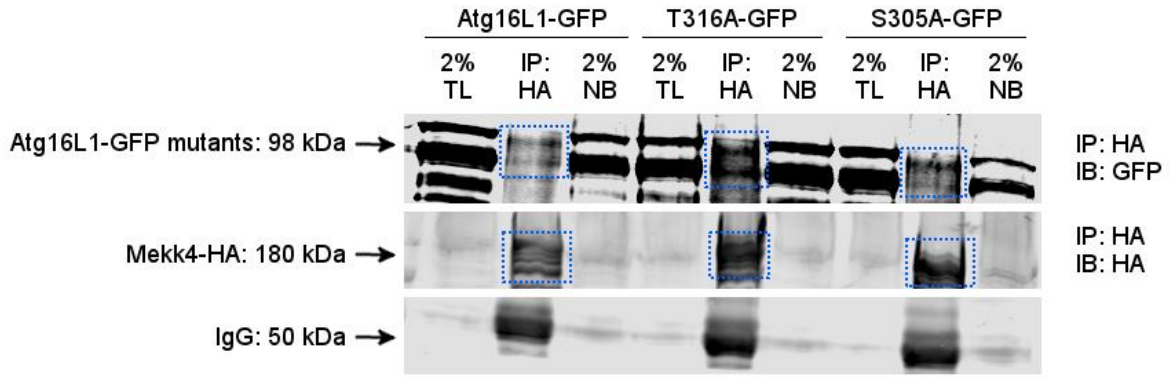

Figure 4.14 The Atg16L1 mutants retain the ability to bind Mekk4.

The Atg16L1-GFP, Atg16L1-T316A-GFP or Atg16L1-S305A-GFP constructs were transiently co-expressed with Mekk4-HA in HEK293 cells. The lysate was collected and the complex immunoprecipitated with anti HA antibody. The proteins were separated by SDS-PAGE. Atg16L1 binding was analysed by immunoblotting with antibodies against GFP and HA. The wild type and mutant Atg16L1 constructs were shown to bind Mekk4-HA (highlighted with blue boxes).

IP = immunoprecipitation. TL = total lysate. NB = non bound protein. IB = immunoblot.

4.3.10 The kinase dead mutant of Mekk4-HA cannot bind Atg16L1-GFP

The kinase activity of MEKK4 is vital for phosphorylation and activation of substrates involved in the MAPK signalling pathways i.e. MAP2Ks. However, not all proteins that bind MEKK4 require kinase activity, including RIP2 (Clark et al, 2008). To determine whether the interaction between Mekk4-HA and Atg16L1-GFP required the kinase activity of Mekk4, a kinase dead mutant of Mekk4-HA, in which lysine 1361 is mutated to methionine (Gerwins et al., 1997) was obtained from Addgene. The kinase dead Mekk4-HA was co-expressed with Atg16L1-GFP in HEK293 cells. Atg16L1-GFP was immunoprecipitated from the lysate and kinase dead Mekk4-HA binding assayed by SDS-PAGE and Western blotting. The kinase dead Mekk4-HA did not bind Atg16L1-GFP (Fig 4.15), indicating that the kinase activity of MEKK4 is required to allow binding of Atg16L1.

4.3.11 NOD2-HA binds Atg16L1-GFP in the absence of autophagy activation and after NOD2 activation with MDP

Previous immunoprecipitation results in this chapter have investigated the interaction between Atg16L1 and Mekk4 in the absence of NOD2. As Mekk4 is a potential candidate for crosstalk between the autophagy and NOD signalling pathways, and previous research has demonstrated an interaction between Atg16L1 and NOD2 (Travassos et al., 2010), NOD2 expression and activation could play an essential role. Therefore, a possible interaction between Atg16L1 and NOD2 in the episomal HEK293 cell line had to be established. The dual episomal HEK293 Atg16L1-GFP & NOD2-HA cells were cultured in supplemented medium or medium with 10 µg/ml MDP for 4 h. Atg16L1-GFP was immunoprecipitated from the lysates and NOD2-HA binding assayed by Western blotting. In both conditions, NOD2-HA bound Atg16L1-GFP (Fig 4.16). This confirmed the interaction published by Travassos et al., (2010) and demonstrated that the interaction between NOD2 and Atg16L1 occurs without MDP activation of NOD2 in the episomal cells.

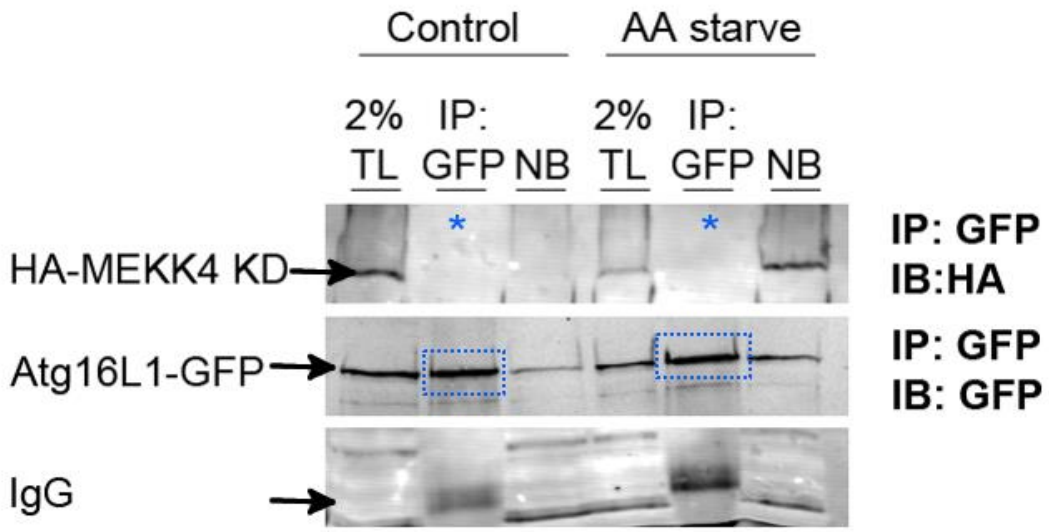

Figure 4.15 The kinase dead Mekk4 does not bind Atg16L1-GFP

Kinase dead Mekk4-HA was transiently expressed in HEK293 Atg16L1-GFP episomal cells. The cells were cultured in nutrient rich media or HBSS to induced autophagy, the lysate collected and immunoprecipitation carried out with an anti-GFP antibody. The proteins were separated by SDS-PAGE., followed by immunoblotting with antibodies against GFP and HA. The kinase dead Mekk4 did not co-precipitate with Atg16L1 (highlighted with blue boxes and asterisks).

IP = immunoprecipitation. TL = total lysate. NB = non bound protein. IB = immunoblot.

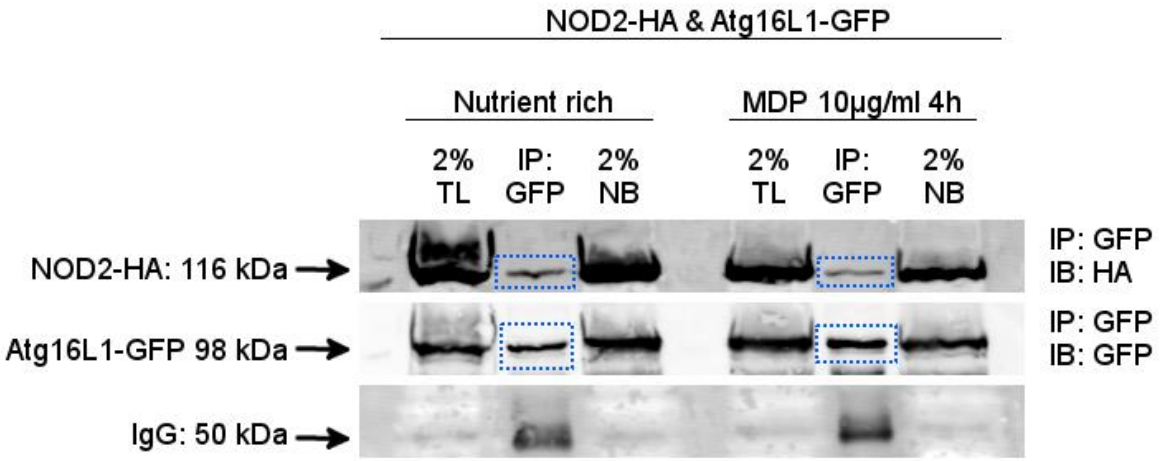

Figure 4.16 NOD2 binds Atg16L1 in HEK293 cells

HEK293 Atg16L1-GFP & NOD2-HA episomal cells were cultured in nutrient rich media or media with the NOD2 agonist MDP, to activate NOD2 signalling and NOD2-directed autophagy. The lysates were collected and immunoprecipitation carried out with an anti-GFP antibody. The proteins were separated by SDS-PAGE. NOD2 binding was analysed by immunoblotting with antibodies against GFP and HA. NOD2 was bound to Atg16L1 in the absence of MDP stimulation and following MDP stimulation (highlighted with blue boxes).

IP = immunoprecipitation. TL = total lysate. NB = non bound protein. IB = immunoblot.

4.3.12 Mekk4 dissociates from Atg16L1 following NOD2 activation in HEK293 episomal cells

So far, the immunoprecipitation results have shown that canonical autophagy does not affect the interaction between Atg16L1 and Mekk4 in episomal cells. To determine whether the activation of NOD-directed autophagy through MDP would alter the interaction between Atg16L1 and Mekk4, HEK293 Atg16L1-GFP & NOD2-HA episomal cells were transfected with Mekk4-HA. The cells were cultured in supplemented media, or in media with 10 µg/ml MDP for 4 h to activate NOD2 directed autophagy. Atg16L1-GFP was immunoprecipitated from the lysates with antibodies against GFP and Mekk4-HA and NOD2-HA binding assayed by Western blotting with antibodies specific for HA. In the absence of NOD2 activation, Atg16L1-GFP precipitated Mekk4-HA and NOD2-HA (Fig 4.17). This is probably not within the same complex, but likely a result of pulling down separate Atg16L1-GFP hetero-dimeric complexes. Following activation of NOD2, Atg16L1-GFP remained bound to NOD2-HA, but Mekk4-HA dissociated from Atg16L1-GFP (Fig. 4.17). This result indicates that the activation of NOD2 signalling leads to the dissociation of Atg16L1 and MEKK4 in the episomal cell model.

4.3.13 Confirmation of the interaction of endogenous Atg16L1 and Mekk4

The characterisation of the interaction between Mekk4 and Atg16L1 has so far been carried out using epitope tagged proteins in episomal and overexpression models. To ensure that the interaction was not an artefact caused by overexpression, the interaction between endogenous Atg16L1 and Mekk4 was validated using two different cell lines. HEK293 cells were used to characterise the human endogenous proteins, and Raw 264.7 cells were chosen to investigate the murine endogenous proteins. Additionally, the Raw 264.7 cell line are a mouse macrophage cell line which respond to MDP by activating NOD2 signalling (Clark et al., 2008). To validate the interaction in a human cell line, HEK293 cells were cultured in nutrient rich medium or HBSS for 2 h to induce autophagy. ATG16L1 was immunoprecipitated from the lysate and MEKK4 binding assayed by Western blotting. In nutrient rich conditions and following the activation of autophagy, ATG16L1 bound MEKK4, confirming the earlier results (Fig. 4.18). This was not a strong interaction, and the results were not as convincing as those in cells overexpressing epitope-tagged proteins. A crosslinker was used to stabilise the interaction between ATG16L1 and MEKK4 prior to cell lysis, which indicates that the interaction may be low affinity or transient. The DSP (Dithiobis[succinimidyl propionate]) crosslinker was used for intracellular conjugation of proteins prior to cell lysis, to preserve weak interactions. This crosslinker has been used

with similar effect to study interactions between Atg16L1 and FIP200 (Nishimura et al., 2013) and Atg16L1 and WIPI2 (Dooley et al., 2014).

To validate the interaction in the mouse macrophage cell line in the context of Nod2 expression, Raw 264.7 cells were cultured in supplemented medium, HBSS for 2 h or MDP 10 µg/ml for 4h. Mekk4 was immunoprecipitated from the lysate and Atg16L1 binding assayed by SDS-PAGE and Western blotting. In the absence of autophagy activation, Mekk4 was bound to Atg16L1 (Fig 4.19). Following activation of canonical autophagy by amino acid starvation there was a small decrease in the binding between Mekk4 and Atg16L1. A similar decrease in binding was also seen in cells where Nod2 was activated by MDP (Fig 4.20). This decrease in binding was difficult to quantify and could be due to background noise in the assay. However, if accurate this result indicates that the expression and activation of endogenous Nod2 in a specialised immune cell affects the interaction between Atg16L1 and Mekk4 during both canonical and selective autophagy, leading to a reduction in binding.

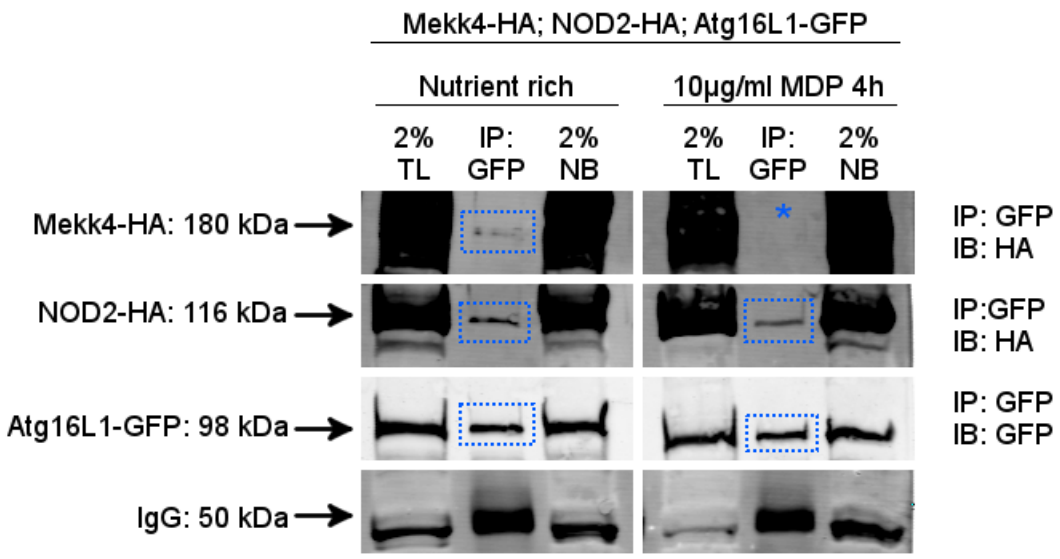

Figure 4.17 Mekk4-HA dissociates from Atg16L1-GFP following activation of NOD2 in HEK293 cells

Mekk4-HA was transiently expressed in HEK293 Atg16L1-GFP & NOD2-HA episomal cells, which were cultured in nutrient rich media or media with the NOD2 agonist MDP. Lysates were collected and immunoprecipitation carried out with an anti-GFP antibody. Mekk4 and NOD2 binding were analysed by immunoblotting with antibodies against HA and GFP. Mekk4 was bound to Atg16L1 in the absence of NOD2 activation (highlighted with blue boxes). When NOD2 was stimulated with MDP, Mekk4 dissociated from Atg16L1 (highlighted with asterisk and blue boxes).

IP = immunoprecipitation. TL = total lysate. NB = non bound protein. IB = immunoblot.

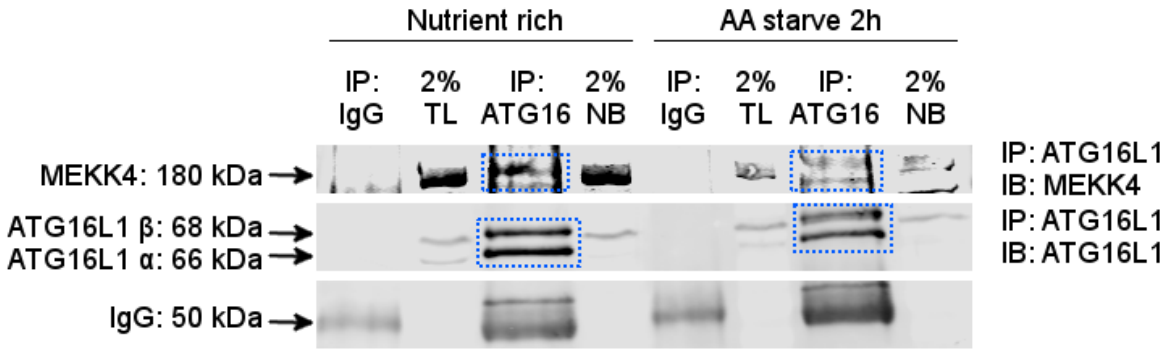

Figure 4.18 Endogenous Atg16L1 and Mekk4 proteins interact in HEK293 cells

HEK293 cells were cultured in nutrient rich media or HBSS to induce autophagy. The lysates were collected and an immunoprecipitation carried out with an anti ATG16L1 antibody. The proteins were separated by SDS-PAGE. MEKK4 binding was analysed by immunoblotting with anti MEKK4 and anti ATG16L1 antibodies. In nutrient rich conditions and following activation of autophagy, the endogenous MEKK4 bound ATG16L1 (highlighted with blue boxes).

IP = immunoprecipitation. TL = total lysate. NB = non bound protein. IB = immunoblot.

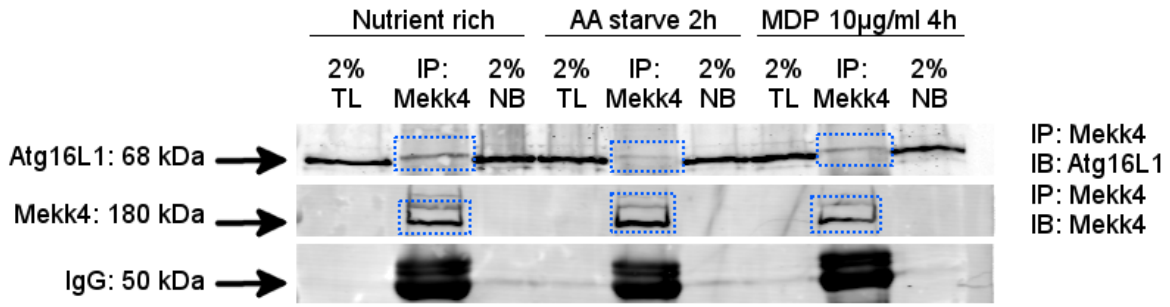

Figure 4.19 Endogenous Atg16L1 and Mekk4 interact in Raw 264.7 cells

Raw 264.7 cells were cultured in nutrient rich media, HBSS to induce autophagy, media with the Nod2 agonist MDP to induce Nod2-directed autophagy. The lysates were collected and immunoprecipitated carried out with an anti Mekk4 antibody. The proteins were separated by SDS-PAGE. Atg16L1 binding was analysed by immunoblotting with anti Atg16L1 and anti Mekk4 antibodies. In nutrient rich conditions, the endogenous Atg16L1 bound Mekk4. Following starvation induced autophagy and Nod2-directed autophagy, there was a decrease in Atg16L1 binding to Mekk4 (highlighted with blue boxes).

IP = immunoprecipitation. TL = total lysate. NB = non bound protein. IB = immunoblot.

4.4 Chapter Discussion

The results of a yeast-two-hybrid screen identified a novel interaction between Atg16L1 and Mekk4. Co-immunoprecipitation studies carried out in this project confirmed the interaction between Atg16L1 and Mekk4, validating the results of the yeast-two-hybrid screen. The Atg16L1 deletion constructs, CCD-GFP and WD40-GFP failed to co-precipitate with Mekk4, whereas the constructs CCD+L-GFP and L+WD40-GFP were able to co-precipitate with Mekk4, suggesting that the linker region of Atg16L1 is responsible for binding Mekk4. Furthermore, the CD-associated Atg16L1 mutant T316A and the serine phosphorylation deficient Atg16L1 mutant S305A retained the ability to bind Mekk4. Both of these mutations reside in the linker region of Atg16L1 (Fig 4.20).

The presence of a putative Atg16L1 binding motif within the N-terminus of Mekk4 raises the possibility that Mekk4 and Atg16L1 interact through the same mechanism as other proteins that contain this motif, including NOD1, NOD2, TLR2 and TMEM59 (Boada-Romero et al., 2013). These proteins play a role in the promotion or activation of autophagy in response to pathogen invasion. The Atg16L1 binding motif was originally identified by Boada-Romero et al (2013) in TMEM59, where deletion constructs of Atg16L1 showed that the region of interaction was in the WD40 domain. This appears to contradict the findings in this chapter, that Mekk4 binds the linker region but not the WD40 domain, despite containing a conserved Atg16L1 binding motif. However, this discrepancy could be caused by two reasons; firstly the different species of Atg16L1 used (human β isoform by Boada-Romero et al., and mouse γ isoform in this thesis), and secondly the precise regions that were deleted in each construct. When each species isoform was aligned, and the regions for the respective deletion constructs mapped, a 10 amino acid discrepancy was revealed between the Boada-Romero et al. ΔWD40 construct and the equivalent CCD+L construct used in this thesis (Appendix 2). It would be appealing to suggest that this 10 amino acid region in Atg16L1 could be responsible for binding proteins containing the Atg16L1 binding motif, but without mutational analysis of the Atg16L1 binding motif in Mekk4, there is little evidence for this argument (Fig. 4.20). However, future work could focus on mutating the Atg16L1 binding motif in Mekk4, to determine if this region is responsible for Mekk4 binding to Atg16L1. Additionally, the 10 amino acid region within the linker of Atg16L1 could be mutated and Atg16L1 binding motif containing proteins could be assayed for binding to this region. As the Atg16L1 binding motif is a novel motif, further characterisation is needed to determine its precise mechanism within autophagy.

The results also demonstrated that a kinase dead Mekk4 lost the ability to bind Atg16L1. If the site of Atg16L1 binding resides within the N-terminus of Mekk4, then this may explain why Atg16L1 cannot bind kinase dead Mekk4. Fully activated Mekk4 requires alleviation of autoinhibition, allowing Mekk4 to change from a closed to an open conformation (Fig 4.21). Overexpression of a kinase dead Mekk4 results in it remaining in a closed conformation, due to its lack of catalytic activity (Miyake et al., 2007). Therefore, the region where Atg16L1 binds on Mekk4 could be masked when it is in a closed conformation, and Mekk4 may need to be activated and in an open conformation to bind Atg16L1. Indeed, the Atg16L1 binding motif lies within the autoinhibitory domain of human and mouse Mekk4 (Fig. 4.22). As kinase-dead Mekk4 lacks any catalytic activity, alleviation autoinhibition would not occur and the protein would remain in closed conformation and never dimerise and become fully activated (Miyake et al., 2007), with the Atg16L1 binding motif revealed only when MEKK4 is in an open confirmation (Fig 4.23). The best characterised activators of Mekk4 are the stress inducible GADD45 family of proteins. These proteins interact with Mekk4 by binding the N-terminus and alleviating auto-inhibition, allowing the catalytic kinase domain to become fully activated and phosphorylate substrate proteins (Figure 4.21) (Mita et al., 2002, Miyake et al., 2007). Interestingly, GADD45β expression is up regulated by cellular stress-induced inflammatory cytokines and LPS (Liebermann et al., 2002; Zhang et al., 2005). A point of future research would be whether Mekk4 activators are required for the interaction between Atg16L1 and Mekk4, and whether their expression can lead to an up regulation of autophagy.

This raises the issue of whether Atg16L1 is a substrate of Mekk4. A mass spec analysis of phosphorylated proteins extracted from mouse liver identified a serine phosphorylation in Atg16L1 (Villén et al., 2007). This serine residue lies 11 amino acids upstream of the equivalent site of the T316A mutation in murine Atg16L1. Mekk4 is described as a ser/thr kinase; its substrate proteins Mkk3/6 in the MAPK pathways are phosphorylated on serine/threonine residues within their activation loop, and autophosphorylation of the human MEKK4 occurs on Thr1493 (Miyake et al., 2007). The conditions that cause Atg16L1 to become phosphorylated, and the consequences of this modification are unknown. However, the evidence in this report that Atg16L1 only binds activated Mekk4 suggests that Mekk4 could be responsible for serine phosphorylation of Atg16L1. Additionally, it would be equally attractive to suggest that the threonine residue at the T316A site is also phosphorylated by Mekk4, and that this somehow promotes or regulates Atg16L1 activity. Whilst both Atg16L1 mutants were able to bind Mekk4, the

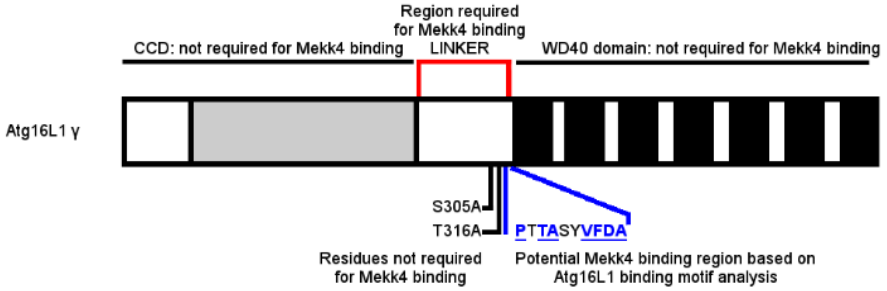

Figure 4.20 Schematic showing regions of Atg16L1 required for Mekk4 binding

The linker region of Atg16L1 is required for Mekk4 binding (red line). Mutation of the S305 and CD associated T316 residue had no effect on Mekk4 binding. Alignment between Atg16L1 WD40 construct used in this thesis and ATG16L1 WD40 construct used by Boada-Romero et al (2013) reveals a 10 amino acid region that may hold residues key for binding of proteins that contain Atg16L1 binding motif. Conserved residues within this region are shown in bold blue underlined typeface.

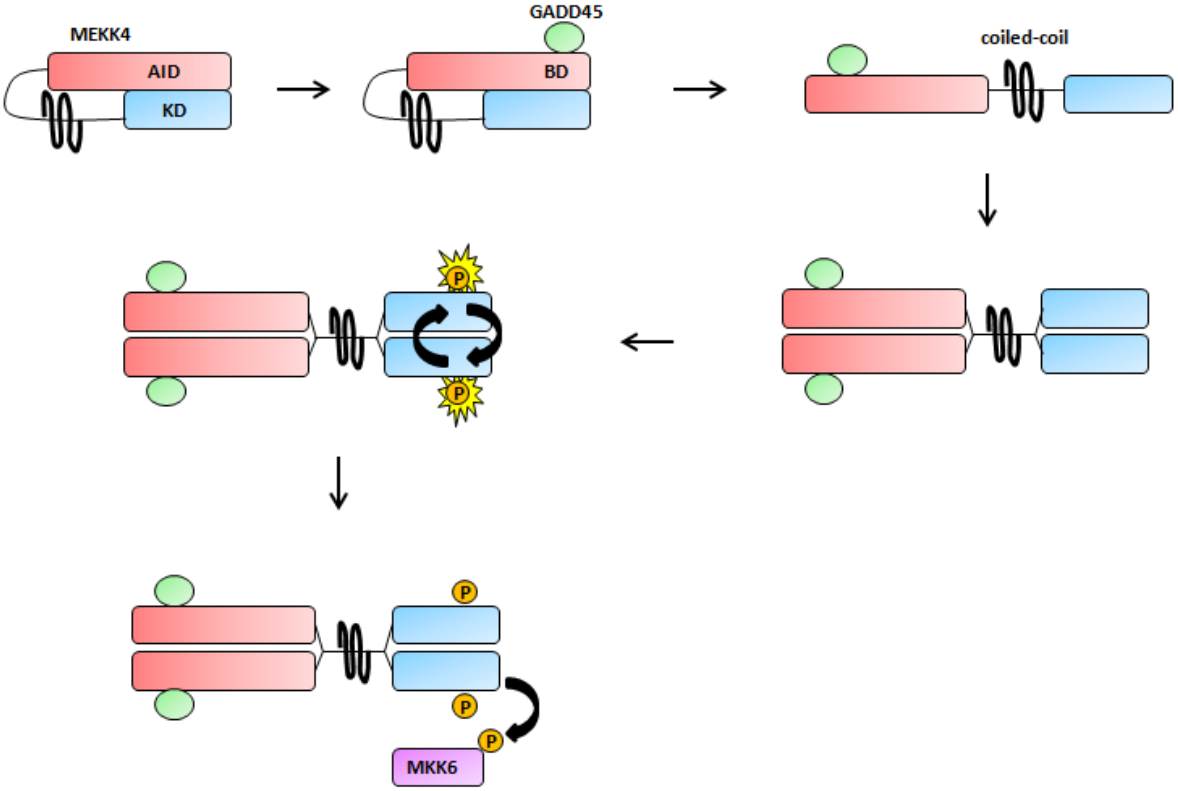

Figure 4.21 Activation of MEKK4 by GADD45 binding

GADD45 is an activator of MEKK4 signalling. When inactive, MEKK4 is in a closed conformation, with the auto-inhibitory domain (AID) blocking the kinase domain. When expressed, GADD45 binds to its N-terminal binding domain, inducing a conformational change in MEKK4 to an open conformation. This allows MEKK4 to dimerise, transphosphorylate on Thr -1493 and become fully activated, allowing it to phosphorylate its substrate protein MKK6 (taken from Miyake et al., 2007). AID = Autoinhibitory domain. KD = kinase domain.

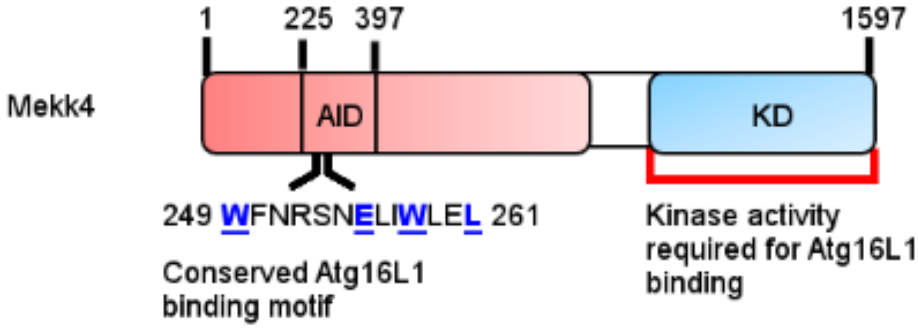

Figure 4.22 Schematic showing regions of Mekk4 required for Atg16L1 binding

The kinase activity of Mekk4 was necessary for Atg16L1 binding. The Atg16L1 binding motif lies in the autoinhibitory domain of Mekk4. Numbering refers to amino acid sequence of *Mus musculus* Mekk4.

AID = autoinhibitory domain. KD = kinase domain

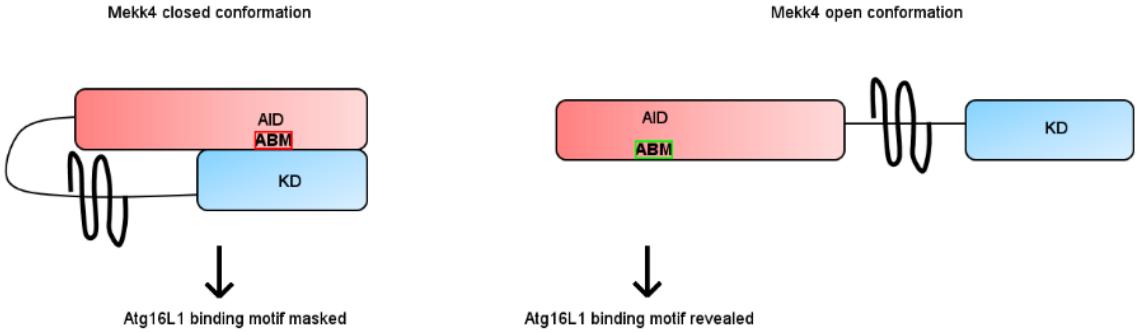

Figure 4.23 Schematic representation of the site of the Atg16L1 binding motif in Mekk4 in closed and open conformations

When Mekk4 is in closed conformation the autoinhibitory domain blocks the kinase domain. This could mask the site of the Atg16L1 binding motif and prevent binding of Atg16L1. When Mekk4 is in open conformation the autoinhibitory domain releases the kinase domain, which would reveal the Atg16L1 binding motif.

AID = Autoinhibitory domain. KD = kinase domain. ABM = Atg16L1 binding motif.

phosphorylation status of these residues in response to autophagy activation was not investigated, as phospho-specific threonine and serine antibodies did not produce consistent results in preliminary tests. Therefore, the phosphorylation of Atg16L1 by Mekk4 on these residues cannot be ruled out.

The nature of the interaction between Mekk4 and Atg16L1 was also determined during the activation of canonical and NOD2 directed autophagy. In cells that do not express NOD2, Atg16L1 co-precipitated with Mekk4 during starvation induced autophagy. In cells where NOD2 was expressed, Mekk4 co-precipitated with Atg16L1 in the absence of autophagy, but when autophagy was induced by MDP, or starvation (macrophage cells with endogenous Nod2 expression only), there was a weakened affinity between Atg16L1 and Mekk4. This suggests that expression of NOD2 alters the dynamic of the interaction between Atg16L1 and Mekk4. This could be related to the interactions between Atg16L1 and NOD2 (Travassos et al., 2010), and Mekk4 and RIP2 (Clark et al., 2008). In the absence of NOD2 stimulation, MEKK4 binds and sequesters RIP2 from the NOD signalling pathway. By outcompeting NOD2 for RIP2 binding, MEKK4 prevents the NOD2-RIP2 complex forming, which has been shown to have a specific inhibitory effect on NF-κB activity (Clark et al., 2008). When NOD2 is activated the ability of MEKK4 to bind RIP2 is abolished. The role of this interaction in autophagy is unclear.

Recently, the assembly of the NOD2-RIP2 complex was shown to be negatively regulated by ATG16L1 (Sorbara et al., 2013). This intricate crosstalk between components of the autophagy pathway and NOD signalling pathways converges around ATG16L1. It would be attractive to suggest that MEKK4 is also able to regulate Atg16L1 activity in selective autophagy as well, in addition to its involvement in regulating NOD2 signalling. Both ATG16L1 and NOD2 mutations have been associated with Crohn's disease (Hampe et al., 2007; Ogura et al., 2001), with defects in bacterial handling and inefficient targeted activation of autophagy against pathogens thought to contribute towards the pathophysiology of the disease. Interestingly, a study has shown that Crohn's disease patients had a reduction in MEKK4 expression, which led to defective IL-1A expression (van der Pouw Kraan et al., 2012). The reduction in MEKK4 expression could be explained by the enhanced degradation of the CD associated ATG16L1 mutation by caspase 3 (Murthy et al., 2014). Degradation of ATG16L1 may lead to a feedback mechanism in the cell resulting in reduced transcription and expression of MEKK4. Additionally, MEKK4 has been linked to the caspase 8/caspase 3 apoptotic signalling. The TNF-related apoptosis-inducing ligand, TRAIL activates apoptosis through activation of caspase 8, which leads to cleavage and activation of caspase 3 (Falschlehner et al., 2007). Treatment of a human prostate

adenocarcinoma cell line with TRAIL induced caspase 8 activation, downstream p38 and JNK activation through MEKK4 (Sun et al., 2011). This further strengthens the argument for the regulation of Atg16L1 in the NOD2: autophagy signalling axis by MEKK4, and highlights an area of future research focus.

The subcellular localisation of Mekk4 and Atg16L1 during both canonical and NOD2-directed autophagy indicates that Mekk4 remains cytosolic during the activation of autophagy, whilst Atg16L1 localises to the autophagosome. Therefore, the interaction does not appear at the autophagosomal membrane, and may not be required for proper localisation of Atg16L1 during autophagy. When combined with the immunoprecipitation results, this suggests that Mekk4 is bound to a subcellular pool of Atg16L1 with a portion released to the autophagosome. It could be that the interaction between Atg16L1 and Mekk4 is a transient interaction, similar to that of ATG16L1 and FIP200, or ATG16L1 and WIPI2, as indicated by the need to use a cross-linker to stabilise the interaction between endogenous proteins (Dooley et al., 2014; Nishimura et al., 2013). On the other hand, the interaction between Atg16L1 and Mekk4 may be a sequestration model, analogous to the MEKK4-RIP2 interaction (Clark et al., 2008). As this is the early stages of dissecting out the interaction, there is not enough evidence to conclude which of these models it is.

The evidence presented in this chapter establishes a novel interaction between Atg16L1 and Mekk4, which is dynamically affected by the expression of NOD2 and activation of autophagy. As the catalytic activity of Mekk4 is required for the interaction, there is the prospect of this interaction playing a key role in the regulation of autophagy. The function of Mekk4 in autophagy is explored in the next chapter.

Chapter 5

Function of MEKK4 in the autophagy pathway

Chapter 5: Function of MEKK4 in the autophagy pathway

5.1 Chapter Aims

The aims of this chapter are to investigate the role of MEKK4 in the autophagy pathway through gene silencing. The effects on autophagy are determined by measuring processing of LC3, degradation of p62, and observing the cellular distribution of autophagosome markers. MEKK4 knockdown is achieved first through the use of short interfering RNAs (siRNAs), and then a number of cell lines are developed and characterised using CRISPR/Cas9 mediated genome editing to knockout MEKK4 gene expression. The proteins of interest are MEKK4, LC3 and p62.

5.2 Introduction

In the previous chapter, Mekk4 was identified and characterised as a novel binding partner of Atg16L1. Though the results have defined the domains and conditions required for the interaction, they do not identify the functional consequence of this interaction in the autophagy pathway.

Mekk4 was originally identified from the yeast-two-hybrid screen due to its role in the negative regulation of NOD2 signalling (Clark et al., 2008). Existing research has established an interaction between NOD2 and Atg16L1, with activation of NOD2 shown to drive autophagy (Travassos et al., 2010; Homer et al., 2010; Cooney et al., 2010). The NOD2-Atg16L1 axis represents an important arm of the innate immune system, and mutation of either of these genes leads to defective microbial handling and failure to target bacteria to autophagosomes in tissue culture (Kuballa et al., 2008; Travassos et al., 2010). Therefore, the interaction between Atg16L1 and Mekk4 may function in regulating the crosstalk between the autophagy and NOD signalling pathways. Silencing of MEKK4 has been shown to inhibit NOD2 mediated autophagy, leading to an increase in the survival of *Salmonella* in infected cells (Homer et al., 2012).

The family of GADD45 proteins that activate MEKK4 are intricately linked to immunity. The expression of GADD45 can be induced by inflammatory cytokines and the bacterial outer-membrane component lipopolysaccharide (LPS) (Liebermann et al., 2002; Zhang et al., 2005). Additionally, GADD45 proteins are important for the function of granulocytes and macrophages (Gupta et al., 2006). In relation to autophagy, GADD45 and MEKK4 have been linked to the regulation of autophagy through p38 mediated phosphorylation of Atg5 (Keil et al., 2013). This modification of Atg5 results in the inhibition of autophagy, linking MEKK4 to the regulation of autophagy once more.

However, the effect of silencing MEKK4 on the autophagy pathway has not been well characterised. Any autophagy specific phenotype arising from gene knockdown could be explained by the interaction between Atg16L1 and MEKK4. Two methods which are used to mediate gene silencing are RNA interference with siRNAs, and genome editing using the CRISPR/Cas9 system.

RNA interference as a tool for gene silencing was first described in *C.elegans* in 1998 (Fire and Mello, 1998). It has since been developed and widely accepted as valuable technology in mammalian systems. Short interfering RNA duplexes of 21bp length are designed to complement the mRNA of the target gene. Upon entering the cell, siRNAs will be incorporated into the RNAi induced silencing complex (RISC), which guides siRNAs to the target RNA sequence (Nykänen et al., 2001). The siRNA duplex will then unwind, and RISC directs the antisense siRNA to the complimentary mRNA sequence, where it is subsequently degraded by endo and exonucleases (Martinez et al., 2002). Gene silencing using this technique relies on careful design of the siRNA target sequence, to ensure there are no off target effects. The reliability of siRNA mediated gene knockdown relies on both transfection efficiency of the siRNAs and the specificity of the siRNA target sequence. The target gene may not achieve 100% knockdown, and it is possible that off-target effects could cause false-positive results. Problems with transfection efficiency can also lead to reliability issues with the experiments. Therefore, this technique lends itself well to an initial screening of whether knockdown of MEKK4 has an effect on autophagy, but is not a long term solution for studying the effects of gene knockout. For a reliable and permanent knockout of gene expression, the genome editing tool CRISPR/Cas9 can be used.

CRISPR/Cas9 is a microbial adaptive immune system that uses an RNA guided nuclease (Cas9) to cleave DNA at a specified locus (Barrangou et al., 2007; Garneau et al., 2010; Ran et al., 2013; Hsu et al., 2014). For two decades, the function of what is now known as the CRISPR locus (clustered regularly interspaced short palindromic repeats) was studied. The first report of CRISPR clustered repeats was in *E.coli* (Ishino et al., 1987). These clustered repeat elements were present in >40% of sequenced bacteria and 90% of archae (Mojica et al., 2000). Subsequently, several clusters of conserved genes adjacent to the CRISPR repeats were identified as CRISPR associated (Cas) genes (Jansen et al., 2002). The key discovery came when analysis identified that regions of the CRISPR repeats were phage or extrachromosomal sequences (Mokica et al., 2005; Pourcel et al., 2005). Following invasion by a phage, Cas genes are rapidly transcribed and translated into proteins, and CRISPR arrays transcribed as single RNA, before processing into shorter CRISPR RNAs (crRNAs). These crRNAs direct the processing and degradation of the phage by the Cas enzymes (Brouns et al., 2008). Soon, this system was engineered for successful genome

editing in mammalian cells. Coexpression of Cas9 from *Streptococcus thermophilus* (Cong et al., 2013) or *S.pyogenes* (Cong et al., 2013; Mali et al., 2013) with single guide RNAs targeted against a genomic locus was able to direct a double stranded break (DSB) within the genome. To design a guide RNA against a genomic target, a 20 nt sequence must be identified which must immediately precede a 5' – NGG sequence, known as a protospacer adjacent motif (PAM) (Fig 5.1). Cas9 from *S.pyogenes* will make a blunt cut between the 17th and 18th bases in the target sequence. This subsequently stimulates the host DNA repair mechanisms; the error prone non-homologous end joining (NHEJ) where in the absence of a repair template DNA is religated with insertion/deletion (indel) mutations, or the more precise homology directed repair (HDR), where a repair template is introduced (Fig 5.2). Should an indel occur within a coding exon, this can lead to frameshift mutations and premature stop codons, making this a useful technique for generating gene knockouts (Ran et al., 2013). This system has been made widely available and is now used by thousands of laboratories in a variety of cell types and organisms (Sander and Joung., 2014), including humans, mice and *C.elegans* (Ran et al., 2013; Cong et al., 2013; Malie et al., 2013; Wang et al., 2013; Friedland et al., 2013).

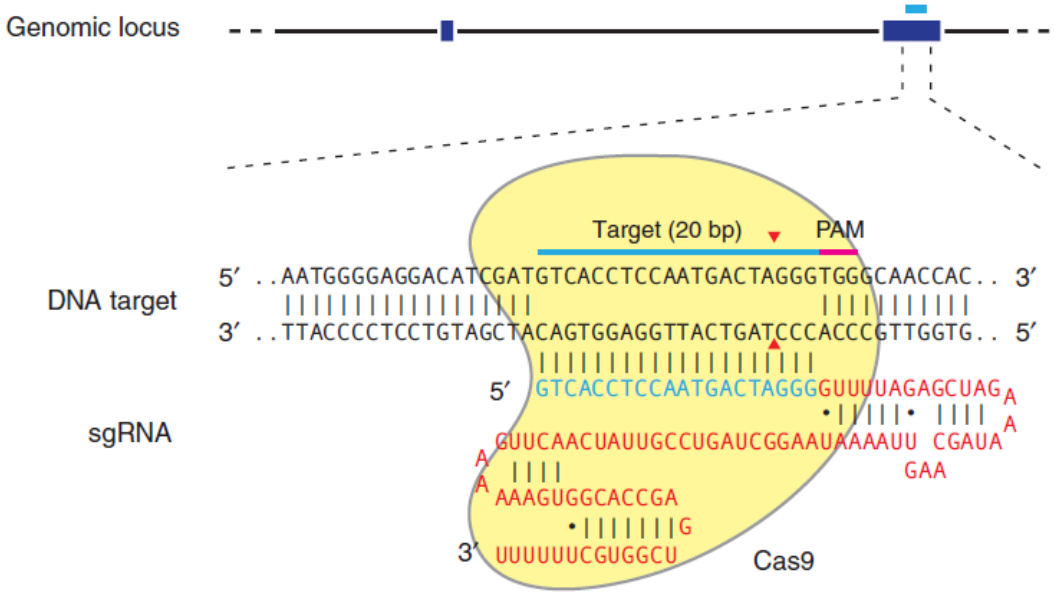

Figure 5.1 Schematic of the RNA guided Cas9 nuclease. The 20 nt guide sequence (blue) plus scaffold (red) acts as the single guide RNA (sgRNA) The guide sequence pairs with the target DNA (blue bar) via Watson-Crick base pairing, upstream of the required NGG protospacer adjacent motif (PAM; pink). Cas9 is directed to the genomic DNA by the sgRNA and generates a double stranded break 3bp upstream of the PAM (red triangle). Modified from Ran et al., 2013.

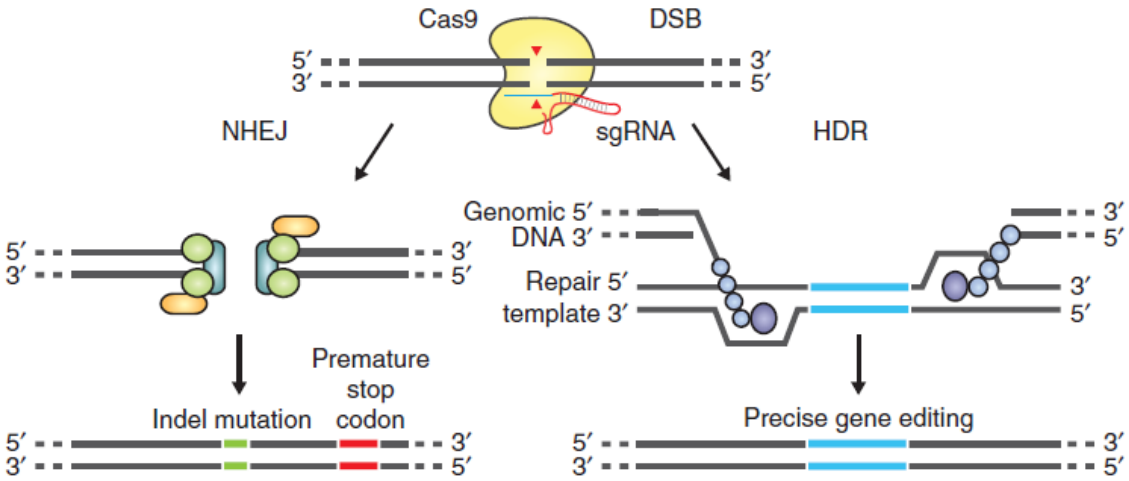

Figure 5.2 DNA damage repair in the CRISPR Cas9 system; NHEJ and HDR. Double stranded breaks induced by Cas9 can be repaired via the NHEJ pathway or by HDR. When the ends of a DSB are repaired by the error prone NHEJ, random insertions/deletions (indels) can result at the site of repair. This leads to frameshift mutations and premature stop codons. The HDR pathway can be utilised for precise gene editing, when a repair template is present e.g. in the form of a plasmid. Modified from Ran et al., 2013.

5.3 Results

5.3.1 siRNA mediated silencing of MEKK4

5.3.1.1 Screening of siRNA oligoprobes identifies s8675 as sufficient to silence MEKK4 expression in HEK293 GFP-LC3 cells

To ascertain whether MEKK4 played a role in autophagy, siRNA probes were used to knockdown expression in HEK293 GFP-LC3 cells. This cell line was chosen for ease of imaging GFP tagged LC3. Two siRNAs (s8673 and s8675) were transfected into cells at different concentrations to determine which probe would effectively knock down MEKK4 expression. A scrambled siRNA was used as a negative control. The lysates were collected and analysed by Western blot. At a concentration of 50 nM, both s8673 and s8675 could efficiently silence MEKK4 expression in HEK293 GFP-LC3 cells (Fig 5.3a, b). Both of these siRNAs were used in tandems in latter experiments to silence MEKK4 expression.

5.3.1.2 Silencing MEKK4 reduces LC3 conversion during starvation induced autophagy in HEK293 GFP-LC3 cells

Having identified suitable siRNA probes, the role of MEKK4 could be examined during starvation induced autophagy. MEKK4 was silenced in HEK293 LC3-GFP cells, and HBSS starved over 6 hours. The lysates were collected and the conversion of LC3 I to LC3 II analysed by Western blot. Compared to the scrambled control, MEKK4 silenced cells showed a loss of LC3 II conversion, as indicated by decreased turnover of LC3 throughout the 6 hour time course (Fig. 5.4 a, b). To determine whether autophagic flux had been disrupted by MEKK4 silencing, the degradation of the adaptor protein p62 was also assessed. As p62 can bind LC3, it is selectively degraded during autophagy (Bjørkøy et al., 2005), and the accumulation of p62 can be an indicator of autophagy deficiency (Mizushima and Yoshimori, 2007). In MEKK4 silenced cells, there were higher levels of p62 present compared to the scrambled control. After 1 h of HBSS starvation, there was an increase of p62 in MEKK4 silenced cells, which was then degraded at a comparable rate compared to the controls (Fig. 5.5 a, b). Taken together, these results indicate that MEKK4 promotes the conversion of LC3 I to LC3 II during starvation induced autophagy, and silencing MEKK4 leads to an accumulation of p62 which is partially degraded during starvation. Therefore, MEKK4 silenced cells are autophagy deficient.

Figure 5.3 MEKK4 expression is knocked down by siRNAs s8673 and s8675

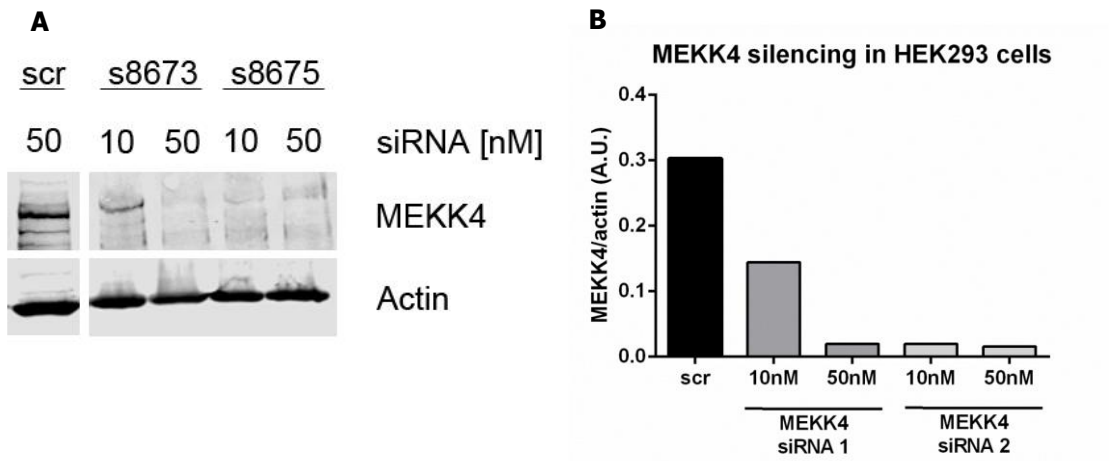

(A) HEK 293 GFP-LC3 cells were transiently transfected with MEKK4 siRNAs at indicated concentrations and analysed by Western blot.
(B) Densitometry analysis of data from experiment in (A). A concentration of 50 nM of both siRNAs is sufficient to knockdown MEKK4 expression.

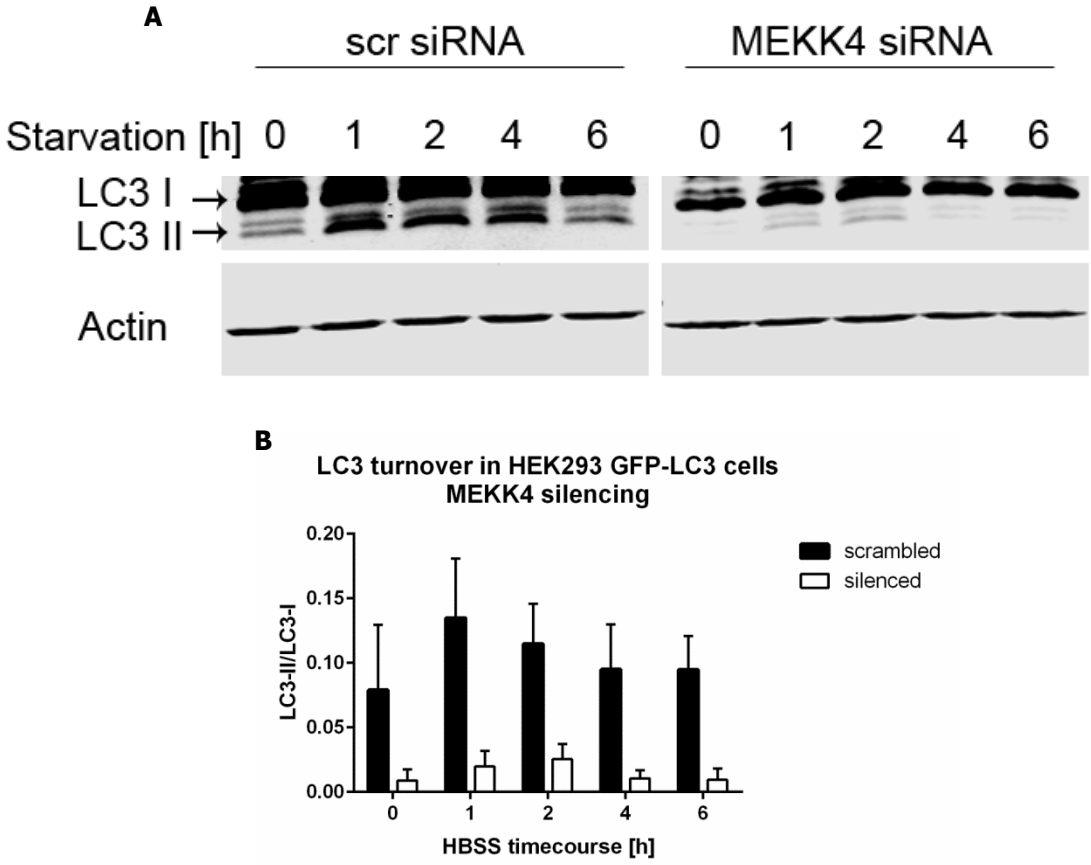

Figure 5.4 Silencing MEKK4 in HEK293 GFP-LC3 cells decreases LC3 turnover

(A) HEK293 GFP-LC3 cells transfected with siRNAs against MEKK4 show reduced levels of LC3 II throughout HBSS starvation. Image representative of two experiments.

(B) Densitometry analysis of experiment in (A). Mean and SEM graphed. A student's t-test was performed, and none of the results were statistically significant.

p values as follows; 0 h = 0.3059, 1 h = 0.2986, 2h = 0.1152, 4 h = 0.1402, 6h = 0.0892.

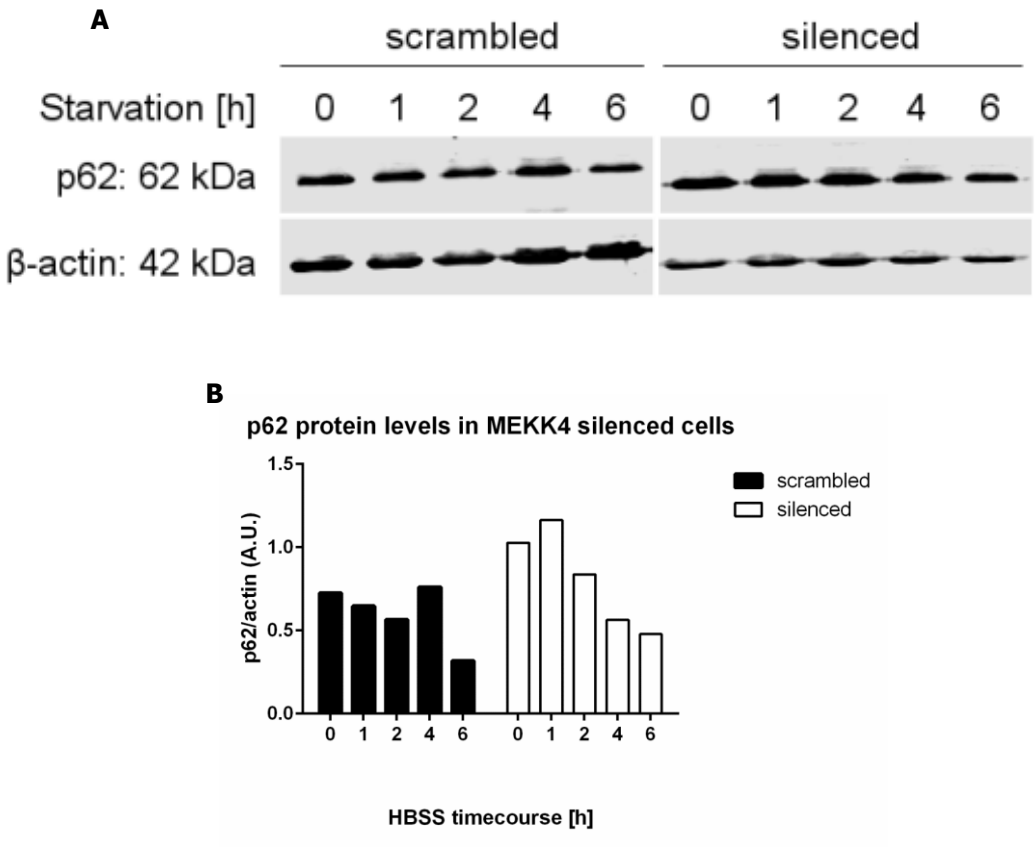

Figure 5.5 Silencing MEKK4 in HEK293 GFP-LC3 cells results in accumulation of p62
(A) HEK293 GFP-LC3 cells were transfected with MEKK4 siRNAs, lysates collected at indicated timepoints during HBSS starvation timecourse and analysed by Western blot.
(B) Densitometry analysis of data from experiment (A). MEKK4 silenced cells have increased levels of p62 compared to the scrambled controls.

5.3.1.3 Silencing MEKK4 redistributes GFP-LC3 to large peri-nuclear puncta that co-localise with p62

With the previous results demonstrating a requirement for MEKK4 for the conversion of LC3 I to LC3 II, the precise effect of MEKK4 silencing on autophagosome formation and dynamics was not known. To see how GFP-LC3 distribution was influenced by MEKK4 silencing, HEK293 LC3-GFP cells were transfected with scrambled siRNA or the two MEKK4 siRNA probes and HBSS starved over a course of 4 hours. The formation of GFP-LC3 puncta and their co-localisation with the early autophagosome marker WIPI2, or the autophagosome cargo marker p62 observed. In the scrambled control, the expected localisation of GFP-LC3 was observed in response to starvation induced autophagy, with an increase of puncta which was sustained over the 4 hour time course (Fig. 5.6, 5.7, 5.10and 5.11). These puncta also co-localised as expected with WIPI2 and p62. Silencing MEKK4 resulted in a dramatic redistribution of GFP-LC3 to large perinuclear puncta (Fig. 5.6, 5.7, 5.10 and 5.11). These large puncta were present even in the absence of autophagy activation (Fig 5.6, 5.10). Additionally, GFP-LC3 was harder to detect in the cytosol of the MEKK4 silenced cells than in the scrambled control cells. WIPI2 was recruited and only partly localised to the large GFP-LC3 puncta when MEKK4 silenced cells were starved (Fig 5.7 a-c), suggesting that upstream of Atg16L1, the autophagy machinery was localised to these large puncta when autophagy was activated. The greatest degree of co-localisation was seen between the large GFP-LC3 puncta and p62 (Fig. 5.10, 5.11), with a number of LC3 puncta surrounded by p62. Due to this level of colocalisation, the nature of the GFP-LC3 puncta and p62 puncta were further quantified.

5.3.1.4 Quantification of autophagosome markers in MEKK4 silenced cells reveals increase in large aggregates

To further characterise the dramatic GFP-LC3 phenotype seen in MEKK4 silenced cells, images from the previous experiment were analysed using Imaris software to determine the number, size and degree of colocalisation of GFP-LC3 and p62 puncta. This was compared to the scrambled control. In MEKK4 silenced cells, the number of GFP-LC3 puncta per cell was decreased compared to the scrambled control throughout the timecourse, and was statistically significant at 1 hour, 2 hours and 4 hours HBSS starvation (Fig 5.8). The diameter of LC3 puncta were then measured and classified into 5 subgroups; 0 – 0.5 µm and 0.51 – 1 µm diameter indicative of the expected sizes of autophagosomes (Mizushima 2004), 1 – 1.5 µm of intermediate autophagosome size, and 1.51 – 2 µm and > 2 µm diameter which would signify a potential aggregate. Throughout the timecourse, there was a higher number of GFP-LC3 puncta in the autophagosome subgroups (0 – 0.5 µm and 0.51

– 1 µm diameter) in scrambled siRNA treated cells, compared to MEKK4 silenced cells. Importantly there was an increase in the number of GFP-LC3 puncta classified as aggregates and intermediate autophagosomes. The number of puncta in these categories remained fairly static during the timecourse. Few cells from the scrambled controls generated puncta in the 1 – 1.5 µm category, and no puncta were measured above 1.51 µm (Fig 5.9 a – d). Overall, this indicates that MEKK4 silenced cells generate fewer GFP-LC3 puncta than the scrambled controls, that these puncta are prone to form aggregates above 1.51 µm diameter, and that following activation of autophagy, there is no dynamic change in the number of aggregates.

The quantification was repeated for p62 puncta, and revealed that the number of p62 puncta per cell were comparable between scrambled controls and MEKK4 silenced cells at 0 hours, 2 hours and 4 hours HBSS. There was a statistically significant decrease at 1 hour HBSS in MEKK4 silenced cells compared to the scrambled control, though it is unclear how this fits with the trend seen throughout the timecourse (Fig 5.12). The p62 puncta were categorised by diameter, as previously with GFP-LC3, and the results demonstrated that there was a small increase in the number p62 puncta in the aggregate and intermediate autophagosome categories at all timepoints. (Fig 5.13 a-d). When the degree of co-localisation between GFP-LC3 and p62 was measured, the scrambled controls showed an increase in the number of colocalised GFP-LC3/p62 puncta following autophagy induction. However, in MEKK4 silenced cells, the number of colocalised GFP-LC3/p62 puncta was significantly lower during starvation induced autophagy than the scrambled controls. The number of co-localised puncta did not differ significantly throughout the timecourse between the MEKK4 silenced cells, indicating that these aggregates are stagnant. The aggregates shared similar characteristics to aggresome-like induced structures (ALIS), which form in response to cellular stress and cleared by autophagy, and are also observed in autophagy deficient cells (Szeto et al., 2006).

5.3.1.5 Confirmation of effects of MEKK4 silencing on autophagy in cells that express NOD2

The effect of MEKK4 silencing on autophagy had been established in HEK293 cells, which do not express NOD2 (Travassos et al., 2010). However, results in chapter 4 indicate that the expression and activation of NOD2 is involved in the interaction between Mekk4 and Atg16L1. To determine whether Mekk4 plays a role in autophagy in cells where Nod2 is expressed, a lentiviral vector containing shRNA against Mekk4 was used to transduce Raw 264.7 cells. This shRNA had been previously validated in this cell line and was shown to

efficiently knockdown Mekk4 expression (Clark et al., 2008). Increasing volumes of prepared shRNA lentiviral particles were added to cells, the lysates collected 5 days post transduction and assayed for Mekk4 expression by Western blot. A 50 µl volume of Mekk4 shRNA lentivirus was sufficient to knockdown Mekk4 expression to 31% of its original levels (Fig 5.14 a, b). Therefore, this volume of lentiviral particles was used to generate a stable knockdown in Raw 264.7 cells.

Cells that had stably incorporated the lentiviral vector were selected using puromycin, as the vector contained a puromycin resistance gene (Fig 5.14 c). The stable Raw 264.7 cells were pooled and subjected to HBSS starvation or MDP treatment to induce autophagy, the lysates collected and LC3 processing analysed by Western blot. The control cell line (Raw 264.7 only) was able to process LC3 following induction of autophagy by HBSS starvation and MDP stimulation. However, the Mekk4 knockdown cell lines showed reduced levels of LC3 I and LC3 II in nutrient rich conditions, and following activation of autophagy by HBSS starvation and MDP stimulation (Fig. 5.14 e-g). Interestingly, when LC3 turnover was calculated, the difference between Raw 264.7 cells and cells where Mekk4 was silenced was less pronounced (Fig. 5.13 h. However, this could be due to a reduction in LC3 I in the silenced cells. These results confirm a role for Mekk4 in the autophagy pathway in both cells that lack or express Nod2.

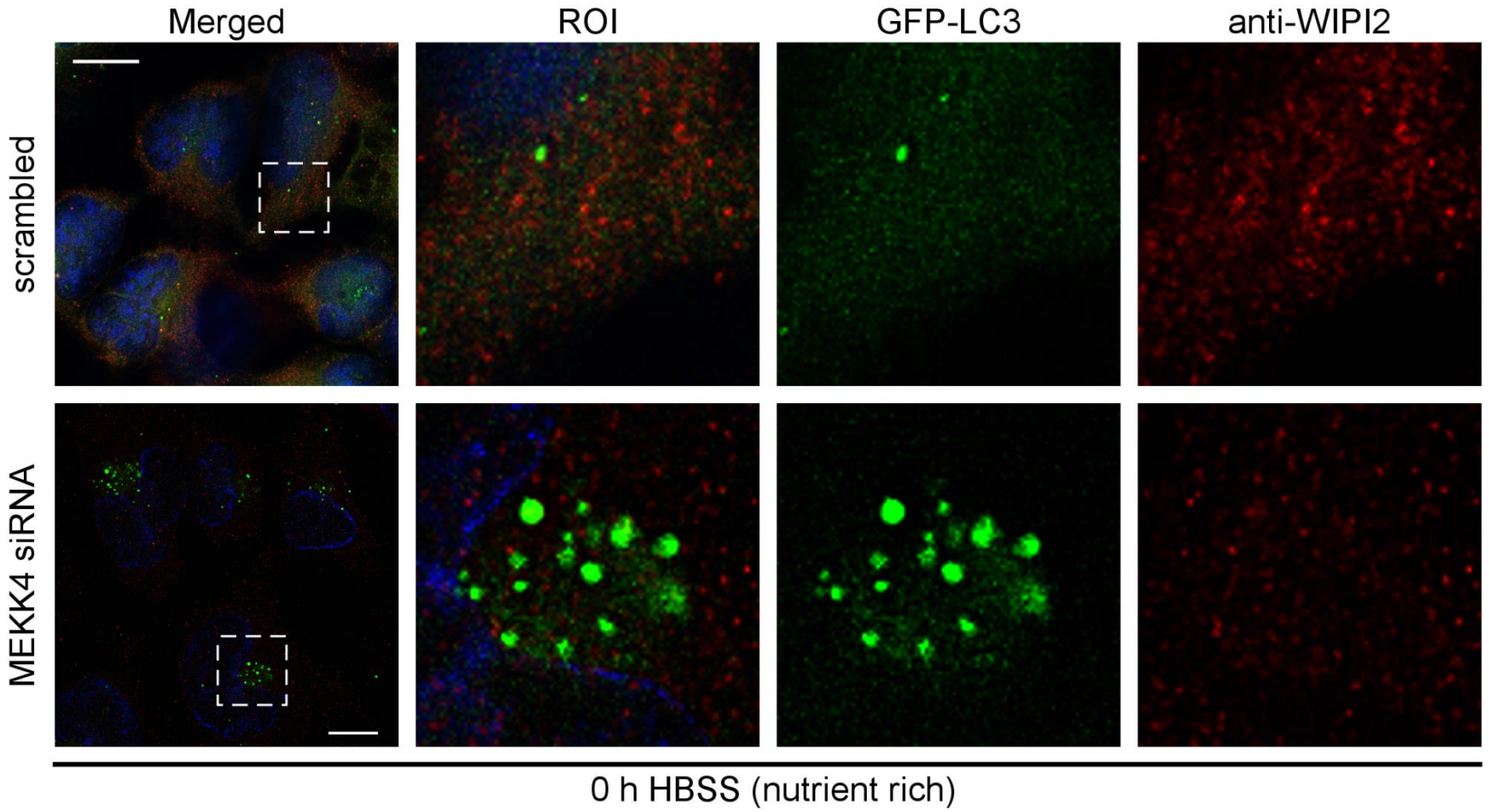

Figure 5.6 MEKK4 silencing induces large perinuclear GFP-LC3 puncta that are negative for WIPI2 in the absence of autophagy

HEK293 GFP-LC3 cells were transfected with scrambled or MEKK4 siRNAs and the localisation of GFP-LC3 and WIPI2 observed in the absence of starvation induced autophagy. WIPI2 was immunostained and the nuclei stained with DAPI. Regions of interest are highlighted in boxes. Scale bars 10 μm

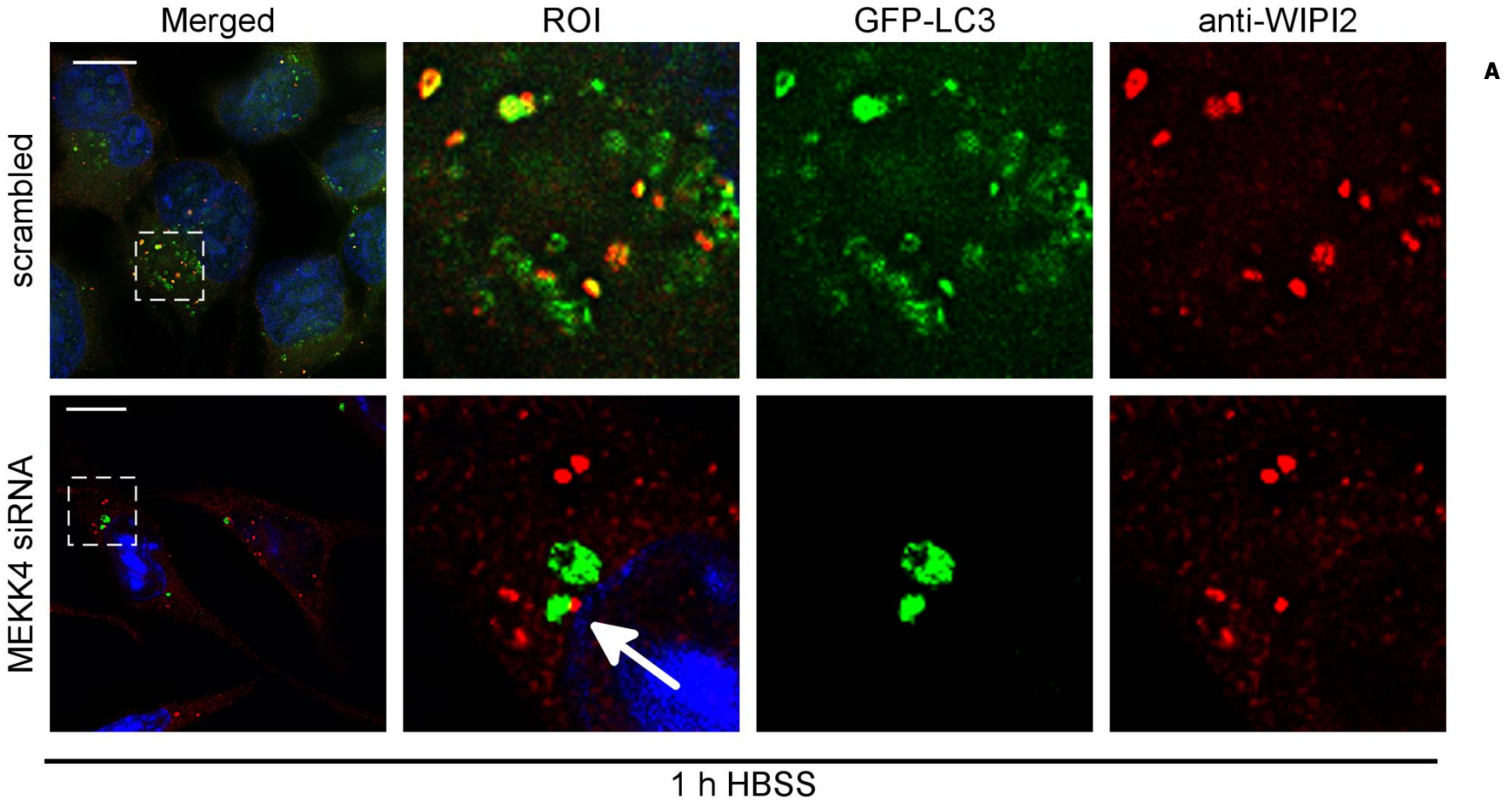

Figure 5.7 WIPI2 is recruited to sites close to the large GFP-LC3 puncta induced by autophagy following MEKK4 silencing

(A) HEK293 GFP-LC3 cells were transfected with scrambled or MEKK4 siRNAs and the localisation of GFP-LC3 and WIPI2 observed after 1 h HBSS to induce autophagy. WIPI2 was immunostained and the nuclei stained with DAPI. Regions of interest are highlighted in boxes. Scale bars 10 μm

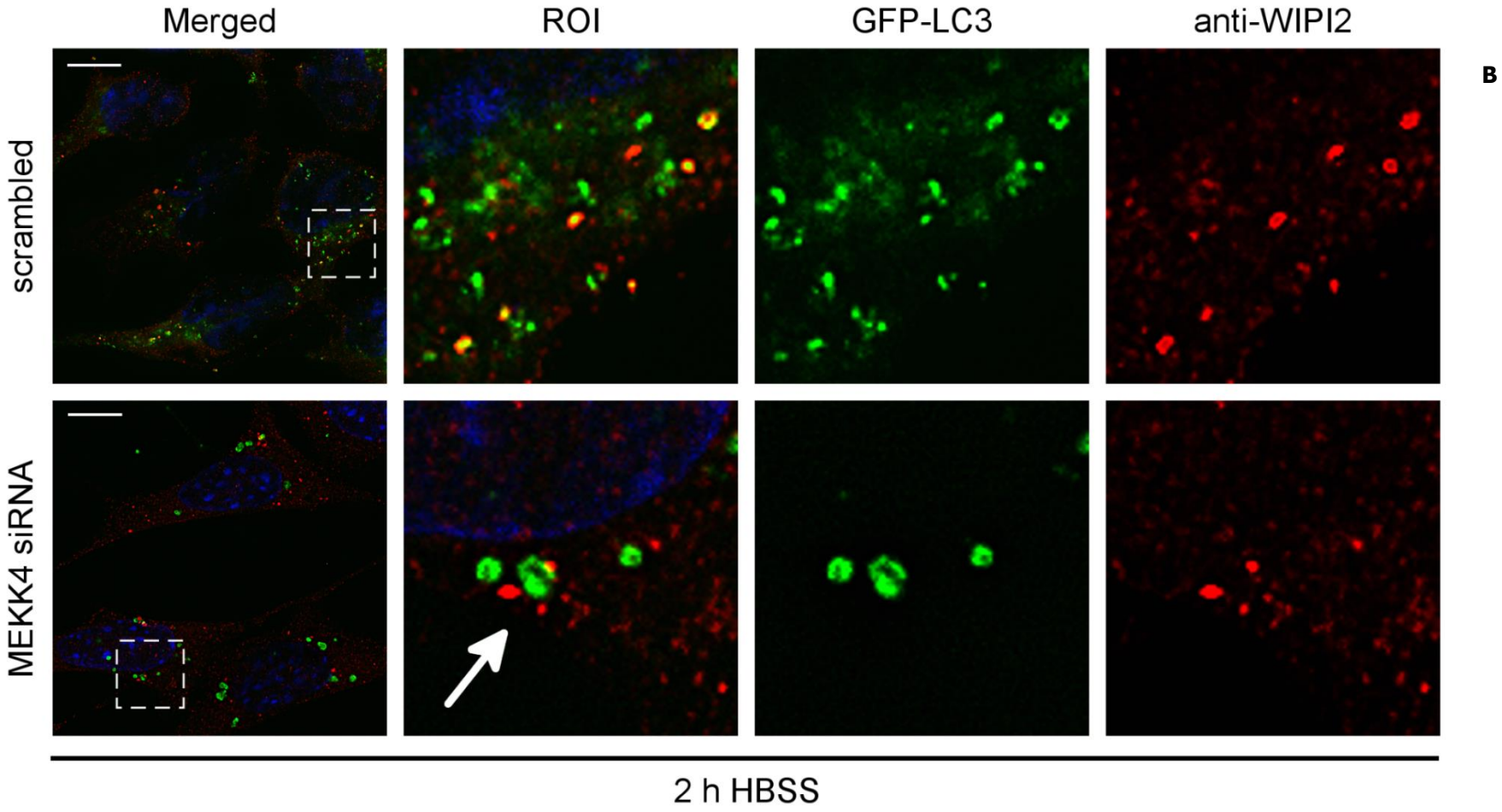

B

Figure 5.7 cont. WIPI2 is recruited to sites close to the large GFP-LC3 puncta induced by autophagy following MEKK4 silencing

(B) HEK293 GFP-LC3 cells were transfected with scrambled or MEKK4 siRNAs and the localisation of GFP-LC3 and WIPI2 observed after 2 h HBSS to induce autophagy. WIPI2 was immunostained and the nuclei stained with DAPI. Regions of interest are highlighted in boxes. Scale bars 10 μm

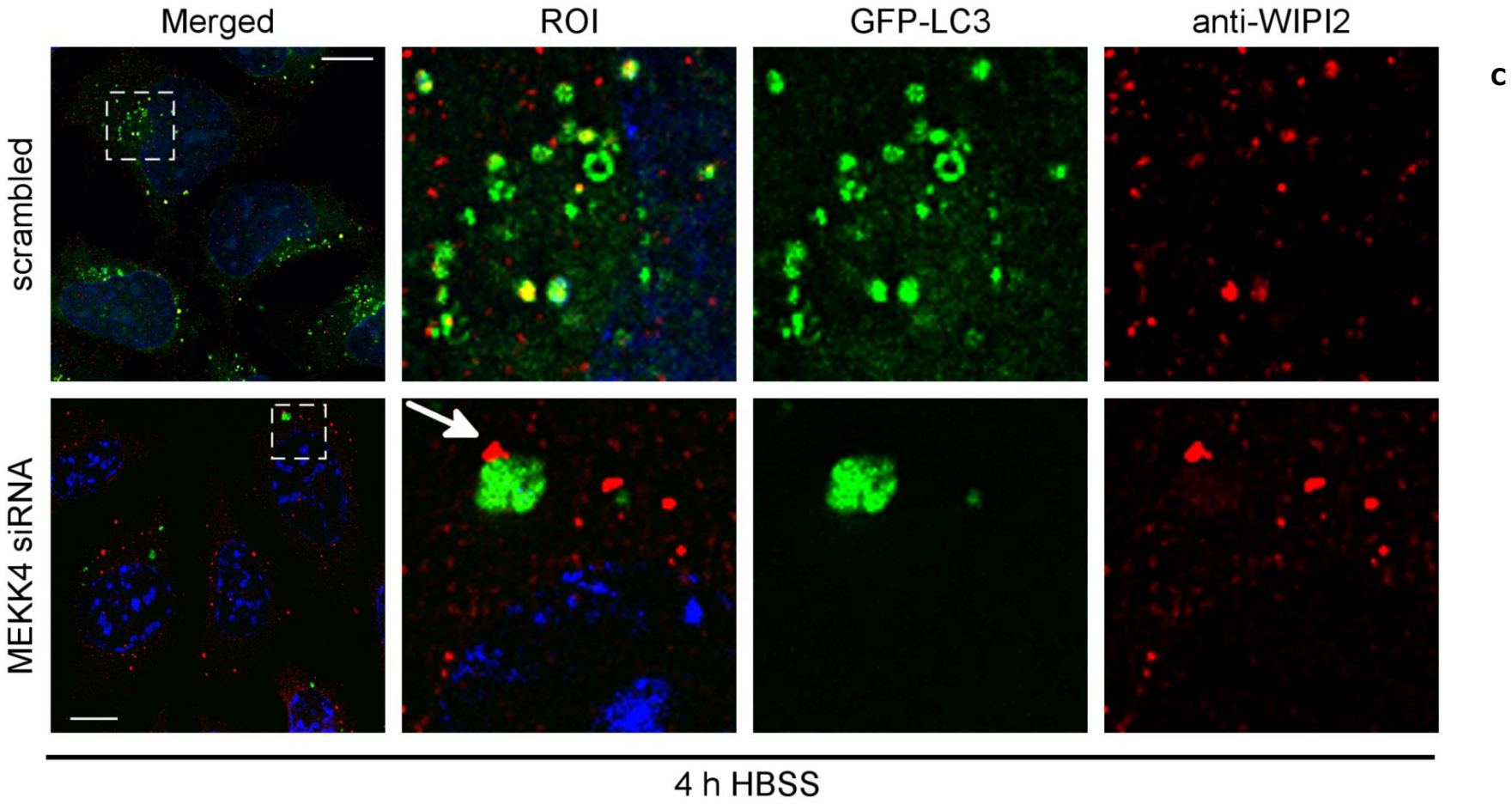

Figure 5.7 cont. WIPI2 is recruited to sites close to the large GFP-LC3 puncta induced by autophagy following MEKK4 silencing

(C) HEK293 GFP-LC3 cells were transfected with scrambled or MEKK4 siRNAs and the localisation of GFP-LC3 and WIPI2 observed after 4 h HBSS to induce autophagy. WIPI2 was immunostained and the nuclei stained with DAPI. Regions of interest are highlighted in boxes. Scale bars 10 μm

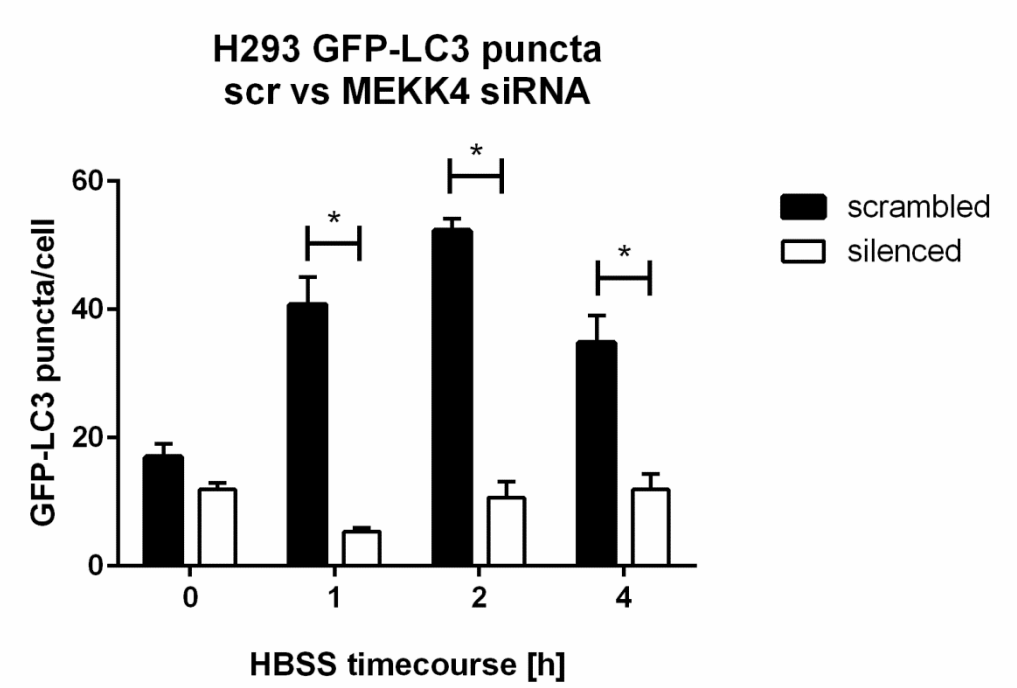

Figure 5.8 MEKK4 silencing decreases GFP-LC3 puncta per cell generated during autophagy

Images from experiments in Fig 5.6 – 5.9 were analysed using Imaris software to quantify GFP-LC3 puncta/cell.

Mean and SEM graphed. A students t-test was performed. * p = < 0.001

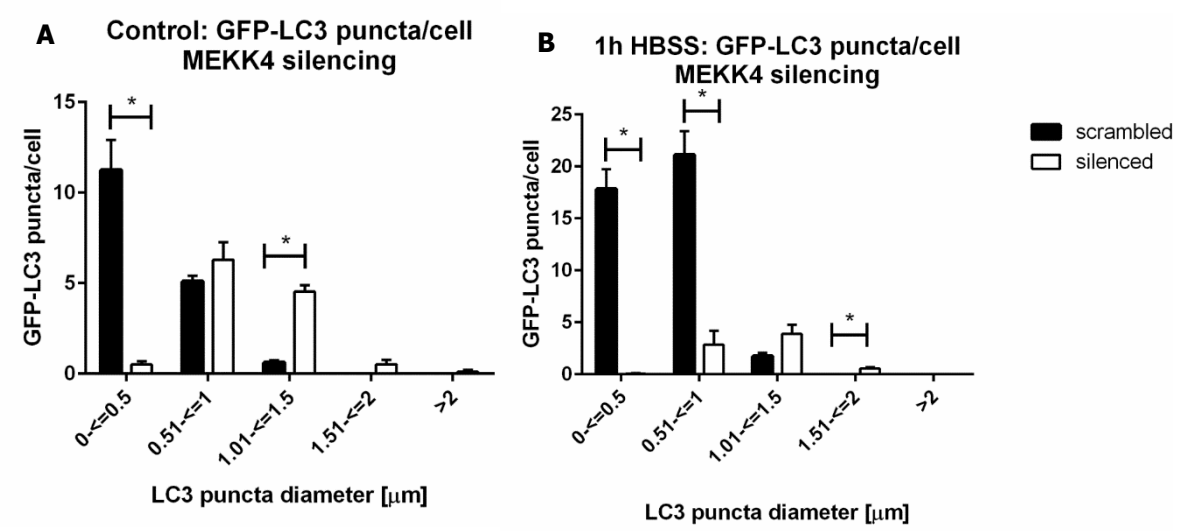

Figure 5.9 MEKK4 silencing leads to an increase in the diameter of GFP-LC3 puncta

(A) Images from experiments performed in Fig 5.6 and 5.10 were analysed using Imaris software. Mean and SEM are graphed. * p = < 0.001

(B) Images from experiments performed in Fig 5.7a and 5.10a were analysed using Imaris software. Mean and SEM are graphed. * p = < 0.0005 for 0 – 0.5 and 0.51 – 1 μm. * p = <0.01 for 1.51 - 2 μm.

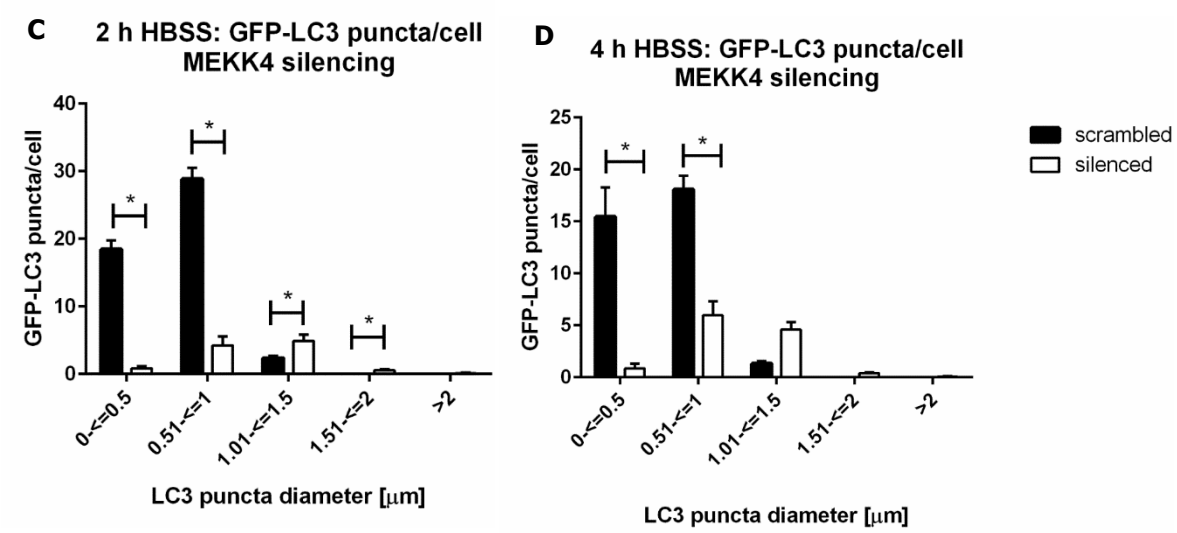

Figure 5.9 cont.

(C) Images from experiments performed in Fig 5.7b and 5.10b were analysed using Imaris software. Mean and SEM are graphed. * p = < 0.01

(D) Images from experiments performed in Fig 5.7c and 5.10c were analysed using Imaris software. Mean and SEM are graphed. * p = < 0.001

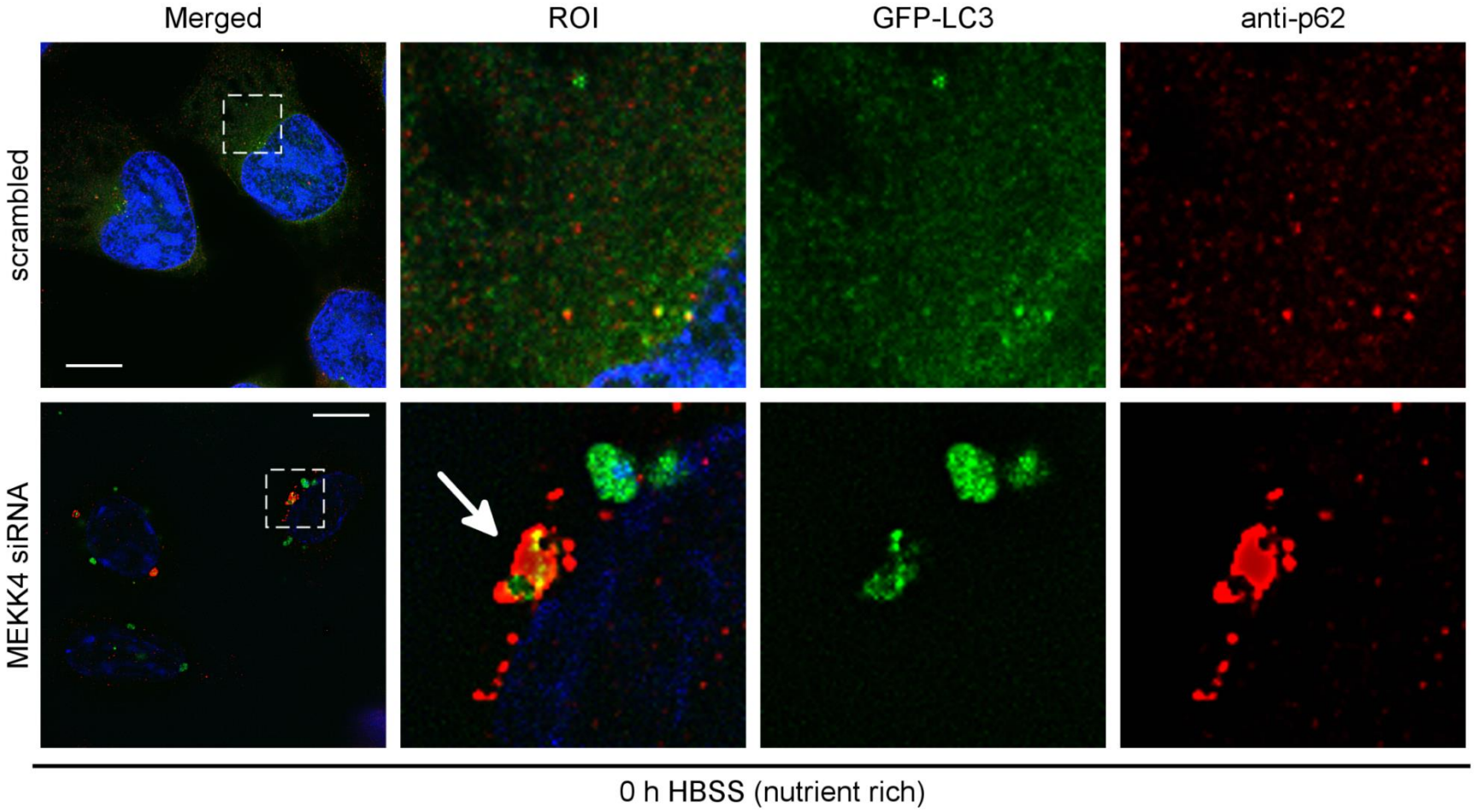

Figure 5.10 p62 colocalised with large GFP-LC3 puncta induced by MEKK4 silencing

HEK293 GFP-LC3 cells were transfected with scrambled or MEKK4 siRNAs and the localisation of GFP-LC3 and p62 observed in the absence of starvation induced autophagy. p62 was immunostained and the nuclei stained with DAPI. Regions of interest are highlighted in boxes. Scale bars 10 μm

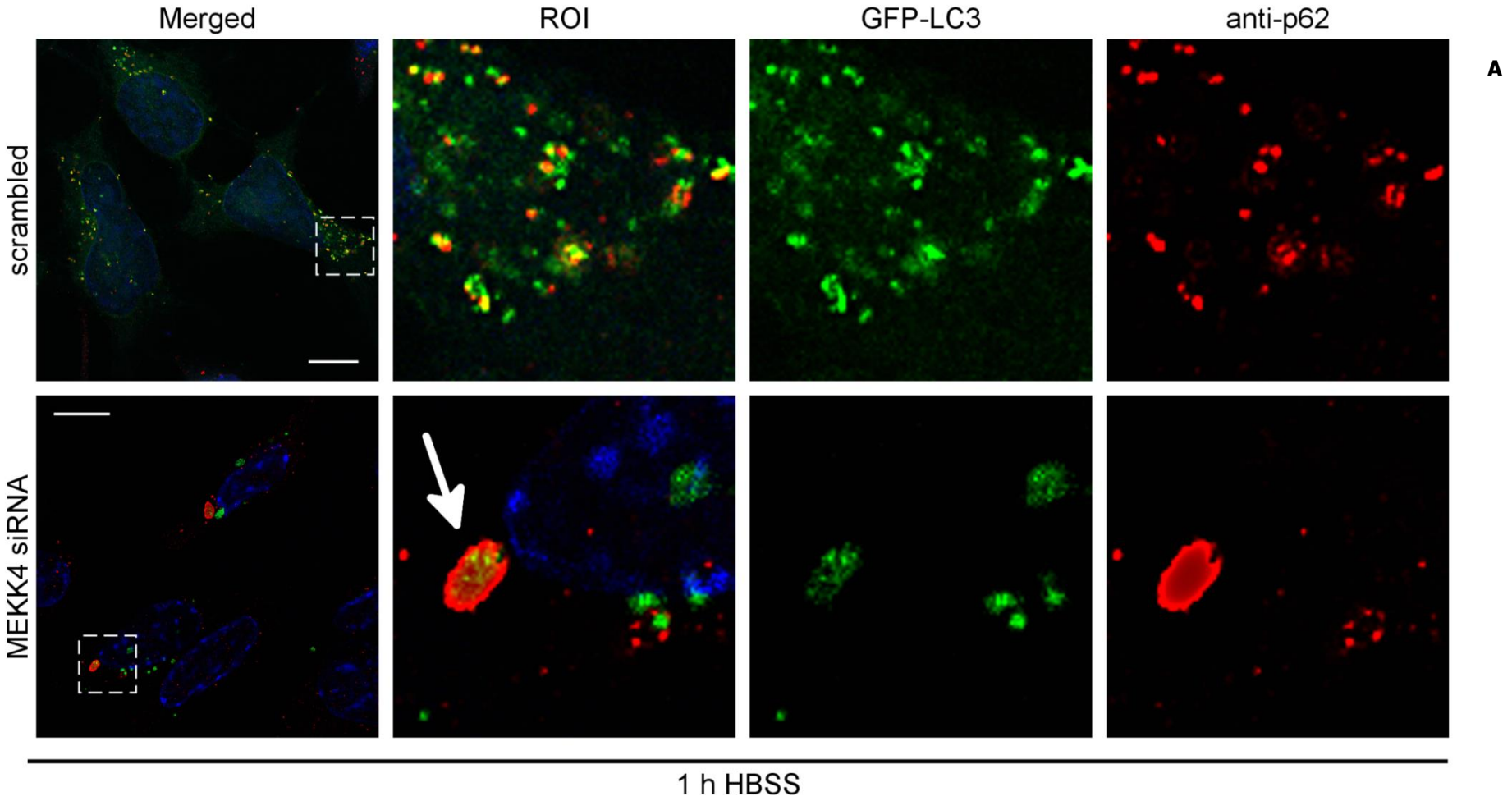

Figure 5.11 p62 continues to co-localise with GFP-LC3 puncta induced by MEKK4 silencing following induction of autophagy

(A) HEK293 GFP-LC3 cells were transfected with scrambled or MEKK4 siRNAs and the localisation of GFP-LC3 and p62 observed after 1 h HBSS to induce autophagy. P62 was immunostained and the nuclei stained with DAPI. Regions of interest are highlighted in boxes. Scale bars 10 μm

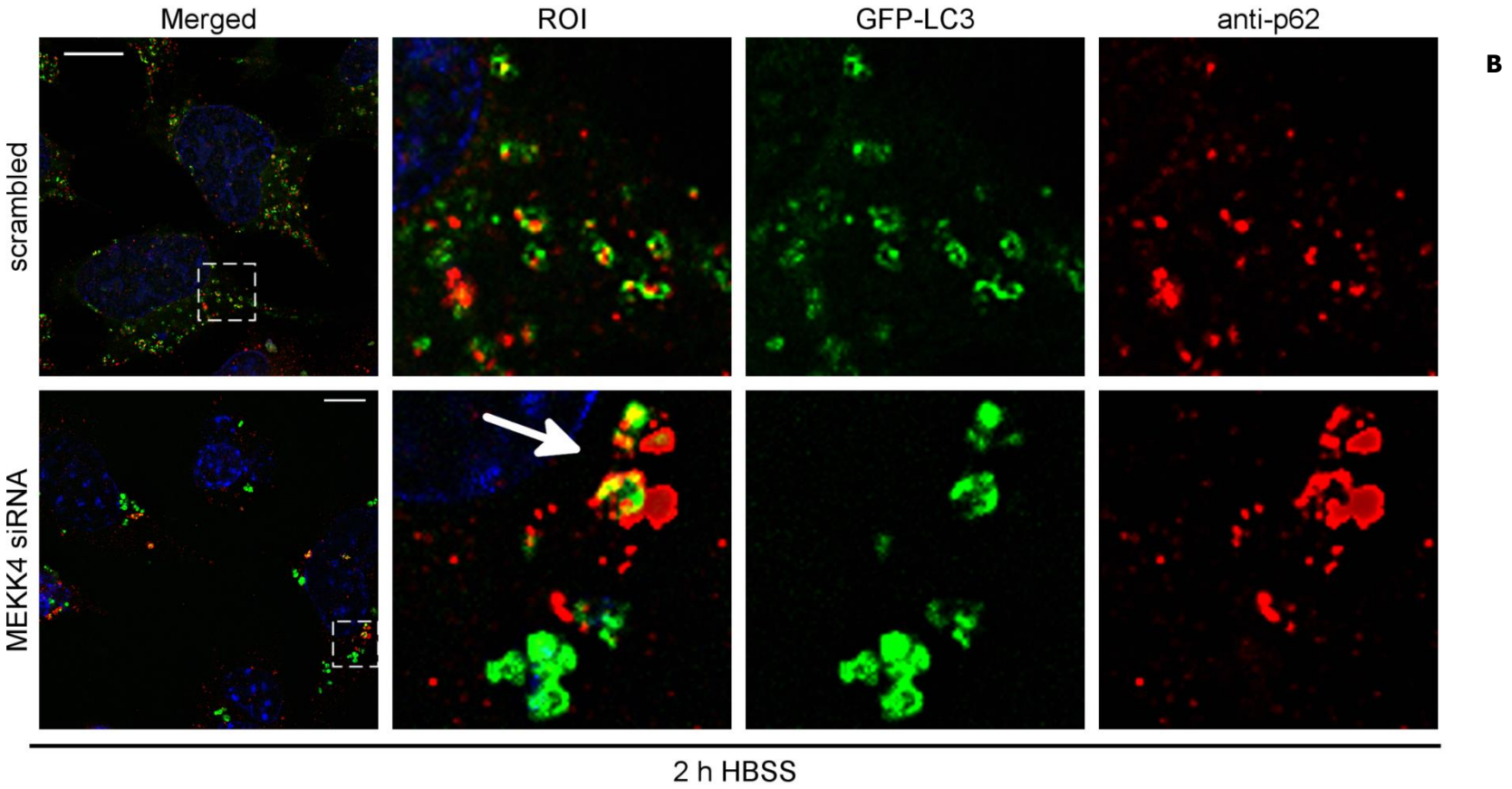

Figure 5.11 cont. p62 continues to co-localise with GFP-LC3 puncta induced by MEKK4 silencing following induction of autophagy

(B) HEK293 GFP-LC3 cells were transfected with scrambled or MEKK4 siRNAs and the localisation of GFP-LC3 and p62 observed after 2 h HBSS to induce autophagy. P62 was immunostained and the nuclei stained with DAPI. Regions of interest are highlighted in boxes. Scale bars 10 μm

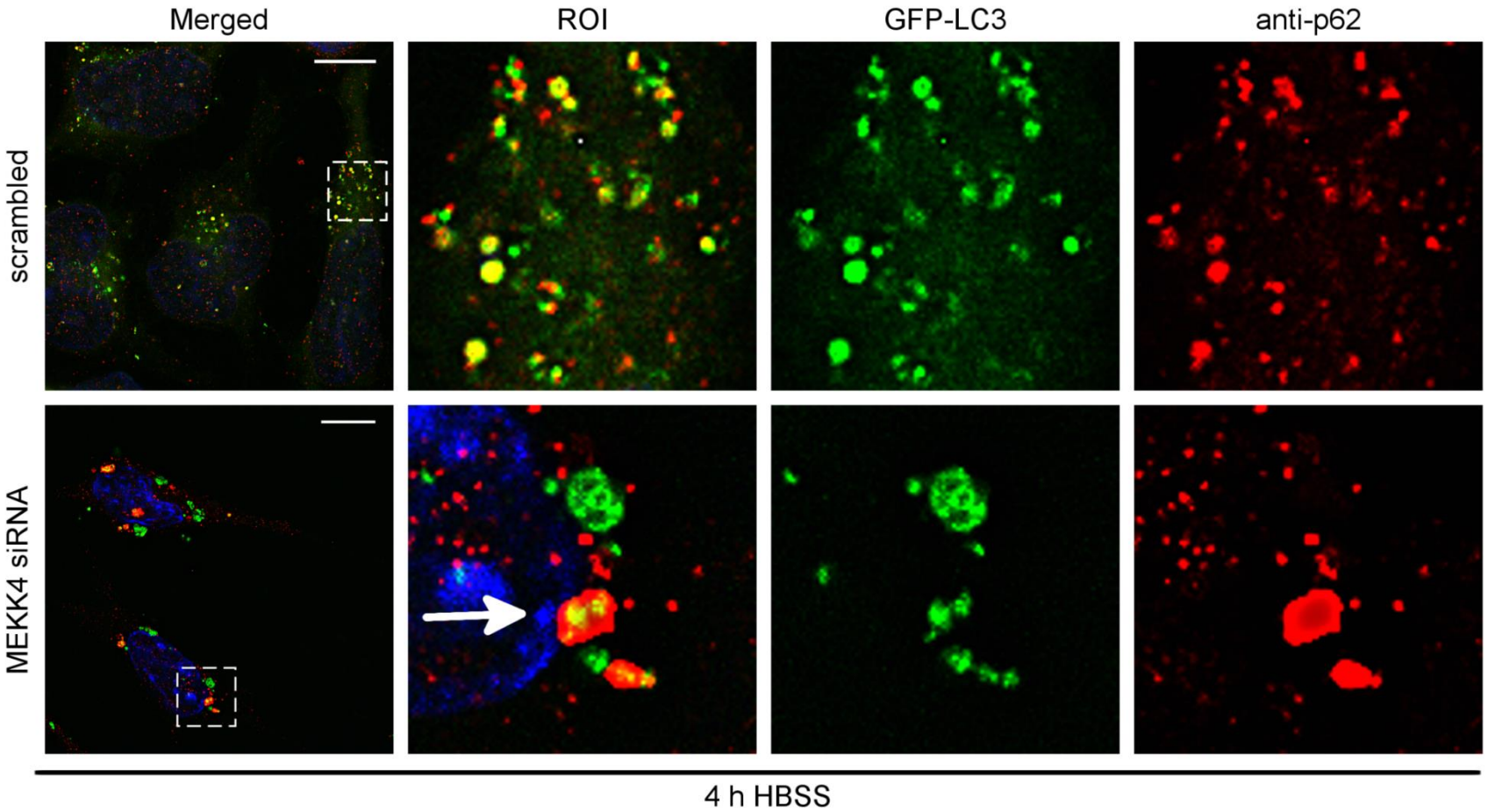

Figure 5.11 cont. p62 continues to co-localise with GFP-LC3 puncta induced by MEKK4 silencing following induction of autophagy

(C) HEK293 GFP-LC3 cells were transfected with scrambled or MEKK4 siRNAs and the localisation of GFP-LC3 and p62 observed after 4 h HBSS to induce autophagy. P62 was immunostained and the nuclei stained with DAPI. Regions of interest are highlighted in boxes. Scale bars 10 μm

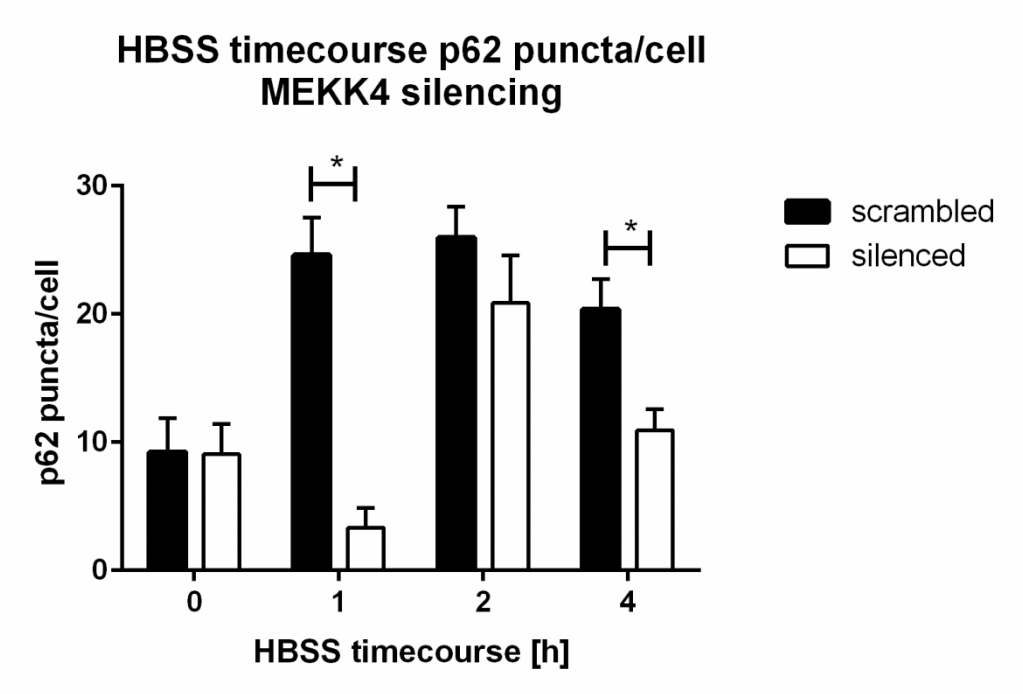

Figure 5.12 MEKK4 silencing does not consistently affect the number of p62 puncta per cell during autophagy
Images from experiments in Fig 5.10 – 5.11 were analysed using Imaris software to quantify p62 puncta/cell. Mean and SEM graphed. A student's t-test was performed. * p = <0.01

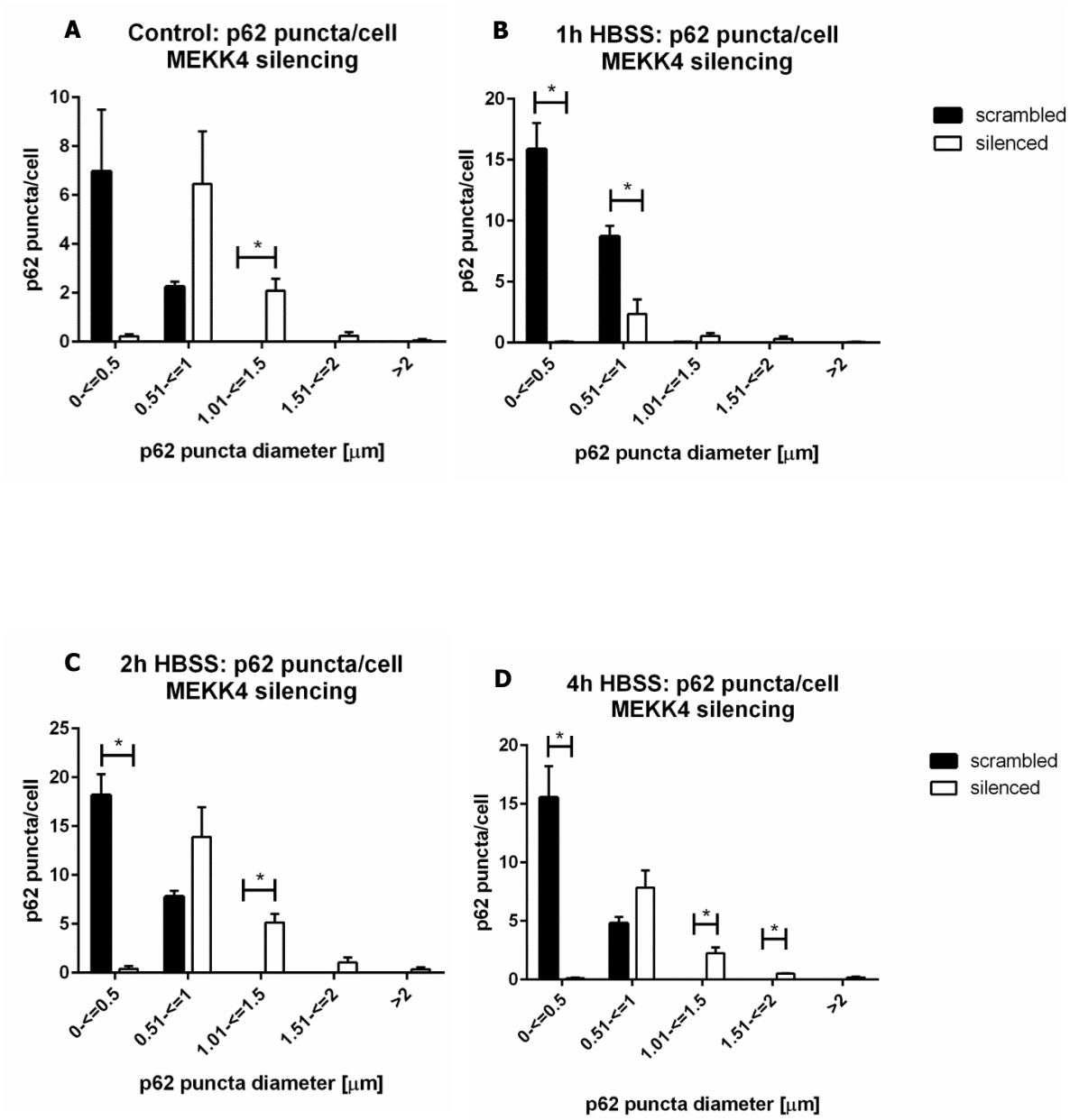

Figure 5.13 MEKK4 silencing leads to an increase in the diameter of p62 puncta

(A-D) Images from experiments 5.10- 5.11 were analysed with Imaris software and the diameter of p62 puncta quantified. A student's t-test was performed.

(A) * p = 0.005
(B) * p = < 0.005
(C) * p = <0005
(D) * p = < 0.001

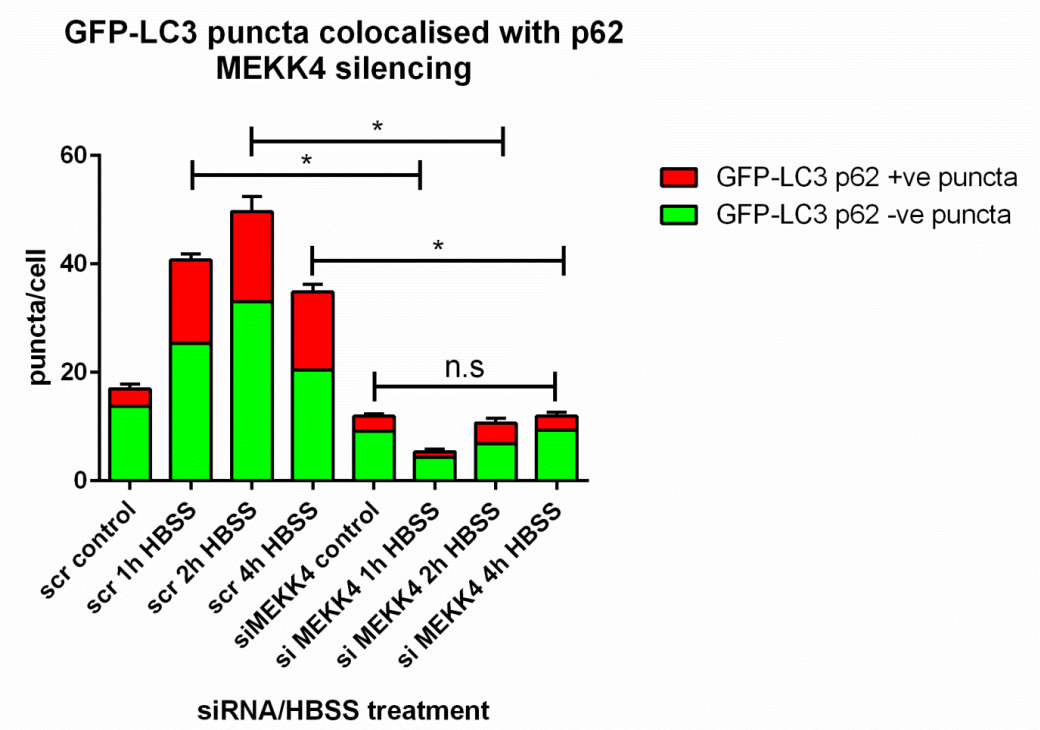

Figure 5.14 Overall co-localisation between p62 and GFP-LC3 is impaired in MEKK4-silenced cells

Images from experiments in 5.10-5.11 were analysed using Imaris and the co-localisation between p62 and GFP-LC3 quantified. Mean and SEM graphed. A student's t-test was performed. * p = < 0.005

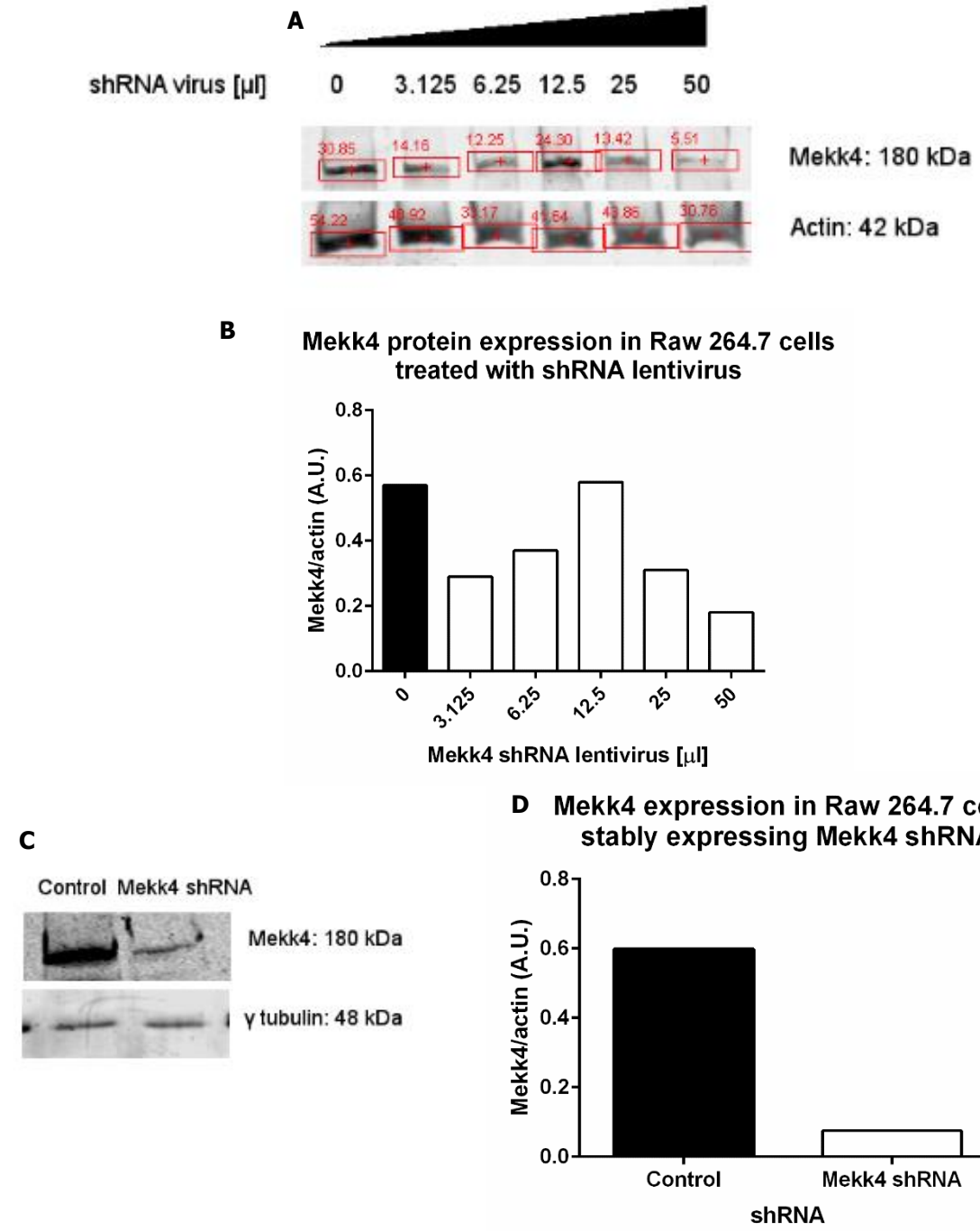

Figure 5.15 Mekk4 shRNA silencing in Raw 264.7 cells leads to decreased LC3 II

(A) Increasing volumes of concentrated shRNA lentiviral particles were added to Raw 264.7 cells, the lysates collected and MEKK4 expression analysed by Western blot.

(B) Densitometry analysis of (A)

(C) Raw 264.7 cells stably expressing MEKK4 shRNA were generated and the lysates analysed by Western blot.

(D) Densitometry analysis of (C)

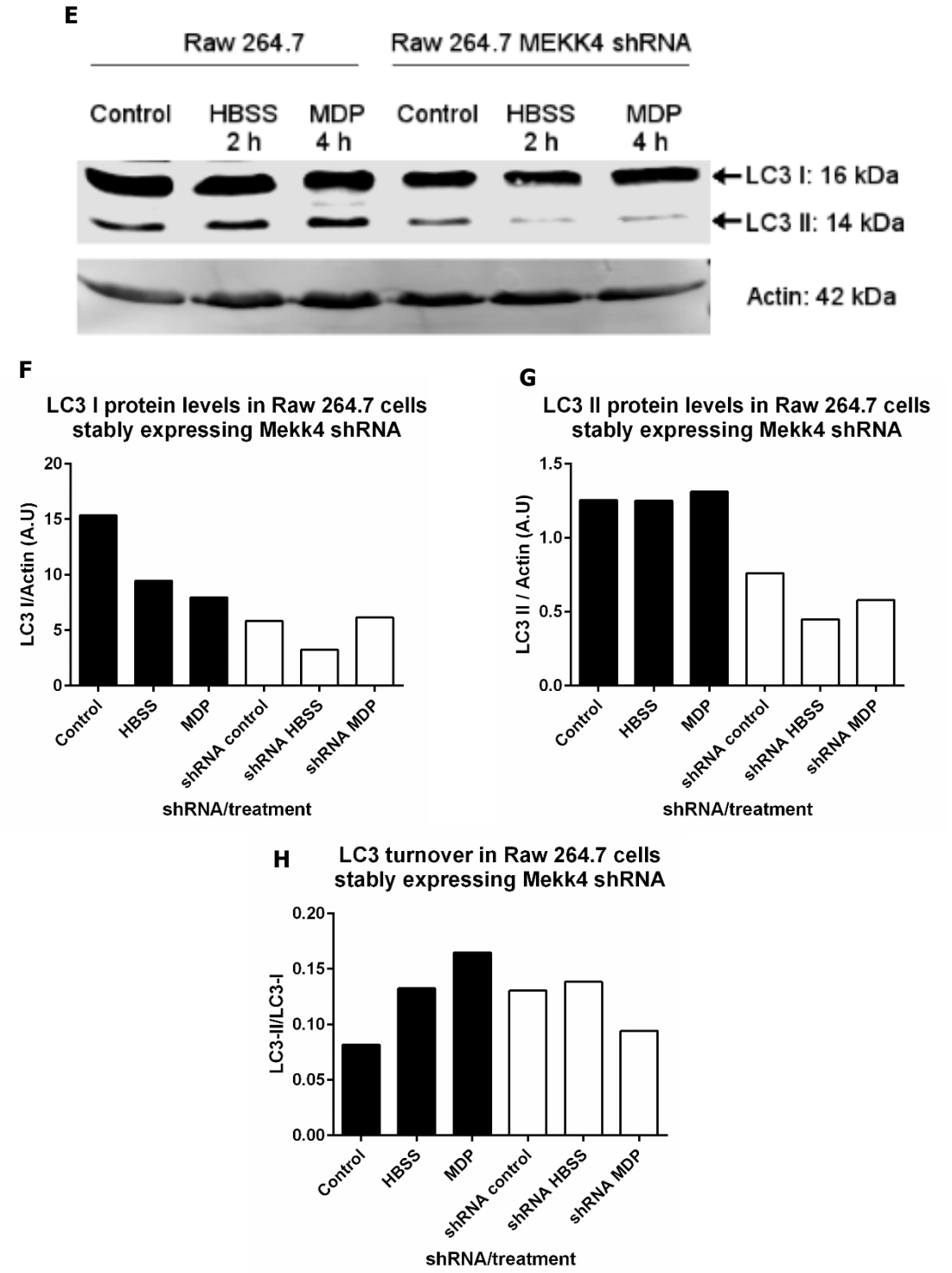

Figure 5.15 cont.

(E) Raw 264.7 MEKK4 shRNA cells were subjected to an HBSS timecourse, the lysates collected and analysed with the indicated antibodies by Western blot.

(F) Densitometry analysis of LC3 I levels in control cells (white) vs MEKK4 shRNA (black)

(G) Densitometry analysis of LC3 II levels in control cells (white) vs MEKK4 shRNA (black)

(H) Densitometry analysis of LC3 turnover in control cells (white) vs MEKK4 shRNA (black)

5.3.2 Generation of MEKK4 knockout cell lines using CRISPR-Cas9 mediated genome editing

Having characterised an autophagy specific defect in MEKK4 silenced cells using siRNA mediated gene silencing, the next step was to repeat the gene silencing using CRISPR-Cas9 genome editing. This would allow comparison to the siRNA experiments, to determine whether the results were due to off-target effects of the siRNAs. In addition to generating MEKK4 knockout cells against a wild type background, Atg5 knockout and p62 knockout cells were also chosen as candidate cell lines for Mekk4 knockout. This was to study the nature of the cellular aggregates, the formation of which is dependent on p62 and are cleared by autophagy (Lelouard et al., 2004; Lamark et al., 2012; Rubinsztein., 2006; Thoreen and Sabatini., 2004).

5.3.2.1 Designing guide oligo targets for sgRNA expression construct

A bicistronic expression vector pSpCas9(BB)-2A-GFP was obtained from www.addgene.org and has been described previously (Ran et al., 2013). Briefly, this vector contains a U6 promoter driven sgRNA expression cassette, with two BbsI cloning sites for the insertion of guide oligo targets. This is followed by a CBh promoter driven Cas9 2A GFP cassette, which allows screening of transfected cells. Both human and murine cell lines were chosen for the generation of MEKK4 knockout cell lines; HEK293, MEFs, MEF Atg5 knockout and MEF p62 knockout. To identify target sites within the MEKK4 gene suitable for use as sgRNA designs, the software tool E-CRISP was used (Heigwer et al., 2014). The algorithms identified target sequences in the human and mouse genes, and sequences were chosen that had low predicted off-target effects. The sgRNA oligos were synthesised and cloned into the vector as described (Ran et al., 2013). The orientation was verified by sequencing, resulting in the generation of pSpCas9(BB)-2A-GFP constructs targeting human MEKK4 or mouse Mekk4.

5.3.2.2 FACS sorting and expansion of transfected cells

The sgRNA Cas9-2A-GFP constructs were transiently transfected into HEK293, MEF, MEF Atg5 knockout and MEF p62 knockout cells. The cells were then analysed and sorted by FACS, with untransfected cells as a negative control (Fig 5.15-5.16). The HEK293 cells showed the greatest enrichment of GFP positive cells, which was confirmed by a post-sort analysis (Fig. 5.15). The assorted MEF cell lines did have some GFP positive cells, though this was reduced in comparison to the HEK293 transfected cells (Fig 5.16). Following

sorting, the GFP positive cells were cultured until enough viable cells were available for analysis.

5.3.2.3 Confirmation of MEKK4 knockdown and ALIS phenotype in CRISPR-Cas9 genome edited cell lines

The expression of an sgRNA and Cas9 protein in the same cell may not guarantee gene knockout in the cell; a double stranded break must be induced in both alleles and the repair pathway must induce indels that lead to frameshift mutations and premature stop codons. Therefore, it is desirable to isolate clonal cells to ensure a homogenous population of cells that likely have the same mutation. However, prior to this, it was necessary to ascertain whether MEKK4 had been knocked down adequately in a non-clonal population. The lysates were collected from the various cell lines and analysed for MEKK4 expression by Western blot. All cell lines demonstrated a subtle reduction in MEKK4 expression compared to the untransfected controls which was confirmed by densitometry (Fig 5. 18 a-d). At the time of writing, analysis of p62 cell lines by Western blot had been unsuccessful due to problems with protein extraction.

In conjunction with this analysis, MEF and p62 knockout cells were immunostained to establish whether the ALIS-like phenotype was replicated in these cells. The autophagy markers LC3 and WIPI were used as autophagosome markers. In a separate immunostaining, GFP-tagged ubiquitin, mCherry-tagged LC3 and p62 were used to determine if any aggregates contained ubiquitin. Advantage was also made of a construct expressing a mutant GFP-LC3-G120A, which cannot be cleaved and processed to LC3 II. This was used to verify whether the p62/LC3 positive aggregates were LC3 I positive.

In MEF MEKK4 Crispr-Cas9 treated cells, there were a small number of cells that contained large LC3 aggregates, which were negative for WIPI2 in the absence of autophagy (Fig 5.18). These aggregates were p62 and ubiquitin positive (Fig 5.19). These aggregates were able to recruit the cleavage defective LC3 mutant, indicating that the aggregates are LC3 I positive, and are likely an ALIS response (Fig 5. 20). Interestingly, there appeared by eye to be fewer ALIS structures in these cells than those seen in the MEKK4 siRNA experiments. This could reflect the short term response to an siRNA experiment versus the long term effects of gene knockout via CRISPR Cas9.

As p62 is required for ALIS formation, it was not expected that ALIS structures would be detected in the MEKK4 CRISPR p62 knockout cells (Fujita et al., 2011). This hypothesis was confirmed as no LC3 aggregates were seen in the immunostained cells, no large ubiquitin

puncta seen, nor were there any LC3 I positive structures (Fig. 5.21-23). These results indicate that any LC3/p62/ubiquitin positive aggregates seen in MEFs are likely an ALIS response to MEKK4 knockdown.

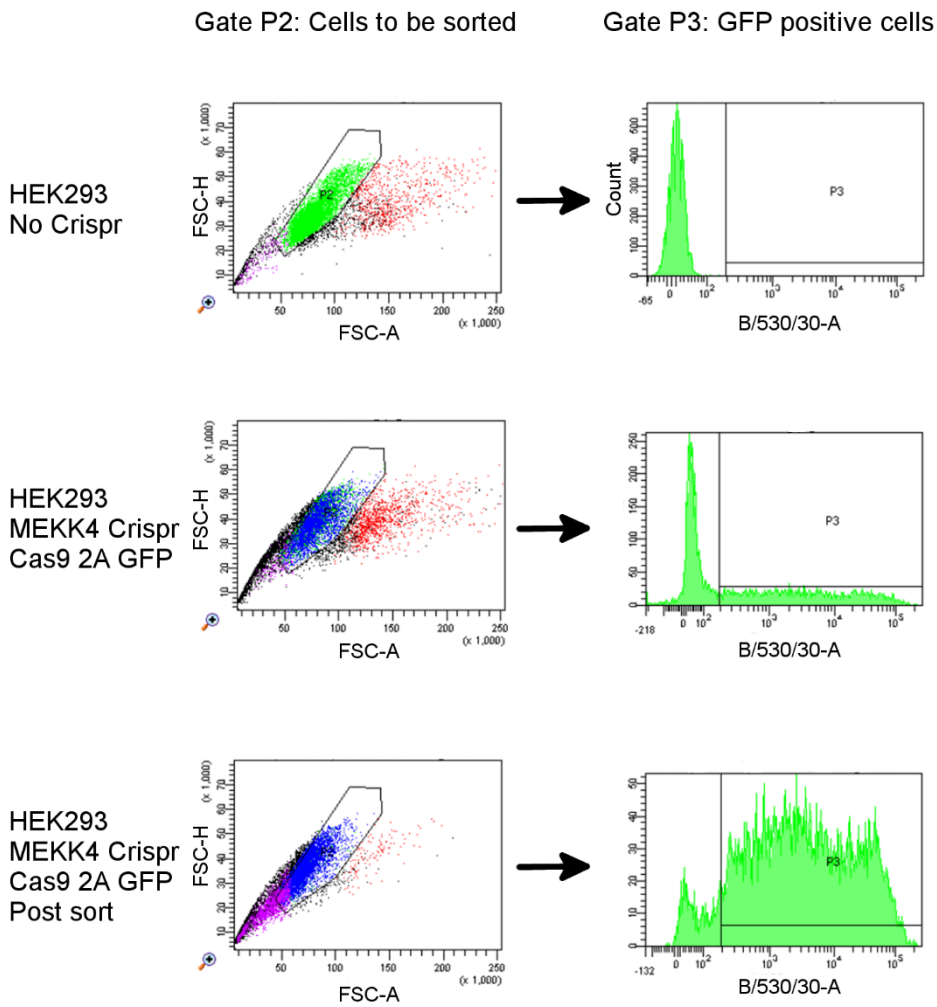

Figure 5.16 FACS sorting of HEK293 cells transfected with Cas9-2A-GFP vector

The population of cells to be sorted was identified in gate P2. GFP cells were sorted using B/530/30-A channel (P3) and subjected to a post-sort enrichment analysis to confirm the isolation of a GFP positive population

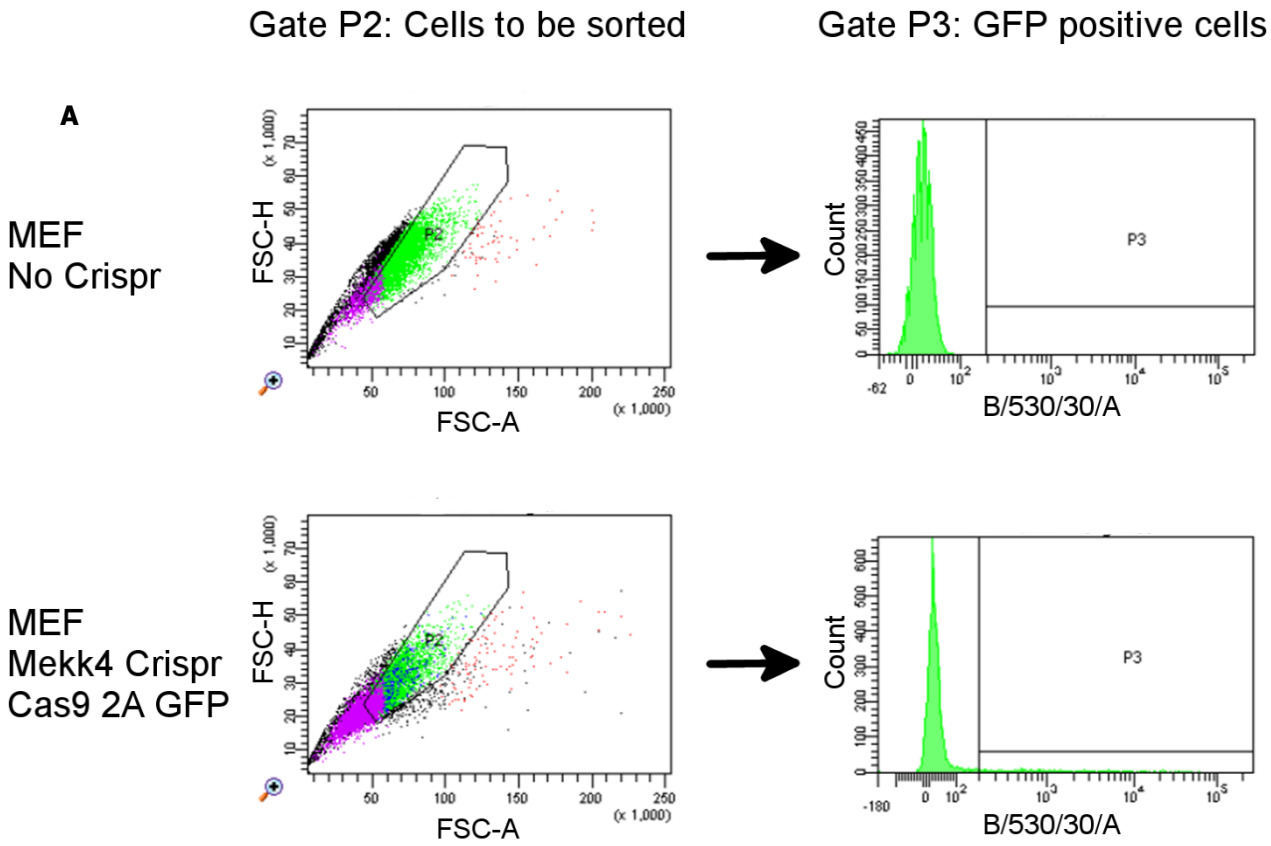

Figure 5.17 FACS sorting of MEF cell lines transfected with Cas9-2A-GFP vector

All cell lines were transfected with the Cas9 plasmid containing sgRNA against the genomic target. The population of cells to be sorted was identified in gate P2. GFP cells were sorted using B/530/30-A channel (P3).

(A) MEF cell line

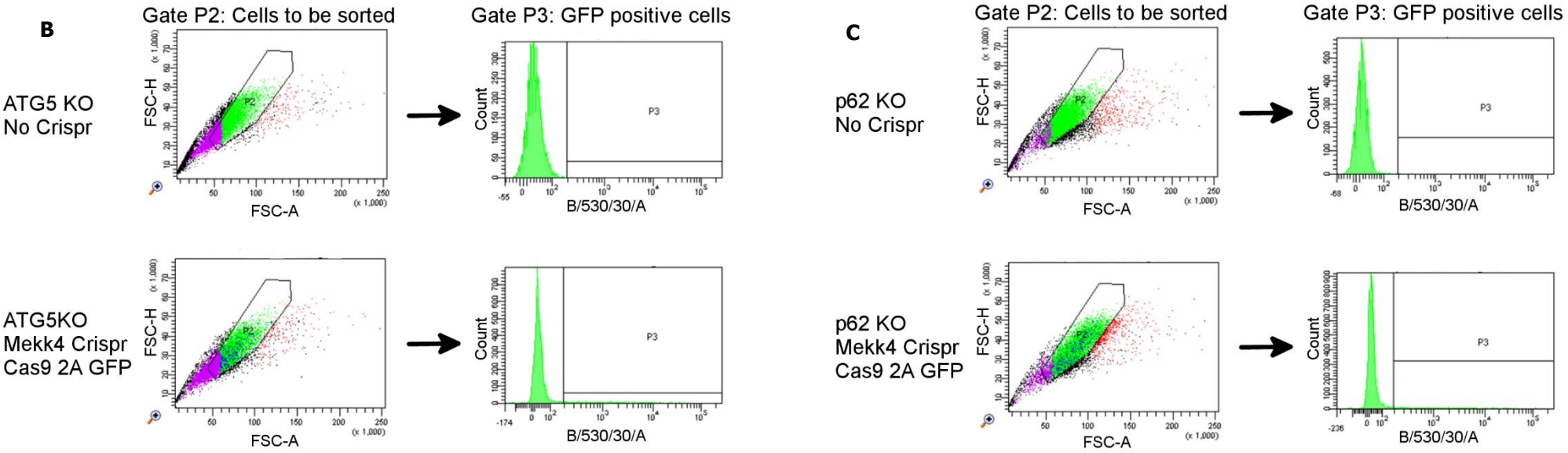

Figure 5.17 cont.

(B) ATG5KO MEF cells sorted for GFP after transfection with the Cas9-2A-GFP vector.

(C) p62 KO MEF cells sorted for GFP after transfection with the Cas9-2A-GFP vector.

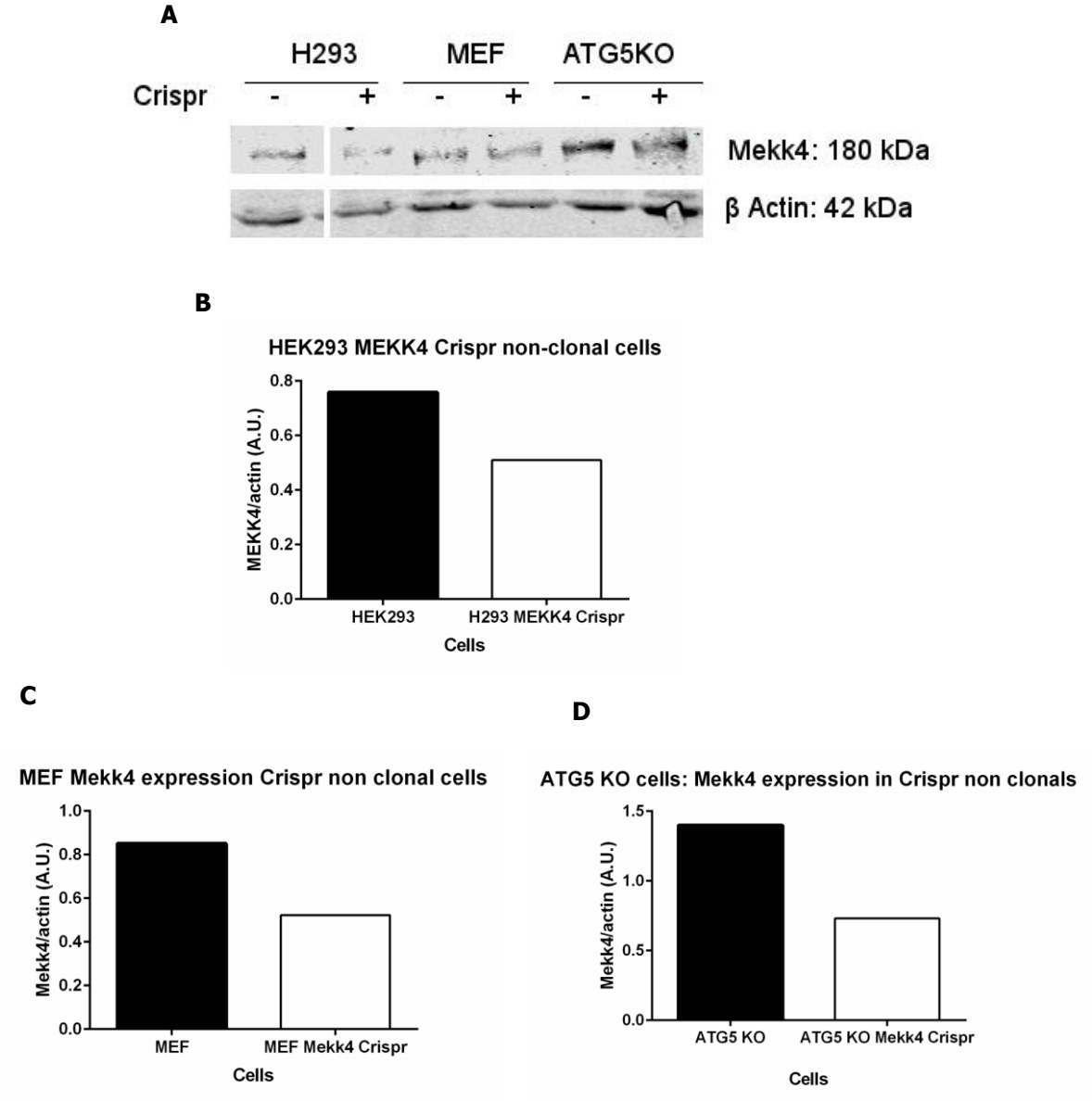

Figure 5.18 CRISPR/Cas9 genome editing results in a small decrease in MEKK4 expression in a non-clonal population of cells

(A) Lysates from non-clonal populations of cells post FACS sorting were analysed for MEKK4 expression by Western blot.

(B) Densitometry analysis of MEKK4 expression in HEK293 cells subjected to CRISPR/Cas9 genome editing

(C) Densitometry analysis of Mekk4 expression in MEF cells subjected to CRISPR/Cas9 genome editing

(D) Densitometry analysis of Mekk4 expression in MEF Atg5 KO cells subjected to CRISPR/Cas9 genome editing

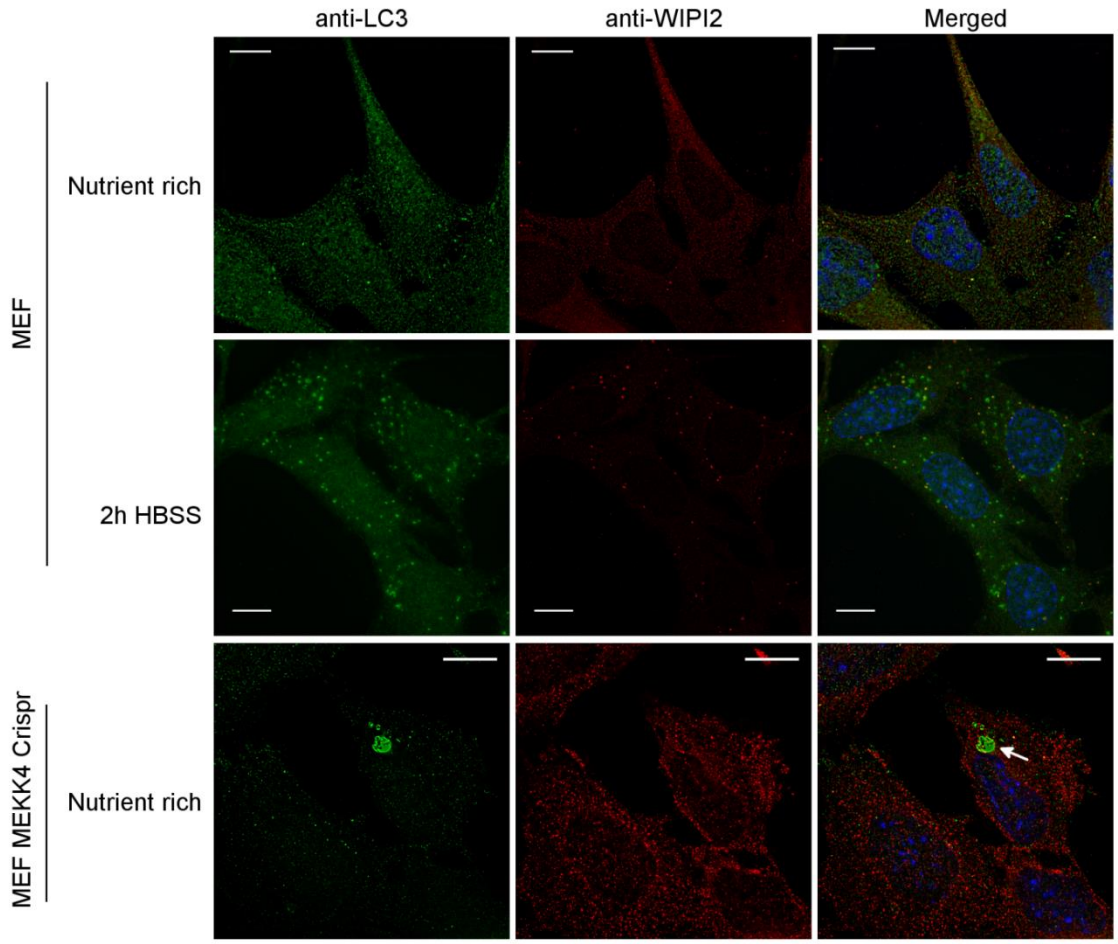

Figure 5.19 A population of Mekk4 CRISPR MEFs generate large perinuclear LC3 aggregates

Non clonal Mekk4 CRISPR MEFs and WT MEFs were immunostained for LC3 and WIPI post FACS sorting and the nuclei stained with DAPI. Scale bars 10 μm

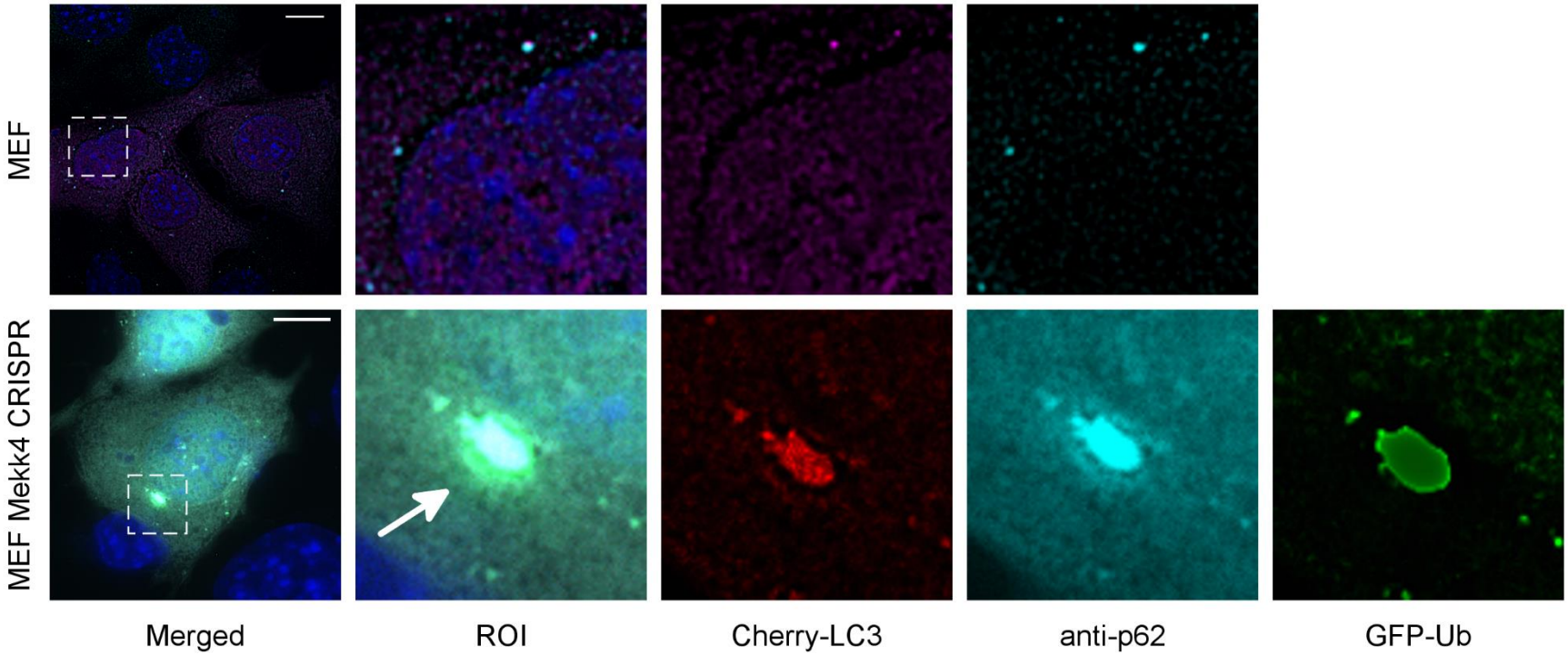

Figure 5.20 LC3 positive aggregates which associate with p62 and ubiquitin are formed in MEKK4 CRISPR knockout cells

Wild type MEFS and MEF Mekk4 CRISPR cells post FACS sorting were transfected with cherry-LC3 and GFP-ubiquitin (CRISPR cells only). The cells were immunostained for p62 (cyan) and the nuclei stained with DAPI. Regions of interest highlighted with boxes. Scale bars 10 μm

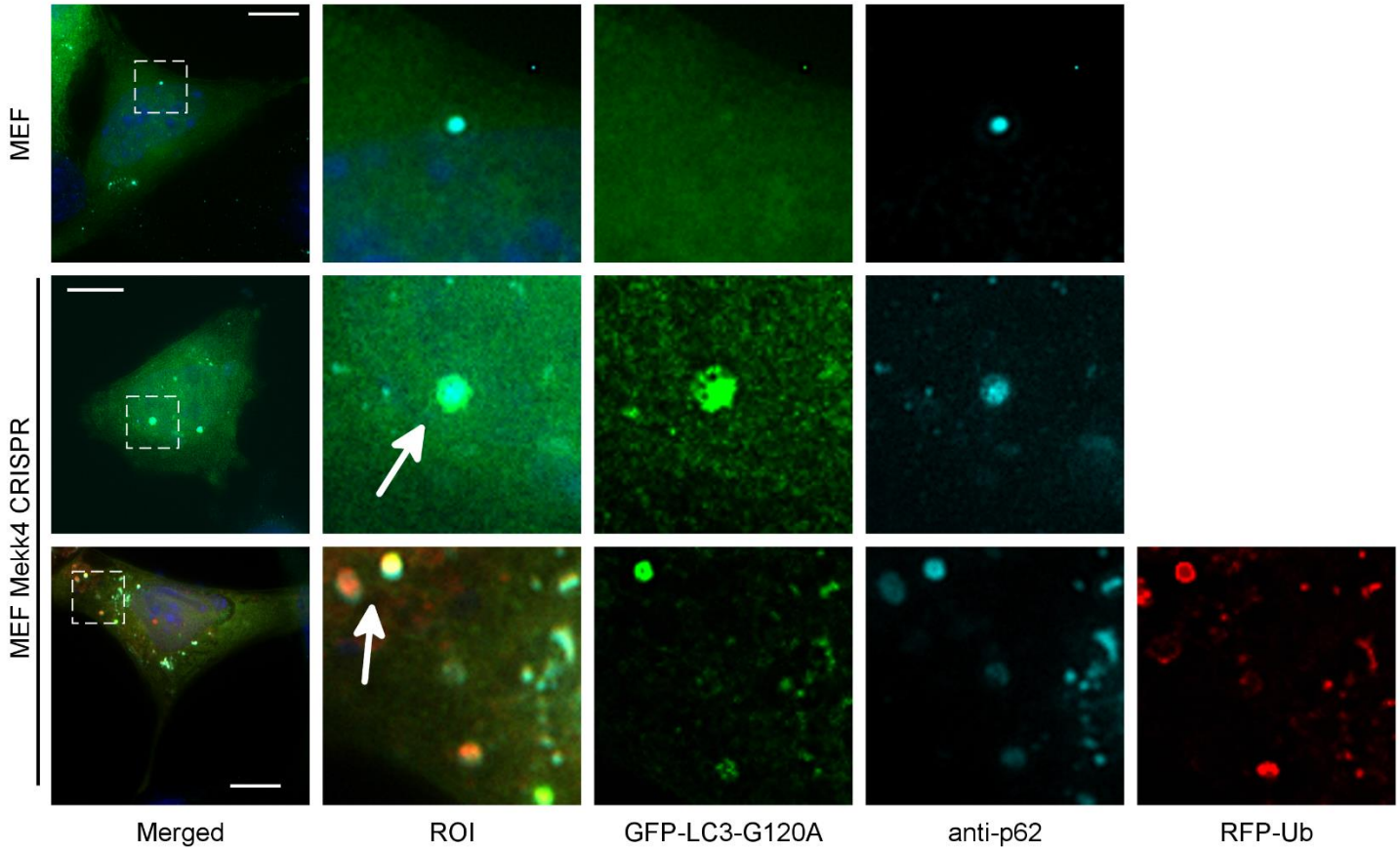

Figure 5.21 LC3 I associates with p62 and ubiquitin positive aggregates following silencing of MEKK4

MEFS were silenced for MEKK4 using CRISPR/CAS. Cells expressing CAS-GFP were sorted by FACS and transfected using plasmids expressing GFP-LC3-G120A and RFP-ubiquitin. The silenced MEFs were compared with control MEFs following immunostaining for p62 (Far red Alexa 647, cyan). The nuclei were stained with DAPI. Regions of interest highlighted with boxes. Scale bars 10 µm

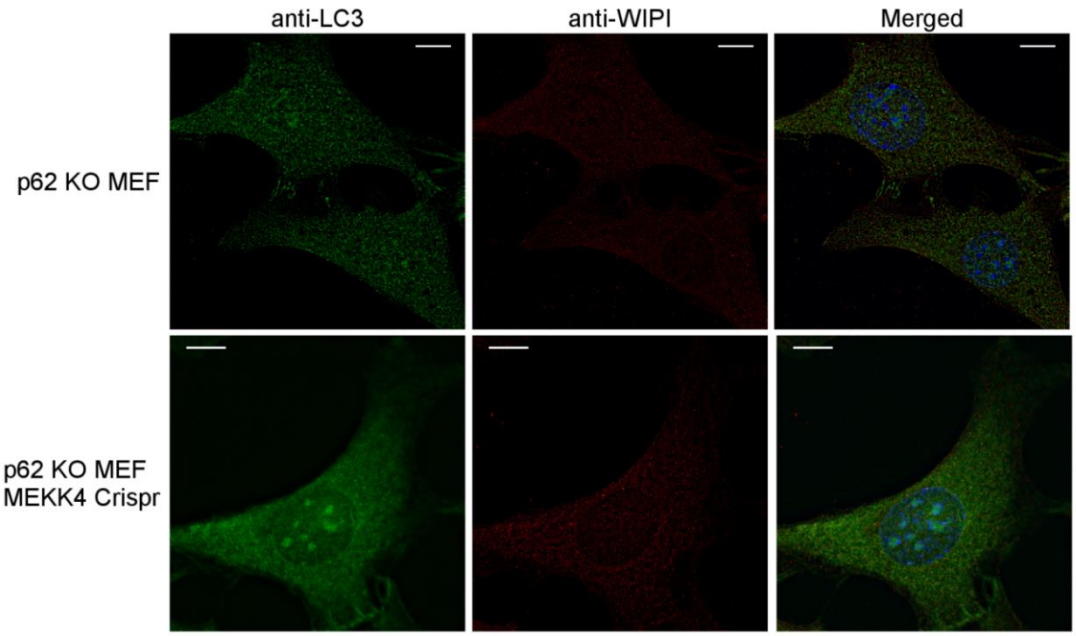

Figure 5.22 LC3 positive aggregates are not formed following silencing of Mekk4 in cells lacking p62

p62 KO MEFS were silenced for MEKK4 using CRISPR/CAS. Cells expressing CAS-GFP were sorted by FACS, and immunostained for LC3 (green Alexa 488) and WIPI (red Alexa 594) and post FACS sorting. The nuclei were stained with DAPI. Scale bars 10 μm

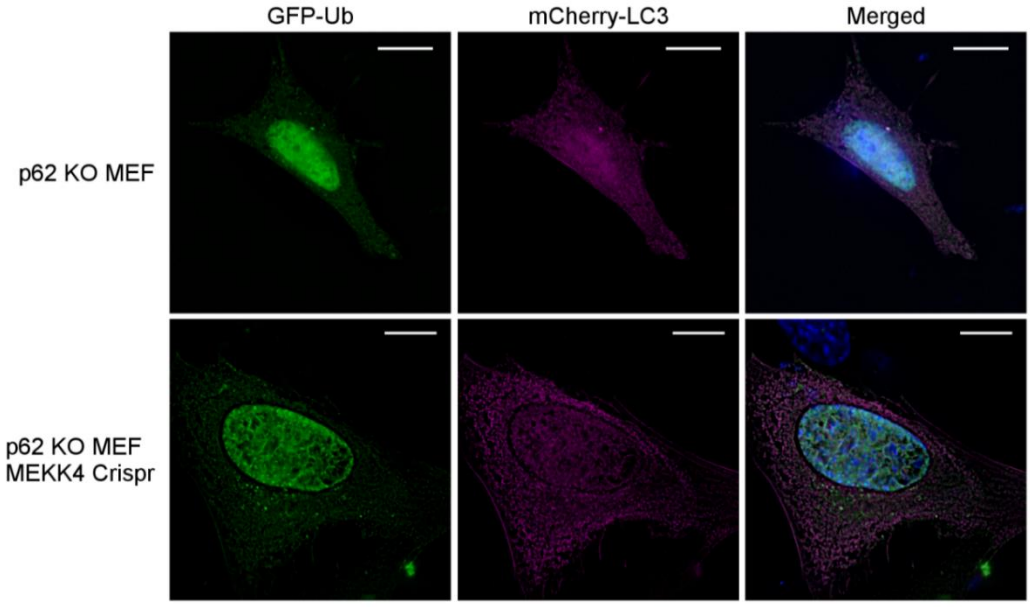

Figure 5.23 Ubiquitin -positive aggregates are not formed following silencing of MEKK4 in cells lacking p62.

MEFS lacking expression of p62 (p62-KO) were silenced for MEKK4 using CRISPR/CAS. Cells expressing CAS-GFP were sorted by FACS and transfected with a plasmid expressing cherry-LC3 and GFP-ubiquitin.

The nuclei were stained with DAPI. Scale bars 10 μm

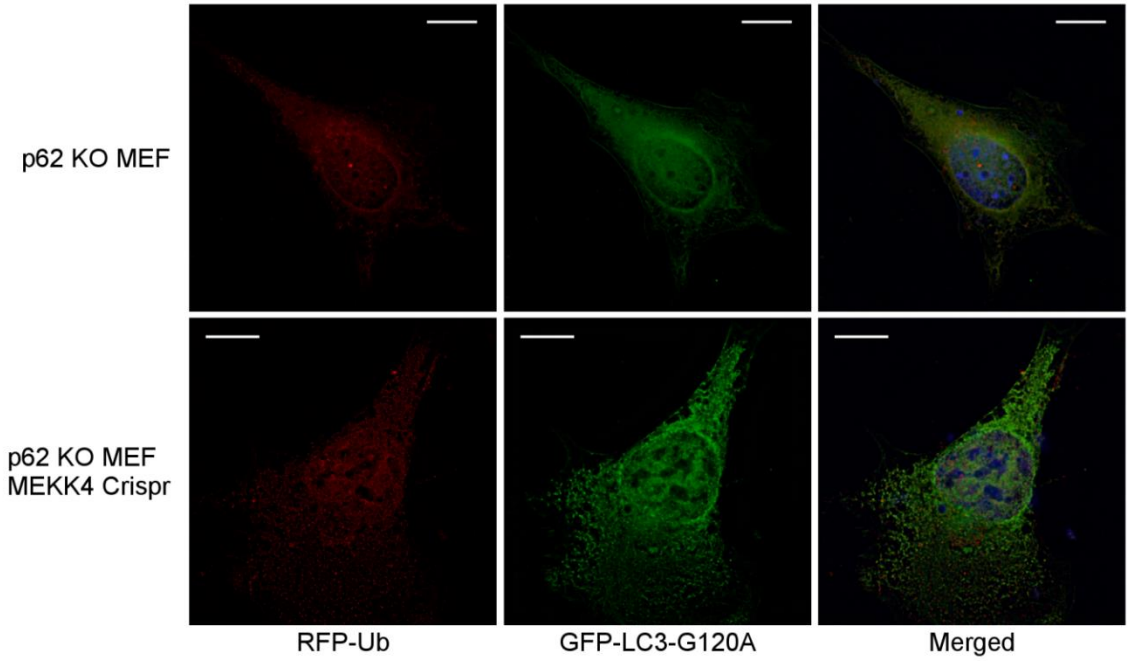

Figure 5.24 LC3 I-positive aggregates are not formed following silencing of MEKK4 in cells lacking p62

MEFS lacking expression of p62 (p62-KO) were silenced for MEKK4 using CRISPR/CAS. Cells expressing CAS-GFP were sorted by FACS and transfected with plasmids expressing GFP-LC3-G120A and RFP-ubiquitin.

The nuclei were stained with DAPI. Scale bars 10 μm

5.4 Chapter Discussion

The main aims of this chapter were to investigate the effect of silencing MEKK4 on the autophagy pathway. A primary screen of siRNAs to transiently knockdown MEKK4 expression was carried out, and the effects on LC3 processing and LC3 distribution were observed. The co-localisation of LC3 with autophagosome and autophagic cargo markers were observed and quantified by Imaris. Cell lines were generated where MEKK4 had been knocked out by CRISPR/Cas9 mediated genome editing, to replicate the earlier siRNA results. This resulted in the generation of a heterogeneous population of cells, some of which may have had Mekk4 knocked out via CRISPR. However, clonal selection to isolate these cells was unsuccessful. The experiments do serve as good preliminary data for analysing the effect of Mekk4 knockdown on the autophagy pathway.

When MEKK4 was transiently knocked down by siRNA, there was a defect in the processing of LC3 I to LC3 II which was indicated by the Western blot results. In this situation, the LC3 was expected to localise in the cytosol, with a reduction in the number of LC3 positive puncta. However, the localisation of LC3 in these cells was to large perinuclear aggregates. These aggregates were p62 positive, and had a larger than expected size of autophagosomes. When the cells were starved, there was no change in the number and size of LC3 puncta in the silenced cells. Interestingly, a small amount of WIPI2 was recruited to the aggregates, but did not fully co-localise with LC3. In cells that had Mekk4 gene expression knocked out by CRISPR/Cas9 mediated genome editing, LC3 positive aggregates were detected that contained p62 and ubiquitin. Interestingly, an LC3 mutant (G120A), which cannot be processed from LC3 I to LC3 II) was also able to form aggregates in the Mekk4 knockout cells, which indicates that the LC3 aggregates are likely LC3 I positive, rather than LC3 II.

The persistent presence of the LC3 positive aggregates in MEKK4 silenced cells during autophagy activation indicates two things. Firstly, that these cells are autophagy deficient and secondly that this defect probably lies downstream of WIPI2 in the autophagy pathway. If the inhibition of autophagy following MEKK4 silencing is a result of disruption of the ATG16L1: MEKK4 interaction, then there would be no expected effects on upstream components of the autophagy pathway e.g. WIPI2. The localisation of ATG16L1 in MEKK4 silenced cells does require further investigation, to determine how this is affected when MEKK4 is depleted. Based on the previous immunoprecipitation and localisation results (chapter 4), it is unlikely that the recruitment of ATG16L1 to the autophagosome will be

attenuated, as MEKK4 doesn't localise to the autophagosome. As the kinase activity of MEKK4 is involved in the interaction, it is possible that MEKK4 is involved in the activation of ATG16L1 by phosphorylation, which acts as a "molecular switch" for autophagic activity. However, the lack of large LC3 positive aggregates in Atg16L1 knockout cells (Saitoh et al., 2008) would imply that the formation of these structures in MEKK4 silenced cells is not solely due to the interaction between Atg16L1 and Mekk4.

The results of this study agree with previous research, which identified a putative role for MEKK4 in NOD2 mediated autophagy, whereby silencing MEKK4 led to an increase in the survival of *Salmonella typhimurium* in cell culture, due to a decrease in autophagy-directed destruction of bacteria (Homer et al., 2012). However, MEKK4 appears to have a role in canonical autophagy rather than just selective autophagy in the work carried out in this thesis. MEKK4 has also been linked to autophagy through its involvement in the GADD45-MEKK4-p38 pathway, which has been shown to regulate autophagy (Keil et al., 2012). When p38 is activated through GADD45 mediated MAPK signalling, ATG5 is phosphorylated, which leads to the inhibition of autophagosome maturation and fusion with the lysosome. As MEKK4 appears to be the main MAP3K involved in this signalling cascade, based on the results of Keil et al., 2012 the expectation would be that a knockdown in MEKK4 expression would lead to an increase in autophagy. Indeed, Gadd45 -/- primary macrophages and p38 -/- MEFs both displayed an increase in basal and autophagy responses to LPS and starvation, respectively (Keil et al., 2012). As this is not the case, this raises issues with the true role of MEKK4 in the GADD45-MEKK4-p38 regulation of autophagy, and demands further investigation into the specific role of MEKK4 in regulating autophagic flux.

The nature of the large perinuclear LC3/p62/ubiquitin aggregates also warrants additional characterisation. The structures share characteristics with ALIS and aggresomes. Both contain p62 and both rely on autophagy for clearance (Lelouard et al., 2004; Lamark et al., 2012; Rubinsztein., 2006; Thoreen and Sabatini., 2004). What was intriguing about the MEKK4 silencing-induced structures was that they had a tendency to localise to the perinuclear region, which is similar to the site of the aggresome. The aggresome is also metabolically stable (Lamark et al., 2012), unlike ALIS which are transient structures (Fujita et al., 2011; Szeto et al., 2006). The microtubule organising centre (MTOC) is the main site of aggresome formation, where protein aggregates are deposited and can accumulate to inclusions of between 1 and 3 μm diameter, when degradation pathways in the cell are overwhelmed (Wileman., 2007). The size of these aggresomes are comparable to those induced by MEKK4 silencing. The transport of ubiquitinated substrates to the aggresome is

mediated by the motor-protein dynein, and facilitated by histone deacetylase 6 (HDAC6), which enables the clearance of aggresomes by autophagy (Kawaguchi et al., 2003; Iwata et al., 2005; Yao et al., 2010). HDAC6 also regulates microtubule deacetylation, and plays an important role in microtubule dynamics, with inhibition altering the rate of growth and shrinkage of microtubules (Zilberman et al., 2009). If the aggregates observed in MEKK4 silenced cells are aggresomes, then their formation would be dependent on HDAC6, therefore inhibition of HDAC6 would be a useful experiment to determine if the aggregates could still form in these conditions. Alternatively, nocodazole treatment would depolymerise the microtubules, which would inditcate if the aggregates relied on the microtubule network for transport. However, the finding that the mutant LC3 G120A, which cannot be processed to LC3 I, is recruited to MEKK4 silencing-induced aggregates would indicate that these structures are a form of ALIS. During aggresome formation the intermediate filament vimentin has been known to collapse and form a cage around the aggresome, sequestering the aggregates and protecting the cell from further damage (Garcia-Mata et al., 1999). The localisation of the MEKK4 silencing aggregates with the MTOC and vimentin, and time-lapse microscopy would help determine whether these structures were ALIS or aggresomes.

The use of CRISPR/Cas9 mediated genome editing in this chapter has facilitated rapid generation of hetergenous knockout cell lines, which is an advantageous technique when studying effects of long term gene knockout versus the effects of transient gene knockdown. The design of the sgRNA target sequence was determined computationally, which allows for a relatively straightforward custom design and construction of the sgRNA. Considerations must be given for off-target cleavage activities of Cas9 (Hsu et al., 2013; Fu et al., 2013; Jiang et al., 2013), which can be determined computationally (Ran et al., 2013). Tolerance for mismatches between the sgRNA target sequence and off-target genomic DNA is position dependent; the first 6 bp of the 5' end of the guide sequence will tolerate mismatches. More than three mismatches will in most instances not be tolerated, and increasing the amount of transfected sgRNA/Cas9 can also increase the number of off-target cleavages (Ran et al., 2013). After the cell lines used in this study were generated, new algorithms and software became available to design sgRNA and calculate off-target effects (http://tools.genome-engineering.org). The suitability of the sgRNA target sequences were assessed and whilst the human sgRNA was deemed as a high quality guide; the number of off-target effects were low with mismatches of 3bp or more and the majority occurring outside of exons (appendix 3). However, the mouse sgRNA used in this thesis was classified as a mid-quality guide, with an increased number of exon off-target effects, with fewer mismatches between the sgRNA and the off-target sequence, increasing the likelihood of off-target cleavage (appendix 4). Therefore, additional mouse sgRNA

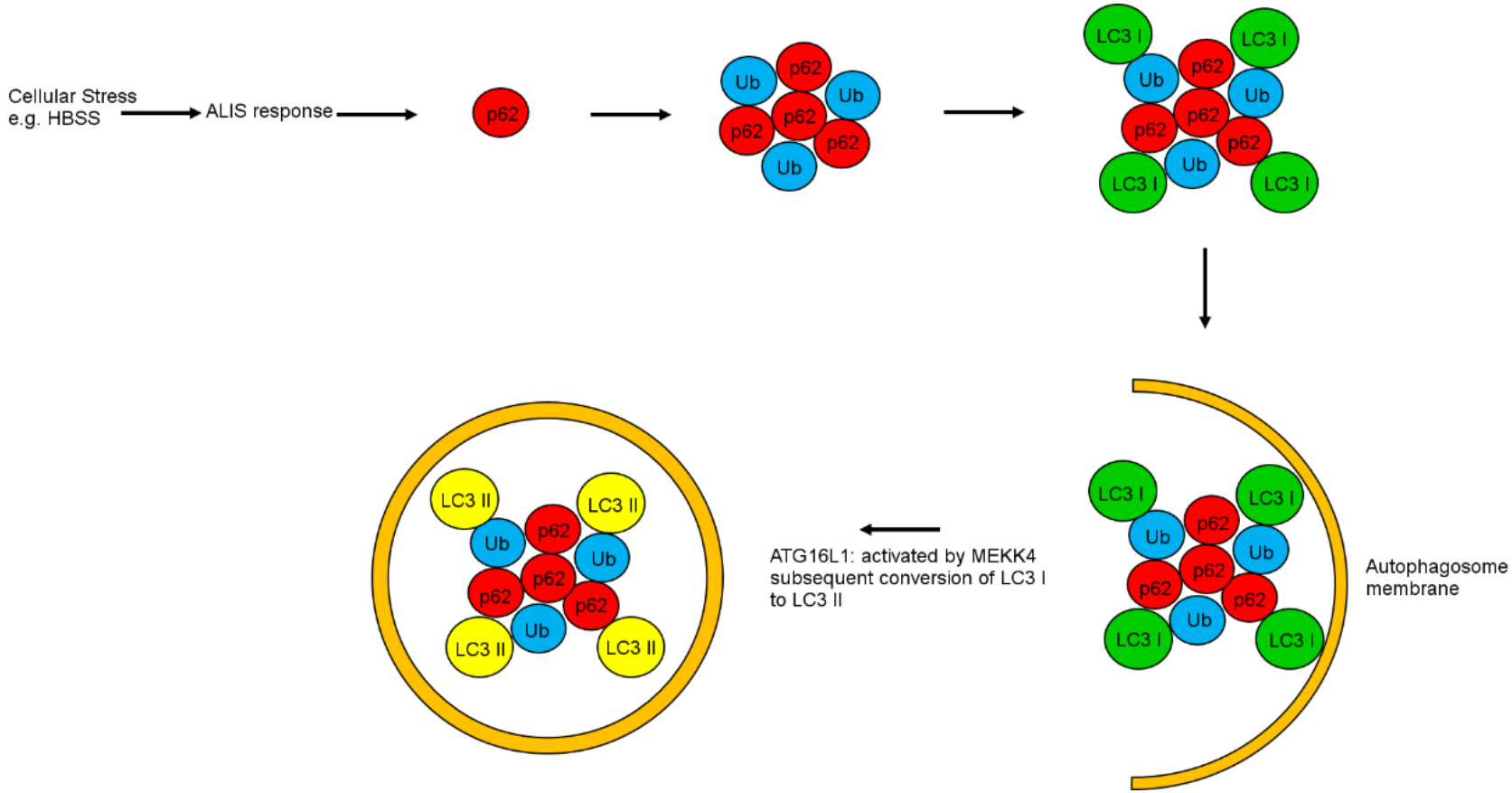

Figure 5.25 Diagrammatic representation of the potential role of ATG16L1 and MEKK4 in the ALIS response
In the response to cellular stress, p62 and ubiquitin accumulate into large aggregates that recruit LC3 I. This promotes the formation of the autophagosomal membrane around the aggregate, where ATG16L1 which may be activated by MEKK4, drives the conversion of LC3 I to LC3 II, facilitating the clearance of the aggregates via autophagy.
Figure assembled using data from Szeto et al., 2006 and Fujita et al., 2011.

sequences could be used to generate MEKK4 knockout cell lines in the MEFs, to ensure that the phenotype observed is not due to off-target effects. These cells were progressed to clonal selection, though this was unsuccessful (data not shown). Primers were also designed for sequencing the genomic target from clonal cells which can be sent for sequencing to detect indels (Appendix 5), which is a technique favoured by Ran et al., 2013.

Overall, the results demonstrate a strong autophagy defective phenotype when MEKK4 is silenced, with LC3 I positive aggregates that share similarities with both aggresomes and ALIS. This could be as a result of the interaction between Atg16L1 and Mekk4, but is likely not the single contributing factor to the defect in autophagy. The further characterisation of these structures in CRISPR/Cas9 mediated MEKK4 knockout cells will help understand how these structures form and how they link MEKK4 to autophagy.

Chapter 6

General Discussion and Future Work

Chapter 6: Discussion

6.1 General Summary

This thesis has studied the Atg16L1 protein in respect of domain function in autophagy, and in the identification and characterisation of a novel interaction with MEKK4. Tools were generated for the study of the domains Atg16L1 and to characterise various point mutants of Atg16l1. This work confirmed the requirement of the coiled-coil domain for autophagy, and identified a defect in the CD associated mutant to form larger autophagosomes, a finding which was later confirmed in other publications.

Tools were generated to verify and study a novel interaction between Atg16L1 and MEKK4, a serine threonine kinase that has shown to be important for regulating NOD2 signalling. Existing research has established an interaction between NOD2 and Atg16L1, with this signalling axis representing an important arm of the innate immune system. Co-immunoprecipitation experiments confirmed the interaction between Atg16L1 and MEKK4, narrowing down the region required for MEKK4 binding to the linker region of Atg16L1. The kinase activity of MEKK4 was also required for the interaction. Whilst MEKK4 did not localise to the autophagosome with Atg16L1, the proteins remained bound during starvation induced autophagy in cells where NOD2 was not expressed. When autophagy was induced by starvation or by MDP in cells that expressed NOD2, there was a reduction in MEKK4 Atg16L1 binding.

The functional role of MEKK4 in autophagy was also studied by various means of gene silencing. Experiments showed that MEKK4 expression is required for LC3 conversion, which phenocopies Atg16L1 knockout in this respect. Furthermore, the lack of MEKK4 expression results in a redistribution of LC3 to perinuclear aggresomes or ALIS structures independently of starvation, which are positive for p62 and ubiquitin. These MEKK4 silencing-induced LC3 structures were distinct from autophagosomes in their number and size, as there were fewer puncta, which had a larger diameter than a normal autophagosome. The formation of these aggregates was dependent on p62 expression, and the aggregates were also able to recruit LC3-I.

6.2 Model of the Atg16L1:MEKK4 interaction in autophagy

The results of chapter 4 have established that in the absence of autophagy, MEKK4 and Atg16L1 form a complex. In cells which have not been silenced for MEKK4, autophagy is

able to proceed normally (Fig 6.1). Starvation induced autophagy inhibits the activity of mTOR, which allows the initiation of the autophagy signalling cascade. Through an unknown mechanism, MEKK4 may be activated by an upstream activator e.g. GADD45, which is known to be upregulated during cellular stress (Liebermann et al., 2002), or by an undiscovered MEKK4 activator. As the kinase activity of MEKK4 is required for the interaction between Atg16L1 and MEKK4, it can be postulated that MEKK4 is in an open conformation, and Atg16L1 could be a substrate for MEKK4. The active MEKK4 then phosphorylates and activates Atg16L1, which could act as a molecular switch for Atg16L1 activity. Several serine phosphorylation sites of unknown function have been documented within Atg16L1, though the mechanism and function of this modification is unclear (Villén et al., 2007; Olsen et al., 2010). What is evident, however, is that the phosphorylation of Atg16L1 does occur and could serve as a potential regulatory mechanism, as has been shown in other autophagy proteins (Keil et al., 2012). The cellular distribution studies of Atg16L1 and MEKK4 show that Atg16L1 localises to the autophagosome, whilst MEKK4 remains in the cytosol. The immunoprecipitation results are less clear however, with Atg16L1 and MEKK4 remaining bound during autophagy activation in cells that lack NOD2 expression. This could represent a pool of Atg16L1 that remains bound to MEKK4, with a portion released to the autophagosome during autophagy. The mechanism behind Atg16L1 recruitment to the autophagosome is predominantly the interaction between WIPI2 and Atg16L1, which is recruited to the early autophagosome upstream of Atg16L1 (Dooley et al., 2014). It is therefore unlikely that phosphorylation of Atg16L1 by MEKK4 is required for recruitment of Atg16L1 to the autophagosome. The experiments showed that MEKK4 was required for LC3 conversion, a process that involves the two ubiquitin-like conjugation pathways; Atg16L1-Atg5-Atg12 and Atg3-LC3. The phosphorylation could result in a conformational change that leads to increased affinity for Atg5 binding, with autophagy being driven through increased recruitment of the Atg5-12 complex which binds and activates Atg3, leading to subsequent lipidation of LC3 (Ichimura et al., 2000; Sakoh-Nakatogawa et al., 2013).This could be a reason as to why MEKK4 is required for LC3 conversion. When MEKK4 has been knocked out or silenced, the phosphorylation of Atg16L1 would no longer occur. Whilst recruitment of Atg16L1 to the autophagosome would still take place, the lack of Atg16L1 activation would result in a failure to recruit members of the Ub-like conjugation pathways, or efficiently carry out the E3-like activity of Atg16L1 required for LC3 conversion. As seen in chapter 5, this results in a failure to activate autophagy in response to starvation, and an abnormal accumulation of aggregates, which cannot be degraded.

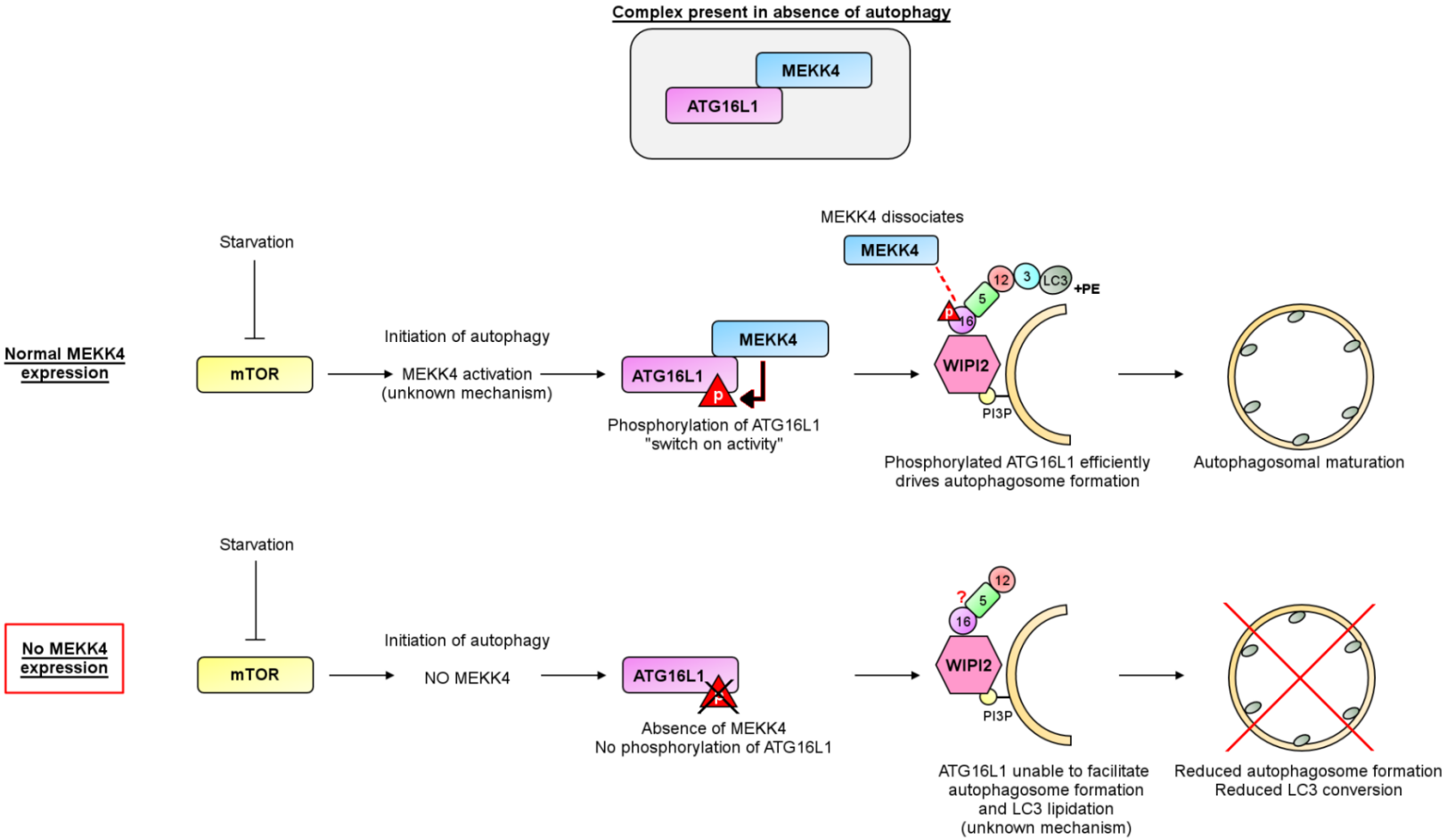

Figure 6.1 Schematic representation of proposed model of Atg16L1 activation by MEKK4

During autophagy initiation, MEKK4 is activated by as yet unknown mechanism, phosphorylates Atg16L1 which activates its autophagic activity. This allows Atg16L1, once recruited to the autophagosome, to efficiently drive LC3 lipidation and autophagy through the ubiquitin-like conjugation pathways.

There are however, gaps in this model which remain unexplained. As autophagy is an essential process, then an important regulator such as MEKK4 would be expected to be broadly expressed in development and in all tissues. Gene expression data in a number of databases indicate that MEKK4 is widely expressed throughout development through to adulthood, with high expression found in skeletal muscle, kidney, testis followed by heart brain and lung (Gerwins et al., 1997; ArrayExpress; Bgee; CleanEx; Genevestigator). This is reassuring, as if MEKK4 is vital for autophagy then expression would not be heavily restricted. MEKK4 knockout and MEKK4 kinase inactive mice display perinatal lethality, with very few mice surviving to adulthood (Chi et al., 2004; Abell et al., 2005), which also demonstrates that MEKK4 expression is vital for development and survival.

It is possible that MEKK4 may be one of many kinases able to activate ATG16L1 activity in response to specific cellular stressors. In the MAPK cascade, the individualised functions of the MAP3Ks (MEKKs) provide for specificity and complexity in the ability to respond to a variety of extra-cellular stresses. As with this system, other kinases could provide alternative means of activating ATG16L1 in response to different autophagic stimuli e.g. mitophagy. What is unclear, is how these kinases would coordinate basal autophagy.

6.3 Future Work

To further dissect the MEKK4:Atg16L1 interaction and its role in regulating the autophagy pathway, further experiments have been proposed.

6.3.1 Short term work

The requirement for MEKK4 in autophagy was based on the results seen in the siRNA screen in chapter 5. To confirm the phenotype and further explore this, knockout Mekk4 MEFs will be generated from Mekk4 flox/flox embryos and immortalised using the Adeno-Cre virus. These mice were a kind gift from Dr Andy Greenfield (MRC Harwell) and are described in Chi et al., 2004. These cells will have their knockout status confirmed by genotyping and Western blot, before autophagy assays are carried out. The cells will be subjected to HBSS starvation with and without the lysosomal inhibitor bafilomycin A1 (BafA1), which inhibits degradation of LC3 II. If the decrease in LC3 II throughout the timecourse is due to an overall decrease/inhibition of autophagosome formation, this will confirm that MEKK4 is required for autophagy. If there is an increase in LC3 II following BafA1 treatment, then this could indicate an increase in autophagic flux, with accelerated degradation of LC3 II.

The nature of the aggregates seen in the siRNA screen and CRISPR/Cas MEKK4 knockout cells also require further investigation. To see whether the recruitment of LC3 to the aggregates is dependent on the interaction with p62, an LC3 mutant defective in p62 binding (where lysine 51 has been mutated to alanine) has been obtained (Ichimura et al., 2008; Fujita et al., 2010). The recruitment of this LC3-K51A mutant to p62/ubiquitin positive aggregates will be compared with wt-LC3 and the cleavage defective LC3-G120A mutant. The LC3-K51A mutant has been shown to colocalise with p62 ALIS structures, so could indicate if the aggregates are ALIS (Fujita et al., 2010). To further characterise the aggregates, their co-localisation with the intermediate filament vimentin should also be considered. Aggresomes are sometimes caged by collapsed vimentin, which acts as a sequestering mechanism (Garcia-Mata et al., 1999). A lack of co-localisation or vimentin cage would indicate that the aggregates were ALIS not aggresomes. The perinuclear location of the aggregates raises the question of how they were transported there in the first place. As aggresome transport to the MTOC is facilitated by HDAC6, inhibitors of HDAC6 or nocodazole will be used to see if the formation or localisation of perinuclear aggregates in the MEKK4 knockout cells. These experiments will aim to determine whether the aggregates in MEKK4 knockout cells are a transient ALIS response or a metabolically stable aggresome.

The identification of an Atg16L1 binding motif in the N-terminus MEKK4 will be confirmed, by mutating the motif using site directed mutagenesis. Co-immunoprecipitations will then be carried out. This will enable a greater understanding of how MEKK4 may interact with Atg16L1, and reveal the importance of the C-terminal kinase activity of MEKK4 in the interaction. Should the motif in MEKK4 be required for Atg16L1 binding, then the previous results demonstrating that kinase activity is required for Atg16L1 binding would indicate that this is due to the conformational state of MEKK4 when active.

6.3.2 Long term work

Two aims have been identified that will address the question; does MEKK4 play a functional role in autophagy by regulating the activation of autophagy through Atg16L1?

The first aim will be to determine if Atg16L1 is a substrate for MEKK4 and if phosphorylation is required for activation of Atg16L1 and lipidation of LC3. Phosphorylation of Atg16L1 could be investigated by Q-MALDI-TOF mass spectrometry to scan Atg16L1 for novel phosphopeptides. Atg16L1 would be isolated from HEK293 Atg16L1-GFP. Atg16L1 will be immmunopurified from control cells cultured in nutrient rich conditions and cells starved to

induce autophagy. Any novel sites could be mutated in the Atg16L1-GFP construct by site-directed mutagenesis. The putative phospho-defective mutants would then be used to reconstitute Atg16L1 KO MEFs to see if there are any changes in autophagosome number and localisation as a result of the mutation. Autophagic flux could also be monitored by analysing the degradation of p62 and conversion of LC3 I to LC3 II by Western blot.
Parallel pull down experiments would determine whether the Atg16L1 phosphorylation mutants retain the ability to bind MEKK4. This aim could be completed using *in vitro* kinase assays to determine whether recombinant active MEKK4 directly phosphorylates recombinant wild type and mutant Atg16L1.

The second aim could be to determine if the MEKK4:Atg16L1 interaction is required for activation of autophagy by NOD2 and if this is regulated by phosphorylation. Whilst MEKK4 was shown to be required for starvation induced autophagy in chapter 5, this work was not extended to investigating NOD2 directed autophagy due to time constraints. Using the HEK293 Atg16L1-GFP NOD2-HA episomal cells, the mass spectrometry analysis could be repeated following MDP incubation and NOD2 activated autophagy. This would indicate whether different phosphorylation sites are involved, if at all, in Atg16L1 activation. To confirm that the interaction between Atg16L1 and MEKK4 controls MDP-activation of autophagy by MEKK4, Atg16L1 -/- MEFs could be reconstituted with NOD2-HA and phosphorylation deficient mutants of Atg16L1 generated in Aim 1. The CRISPR/Cas MEKK4 knockout cell lines would then be used to see if MEKK4 is required for MDP induced autophagy.

6.4 Concluding Remarks

The discovery and characterisation of a novel interaction between Atg16L1 and MEKK4 has demonstrated a functional role for MEKK4 in the regulation of the autophagy pathway. Whilst previous literature had shown an indirect involvement for MEKK4 in autophagy through undefined mechanisms, this body of work presents a feasible molecular basis for the involvement of MEKK4 in autophagy. Should future work be able to elucidate how this interaction contributes towards regulating the ATG16L1:NOD2 signalling axis, then there is great potential for understanding how autophagy is activated in response to infection. This would represent a specific druggable target for the control of autophagy, which would be worth developing. However, it is clear that further investigation into the activation of Atg16L1 is required to determine whether the vital role of MEKK4 in autophagy is directly as a consequence of its interaction with Atg16L1

Appendix 1

Schematic representation of the splice variants of Atg16L1

Three isoforms of murine Atg16L1 have been described, Atg16L1 α, β and γ. Atg16L1 γ contains exons 1-19, and is the longest splice variant. Atg16L1 β is referred to as the canonical sequence (Mizushima et al., 2003) and lacks exon 9, whereas Atg16L1 α is missing exon 8 and 9.

Modified from an original figure created by Dr Ernst Poschl

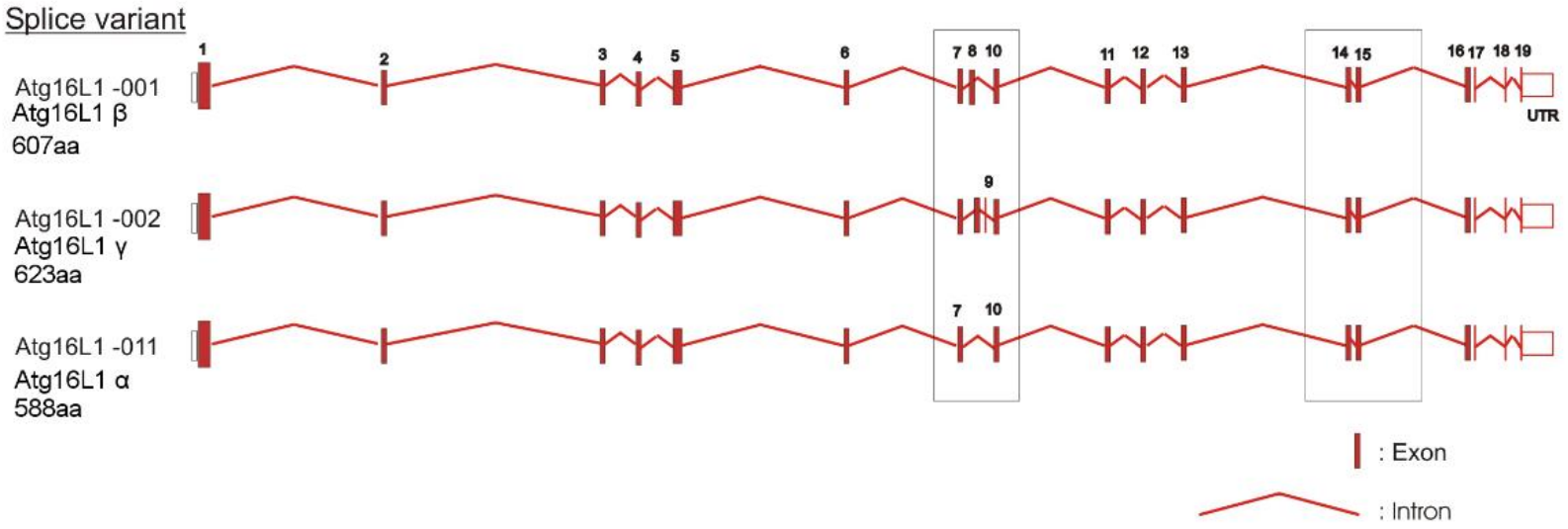
Splice variant
Atg16L1 -001
Atg16L1 β
607aa
Atg16L1 -002
Atg16L1 γ
623aa
Atg16L1 -011
Atg16L1 α
588aa
1
2
3
4
5
6
7 8 10
9
7
10
11
12
13
14 15
16 17 18 19
UTR
: Exon
: Intron

Appendix 2

Alignment between Human ATG16L1 β and Mouse Atg16L1 γ protein sequences to highlight potential region for binding of proteins containing Atg16L1 binding motif

```
CLUSTAL 2.1 multiple sequence alignment


humanatg16l1beta       MSSGLRAADFPRWKRHISEQLRRRDRLQRQAFEEIILQYNKLLEKSDLHSVLAQKLQAEK 60
mouseatg16L1gamma      MSSGLRAADFPRWKRHIAEELRRRDRLQRQAFEEIILQYTKLLEKSDLHSVLTQKLQAEK 60
                       ******************:*:*******************.************:*******

humanatg16l1beta       HDVPNRHEISPGHDGTWNDNQLQEMAQLRIKHQEELTELHKKRGELAQLVIDLNNQMQRK 120
mouseatg16L1gamma      HDMPNRHEISPGHDGAWNDSQLQEMAQLRIKHQEELTELHKKRGELAQLVIDLNNQMQQK 120
                       **:************:***.****************************************:*

humanatg16l1beta       DREMQMNEAKIAECLQTISDLETECLDLRTKLCDLERANQTLKDEYDALQITFTALEGKL 180
mouseatg16L1gamma      DKEIQMNEAKISEYLQTISDLETNCLDLRTKLQDLEVANQTLKDEYDALQITFTALEEKL 180
                       *:*:*******:* *********:******** *** ********************* **

humanatg16l1beta       RKTTEENQELVTRWMAEKAQEANRLNAENEKDSRRRQARLQKELAEAAKEPLPVEQDDDI 240
mouseatg16L1gamma      RKTTEENQELVTRWMAEKAQEANRLNAENEKDSRRRQARLQKELAEAAKEPLPVEQDDDI 240
                       ************************************************************

humanatg16l1beta       EVIVDETSDHTEETSPVRAISRAATKRLSQPAGGLLDSITNIFG---------------- 284
mouseatg16L1gamma      EVIVDETSDHTEETSPVRAVSRAATKRLSQPAGGLLDSITNIFGLSESPLLGHHSSDAAR 300
                       ******************:************************

humanatg16l1beta       RRSVSSFPVPQDNVDTHPGSGKEVRVPATALCVFDAHDGEVNAVQFSPGSRLLATGGMDR 344
mouseatg16L1gamma      RRSVSSIPVPQDIMDTHPASGKDVRVPTTASYVFDAHDGEVNAVQFSPGSRLLATGGMDR 360
                       ******:***** :****.***:****.**  ****************************

humanatg16l1beta       RVKLWEVFGEKCEFKGSLSGSNAGITSIEFDSAGSYLLAASNDFASRIWTVDDYRLRHTL 404
mouseatg16L1gamma      RVKLWEAFGDKCEFKGSLSGSNAGITSIEFDSAGAYLLAASNDFASRIWTVDDYRLRHTL 420
                       ******.**:************************:************************

humanatg16l1beta       TGHSGKVLSAKFLLDNARIVSGSHDRTLKLWDLRSKVCIKTVFAGSSCNDIVCTEQCVMS 464
mouseatg16L1gamma      TGHSGKVLSAKFLLDNARIVSGSHDRTLKLWDLRSKVCIKTVFAGSSCNDIVCTEQCVMS 480
                       ************************************************************

humanatg16l1beta       GHFDKKIRFWDIRSESIVREMELLGKITALDLNPERTELLSCSRDDLLKVIDLRTNAIKQ 524
mouseatg16L1gamma      GHFDKKIRFWDIRSESVVREMELLGKITALDLNPERTELLSCSRDDLLKVIDLRTNAVKQ 540
                       ****************:****************************************:**

humanatg16l1beta       TFSAPGFKCGSDWTRVVFSPDGSYVAAGSAEGSLYIWSVLTGKVEKVLSKQHSSSINAVA 584
mouseatg16L1gamma      TFSAPGFKCGSDWTRVVFSPDGSYVAAGSAEGSLYVWSVLTGKVEKVLSKQHSSSINAVA 600
                       ************************************:************************

humanatg16l1beta       WSPSGSHVVSVDKGCKAVLWAQY 607
mouseatg16L1gamma      WAPSGLHVVSVDKGSRAVLWAQP 623
                       *:*** ********.:******
```

Boada-Romero WD40 construct

Atg16L1 WD40 construct used in this thesis

[ ] = 10 aa region of difference between constructs

Alignments were carried out using the Clustal 2.1 algorithm, to align the sequences of human ATG16L1 β and mouse Atg16L1 γ. This allowed determination of the regions of discrepancy between the WD40 construct used for interaction studies by Boada-Romero et al., (320-607aa) and the WD40 construct used in this thesis (327-623aa). The alignments reveal a 10 amino acid region which is present in the WD40 construct used in this thesis, which is missing from the Boada-Romero WD40 construct. This region may explain why Mekk4, which contains an Atg16L1 interacting motif, cannot bind the WD40 construct used in this thesis.

Appendix 3

Updated sgRNA design for human MEKK4 using http://tools.genome-engineering.org software from Dr Fen Zhang.

all guides

scored by inverse likelihood of offtarget binding
mouse over for details ... show legend

	score	sequence	
Guide #1	91	CTCGGGTTCTGACTCGGTCT	CGG
Guide #2	90	TCGGTCTCGGGTTCCGGTGG	CGG
Guide #3	90	TCGGGTTCTGACTCGGTCTC	GGG
Guide #4	89	GACTCGGTCTCGGGTTCCGG	TGG
Guide #5	87	TCTGACTCGGTCTCGGGTTC	CGG
Guide #6	85	GGCGGCAGGCGTGACGGCAA	AGG
Guide #7	83	GAGAGAAGCCGCTGCCGCGC	TGG
Guide #8	83	GTCTCGGGTTCCGGTGGCGG	TGG
Guide #9	81	CATGGCGGCGGCAGGCGTGA	CGG
Guide #10	78	GCAGCACTCGGGTTCTGACT	CGG
Guide #11	75	CTCGCCGCCAAGCAGCACTC	GGG
Guide #12	75	CGGCGGCTCCTCCATGGCGG	CGG
Guide #13	74	GGCGTGACGGCAAAGGCGGG	AGG
Guide #14	73	GCAGGCGTGACGGCAAAGGC	GGG
Guide #15	72	GTCAGAACCCGAGTGCTGCT	TGG
Guide #16	72	GGCAGGCGTGACGGCAAAGG	CGG
Guide #17	70	CACGCCTGCCGCCGCCATGG	AGG
Guide #18	68	CGTCACGCCTGCCGCCGCCA	TGG
Guide #19	68	TCGGGTTCCGGTGGCGGTGG	TGG
Guide #20	66	AGAACCCGAGTGCTGCTTGG	CGG
Guide #21	61	AGGAGGGACCAGCGCGGCAG	CGG
Guide #22	59	TGGCGGCGGCTCCTCCATGG	CGG
Guide #23	55	TGACGGCAAAGGCGGGAGGA	GGG
Guide #24	50	GTGACGGCAAAGGCGGGAGG	AGG
Guide #25	48	CGGTGGCGGCGGCTCCTCCA	TGG
Guide #26	47	GGCTCCTCCATGGCGGCGGC	AGG
Guide #27	45	GGCGGGAGGAGGGACCAGCG	CGG
Guide #28	40	GCCGCCGCCACCACCGCCAC	CGG
Guide #29	30	TCCGGTGGCGGTGGTGGCGG	CGG
Guide #30	28	GGTTCCGGTGGCGGTGGTGG	CGG
Guide #31	12	GGTGGCGGTGGTGGCGGCGG	CGG
Guide #32	9	GGTGGCGGCGGCGGCGGTGG	CGG
Guide #33	9	GGCGGCGGCGGCGGTGGCGG	CGG
Guide #34	9	GGCGGTGGTGGCGGCGGCGG	CGG
Guide #35	7	GGTGGTGGCGGCGGCGGCGG	TGG

guide #7 quality score: 83

guide sequence: GAGAGAAGCCGCTGCCGCGC TGG
on-target locus: unknown
number of offtarget sites: 133 (45 are in genes)

top 20 genome-wide off-target sites

sequence	score	mismatches
GTCACACGCCGCTGCCGCGCAAG	0.9	4MMs [2:3:5:7]
CCGAGACGCAGCTGCCGCGCCGG	0.9	4MMs [1:2:7:10]
CAAAGAGGCGGCTGCCGCGCGGG	0.9	4MMs [1:3:7:10]
GGGAGGAGCCGCCGCCGCGCCGG	0.7	3MMs [2:6:13]
GGGTGAAGCAGCTGCCGCGACGG	0.6	4MMs [2:4:10:20]
CCCAGAAGCCGCTGCCCCGCCGG	0.6	4MMs [1:2:3:17]
GCGAGAAGCCGCGGCCGCGGGAG	0.6	3MMs [2:13:20]
CAGTGAAGCAGCTGCCCCGCGAG	0.6	4MMs [1:4:10:17]
GCGAGCCACCGCTGCCGCGCCAG	0.6	4MMs [2:6:7:8]
GCGAGGGGCTGCTGCCGCGCGGG	0.5	4MMs [2:6:7:10]
GAGACAATTCCCTGCCGCGCCGG	0.5	4MMs [5:8:9:11]
GAAGGACGCCGCCGCCGCGCAGG	0.4	4MMs [3:4:7:13]
GTGGGAAGTCGCTGCCTCGCGGG	0.4	4MMs [2:4:9:17]
GCGGGGAGCCGCGGCCGCGCTGG	0.3	4MMs [2:4:6:13]
GGGAGGAGCCGCTGCAGCGCCGG	0.3	3MMs [2:6:16]
AGGAGCAGCCGCTGCCGCCCAGG	0.3	4MMs [1:2:6:19]
GAGTGAAGGCGCTGCAGCGCTGG	0.3	3MMs [4:9:16]
GATGGCAGCCGCTGCCGCCCTAG	0.3	4MMs [3:4:6:19]
GAGAGACGCCGCAGCCTCGCGGG	0.3	3MMs [7:13:17]
CAGGGAAGCCGCGGCCGCGTGGG	0.3	4MMs [1:4:13:20]
GGAAAAAGCCGCTGCAGCGCCGG	0.3	4MMs [2:3:5:16]
GAGAGAAGAGGCTGCAGCGCCAG	0.3	3MMs [9:10:16]
GGGAGAAGCAGCAGCCGCGTGGG	0.2	4MMs [2:10:13:20]
GAAAGAAGCCGCTGCTGCGGGGG	0.2	3MMs [3:16:20]
GAAAGAAGCAGCGGCCGCGGCGG	0.2	4MMs [3:10:13:20]

= sgRNA used in thesis to generate HEK293 MEKK4 Crispr genome edited cells.

Appendix 4

Updated sgRNA design for mouse using http://tools.genome-engineering.org software from Dr Fen Zhang.

all guides

scored by inverse likelihood of offtarget binding
mouse over for details ... show legend

	score	sequence	
Guide #1	97	CAAGCTTCGCATGACCGCGG	CGG
Guide #2	96	CGCCGCGGTCATGCGAAGCT	TGG
Guide #3	96	AAGCTTCGCATGACCGCGGC	GGG
Guide #4	94	GAGAGACGCCATCGCCGAGC	CGG
Guide #5	94	CACCAAGCTTCGCATGACCG	CGG
Guide #6	91	AGGGGGCACCGGCTCGGCGA	TGG
Guide #7	86	GGCTGCAGGGGTGTCGGCGA	GGG
Guide #8	86	GCTGGGCAGCACTCCGGATC	CGG
Guide #9	82	CGGCTGCAGGGGTGTCGGCG	AGG
Guide #10	82	GCCACAGCCCGAGCCGGATC	CGG
Guide #11	82	TCCGGATCCGGCTCGGGCTG	TGG
Guide #12	80	CTCGCCGCTGGGCAGCACTC	CGG
Guide #13	80	GTCATGCGAAGCTTGGTGCA	CGG
Guide #14	79	ACCGCCGCCACAGCCCGAGC	CGG
Guide #15	77	TCGGGCTGTGGCGGCGGTGC	TGG
Guide #16	73	GCAGCACTCCGGATCCGGCT	CGG
Guide #17	73	AGCTCCTCCATGGCGGCTGC	AGG
Guide #18	71	TCCGGCTCGGGCTGTGGCGG	CGG
Guide #19	71	CGACACCCCTGCAGCCGCCA	TGG
Guide #20	70	GCAGGGGTGTCGGCGAGGGC	AGG
Guide #21	69	GGATCCGGAGTGCTGCCCAG	CGG
Guide #22	69	GGATCCGGCTCGGGCTGTGG	CGG
Guide #23	66	CACCCCTGCAGCCGCCATGG	AGG
Guide #24	61	TGGCCGCAGCTCCTCCATGG	CGG
Guide #25	59	CTCCTCCATGGCGGCTGCAG	GGG
Guide #18	71	TCCGGCTCGGGCTGTGGCGG	CGG
Guide #19	71	CGACACCCCTGCAGCCGCCA	TGG
Guide #20	70	GCAGGGGTGTCGGCGAGGGC	AGG
Guide #21	69	GGATCCGGAGTGCTGCCCAG	CGG
Guide #22	69	GGATCCGGCTCGGGCTGTGG	CGG
Guide #23	66	CACCCCTGCAGCCGCCATGG	AGG
Guide #24	61	TGGCCGCAGCTCCTCCATGG	CGG
Guide #25	59	CTCCTCCATGGCGGCTGCAG	GGG
Guide #26	57	CATGGCGGCTGCAGGGGTGT	CGG
Guide #27	56	GCTCCTCCATGGCGGCTGCA	GGG
Guide #28	56	CAGCACTCCGGATCCGGCTC	GGG
Guide #29	55	GGCAGGAGGGGGCACCGGCT	CGG
Guide #30	54	GGGTGTCGGCGAGGGCAGGA	GGG
Guide #31	51	GGTGTCGGCGAGGGCAGGAG	GGG
Guide #32	50	TGCTGGCCGCAGCTCCTCCA	TGG
Guide #33	46	GGGGTGTCGGCGAGGGCAGG	AGG
Guide #34	39	GTGTCGGCGAGGGCAGGAGG	GGG
Guide #35	36	CAGCCGCCATGGAGGAGCTG	CGG
Guide #36	35	GCGAGGGCAGGAGGGGGCAC	CGG

guide #33 **quality score:** 46

guide sequence: GGGGTGTCGGCGAGGGCAGG AGG
on-target locus: unknown
number of offtarget sites: 360 (62 are in genes)

top 20 genome-wide off-target sites

sequence	score	mismatches
GGGGTGTGGGGGAGGGCAGGCAG	3.2	2MMs [8:11]
GGGGTGTTGGCGGGGGCAGGAGG	2.5	2MMs [8:13]
GGTGGGTGGGCGAGGGCAGGAAG	2.4	3MMs [3:5:8]
GGGCTGGGGGCGAGGGCAGGGGG	1.7	3MMs [4:7:8]
GTGGTGTGGGGGAGGGCAGGAAG	1.5	3MMs [2:8:11]
GGCGTGTCCCCGAGGGCAGGGGG	1.4	3MMs [3:9:10]
GGGGGGTGGGTGAGGGCAGGGAG	1.4	3MMs [5:8:11]
GGGGAGTGGGGGAGGGCAGGGAG	1.4	3MMs [5:8:11]
GGGGGGTAGGGGAGGGCAGGGAG	1.4	3MMs [5:8:11]
GTGGTGTAGGCCAGGGCAGGCAG	1.4	3MMs [2:8:12]
GGCCAGTAGGCGAGGGCAGGCAG	1.3	4MMs [3:4:5:8]
GGGGTGTTGAGGAGGGCAGGAAG	1.2	3MMs [8:10:11]
TGGGTGTTGGCGGGGGCAGGGGG	1.2	3MMs [1:8:13]
GCGGGGTCGGCGTGGGCAGGAAG	1.1	3MMs [2:5:13]
GGGGGGTAGGCGGGGGCAGGGAG	1.0	3MMs [5:8:13]
GGGGTGCTGGGGAGGGCAGGTGG	0.9	3MMs [7:8:11]
GGGCCGAGGGCGAGGGCAGGAGG	0.9	4MMs [4:5:7:8]
GGGAGGGGGGCGAGGGCAGGAAG	0.9	4MMs [4:5:7:8]
GGGATGCCGGCCAGGGCAGGAGG	0.9	3MMs [4:7:12]
GGGGTGATGGCGAGGGCAGTCAG	0.9	3MMs [7:8:20]
GGGGTTTGGGGGAGGGCAGGGAG	0.8	3MMs [6:8:11]
TGGGGGTGGGGGAGGGCAGGGAG	0.8	4MMs [1:5:8:11]
TGGGGGTGGGGGAGGGCAGGGAG	0.8	4MMs [1:5:8:11]
GGAGAATAGGCGAGGGCAGGAAG	0.8	4MMs [3:5:6:8]
GGATTGTTGGGGAGGGCAGGAGG	0.8	4MMs [3:4:8:11]
GGTGAGTGGGGGAGGGCAGGCAG	0.8	4MMs [3:5:8:11]
GGGAGGTGGGGGAGGGCAGGGAG	0.8	4MMs [4:5:8:11]

= sgRNA used in thesis to generate MEF Mekk4 Crispr genome edited cell lines.

Appendix 5

Designing primers to amplify Mouse Mekk4 Cas9 target for Surveyor/sequencing assays

MAP3K4-201 ENSMUSG00000014426

Mekk4 on the chromosome

>chromosome:GRCm38:17:12227021:12319260:-1

Primer-BLAST in order to avoid nonspecific amplification. SURVEYOR primers should be designed to amplify 200–400 bp on either side of the Cas9 target (for a total amplicon 400–800 bp long) to allow clear visualization of cleavage bands by gel electrophoresis. To prevent excessive primer dimer formation, SURVEYOR primers should be designed to be typically 18 to 25 nt long with melting temperatures of ~60 °C. For SURVEYOR assay or sequencing analysis, we recommend testing that each pair of candidate primers produces a single PCR product, as well as testing for the absence of nonspecific cleavage during the SURVEYOR nuclease digestion process

Design primers to amplify this region

GCAGAATCCAGTGGCGCAGAGACCTTGAGCTCCAGTTTATGAAGCATTCCTGCTCGCCCAGACAACC
CTACCTCTCCAAATGTCTCCTGTGCCCTTAGCCTCAGGACCTCCCGAGGCCACCCGCGGTCACCCAGC
GACACCTGATTTACCACTGGCCAGTGCGCTCCTCCCTCCCGCCTCGCCCCGCCCAGGCGGACTCAGCC
GCCCGCCGAGGCGTGTCCCTCGCTGCCCGCCGTAGCCCAGCGTTCGGCCGGCCGCCGTTCCCAAGAT
GGCCGCTGCGCGCACGGCTCCTGCGGCGGGCTAGAGGCGGAGGCGGAGTCGAGTCACTCCCTCACCC
CGCGGCTCCTGGTCTTCCCGCACCAGGCTGCAGCTGACGA**CCCGCCGCGGTCATGCGAAGCTTGGT**
GCACGGATGAGAGACGCCATCGCCGAGCCGGTGCCCCCTCCTGCCCTCGCCGACACCCCTGCA
GCCGCCATGGAGGAGCTGCGGCCAGCACCGCCGCCACAGCCCGAGCCGGATCCGGAGTGCTG
CCCAGCGGCGAGGTGAGTGCACGGCTGCAGCTGCAGCTCGGAGGGAGCAGGGTGGCGCGTGAAGG
GGGCGTGGGGTCCTCGGCTGCGCGCCAGGTGGGCGCGGAGCATCCGGACCTCCGGTGGCGGGAGGG
GCGCGGTGCAGCGCGGAGCCCGGTGCTCCGCTTCCGCGCGACCCCTGCCCGGGCTCGGAGGCCAAGC
TCCCGAGCGACCCTGGCCTTTGCAGTAGTGCTCCCCGGGGCCCTGCTGCAGACAGCCCCAGCTTGCCC
CGGACTGCCGCTCGGGCTCGGATCAGTGATCGGATGGAAGGAAGGTGGTCCATCTTTCTCCTTTTTCC
AGGAAAAGAGAGGCGACGTGCCTCTCGGCAGTTC

660 896

Primers designed using Primer blast

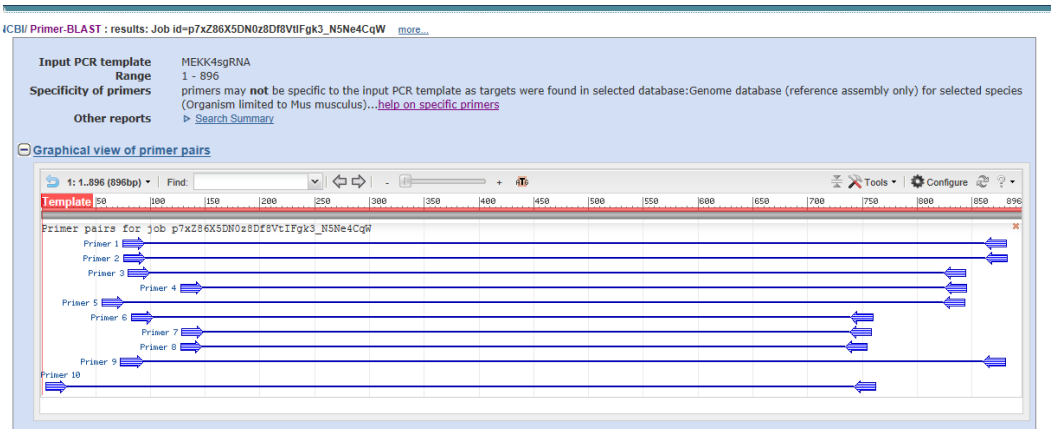

Primer pair 1

	Sequence (5'->3')	Template strand	Length	Start	Stop	Tm	GC %	Self complementarity	Self 3' complementarity
Forward primer	TCCAAATGTCTCCTGTGCCC	Plus	20	75	94	59.96	55.00	2.00	2.00
Reverse primer	ACGTCGCCTCTCTTTTCCTG	Minus	20	881	862	60.04	55.00	4.00	1.00
Internal oligo		Plus							
Product length	807								
Product Tm									
Product Tm - min(OLIGO Tm)									
Exon junction									
Total intron size									

Products on intended target

>NC_000083.6 Mus musculus strain C57BL/6J chromosome 17, GRCm38.p2 C57BL/6J

```
product length = 807
Features associated with this product:
   mitogen-activated protein kinase kinase kinase 4 isoform X1

   mitogen-activated protein kinase kinase kinase 4

Forward primer  1         TCCAAATGTCTCCTGTGCCC  20
Template        12318963  ....................  12318944

Reverse primer  1         ACGTCGCCTCTCTTTTCCTG  20
Template        12318157  ....................  12318176
```

Products on allowed transcript variants

Products on potentially unintended templates

Primer pair 2

	Sequence (5'->3')	Template strand	Length	Start	Stop	Tm	GC %	Self complementarity	Self 3' complementarity
Forward primer	CCAAATGTCTCCTGTGCCCT	Plus	20	76	95	59.96	55.00	2.00	0.00
Reverse primer	CACGTCGCCTCTCTTTTCCT	Minus	20	882	863	60.04	55.00	4.00	0.00
Internal oligo		Plus							
Product length	807								

Product Tm

Product Tm - min(OLIGO Tm)

Exon junction

Total intron size

Products on intended target

>NC_000083.6 Mus musculus strain C57BL/6J chromosome 17, GRCm38.p2 C57BL/6J

```
product length = 807
Features associated with this product:
   mitogen-activated protein kinase kinase kinase 4 isoform X1

   mitogen-activated protein kinase kinase kinase 4

Forward primer  1         CCAAATGTCTCCTGTGCCCT  20
Template        12318962  ....................  12318943

Reverse primer  1         CACGTCGCCTCTCTTTTCCT  20
Template        12318156  ....................  12318175
```

Products on allowed transcript variants

Products on target templates

Primer pair 3

	Sequence (5'->3')	Template strand	Length	Start	Stop	Tm	GC %	Self complementarity	Self 3' complementarity
Forward primer	ATGTCTCCTGTGCCCTTAGC	Plus	20	80	99	59.46	55.00	3.00	2.00
Reverse primer	GACCACCTTCCTTCCATCCG	Minus	20	844	825	60.11	60.00	2.00	2.00
Internal oligo		Plus							
Product length	765								
Product Tm									
Product Tm - min(OLIGO Tm)									
Exon junction									
Total intron size									

Products on intended target

>NC_000083.6 Mus musculus strain C57BL/6J chromosome 17, GRCm38.p2 C57BL/6J

```
product length = 765
Features associated with this product:
   mitogen-activated protein kinase kinase kinase 4 isoform X1

   mitogen-activated protein kinase kinase kinase 4

Forward primer  1         ATGTCTCCTGTGCCCTTAGC  20
Template        12318958  ....................  12318939

Reverse primer  1         GACCACCTTCCTTCCATCCG  20
Template        12318194  ....................  12318213
```

Products on allowed transcript variants

Products on target templates

Primer pair 4

	Sequence (5'->3')	Template strand	Length	Start	Stop	Tm	GC %	Self complementarity	Self 3' complementarity
Forward primer	CACCCAGCGACACCTGATTT	Plus	20	128	147	60.61	55.00	3.00	1.00
Reverse primer	GGACCACCTTCCTTCCATCC	Minus	20	845	826	59.74	60.00	3.00	0.00
Internal oligo		Plus							
Product length	718								
Product Tm									
Product Tm - min(OLIGO Tm)									
Exon junction									
Total intron size									

Products on intended target

>NC_000083.6 Mus musculus strain C57BL/6J chromosome 17, GRCm38.p2 C57BL/6J

```
product length = 718
Features associated with this product:
   mitogen-activated protein kinase kinase kinase 4 isoform X1

   mitogen-activated protein kinase kinase kinase 4

Forward primer  1         CACCCAGCGACACCTGATTT  20
Template        12318910  ....................  12318891

Reverse primer  1         GGACCACCTTCCTTCCATCC  20
Template        12318193  ....................  12318212
```

Products on allowed transcript variants

Primer pair 5

	Sequence (5'->3')	Template strand	Length	Start	Stop	Tm	GC %	Self complementarity	Self 3' complementarity
Forward primer	GCCCAGACAACCCTACCTCT	Plus	20	56	75	60.91	60.00	3.00	0.00
Reverse primer	ACCACCTTCCTTCCATCCGA	Minus	20	843	824	60.55	55.00	3.00	3.00
Internal oligo		Plus							
Product length	788								
Product Tm									
Product Tm - min(OLIGO Tm)									
Exon junction									
Total intron size									

Products on intended target

>NC_000083.6 Mus musculus strain C57BL/6J chromosome 17, GRCm38.p2 C57BL/6J

```
product length = 788
Features associated with this product:
   mitogen-activated protein kinase kinase kinase 4 isoform X1

   mitogen-activated protein kinase kinase kinase 4
```

```
Forward primer  1         GCCCAGACAACCCTACCTCT  20
Template        12318982  ....................  12318963

Reverse primer  1         ACCACCTTCCTTCCATCCGA  20
Template        12318195  ....................  12318214
```

Products on allowed transcript variants

Products on target templates

Primer pair 6

	Sequence (5'->3')	Template strand	Length	Start	Stop	Tm	GC %	Self complementarity	Self 3' complementarity
Forward primer	TCTCCTGTGCCCTTAGCCTC	Plus	20	83	102	60.98	60.00	3.00	1.00
Reverse primer	GAGCACTACTGCAAAGGCCA	Minus	20	759	740	60.61	55.00	6.00	2.00
Internal oligo		Plus							
Product length	677								
Product Tm									
Product Tm - min(OLIGO Tm)									
Exon junction									
Total intron size									

Products on intended target

>NC_000083.6 Mus musculus strain C57BL/6J chromosome 17, GRCm38.p2 C57BL/6J

```
product length = 677
Features associated with this product:
   mitogen-activated protein kinase kinase kinase 4 isoform X1

   mitogen-activated protein kinase kinase kinase 4

Forward primer  1         TCTCCTGTGCCCTTAGCCTC  20
Template        12318955  ....................  12318936

Reverse primer  1         GAGCACTACTGCAAAGGCCA  20
Template        12318279  ....................  12318298
```

Products on allowed transcript variants

Products on target templates

Primer pair 7

	Sequence (5'->3')	Template strand	Length	Start	Stop	Tm	GC %	Self complementarity	Self 3' complementarity
Forward primer	ACCCAGCGACACCTGATTTA	Plus	20	129	148	59.02	50.00	3.00	2.00
Reverse primer	AGCACTACTGCAAAGGCCAG	Minus	20	758	739	60.61	55.00	6.00	1.00
Internal oligo		Plus							
Product length	630								
Product Tm									
Product Tm - min(OLIGO Tm)									

Exon junction

Total intron size

Products on intended target

>NC_000083.6 Mus musculus strain C57BL/6J chromosome 17, GRCm38.p2 C57BL/6J

```
product length = 630
Features associated with this product:
   mitogen-activated protein kinase kinase kinase 4 isoform X1

   mitogen-activated protein kinase kinase kinase 4

Forward primer  1         ACCCAGCGACACCTGATTTA  20
Template        12318909  ....................  12318890

Reverse primer  1         AGCACTACTGCAAAGGCCAG  20
Template        12318280  ....................  12318299
```

Products on allowed transcript variants

Products on potentially unintended templates

Products on target templates

Primer pair 8

	Sequence (5'->3')	Template strand	Length	Start	Stop	Tm	GC %	Self complementarity	Self 3' complementarity
Forward primer	CACCCAGCGACACCTGATT	Plus	19	128	146	60.00	57.89	3.00	1.00
Reverse primer	CTACTGCAAAGGCCAGGGTC	Minus	20	754	735	60.68	60.00	4.00	2.00
Internal oligo		Plus							
Product length	627								
Product Tm									
Product Tm - min(OLIGO Tm)									
Exon junction									
Total intron size									

Products on intended target

>NC_000083.6 Mus musculus strain C57BL/6J chromosome 17, GRCm38.p2 C57BL/6J

```
product length = 627
Features associated with this product:
   mitogen-activated protein kinase kinase kinase 4 isoform X1

   mitogen-activated protein kinase kinase kinase 4

Forward primer  1         CACCCAGCGACACCTGATT  19
Template        12318910  ...................  12318892

Reverse primer  1         CTACTGCAAAGGCCAGGGTC  20
Template        12318284  ....................  12318303
```

Products on allowed transcript variants

Products on target templates

Primer pair 9

	Sequence (5'->3')	Template strand	Length	Start	Stop	Tm	GC %	Self complementarity	Self 3' complementarity
Forward primer	TCTCCAAATGTCTCCTGTGCC	Plus	21	73	93	60.00	52.38	2.00	1.00
Reverse primer	CGTCGCCTCTCTTTTCCTGG	Minus	20	880	861	60.74	60.00	3.00	3.00
Internal oligo		Plus							
Product length	808								
Product Tm									
Product Tm - min(OLIGO Tm)									
Exon junction									
Total intron size									

Products on intended target

>NC_000083.6 Mus musculus strain C57BL/6J chromosome 17, GRCm38.p2 C57BL/6J

```
product length = 808
Features associated with this product:
   mitogen-activated protein kinase kinase kinase 4 isoform X1

   mitogen-activated protein kinase kinase kinase 4

Forward primer  1         TCTCCAAATGTCTCCTGTGCC  21
Template        12318965  ......................  12318945

Reverse primer  1         CGTCGCCTCTCTTTTCCTGG  20
Template        12318158  ....................  12318177
```

Products on allowed transcript variants

Primer pair 10

	Sequence (5'->3')	Template strand	Length	Start	Stop	Tm	GC %	Self complementarity	Self 3' complementarity
Forward primer	AATCCAGTGGCGCAGAGAC	Plus	19	5	23	60.08	57.89	5.00	1.00
Reverse primer	GGGGAGCACTACTGCAAAGG	Minus	20	762	743	60.68	60.00	6.00	0.00
Internal oligo		Plus							
Product length	758								
Product Tm									
Product Tm - min(OLIGO Tm)									
Exon junction									
Total intron size									

Products on intended target

>NC_000083.6 Mus musculus strain C57BL/6J chromosome 17, GRCm38.p2 C57BL/6J

```
product length = 758
Features associated with this product:
   mitogen-activated protein kinase kinase kinase 4 isoform X1

   mitogen-activated protein kinase kinase kinase 4
```

```
Forward primer  1         AATCCAGTGGCGCAGAGAC  19
Template        12319033  ...................  12319015

Reverse primer  1         GGGGAGCACTACTGCAAAGG  20
Template        12318276  ...................  12318295
```

Products on allowed transcript variants

Products on potentially unintended templates

Designing primers to amplify human MEKK4 Cas9 target for Surveyor/sequencing assays

Human MEKK4

Ensembl summary

Name	Transcript ID	Length (bp)	Protein ID	Length (aa)	Biotyp
MAP3K4-001	ENST00000392142	5490	ENSP00000375986	1608	Protein

Primer-BLAST in order to avoid nonspecific amplification. SURVEYOR primers should be designed to amplify 200–400 bp on either side of the Cas9 target (for a total amplicon 400–800 bp long) to allow clear visualization of cleavage bands by gel electrophoresis. To prevent excessive primer dimer formation, SURVEYOR primers should be designed to be typically 18 to 25 nt long with melting temperatures of ~60 °C. For SURVEYOR assay or sequencing analysis, we recommend testing that each pair of candidate primers produces a single PCR product, as well as testing for the absence of nonspecific cleavage during the SURVEYOR nuclease digestion process

Design primes to amplify this region with Primer blast

GAGCTCCCAGCCCGCTGCACAGCCCGGCTCCGCTCCACAGTCCCCCACTGCCACCGGCCGGGGCGACACCGGGCGAG
CTGGCGAGACCCGGCTCCAGGACCGAATCGCGCCGACACTTGACGGCGCTCCCCGCCCCTCCCTGCCGCCGTCTCCG
CCCCCGTCCGGTCGCATTCCGGCGCCCGCCGCCGCCGCCGCCACCGCCGCCGATCTGGGAGGCTTGTCCCTCGCCGC
CCACCGTAGCCCCGGCGCTCGGCCGGTCGCCGTTTCCAAGATGGCCGCGGCGCGCACGGCTCCTGCGGCGGGGTAGA
GGCGGAGGCGGAGTCGAGTCACTCCCGCACTTCGGGGCTCCGGTGCCCCGCGCCAGGCTGCAGCTTACTGCCCGCCG
CGGCCATGCGGGGCTCCGTGCACGGATGAGAGAAGCCGCTGCCGCGCTGGTCCCTCCTCCCGCCTTTGCCGTCACGC
CTGCCGCCGCCATGGAGGAGCCGCCGCCACCGCCGCCGCCGCCACCACCGCCACCGGAACCCGAGACCGAGTCAGAA
CCCGAGTGCTGCTTGGCGGCGAGGTGAGTGTGGCGGCCGCAGTCGGTCGCTCGCAGAAAGCGGGGCGGGTCCTGGCC
CGAACTCGGTCGGGCCCGAGGGCCTCTGCTTCCCGCCAGGTGGGGAGGGAAGCATCCAGTCTCTGCAGGCTGGGGCG
GGAGGGGCGCGGTGCATCCCTGGGTCCCAGGGGACCGCGTCTGAGTCTGTCCGGCGACTCCTCCCGGGGGTTGCAGCT
CCGCAGGGTTCCGCTCGAGCGTGTTGCCGGCTCCCCTTCCCTTGTAGACTCCCCCAGCTCACCCTCAACGTTGCGGG
GGCTGGGAGCAGAGTGC

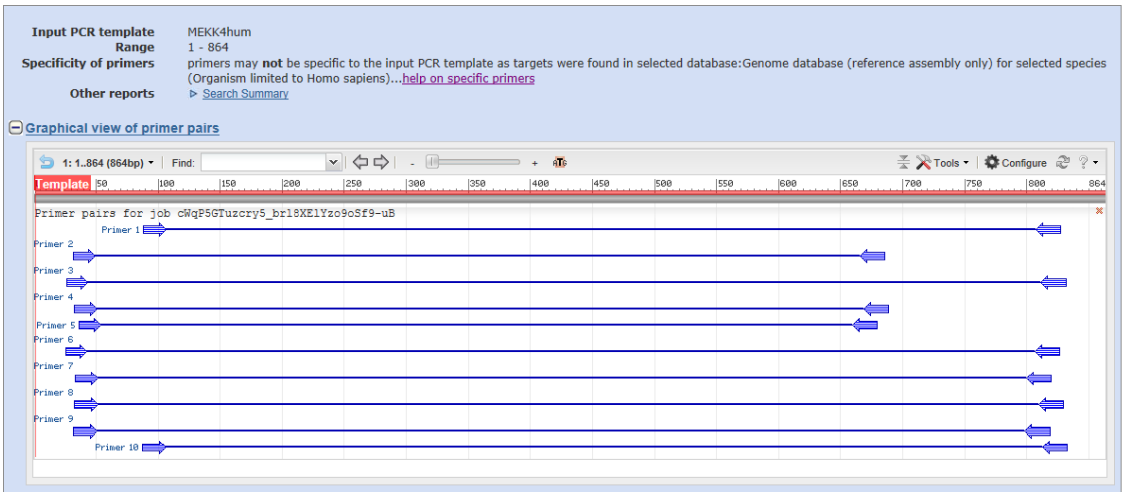

Primer pair 1

	Sequence (5'->3')	Template strand	Length	Start	Stop	Tm	GC %	Self complementarity	Self 3' complementarity
Forward primer	CGGCTCCAGGACCGAATC	Plus	18	89	106	59.89	66.67	7.00	3.00
Reverse primer	CTGGGGGAGTCTACAAGGGA	Minus	20	827	808	59.96	60.00	3.00	0.00
Internal oligo		Plus							
Product length	739								
Product Tm									
Product Tm - min(OLIGO Tm)									
Exon junction									
Total intron size									

Products on intended target

>NC_000006.12 Homo sapiens chromosome 6, GRCh38 Primary Assembly

```
product length = 739
Features associated with this product:
   mitogen-activated protein kinase kinase kinase 4 isoform a

   mitogen-activated protein kinase kinase kinase 4 isoform b

Forward primer  1          CGGCTCCAGGACCGAATC  18
Template        160991610  ..................  160991627

Reverse primer  1          CTGGGGGAGTCTACAAGGGA  20
Template        160992348  ....................  160992329
```

Products on allowed transcript variants

Products on potentially unintended templates

Primer pair 2

	Sequence (5'->3')	Template strand	Length	Start	Stop	Tm	GC %	Self complementarity	Self 3' complementarity
Forward primer	GCTCCACAGTCCCCCACT	Plus	18	32	49	60.93	66.67	3.00	1.00
Reverse primer	CCTGCAGAGACTGGATGCTT	Minus	20	685	666	59.75	55.00	6.00	2.00
Internal oligo		Plus							
Product length	654								
Product Tm									
Product Tm - min(OLIGO Tm)									
Exon junction									
Total intron size									

Products on intended target

>NC_000006.12 Homo sapiens chromosome 6, GRCh38 Primary Assembly

```
product length = 654
Features associated with this product:
   mitogen-activated protein kinase kinase kinase 4 isoform a

   mitogen-activated protein kinase kinase kinase 4 isoform b

Forward primer  1          GCTCCACAGTCCCCCACT  18
Template        160991553  ..................  160991570

Reverse primer  1          CCTGCAGAGACTGGATGCTT  20
Template        160992206  ....................  160992187
```

Products on allowed transcript variants

Products on potentially unintended templates

Primer pair 3

	Sequence (5'->3')	Template strand	Length	Start	Stop	Tm	GC %	Self complementarity	Self 3' complementarity
Forward primer	GCTCCGCTCCACAGTCC	Plus	17	27	43	59.77	70.59	3.00	0.00
Reverse primer	TGAGCTGGGGGAGTCTACAA	Minus	20	831	812	59.88	55.00	4.00	1.00
Internal oligo		Plus							
Product length	805								
Product Tm									
Product Tm - min(OLIGO Tm)									
Exon junction									
Total intron size									

Products on intended target

>NC_000006.12 Homo sapiens chromosome 6, GRCh38 Primary Assembly

```
product length = 805
Features associated with this product:
   mitogen-activated protein kinase kinase kinase 4 isoform a

   mitogen-activated protein kinase kinase kinase 4 isoform b

Forward primer  1          GCTCCGCTCCACAGTCC  17
Template        160991548  ..................  160991564

Reverse primer  1          TGAGCTGGGGGAGTCTACAA  20
Template        160992352  ....................  160992333
```

Products on allowed transcript variants

Primer pair 4

	Sequence (5'->3')	Template strand	Length	Start	Stop	Tm	GC %	Self complementarity	Self 3' complementarity
Forward primer	CTCCACAGTCCCCCACTG	Plus	18	33	50	58.93	66.67	4.00	3.00
Reverse primer	CAGCCTGCAGAGACTGGATG	Minus	20	688	669	60.46	60.00	6.00	3.00
Internal oligo		Plus							
Product length	656								
Product Tm									

Product Tm - min(OLIGO Tm)	
Exon junction	
Total intron size	

Products on intended target

>NC_000006.12 Homo sapiens chromosome 6, GRCh38 Primary Assembly

```
product length = 656
Features associated with this product:
   mitogen-activated protein kinase kinase kinase 4 isoform a

   mitogen-activated protein kinase kinase kinase 4 isoform b

Forward primer  1          CTCCACAGTCCCCCACTG  18
Template        160991554  ..................  160991571

Reverse primer  1          CAGCCTGCAGAGACTGGATG  20
Template        160992209  ....................  160992190
```

Products on allowed transcript variants

Primer pair 5

	Sequence (5'->3')	Template strand	Length	Start	Stop	Tm	GC %	Self complementarity	Self 3' complementarity
Forward primer	ACAGTCCCCCACTGCCA	Plus	17	37	53	60.09	64.71	4.00	3.00
Reverse primer	GAGACTGGATGCTTCCCTCC	Minus	20	679	660	59.53	60.00	6.00	2.00
Internal oligo		Plus							
Product length	643								
Product Tm									
Product Tm - min(OLIGO Tm)									
Exon junction									
Total intron size									

Products on intended target

>NC_000006.12 Homo sapiens chromosome 6, GRCh38 Primary Assembly

```
product length = 643
Features associated with this product:
   mitogen-activated protein kinase kinase kinase 4 isoform a

   mitogen-activated protein kinase kinase kinase 4 isoform b

Forward primer  1          ACAGTCCCCCACTGCCA  17
Template        160991558  .................  160991574

Reverse primer  1          GAGACTGGATGCTTCCCTCC  20
Template        160992200  ....................  160992181
```

Products on allowed transcript variants

Primer pair 6

	Sequence (5'->3')	Template strand	Length	Start	Stop	Tm	GC %	Self complementarity	Self 3' complementarity
Forward primer	GGCTCCGCTCCACAGTC	Plus	17	26	42	59.77	70.59	3.00	1.00

Reverse primer	TGGGGGAGTCTACAAGGGAA	Minus	20	826	807	59.51	55.00	3.00	0.00
Internal oligo		Plus							
Product length	801								
Product Tm									
Product Tm - min(OLIGO Tm)									
Exon junction									
Total intron size									

Products on intended target

>NC_000006.12 Homo sapiens chromosome 6, GRCh38 Primary Assembly

```
product length = 801
Features associated with this product:
   mitogen-activated protein kinase kinase kinase 4 isoform a

   mitogen-activated protein kinase kinase kinase 4 isoform b

Forward primer  1          GGCTCCGCTCCACAGTC  17
Template        160991547  .................  160991563

Reverse primer  1          TGGGGGAGTCTACAAGGGAA  20
Template        160992347  ....................  160992328
```

Products on allowed transcript variants

Primer pair 7

	Sequence (5'->3')	Template strand	Length	Start	Stop	Tm	GC %	Self complementarity	Self 3' complementarity
Forward primer	TCCACAGTCCCCCACTGC	Plus	18	34	51	61.25	66.67	4.00	2.00
Reverse primer	GTCTACAAGGGAAGGGGAGC	Minus	20	819	800	59.46	60.00	2.00	2.00
Internal oligo		Plus							
Product length	786								
Product Tm									
Product Tm - min(OLIGO Tm)									
Exon junction									
Total intron size									

Products on intended target

>NC_000006.12 Homo sapiens chromosome 6, GRCh38 Primary Assembly

```
product length = 786
Features associated with this product:
   mitogen-activated protein kinase kinase kinase 4 isoform a

   mitogen-activated protein kinase kinase kinase 4 isoform b

Forward primer  1          TCCACAGTCCCCCACTGC  18
Template        160991555  ..................  160991572

Reverse primer  1          GTCTACAAGGGAAGGGGAGC  20
Template        160992340  ....................  160992321
```

Products on allowed transcript variants

Products on potentially unintended templates

Primer pair 8

	Sequence (5'->3')	Template strand	Length	Start	Stop	Tm	GC %	Self complementarity	Self 3' complementarity
Forward primer	CTCCACAGTCCCCCACTGC	Plus	19	33	51	62.26	68.42	4.00	2.00
Reverse primer	AGCTGGGGGAGTCTACAAGG	Minus	20	829	810	60.62	60.00	4.00	1.00
Internal oligo		Plus							
Product length	797								
Product Tm									
Product Tm - min(OLIGO Tm)									
Exon junction									
Total intron size									

Products on intended target

>NC_000006.12 Homo sapiens chromosome 6, GRCh38 Primary Assembly

```
product length = 797
Features associated with this product:
   mitogen-activated protein kinase kinase kinase 4 isoform a

   mitogen-activated protein kinase kinase kinase 4 isoform b

Forward primer  1          CTCCACAGTCCCCCACTGC  19
Template        160991554  ..................  160991572

Reverse primer  1          AGCTGGGGGAGTCTACAAGG  20
Template        160992350  ....................  160992331
```

Products on allowed transcript variants

Primer pair 9

	Sequence (5'->3')	Template strand	Length	Start	Stop	Tm	GC %	Self complementarity	Self 3' complementarity
Forward primer	GCTCCACAGTCCCCCACTG	Plus	19	32	50	62.26	68.42	4.00	3.00
Reverse primer	TCTACAAGGGAAGGGGAGCC	Minus	20	818	799	60.62	60.00	2.00	2.00
Internal oligo		Plus							
Product length	787								
Product Tm									
Product Tm -									

min(OLIGO Tm)	
Exon junction	
Total intron size	

Products on intended target

>NC_000006.12 Homo sapiens chromosome 6, GRCh38 Primary Assembly

```
product length = 787
Features associated with this product:
   mitogen-activated protein kinase kinase kinase 4 isoform a

   mitogen-activated protein kinase kinase kinase 4 isoform b

Forward primer  1          GCTCCACAGTCCCCCACTG  19
Template        160991553  ...................  160991571

Reverse primer  1          TCTACAAGGGAAGGGGAGCC  20
Template        160992339  ....................  160992320
```

Products on allowed transcript variants

Primer pair 10

	Sequence (5'->3')	Template strand	Length	Start	Stop	Tm	GC %	Self complementarity	Self 3' complementarity
Forward primer	CCGGCTCCAGGACCGAATC	Plus	19	88	106	62.45	68.42	7.00	3.00
Reverse primer	GTGAGCTGGGGGAGTCTACA	Minus	20	832	813	60.61	60.00	4.00	2.00
Internal oligo		Plus							
Product length	745								
Product Tm									
Product Tm - min(OLIGO Tm)									
Exon junction									
Total intron size									

Products on intended target

>NC_000006.12 Homo sapiens chromosome 6, GRCh38 Primary Assembly

```
product length = 745
Features associated with this product:
   mitogen-activated protein kinase kinase kinase 4 isoform a

   mitogen-activated protein kinase kinase kinase 4 isoform b

Forward primer  1          CCGGCTCCAGGACCGAATC  19
Template        160991609  ...................  160991627

Reverse primer  1          GTGAGCTGGGGGAGTCTACA  20
Template        160992353  ....................  160992334
```

Products on allowed transcript variants

References

Abbott, D.W., A. Wilkins, J.M. Asara, and L.C. Cantley. 2004. The Crohn's disease protein, NOD2, requires RIP2 in order to induce ubiquitinylation of a novel site on NEMO. Curr Biol. 14:2217-2227.

Abbott, D.W., Y. Yang, J.E. Hutti, S. Madhavarapu, M.A. Kelliher, and L.C. Cantley. 2007. Coordinated regulation of Toll-like receptor and NOD2 signaling by K63-linked polyubiquitin chains. Mol Cell Biol. 27:6012-6025.
Abell, A.N., and G.L. Johnson. 2005. MEKK4 is an effector of the embryonic TRAF4 for JNK activation. J Biol Chem. 280:35793-35796.

Abell, A.N., J.A. Rivera-Perez, B.D. Cuevas, M.T. Uhlik, S. Sather, N.L. Johnson, S.K. Minton, J.M. Lauder, A.M. Winter-Vann, K. Nakamura, T. Magnuson, R.R. Vaillancourt, L.E. Heasley, and G.L. Johnson. 2005. Ablation of MEKK4 kinase activity causes neurulation and skeletal patterning defects in the mouse embryo. Mol Cell Biol. 25:8948-8959.

Aiastui, A., M.G. Pucciarelli, and F. García-del Portillo. 2010. Salmonella enterica serovar typhimurium invades fibroblasts by multiple routes differing from the entry into epithelial cells. Infect Immun. 78:2700-2713.

Aissouni, Y., G. Zapart, J.L. Iovanna, I. Dikic, and P. Soubeyran. 2005. CIN85 regulates the ability of MEKK4 to activate the p38 MAP kinase pathway. Biochem Biophys Res Commun. 338:808-814.

Alers, S., A.S. Löffler, S. Wesselborg, and B. Stork. 2012. The incredible ULKs. Cell Commun Signal. 10:7.

Ashwell, J.D. 2006. The many paths to p38 mitogen-activated protein kinase activation in the immune system. Nat Rev Immunol. 6:532-540.

Axe, E.L., S.A. Walker, M. Manifava, P. Chandra, H.L. Roderick, A. Habermann, G. Griffiths, and N.T. Ktistakis. 2008. Autophagosome formation from membrane compartments enriched in phosphatidylinositol 3-phosphate and dynamically connected to the endoplasmic reticulum. J Cell Biol. 182:685-701.

Bandyopadhyay, U., S. Kaushik, L. Varticovski, and A.M. Cuervo. 2008. The chaperone-mediated autophagy receptor organizes in dynamic protein complexes at the lysosomal membrane. Mol Cell Biol. 28:5747-5763.

Barrangou, R., C. Fremaux, H. Deveau, M. Richards, P. Boyaval, S. Moineau, D.A. Romero, and P. Horvath. 2007. CRISPR provides acquired resistance against viruses in prokaryotes. Science. 315:1709-1712.

Barrett, J.C., S. Hansoul, D.L. Nicolae, J.H. Cho, R.H. Duerr, J.D. Rioux, S.R. Brant, M.S. Silverberg, K.D. Taylor, M.M. Barmada, A. Bitton, T. Dassopoulos, L.W. Datta, T. Green, A.M. Griffiths, E.O. Kistner, M.T. Murtha, M.D. Regueiro, J.I. Rotter, L.P. Schumm, A.H. Steinhart, S.R. Targan, R.J. Xavier, C. Libioulle, C. Sandor, M. Lathrop, J. Belaiche, O. Dewit, I. Gut, S. Heath, D. Laukens, M. Mni, P. Rutgeerts, A. Van Gossum, D. Zelenika, D. Franchimont, J.P. Hugot, M. de Vos, S. Vermeire, E. Louis, L.R. Cardon, C.A. Anderson, H. Drummond, E. Nimmo, T. Ahmad, N.J. Prescott, C.M. Onnie, S.A. Fisher, J. Marchini, J. Ghori, S. Bumpstead, R. Gwilliam, M. Tremelling, P. Deloukas, J. Mansfield, D. Jewell, J.

Satsangi, C.G. Mathew, M. Parkes, M. Georges, M.J. Daly, N.I.G. Consortium, B.-F.I. Consortium, and W.T.C.C. Consortium. 2008. Genome-wide association defines more than 30 distinct susceptibility loci for Crohn's disease. Nat Genet. 40:955-962.

Bastian, F., G. Parmentier, J. Roux, S. Moretti, V. Laudent, and M. Robinson-Rechavi. 2008. Bgee: Integrating and Comparing Heterogeneous Transcriptome Data Among Species. In Data Integration in the Life Sciences 5th International Workshop, DILS 2008. Evry, France, June 2008. A. Barioch, S. Cohen-Boulakia, and C. Froidevaux, editors. Springer. 124-131.

Behrends, C., M.E. Sowa, S.P. Gygi, and J.W. Harper. 2010. Network organization of the human autophagy system. Nature. 466:68-76.

Belt, P.B., W. Jongmans, J. de Wit, J.H. Hoeijmakers, P. van de Putte, and C. Backendorf. 1991. Efficient cDNA cloning by direct phenotypic correction of a mutant human cell line (HPRT-) using an Epstein-Barr virus-derived cDNA expression vector. Nucleic Acids Res. 19:4861-4866.

Bergink, S., F.A. Salomons, D. Hoogstraten, T.A. Groothuis, H. de Waard, J. Wu, L. Yuan, E. Citterio, A.B. Houtsmuller, J. Neefjes, J.H. Hoeijmakers, W. Vermeulen, and N.P. Dantuma. 2006. DNA damage triggers nucleotide excision repair-dependent monoubiquitylation of histone H2A. Genes Dev. 20:1343-1352.

Bertrand, M.J., K. Doiron, K. Labbé, R.G. Korneluk, P.A. Barker, and M. Saleh. 2009. Cellular inhibitors of apoptosis cIAP1 and cIAP2 are required for innate immunity signaling by the pattern recognition receptors NOD1 and NOD2. Immunity. 30:789-801.

Bettinger, B.T., and D.C. Amberg. 2007. The MEK kinases MEKK4/Ssk2p facilitate complexity in the stress signaling responses of diverse systems. J Cell Biochem. 101:34-43.

Bhinder, G., H.P. Sham, J.M. Chan, V. Morampudi, K. Jacobson, and B.A. Vallance. 2013. The Citrobacter rodentium mouse model: studying pathogen and host contributions to infectious colitis. J Vis Exp:e50222.

Billmann-Born, S., S. Lipinski, J. Böck, A. Till, P. Rosenstiel, and S. Schreiber. 2011. The complex interplay of NOD-like receptors and the autophagy machinery in the pathophysiology of Crohn disease. Eur J Cell Biol. 90:593-602.

Bjørkøy, G., T. Lamark, A. Brech, H. Outzen, M. Perander, A. Overvatn, H. Stenmark, and T. Johansen. 2005. p62/SQSTM1 forms protein aggregates degraded by autophagy and has a protective effect on huntingtin-induced cell death. J Cell Biol. 171:603-614.

Boada-Romero, E., M. Letek, A. Fleischer, K. Pallauf, C. Ramón-Barros, and F.X. Pimentel-Muiños. 2013. TMEM59 defines a novel ATG16L1-binding motif that promotes local activation of LC3. EMBO J. 32:566-582.

Brazma, A., H. Parkinson, U. Sarkans, M. Shojatalab, J. Vilo, N. Abeygunawardena, E. Holloway, M. Kapushesky, P. Kemmeren, G.G. Lara, A. Oezcimen, P. Rocca-Serra, and S.A. Sansone. 2003. ArrayExpress--a public repository for microarray gene expression data at the EBI. Nucleic Acids Res. 31:68-71.

Breslin, N.P., A. Todd, C. Kilgallen, and C. O'Morain. 1997. Monozygotic twins with Crohn's disease and ulcerative colitis: a unique case report. Gut. 41:557-560.

Brouns, S.J., M.M. Jore, M. Lundgren, E.R. Westra, R.J. Slijkhuis, A.P. Snijders, M.J. Dickman, K.S. Makarova, E.V. Koonin, and J. van der Oost. 2008. Small CRISPR RNAs guide antiviral defense in prokaryotes. Science. 321:960-964.

Cadwell, K., J.Y. Liu, S.L. Brown, H. Miyoshi, J. Loh, J.K. Lennerz, C. Kishi, W. Kc, J.A. Carrero, S. Hunt, C.D. Stone, E.M. Brunt, R.J. Xavier, B.P. Sleckman, E. Li, N. Mizushima, T.S. Stappenbeck, and H.W. Virgin. 2008. A key role for autophagy and the autophagy gene Atg16l1 in mouse and human intestinal Paneth cells. Nature. 456:259-263.

Cadwell, K., K.K. Patel, N.S. Maloney, T.C. Liu, A.C. Ng, C.E. Storer, R.D. Head, R. Xavier, T.S. Stappenbeck, and H.W. Virgin. 2010. Virus-plus-susceptibility gene interaction determines Crohn's disease gene Atg16L1 phenotypes in intestine. Cell. 141:1135-1145.

Cecconi, F., and B. Levine. 2008. The role of autophagy in mammalian development: cell makeover rather than cell death. Dev Cell. 15:344-357.
Celis, J.E. 2006. Cell biology : a laboratory handbook. Oxford ; Boston : Elsevier Academic, Amsterdam.

Chauhan, S., M.A. Mandell, V. Deretic. 2015. IGRM Governs the Core Autophagy Machinery to Conduct Antimicrobial Defense. Mol Cell. 58:507-21.

Cheng, J.F., Y.J. Ning, W. Zhang, Z.H. Lu, and L. Lin. 2010. T300A polymorphism of ATG16L1 and susceptibility to inflammatory bowel diseases: a meta-analysis. World J Gastroenterol. 16:1258-1266.

Chi, H., B. Lu, M. Takekawa, R.J. Davis, and R.A. Flavell. 2004. GADD45beta/GADD45gamma and MEKK4 comprise a genetic pathway mediating STAT4-independent IFNgamma production in T cells. EMBO J. 23:1576-1586.

Cho, J.H. 2008. The genetics and immunopathogenesis of inflammatory bowel disease. Nat Rev Immunol. 8:458-466.

Choi, J., S. Park, S.B. Biering, E. Selleck, C.Y. Liu, X. Zhang, N. Fujita, T. Saitoh, S. Akira, T. Yoshimori, L.D. Sibley, S. Hwang, and H.W. Virgin. 2014. The parasitophorous vacuole membrane of Toxoplasma gondii is targeted for disruption by ubiquitin-like conjugation systems of autophagy. Immunity. 40:924-935.

Clark, N.M., J.M. Marinis, B.A. Cobb, and D.W. Abbott. 2008. MEKK4 sequesters RIP2 to dictate NOD2 signal specificity. Curr Biol. 18:1402-1408.

Cong, L., F.A. Ran, D. Cox, S. Lin, R. Barretto, N. Habib, P.D. Hsu, X. Wu, W. Jiang, L.A. Marraffini, and F. Zhang. 2013. Multiplex genome engineering using CRISPR/Cas systems. Science. 339:819-823.

Consortium, W.T.C.C. 2007. Genome-wide association study of 14,000 cases of seven common diseases and 3,000 shared controls. Nature. 447:661-678.

Conway, K.L., P. Kuballa, J.H. Song, K.K. Patel, A.B. Castoreno, O.H. Yilmaz, H.B. Jijon, M. Zhang, L.N. Aldrich, E.J. Villablanca, J.M. Peloquin, G. Goel, I.A. Lee, E. Mizoguchi, H.N. Shi, A.K. Bhan, S.Y. Shaw, S.L. Schreiber, H.W. Virgin, A.F. Shamji, T.S. Stappenbeck, H.C. Reinecker, and R.J. Xavier. 2013. Atg16l1 is required for autophagy in intestinal

epithelial cells and protection of mice from Salmonella infection. Gastroenterology. 145:1347-1357.

Cooney, R., J. Baker, O. Brain, B. Danis, T. Pichulik, P. Allan, D.J. Ferguson, B.J. Campbell, D. Jewell, and A. Simmons. 2010. NOD2 stimulation induces autophagy in dendritic cells influencing bacterial handling and antigen presentation. Nat Med. 16:90-97.

Corpet, F. 1988. Multiple sequence alignment with hierarchical clustering. Nucleic Acids Res. 16:10881-10890.

Dantuma, N.P., T.A. Groothuis, F.A. Salomons, and J. Neefjes. 2006. A dynamic ubiquitin equilibrium couples proteasomal activity to chromatin remodeling. J Cell Biol. 173:19-26.

de Castro, E., C.J. Sigrist, A. Gattiker, V. Bulliard, P.S. Langendijk-Genevaux, E. Gasteiger, A. Bairoch, and N. Hulo. 2006. ScanProsite: detection of PROSITE signature matches and ProRule-associated functional and structural residues in proteins. Nucleic Acids Res. 34:W362-365.

Deretic, V., and B. Levine. 2009. Autophagy, immunity, and microbial adaptations. Cell Host Microbe. 5:527-549.

Dooley, H.C., M. Razi, H.E. Polson, S.E. Girardin, M.I. Wilson, and S.A. Tooze. 2014. WIPI2 links LC3 conjugation with PI3P, autophagosome formation, and pathogen clearance by recruiting Atg12-5-16L1. Mol Cell. 55:238-252.

Elson, C.O., Y. Cong, V.J. McCracken, R.A. Dimmitt, R.G. Lorenz, and C.T. Weaver. 2005. Experimental models of inflammatory bowel disease reveal innate, adaptive, and regulatory mechanisms of host dialogue with the microbiota. Immunol Rev. 206:260-276.

English, L., M. Chemali, and M. Desjardins. 2009. Nuclear membrane-derived autophagy, a novel process that participates in the presentation of endogenous viral antigens during HSV-1 infection. Autophagy. 5:1026-1029.

Falschlehner, C., C.H. Emmerich, B. Gerlach, and H. Walczak. 2007. TRAIL signalling: decisions between life and death. Int J Biochem Cell Biol. 39:1462-1475.

Fass, E., E. Shvets, I. Degani, K. Hirschberg, and Z. Elazar. 2006. Microtubules support production of starvation-induced autophagosomes but not their targeting and fusion with lysosomes. J Biol Chem. 281:36303-36316.

Fire, A., S. Xu, M.K. Montgomery, S.A. Kostas, S.E. Driver, and C.C. Mello. 1998. Potent and specific genetic interference by double-stranded RNA in Caenorhabditis elegans. Nature. 391:806-811.

Friedland, A.E., Y.B. Tzur, K.M. Esvelt, M.P. Colaiácovo, G.M. Church, and J.A. Calarco. 2013. Heritable genome editing in C. elegans via a CRISPR-Cas9 system. Nat Methods. 10:741-743.

Fu, Y., J.A. Foden, C. Khayter, M.L. Maeder, D. Reyon, J.K. Joung, and J.D. Sander. 2013. High-frequency off-target mutagenesis induced by CRISPR-Cas nucleases in human cells. Nat Biotechnol. 31:822-826.

Fujioka, Y., N.N. Noda, H. Nakatogawa, Y. Ohsumi, and F. Inagaki. 2010. Dimeric coiled-coil structure of Saccharomyces cerevisiae Atg16 and its functional significance in autophagy. J Biol Chem. 285:1508-1515.

Fujita, K., D. Maeda, Q. Xiao, and S.M. Srinivasula. 2011. Nrf2-mediated induction of p62 controls Toll-like receptor-4-driven aggresome-like induced structure formation and autophagic degradation. Proc Natl Acad Sci U S A. 108:1427-1432.

Fujita, N., M. Hayashi-Nishino, H. Fukumoto, H. Omori, A. Yamamoto, T. Noda, and T. Yoshimori. 2008. An Atg4B mutant hampers the lipidation of LC3 paralogues and causes defects in autophagosome closure. Mol Biol Cell. 19:4651-4659.

Fujita, N., T. Itoh, H. Omori, M. Fukuda, T. Noda, and T. Yoshimori. 2008. The Atg16L complex specifies the site of LC3 lipidation for membrane biogenesis in autophagy. Mol Biol Cell. 19:2092-2100.

Fujita, N., E. Morita, T. Itoh, A. Tanaka, M. Nakaoka, Y. Osada, T. Umemoto, T. Saitoh, H. Nakatogawa, S. Kobayashi, T. Haraguchi, J.L. Guan, K. Iwai, F. Tokunaga, K. Saito, K. Ishibashi, S. Akira, M. Fukuda, T. Noda, and T. Yoshimori. 2013. Recruitment of the autophagic machinery to endosomes during infection is mediated by ubiquitin. J Cell Biol. 203:115-128.

Fujita, N., T. Saitoh, S. Kageyama, S. Akira, T. Noda, and T. Yoshimori. 2009. Differential involvement of Atg16L1 in Crohn disease and canonical autophagy: analysis of the organization of the Atg16L1 complex in fibroblasts. J Biol Chem. 284:32602-32609.

Gammoh, N., O. Florey, M. Overholtzer, and X. Jiang. 2013. Interaction between FIP200 and ATG16L1 distinguishes ULK1 complex-dependent and -independent autophagy. Nat Struct Mol Biol. 20:144-149.

García-Mata, R., Z. Bebök, E.J. Sorscher, and E.S. Sztul. 1999. Characterization and dynamics of aggresome formation by a cytosolic GFP-chimera. J Cell Biol. 146:1239-1254.

Garneau, J.E., M. Dupuis, M. Villion, D.A. Romero, R. Barrangou, P. Boyaval, C. Fremaux, P. Horvath, A.H. Magadán, and S. Moineau. 2010. The CRISPR/Cas bacterial immune system cleaves bacteriophage and plasmid DNA. Nature. 468:67-71.

Ge, L., and R. Schekman. 2014. The ER-Golgi intermediate compartment feeds the phagophore membrane. Autophagy. 10:170-172.

Geng, J., and D.J. Klionsky. 2008. The Atg8 and Atg12 ubiquitin-like conjugation systems in macroautophagy. 'Protein modifications: beyond the usual suspects' review series. EMBO Rep. 9:859-864.

Gerwins, P., J.L. Blank, and G.L. Johnson. 1997. Cloning of a novel mitogen-activated protein kinase kinase kinase, MEKK4, that selectively regulates the c-Jun amino terminal kinase pathway. J Biol Chem. 272:8288-8295.

Gould, C.M., F. Diella, A. Via, P. Puntervoll, C. Gemünd, S. Chabanis-Davidson, S. Michael, A. Sayadi, J.C. Bryne, C. Chica, M. Seiler, N.E. Davey, N. Haslam, R.J. Weatheritt, A. Budd, T. Hughes, J. Pas, L. Rychlewski, G. Travé, R. Aasland, M. Helmer-Citterich, R. Linding, and T.J. Gibson. 2010. ELM: the status of the 2010 eukaryotic linear motif resource. Nucleic Acids Res. 38:D167-180.

Guo, W., and H. Wu. 2008. Detection of LacZ expression by FACS-Gal analysis. Protocol Exchange.

Gupta, M., S.K. Gupta, B. Hoffman, and D.A. Liebermann. 2006. Gadd45a and Gadd45b protect hematopoietic cells from UV-induced apoptosis via distinct signaling pathways, including p38 activation and JNK inhibition. J Biol Chem. 281:17552-17558.

Hampe, J., A. Franke, P. Rosenstiel, A. Till, M. Teuber, K. Huse, M. Albrecht, G. Mayr, F.M. De La Vega, J. Briggs, S. Günther, N.J. Prescott, C.M. Onnie, R. Häsler, B. Sipos, U.R. Fölsch, T. Lengauer, M. Platzer, C.G. Mathew, M. Krawczak, and S. Schreiber. 2007. A genome-wide association scan of nonsynonymous SNPs identifies a susceptibility variant for Crohn disease in ATG16L1. Nat Genet. 39:207-211.

Harlow, E., and D. Lane. 2006. Mounting samples in gelvatol or mowiol. CSH Protoc. 2006.

Heigwer, F., G. Kerr, and M. Boutros. 2014. E-CRISP: fast CRISPR target site identification. Nat Methods. 11:122-123.

Hisamatsu, T., M. Suzuki, and D.K. Podolsky. 2003. Interferon-gamma augments CARD4/NOD1 gene and protein expression through interferon regulatory factor-1 in intestinal epithelial cells. J Biol Chem. 278:32962-32968.

Hisamatsu, T., M. Suzuki, H.C. Reinecker, W.J. Nadeau, B.A. McCormick, and D.K. Podolsky. 2003. CARD15/NOD2 functions as an antibacterial factor in human intestinal epithelial cells. Gastroenterology. 124:993-1000.

Homer, C.R., A. Kabi, N. Marina-García, A. Sreekumar, A.I. Nesvizhskii, K.P. Nickerson, A.M. Chinnaiyan, G. Nuñez, and C. McDonald. 2012. A dual role for receptor-interacting protein kinase 2 (RIP2) kinase activity in nucleotide-binding oligomerization domain 2 (NOD2)-dependent autophagy. J Biol Chem. 287:25565-25576.

Homer, C.R., A.L. Richmond, N.A. Rebert, J.P. Achkar, and C. McDonald. 2010. ATG16L1 and NOD2 interact in an autophagy-dependent antibacterial pathway implicated in Crohn's disease pathogenesis. Gastroenterology. 139:1630-1641, 1641.e1631-1632.

Hosokawa, N., T. Sasaki, S. Iemura, T. Natsume, T. Hara, and N. Mizushima. 2009. Atg101, a novel mammalian autophagy protein interacting with Atg13. Autophagy. 5:973-979.

Hsu, P.D., E.S. Lander, and F. Zhang. 2014. Development and applications of CRISPR-Cas9 for genome engineering. Cell. 157:1262-1278.

Huang, J., and D.J. Klionsky. 2007. Autophagy and human disease. Cell Cycle. 6:1837-1849.

Huebner, C., I. Petermann, W.J. Lam, A.N. Shelling, and L.R. Ferguson. 2010. Characterization of single-nucleotide polymorphisms relevant to inflammatory bowel disease in commonly used gastrointestinal cell lines. Inflamm Bowel Dis. 16:282-295.

Humphries, F., S. Yang, B. Wang, and P.N. Moynagh. 2014. RIP kinases: key decision makers in cell death and innate immunity. Cell Death Differ.

Ichimura, Y., T. Kirisako, T. Takao, Y. Satomi, Y. Shimonishi, N. Ishihara, N. Mizushima, I. Tanida, E. Kominami, M. Ohsumi, T. Noda, and Y. Ohsumi. 2000. A ubiquitin-like system mediates protein lipidation. Nature. 408:488-492.

Ichimura, Y., T. Kumanomidou, Y.S. Sou, T. Mizushima, J. Ezaki, T. Ueno, E. Kominami, T. Yamane, K. Tanaka, and M. Komatsu. 2008. Structural basis for sorting mechanism of p62 in selective autophagy. J Biol Chem. 283:22847-22857.

Inohara, N., T. Koseki, J. Lin, L. del Peso, P.C. Lucas, F.F. Chen, Y. Ogura, and G. Núñez. 2000. An induced proximity model for NF-kappa B activation in the Nod1/RICK and RIP signaling pathways. J Biol Chem. 275:27823-27831.

Ishibashi, K., N. Fujita, E. Kanno, H. Omori, T. Yoshimori, T. Itoh, and M. Fukuda. 2011. Atg16L2, a novel isoform of mammalian Atg16L that is not essential for canonical autophagy despite forming an Atg12–5-16L2 complex. Autophagy. 7:1500-1513.

Ishino, Y., H. Shinagawa, K. Makino, M. Amemura, and A. Nakata. 1987. Nucleotide sequence of the iap gene, responsible for alkaline phosphatase isozyme conversion in Escherichia coli, and identification of the gene product. J Bacteriol. 169:5429-5433.

Itakura, E., C. Kishi, K. Inoue, and N. Mizushima. 2008. Beclin 1 forms two distinct phosphatidylinositol 3-kinase complexes with mammalian Atg14 and UVRAG. Mol Biol Cell. 19:5360-5372.

Itakura, E., and N. Mizushima. 2010. Characterization of autophagosome formation site by a hierarchical analysis of mammalian Atg proteins. Autophagy. 6:764-776.

Itoh, T., N. Fujita, E. Kanno, A. Yamamoto, T. Yoshimori, and M. Fukuda. 2008. Golgi-resident small GTPase Rab33B interacts with Atg16L and modulates autophagosome formation. Mol Biol Cell. 19:2916-2925.

Iwata, A., B.E. Riley, J.A. Johnston, and R.R. Kopito. 2005. HDAC6 and microtubules are required for autophagic degradation of aggregated huntingtin. J Biol Chem. 280:40282-40292.

Jahreiss, L., F.M. Menzies, and D.C. Rubinsztein. 2008. The itinerary of autophagosomes: from peripheral formation to kiss-and-run fusion with lysosomes. Traffic. 9:574-587.

Jiang, W., D. Bikard, D. Cox, F. Zhang, and L.A. Marraffini. 2013. RNA-guided editing of bacterial genomes using CRISPR-Cas systems. Nat Biotechnol. 31:233-239.

Kabeya, Y., N. Mizushima, T. Ueno, A. Yamamoto, T. Kirisako, T. Noda, E. Kominami, Y. Ohsumi, and T. Yoshimori. 2000. LC3, a mammalian homologue of yeast Apg8p, is localized in autophagosome membranes after processing. EMBO J. 19:5720-5728.

Kamijo, T., F. Zindy, M.F. Roussel, D.E. Quelle, J.R. Downing, R.A. Ashmun, G. Grosveld, and C.J. Sherr. 1997. Tumor suppression at the mouse INK4a locus mediated by the alternative reading frame product p19ARF. Cell. 91:649-659.

Kanayama, A., R.B. Seth, L. Sun, C.K. Ea, M. Hong, A. Shaito, Y.H. Chiu, L. Deng, and Z.J. Chen. 2004. TAB2 and TAB3 activate the NF-kappaB pathway through binding to polyubiquitin chains. Mol Cell. 15:535-548.

Karanasios, E., E. Stapleton, M. Manifava, T. Kaizuka, N. Mizushima, S.A. Walker, and N.T. Ktistakis. 2013. Dynamic association of the ULK1 complex with omegasomes during autophagy induction. J Cell Sci. 126:5224-5238.

Kawaguchi, Y., J.J. Kovacs, A. McLaurin, J.M. Vance, A. Ito, and T.P. Yao. 2003. The deacetylase HDAC6 regulates aggresome formation and cell viability in response to misfolded protein stress. Cell. 115:727-738.

Keil, E., R. Höcker, M. Schuster, F. Essmann, N. Ueffing, B. Hoffman, D.A. Liebermann, K. Pfeffer, K. Schulze-Osthoff, and I. Schmitz. 2013. Phosphorylation of Atg5 by the Gadd45β-MEKK4-p38 pathway inhibits autophagy. Cell Death Differ. 20:321-332.

Kirkin, V., T. Lamark, Y.S. Sou, G. Bjørkøy, J.L. Nunn, J.A. Bruun, E. Shvets, D.G. McEwan, T.H. Clausen, P. Wild, I. Bilusic, J.P. Theurillat, A. Øvervatn, T. Ishii, Z. Elazar, M. Komatsu, I. Dikic, and T. Johansen. 2009. A role for NBR1 in autophagosomal degradation of ubiquitinated substrates. Mol Cell. 33:505-516.

Klionsky, D.J., F.C. Abdalla, H. Abeliovich, R.T. Abraham, A. Acevedo-Arozena, K. Adeli, L. Agholme, M. Agnello, P. Agostinis, J.A. Aguirre-Ghiso, H.J. Ahn, O. Ait-Mohamed, S. Ait-Si-Ali, T. Akematsu, S. Akira, H.M. Al-Younes, M.A. Al-Zeer, M.L. Albert, R.L. Albin, J. Alegre-Abarrategui, M.F. Aleo, M. Alirezaei, A. Almasan, M. Almonte-Becerril, A. Amano, R. Amaravadi, S. Amarnath, A.O. Amer, N. Andrieu-Abadie, V. Anantharam, D.K. Ann, S. Anoopkumar-Dukie, H. Aoki, N. Apostolova, G. Arancia, J.P. Aris, K. Asanuma, N.Y. Asare, H. Ashida, V. Askanas, D.S. Askew, P. Auberger, M. Baba, S.K. Backues, E.H. Baehrecke, B.A. Bahr, X.Y. Bai, Y. Bailly, R. Baiocchi, G. Baldini, W. Balduini, A. Ballabio, B.A. Bamber, E.T. Bampton, G. Bánhegyi, C.R. Bartholomew, D.C. Bassham, R.C. Bast, H. Batoko, B.H. Bay, I. Beau, D.M. Béchet, T.J. Begley, C. Behl, C. Behrends, S. Bekri, B. Bellaire, L.J. Bendall, L. Benetti, L. Berliocchi, H. Bernardi, F. Bernassola, S. Besteiro, I. Bhatia-Kissova, X. Bi, M. Biard-Piechaczyk, J.S. Blum, L.H. Boise, P. Bonaldo, D.L. Boone, B.C. Bornhauser, K.R. Bortoluci, I. Bossis, F. Bost, J.P. Bourquin, P. Boya, M. Boyer-Guittaut, P.V. Bozhkov, N.R. Brady, C. Brancolini, A. Brech, J.E. Brenman, A. Brennand, E.H. Bresnick, P. Brest, D. Bridges, M.L. Bristol, P.S. Brookes, E.J. Brown, J.H. Brumell, et al. 2012. Guidelines for the use and interpretation of assays for monitoring autophagy. Autophagy. 8:445-544.

Knævelsrud, H., K. Søreng, C. Raiborg, K. Håberg, F. Rasmuson, A. Brech, K. Liestøl, T.E. Rusten, H. Stenmark, T.P. Neufeld, S.R. Carlsson, and A. Simonsen. 2013. Membrane remodeling by the PX-BAR protein SNX18 promotes autophagosome formation. J Cell Biol. 202:331-349.

Köchl, R., X.W. Hu, E.Y. Chan, and S.A. Tooze. 2006. Microtubules facilitate autophagosome formation and fusion of autophagosomes with endosomes. Traffic. 7:129-145.

Kohfeldt, E., P. Maurer, C. Vannahme, and R. Timpl. 1997. Properties of the extracellular calcium binding module of the proteoglycan testican. FEBS Lett. 414:557-561.

Komatsu, M., S. Waguri, M. Koike, Y.S. Sou, T. Ueno, T. Hara, N. Mizushima, J. Iwata, J. Ezaki, S. Murata, J. Hamazaki, Y. Nishito, S. Iemura, T. Natsume, T. Yanagawa, J. Uwayama, E. Warabi, H. Yoshida, T. Ishii, A. Kobayashi, M. Yamamoto, Z. Yue, Y. Uchiyama, E. Kominami, and K. Tanaka. 2007. Homeostatic levels of p62 control cytoplasmic inclusion body formation in autophagy-deficient mice. Cell. 131:1149-1163.

Komatsu, M., S. Waguri, T. Ueno, J. Iwata, S. Murata, I. Tanida, J. Ezaki, N. Mizushima, Y. Ohsumi, Y. Uchiyama, E. Kominami, K. Tanaka, and T. Chiba. 2005. Impairment of starvation-induced and constitutive autophagy in Atg7-deficient mice. J Cell Biol. 169:425-434.

Koyama-Honda, I., E. Itakura, T.K. Fujiwara, and N. Mizushima. 2013. Temporal analysis of recruitment of mammalian ATG proteins to the autophagosome formation site. Autophagy. 9:1491-1499.

Krieg, A., R.G. Correa, J.B. Garrison, G. Le Negrate, K. Welsh, Z. Huang, W.T. Knoefel, and J.C. Reed. 2009. XIAP mediates NOD signaling via interaction with RIP2. Proc Natl Acad Sci U S A. 106:14524-14529.

Kuballa, P., A. Huett, J.D. Rioux, M.J. Daly, and R.J. Xavier. 2008. Impaired autophagy of an intracellular pathogen induced by a Crohn's disease associated ATG16L1 variant. PLoS One. 3:e3391.

Kuma, A., M. Hatano, M. Matsui, A. Yamamoto, H. Nakaya, T. Yoshimori, Y. Ohsumi, T. Tokuhisa, and N. Mizushima. 2004. The role of autophagy during the early neonatal starvation period. Nature. 432:1032-1036.

Kumar, H., T. Kawai, and S. Akira. 2009. Pathogen recognition in the innate immune response. Biochem J. 420:1-16.

Lamark, T., and T. Johansen. 2012. Aggrephagy: selective disposal of protein aggregates by macroautophagy. Int J Cell Biol. 2012:736905.

Lamb, C.A., T. Yoshimori, and S.A. Tooze. 2013. The autophagosome: origins unknown, biogenesis complex. Nat Rev Mol Cell Biol. 14:759-774.

Lassen, K.G., P. Kuballa, K.L. Conway, K.K. Patel, C.E. Becker, J.M. Peloquin, E.J. Villablanca, J.M. Norman, T.C. Liu, R.J. Heath, M.L. Becker, L. Fagbami, H. Horn, J. Mercer, O.H. Yilmaz, J.D. Jaffe, A.F. Shamji, A.K. Bhan, S.A. Carr, M.J. Daly, H.W. Virgin, S.L. Schreiber, T.S. Stappenbeck, and R.J. Xavier. 2014. Atg16L1 T300A variant decreases selective autophagy resulting in altered cytokine signaling and decreased antibacterial defense. Proc Natl Acad Sci U S A. 111:7741-7746.

Laule, O., M. Hirsch-Hoffmann, T. Hruz, W. Gruissem, and P. Zimmermann. 2006. Web-based analysis of the mouse transcriptome using Genevestigator. BMC Bioinformatics. 7:311.

Le Lay, J., and K.H. Kaestner. 2010. The Fox genes in the liver: from organogenesis to functional integration. Physiol Rev. 90:1-22.

Lee, I.H., and T. Finkel. 2009. Regulation of autophagy by the p300 acetyltransferase. J Biol Chem. 284:6322-6328.

Lelouard, H., V. Ferrand, D. Marguet, J. Bania, V. Camosseto, A. David, E. Gatti, and P. Pierre. 2004. Dendritic cell aggresome-like induced structures are dedicated areas for ubiquitination and storage of newly synthesized defective proteins. J Cell Biol. 164:667-675.

Levine, B., and D.J. Klionsky. 2004. Development by self-digestion: molecular mechanisms and biological functions of autophagy. Dev Cell. 6:463-477.

Levine, B., and G. Kroemer. 2008. Autophagy in the pathogenesis of disease. Cell. 132:27-42.

Liebermann, D.A., and B. Hoffman. 2002. Myeloid differentiation (MyD) primary response genes in hematopoiesis. Oncogene. 21:3391-3402.

Linderson, Y., F. Bresso, E. Buentke, S. Pettersson, and M. D'Amato. 2005. Functional interaction of CARD15/NOD2 and Crohn's disease-associated TNFalpha polymorphisms. Int J Colorectal Dis. 20:305-311.

Liou, W., H.J. Geuze, M.J. Geelen, and J.W. Slot. 1997. The autophagic and endocytic pathways converge at the nascent autophagic vacuoles. J Cell Biol. 136:61-70.

Longatti, A., and S.A. Tooze. 2009. Vesicular trafficking and autophagosome formation. Cell Death Differ. 16:956-965.

Luo, W., W.W. Ng, L.H. Jin, Z. Ye, J. Han, and S.C. Lin. 2003. Axin utilizes distinct regions for competitive MEKK1 and MEKK4 binding and JNK activation. J Biol Chem. 278:37451-37458.

Mali, P., K.M. Esvelt, and G.M. Church. 2013. Cas9 as a versatile tool for engineering biology. Nat Methods. 10:957-963.

Marchiando, A.M., D. Ramanan, Y. Ding, L.E. Gomez, V.M. Hubbard-Lucey, K. Maurer, C. Wang, J.W. Ziel, N. van Rooijen, G. Nuñez, B.B. Finlay, I.U. Mysorekar, and K. Cadwell. 2013. A deficiency in the autophagy gene Atg16L1 enhances resistance to enteric bacterial infection. Cell Host Microbe. 14:216-224.

Marinis, J.M., C.R. Homer, C. McDonald, and D.W. Abbott. 2011. A novel motif in the Crohn's disease susceptibility protein, NOD2, allows TRAF4 to down-regulate innate immune responses. J Biol Chem. 286:1938-1950.

Martinez, J., A. Patkaniowska, H. Urlaub, R. Lührmann, and T. Tuschl. 2002. Single-stranded antisense siRNAs guide target RNA cleavage in RNAi. Cell. 110:563-574.

Medzhitov, R. 2007. Recognition of microorganisms and activation of the immune response. Nature. 449:819-826.

Mehrpour, M., A. Esclatine, I. Beau, and P. Codogno. 2010. Autophagy in health and disease. 1. Regulation and significance of autophagy: an overview. Am J Physiol Cell Physiol. 298:C776-785. a

Mehrpour, M., A. Esclatine, I. Beau, and P. Codogno. 2010. Overview of macroautophagy regulation in mammalian cells. Cell Res. 20:748-762. b

Messer, J.S., S.F. Murphy, M.F. Logsdon, J.P. Lodolce, W.A. Grimm, S.J. Bartulis, T.P. Vogel, M. Burn, and D.L. Boone. 2013. The Crohn's disease: associated ATG16L1 variant and Salmonella invasion. BMJ Open. 3.

Mita, H., J. Tsutsui, M. Takekawa, E.A. Witten, and H. Saito. 2002. Regulation of MTK1/MEKK4 kinase activity by its N-terminal autoinhibitory domain and GADD45 binding. Mol Cell Biol. 22:4544-4555.

Miyake, Z., M. Takekawa, Q. Ge, and H. Saito. 2007. Activation of MTK1/MEKK4 by GADD45 through induced N-C dissociation and dimerization-mediated trans autophosphorylation of the MTK1 kinase domain. Mol Cell Biol. 27:2765-2776.

Mizushima, N. 2004. Methods for monitoring autophagy. Int J Biochem Cell Biol. 36:2491-2502.

Mizushima, N., A. Kuma, Y. Kobayashi, A. Yamamoto, M. Matsubae, T. Takao, T. Natsume, Y. Ohsumi, and T. Yoshimori. 2003. Mouse Apg16L, a novel WD-repeat protein, targets to the autophagic isolation membrane with the Apg12-Apg5 conjugate. J Cell Sci. 116:1679-1688.

Mizushima, N., B. Levine, A.M. Cuervo, and D.J. Klionsky. 2008. Autophagy fights disease through cellular self-digestion. Nature. 451:1069-1075.

Mizushima, N., A. Yamamoto, M. Hatano, Y. Kobayashi, Y. Kabeya, K. Suzuki, T. Tokuhisa, Y. Ohsumi, and T. Yoshimori. 2001. Dissection of autophagosome formation using Apg5-deficient mouse embryonic stem cells. J Cell Biol. 152:657-668.

Mizushima, N., and T. Yoshimori. 2007. How to interpret LC3 immunoblotting. Autophagy. 3:542-545.

Mojica, F.J., C. Díez-Villaseñor, E. Soria, and G. Juez. 2000. Biological significance of a family of regularly spaced repeats in the genomes of Archaea, Bacteria and mitochondria. Mol Microbiol. 36:244-246.

Morita, S., T. Kojima, and T. Kitamura. 2000. Plat-E: an efficient and stable system for transient packaging of retroviruses. Gene Ther. 7:1063-1066.

Murthy, A., Y. Li, I. Peng, M. Reichelt, A.K. Katakam, R. Noubade, M. Roose-Girma, J. DeVoss, L. Diehl, R.R. Graham, and M. van Lookeren Campagne. 2014. A Crohn's disease variant in Atg16l1 enhances its degradation by caspase 3. Nature. 506:456-462.

Murthy, A., Y. Li, I. Peng, M. Reichelt, A.K. Katakam, R. Noubade, M. Roose-Girma, J. DeVoss, L. Diehl, R.R. Graham, and M. van Lookeren Campagne. 2014. A Crohn's disease variant in Atg16l1 enhances its degradation by caspase 3. Nature. 506:456-462.

Nigro, G., R. Rossi, P.H. Commere, P. Jay, and P.J. Sansonetti. 2014. The cytosolic bacterial peptidoglycan sensor Nod2 affords stem cell protection and links microbes to gut epithelial regeneration. Cell Host Microbe. 15:792-798.

Nishimura, T., T. Kaizuka, K. Cadwell, M.H. Sahani, T. Saitoh, S. Akira, H.W. Virgin, and N. Mizushima. 2013. FIP200 regulates targeting of Atg16L1 to the isolation membrane. EMBO Rep. 14:284-291.

Nykänen, A., B. Haley, and P.D. Zamore. 2001. ATP requirements and small interfering RNA structure in the RNA interference pathway. Cell. 107:309-321.

Ogura, Y., N. Inohara, A. Benito, F.F. Chen, S. Yamaoka, and G. Nunez. 2001. Nod2, a Nod1/Apaf-1 family member that is restricted to monocytes and activates NF-kappaB. J Biol Chem. 276:4812-4818.

Ogura, Y., S. Lala, W. Xin, E. Smith, T.A. Dowds, F.F. Chen, E. Zimmermann, M. Tretiakova, J.H. Cho, J. Hart, J.K. Greenson, S. Keshav, and G. Nuñez. 2003. Expression of NOD2 in Paneth cells: a possible link to Crohn's ileitis. Gut. 52:1591-1597.

Olsen, J.V., M. Vermeulen, A. Santamaria, C. Kumar, M.L. Miller, L.J. Jensen, F. Gnad, J. Cox, T.S. Jensen, E.A. Nigg, S. Brunak, and M. Mann. 2010. Quantitative phosphoproteomics reveals widespread full phosphorylation site occupancy during mitosis. Sci Signal. 3:ra3.

Paludan, C., D. Schmid, M. Landthaler, M. Vockerodt, D. Kube, T. Tuschl, and C. Münz. 2005. Endogenous MHC class II processing of a viral nuclear antigen after autophagy. Science. 307:593-596.

Polson, H.E., J. de Lartigue, D.J. Rigden, M. Reedijk, S. Urbé, M.J. Clague, and S.A. Tooze. 2010. Mammalian Atg18 (WIPI2) localizes to omegasome-anchored phagophores and positively regulates LC3 lipidation. Autophagy. 6:506-522.

Porter, E.M., C.L. Bevins, D. Ghosh, and T. Ganz. 2002. The multifaceted Paneth cell. Cell Mol Life Sci. 59:156-170.

Pourcel, C., G. Salvignol, and G. Vergnaud. 2005. CRISPR elements in Yersinia pestis acquire new repeats by preferential uptake of bacteriophage DNA, and provide additional tools for evolutionary studies. Microbiology. 151:653-663.

Praz, V., V. Jagannathan, and P. Bucher. 2004. CleanEx: a database of heterogeneous gene expression data based on a consistent gene nomenclature. Nucleic Acids Res. 32:D542-547.

Proikas-Cezanne, T., S. Waddell, A. Gaugel, T. Frickey, A. Lupas, and A. Nordheim. 2004. WIPI-1alpha (WIPI49), a member of the novel 7-bladed WIPI protein family, is aberrantly expressed in human cancer and is linked to starvation-induced autophagy. Oncogene. 23:9314-9325.

Ran, F.A., P.D. Hsu, J. Wright, V. Agarwala, D.A. Scott, and F. Zhang. 2013. Genome engineering using the CRISPR-Cas9 system. Nat Protoc. 8:2281-2308.

Ravikumar, B., K. Moreau, L. Jahreiss, C. Puri, and D.C. Rubinsztein. 2010. Plasma membrane contributes to the formation of pre-autophagosomal structures. Nat Cell Biol. 12:747-757.

Razi, M., E.Y. Chan, and S.A. Tooze. 2009. Early endosomes and endosomal coatomer are required for autophagy. J Cell Biol. 185:305-321.

Rioux, J.D., R.J. Xavier, K.D. Taylor, M.S. Silverberg, P. Goyette, A. Huett, T. Green, P. Kuballa, M.M. Barmada, L.W. Datta, Y.Y. Shugart, A.M. Griffiths, S.R. Targan, A.F. Ippoliti, E.J. Bernard, L. Mei, D.L. Nicolae, M. Regueiro, L.P. Schumm, A.H. Steinhart, J.I. Rotter, R.H. Duerr, J.H. Cho, M.J. Daly, and S.R. Brant. 2007. Genome-wide association study identifies new susceptibility loci for Crohn disease and implicates autophagy in disease pathogenesis. Nat Genet. 39:596-604.

Roberts, R., W.T. Al-Jamal, M. Whelband, P. Thomas, M. Jefferson, J. van den Bossche, P.P. Powell, K. Kostarelos, and T. Wileman. 2013. Autophagy and formation of tubulovesicular autophagosomes provide a barrier against nonviral gene delivery. Autophagy. 9:667-682.

Rubinsztein, D.C. 2006. The roles of intracellular protein-degradation pathways in neurodegeneration. Nature. 443:780-786.

Russell, R.C., Y. Tian, H. Yuan, H.W. Park, Y.Y. Chang, J. Kim, H. Kim, T.P. Neufeld, A. Dillin, and K.L. Guan. 2013. ULK1 induces autophagy by phosphorylating Beclin-1 and activating VPS34 lipid kinase. Nat Cell Biol. 15:741-750.

Saitoh, T., N. Fujita, M.H. Jang, S. Uematsu, B.G. Yang, T. Satoh, H. Omori, T. Noda, N. Yamamoto, M. Komatsu, K. Tanaka, T. Kawai, T. Tsujimura, O. Takeuchi, T. Yoshimori, and S. Akira. 2008. Loss of the autophagy protein Atg16L1 enhances endotoxin-induced IL-1beta production. Nature. 456:264-268.

Sakoh-Nakatogawa, M., K. Matoba, E. Asai, H. Kirisako, J. Ishii, N.N. Noda, F. Inagaki, H. Nakatogawa, and Y. Ohsumi. 2013. Atg12-Atg5 conjugate enhances E2 activity of Atg3 by rearranging its catalytic site. Nat Struct Mol Biol. 20:433-439.

Sander, J.D., and J.K. Joung. 2014. CRISPR-Cas systems for editing, regulating and targeting genomes. Nat Biotechnol. 32:347-355.

Schmid, D., M. Pypaert, and C. Münz. 2007. Antigen-loading compartments for major histocompatibility complex class II molecules continuously receive input from autophagosomes. Immunity. 26:79-92.

Sclimenti, C.R., and M.P. Calos. 1998. Epstein-Barr virus vectors for gene expression and transfer. Curr Opin Biotechnol. 9:476-479.

Shaw, M.H., T. Reimer, Y.G. Kim, and G. Nuñez. 2008. NOD-like receptors (NLRs): bona fide intracellular microbial sensors. Curr Opin Immunol. 20:377-382.

Shintani, T., and D.J. Klionsky. 2004. Autophagy in health and disease: a double-edged sword. Science. 306:990-995.

Simmons, A. 2010. Crohn's disease: Genes, viruses and microbes. Nature. 466:699-700.

Simonsen, A., and S.A. Tooze. 2009. Coordination of membrane events during autophagy by multiple class III PI3-kinase complexes. J Cell Biol. 186:773-782.

Smith, T.F. 2008. Diversity of WD-repeat proteins. Subcell Biochem. 48:20-30.

Smith, T.F., C. Gaitatzes, K. Saxena, and E.J. Neer. 1999. The WD repeat: a common architecture for diverse functions. Trends Biochem Sci. 24:181-185.

Sorbara, M.T., L.K. Ellison, M. Ramjeet, L.H. Travassos, N.L. Jones, S.E. Girardin, and D.J. Philpott. 2013. The protein ATG16L1 suppresses inflammatory cytokines induced by the intracellular sensors Nod1 and Nod2 in an autophagy-independent manner. Immunity. 39:858-873.

Stappenbeck, T.S., J.D. Rioux, A. Mizoguchi, T. Saitoh, A. Huett, A. Darfeuille-Michaud, T. Wileman, N. Mizushima, S. Carding, S. Akira, M. Parkes, and R.J. Xavier. 2011. Crohn disease: a current perspective on genetics, autophagy and immunity. Autophagy. 7:355-374.

Sun, B.K., J.H. Kim, H.N. Nguyen, S. Oh, S.Y. Kim, S. Choi, H.J. Choi, Y.J. Lee, and J.J. Song. 2011. MEKK1/MEKK4 are responsible for TRAIL-induced JNK/p38 phosphorylation. Oncol Rep. 25:537-544.

Sun, Q., W. Fan, K. Chen, X. Ding, S. Chen, and Q. Zhong. 2008. Identification of Barkor as a mammalian autophagy-specific factor for Beclin 1 and class III phosphatidylinositol 3-kinase. Proc Natl Acad Sci U S A. 105:19211-19216.

Sventoraityte, J., A. Zvirbliene, A. Franke, R. Kwiatkowski, G. Kiudelis, L. Kupcinskas, and S. Schreiber. 2010. NOD2, IL23R and ATG16L1 polymorphisms in Lithuanian patients with inflammatory bowel disease. World J Gastroenterol. 16:359-364.

Szeto, J., N.A. Kaniuk, V. Canadien, R. Nisman, N. Mizushima, T. Yoshimori, D.P. Bazett-Jones, and J.H. Brumell. 2006. ALIS are stress-induced protein storage compartments for substrates of the proteasome and autophagy. Autophagy. 2:189-199.

Takekawa, M., F. Posas, and H. Saito. 1997. A human homolog of the yeast Ssk2/Ssk22 MAP kinase kinase kinases, MTK1, mediates stress-induced activation of the p38 and JNK pathways. EMBO J. 16:4973-4982.

Tao, M., P.C. Scacheri, J.M. Marinis, E.W. Harhaj, L.E. Matesic, and D.W. Abbott. 2009. ITCH K63-ubiquitinates the NOD2 binding protein, RIP2, to influence inflammatory signaling pathways. Curr Biol. 19:1255-1263.

Thoreen, C.C., S.A. Kang, J.W. Chang, Q. Liu, J. Zhang, Y. Gao, L.J. Reichling, T. Sim, D.M. Sabatini, and N.S. Gray. 2009. An ATP-competitive mammalian target of rapamycin inhibitor reveals rapamycin-resistant functions of mTORC1. J Biol Chem. 284:8023-8032.

Thoreen, C.C., and D.M. Sabatini. 2004. Huntingtin aggregates ask to be eaten. Nat Genet. 36:553-554.

Tigno-Aranjuez, J.T., J.M. Asara, and D.W. Abbott. 2010. Inhibition of RIP2's tyrosine kinase activity limits NOD2-driven cytokine responses. Genes Dev. 24:2666-2677.

Travassos, L.H., L.A. Carneiro, M. Ramjeet, S. Hussey, Y.G. Kim, J.G. Magalhães, L. Yuan, F. Soares, E. Chea, L. Le Bourhis, I.G. Boneca, A. Allaoui, N.L. Jones, G. Nuñez, S.E. Girardin, and D.J. Philpott. 2010. Nod1 and Nod2 direct autophagy by recruiting ATG16L1 to the plasma membrane at the site of bacterial entry. Nat Immunol. 11:55-62.

Van Craenenbroeck, K., P. Vanhoenacker, and G. Haegeman. 2000. Episomal vectors for gene expression in mammalian cells. Eur J Biochem. 267:5665-5678.

van der Pouw Kraan, C.T., J.M. Baggen, A.A. van Bodegraven, C.J. Mulder, A. Zwiers, D. Geerts, G. Kraal, A.J. Horrevoets, and G. Bouma. 2012. Defective IL-1A expression in patients with Crohn's disease is related to attenuated MAP3K4 signaling. Hum Immunol. 73:912-919.

Villén, J., S.A. Beausoleil, S.A. Gerber, and S.P. Gygi. 2007. Large-scale phosphorylation analysis of mouse liver. Proc Natl Acad Sci U S A. 104:1488-1493.

Wang, H., H. Yang, C.S. Shivalila, M.M. Dawlaty, A.W. Cheng, F. Zhang, and R. Jaenisch. 2013. One-step generation of mice carrying mutations in multiple genes by CRISPR/Cas-mediated genome engineering. Cell. 153:910-918.

Webber, J.L., and S.A. Tooze. 2010. Coordinated regulation of autophagy by p38alpha MAPK through mAtg9 and p38IP. EMBO J. 29:27-40.

Weidberg, H., T. Shpilka, E. Shvets, A. Abada, F. Shimron, and Z. Elazar. 2011. LC3 and GATE-16 N termini mediate membrane fusion processes required for autophagosome biogenesis. Dev Cell. 20:444-454.

Wileman, T. 2007. Aggresomes and pericentriolar sites of virus assembly: cellular defense or viral design? Annu Rev Microbiol. 61:149-167.
Wirth, M., J. Joachim, and S.A. Tooze. 2013. Autophagosome formation--the role of ULK1 and Beclin1-PI3KC3 complexes in setting the stage. Semin Cancer Biol. 23:301-309.

Xavier, R.J., and J.D. Rioux. 2008. Genome-wide association studies: a new window into immune-mediated diseases. Nat Rev Immunol. 8:631-643.

Xie, Z., and D.J. Klionsky. 2007. Autophagosome formation: core machinery and adaptations. Nat Cell Biol. 9:1102-1109.

Xie, Z., U. Nair, and D.J. Klionsky. 2008. Atg8 controls phagophore expansion during autophagosome formation. Mol Biol Cell. 19:3290-3298.

Yang, Z., and D.J. Klionsky. 2009. An overview of the molecular mechanism of autophagy. Curr Top Microbiol Immunol. 335:1-32.

Yang, Z., and D.J. Klionsky. 2010. Eaten alive: a history of macroautophagy. Nat Cell Biol. 12:814-822.

Yang, Z., and D.J. Klionsky. 2010. Mammalian autophagy: core molecular machinery and signaling regulation. Curr Opin Cell Biol. 22:124-131.

Yao, T.P. 2010. The role of ubiquitin in autophagy-dependent protein aggregate processing. Genes Cancer. 1:779-786.

Yates, J., N. Warren, D. Reisman, and B. Sugden. 1984. A cis-acting element from the Epstein-Barr viral genome that permits stable replication of recombinant plasmids in latently infected cells. Proc Natl Acad Sci U S A. 81:3806-3810.

Young, A.R., E.Y. Chan, X.W. Hu, R. Köchl, S.G. Crawshaw, S. High, D.W. Hailey, J. Lippincott-Schwartz, and S.A. Tooze. 2006. Starvation and ULK1-dependent cycling of mammalian Atg9 between the TGN and endosomes. J Cell Sci. 119:3888-3900.

Zhang, N., M.H. Ahsan, L. Zhu, L.C. Sambucetti, A.F. Purchio, and D.B. West. 2005. NF-kappaB and not the MAPK signaling pathway regulates GADD45beta expression during acute inflammation. J Biol Chem. 280:21400-21408.

Zilberman, Y., C. Ballestrem, L. Carramusa, R. Mazitschek, S. Khochbin and A. Bershadsky. 2009. J Cell Sci. 122: 3531-41.